

**Polymerization And Oligomerization Reactions Mediated
By Metallo dendrimers Of Zinc And Palladium**

By

Jane Ng̃ima Mũgo



**A dissertation in fulfilment of the requirement for the degree of PhD in
Chemistry in the Department of Chemistry and Polymer Science,
University of Stellenbosch**

Supervisor: Prof. S. F. Mapolie

March 2012

Declaration

I declare that the thesis "*Polymerization And Oligomerization Reactions Mediated By Metallo dendrimers Of Zinc and Palladium*" is my own work, that it has not been submitted before for any degree or examination in any other university, and that all the sources I have used or quoted have been indicated and acknowledged as complete references.

"

"

"

"

"

"

"

"

"

"

Eqr { tki j vÍ "4234"Uvgmgpdquej "Wplxgtukv{

Cmłki j w'tgugtxgf "

.....

Jane Ngĩma Mũgo

Abstract

In this thesis the synthesis and catalytic applications of new mononuclear and multinuclear transition metal complexes derived from salicylaldimine (N,O) and pyrrolylaldimine (N,N) ligands are described. The mononuclear complexes were obtained from monofunctional ligands while the multinuclear complexes were derived from dendritic ligands.

The monofunctional salicylaldimine ligands (**L1 – L3**) were prepared by Schiff base condensation of n-propyl amine with the appropriate aldehyde; 2-hydroxybenzaldehyde, 3-*t*-butyl-2-hydroxybenzaldehyde and 3,5-*t*-di-butyl-2-hydroxybenzaldehyde respectively. The dendritic analogues were obtained by modifying the peripheral groups of the first or second generation poly(propyleneimine) dendrimer, (DAB-(NH₂)_n (n = 4 or 8), which are commercially available with the aforementioned aldehydes to produce ligands, (**L4 – L9**). The zinc complexes (**C1 – C9**) and those of palladium (**C14 – C17**) were subsequently obtained by reacting each of the ligands with either diethyl zinc or palladium acetate respectively.

The pyrrolylaldiminato Pd(II) complexes were synthesized using a similar protocol to that of the salicylaldimine analogues. The ligands were first prepared by the condensation of pyrrole-2-carboxylaldehyde with either n-propyl amine, 2,6-diisopropylaniline or the 1st and 2nd generation DAB-(NH₂)_n dendrimer to produce ligands (**L10 – L13**). These ligands were later reacted with palladium acetate yielding complexes **C10 – C13**.

The ligands and metal complexes were fully characterized using various analytical techniques. These include NMR, FT-IR and ICP-AE spectroscopy, mass spectrometry and microanalysis. Thermal analyses (TGA and DSC) were also performed to establish the thermal properties of the metallodendrimers. Single crystal x-ray diffraction of complex **C14** was performed to determine the molecular structure. The structure reveals a slightly distorted

square planar geometry around the metal center with the imino nitrogens positioned *trans* relative to each other.

The Zn(II) complexes were evaluated as catalysts in the ring opening polymerization (ROP) of D, L-Lactide (D,L-LA). The reactions were followed by ¹H-NMR and the polylactides obtained characterized by FT-IR and NMR spectroscopy, GPC, SEM, TGA and DSC.

Five mononuclear complexes (**C1** – **C3**, **C18** and **C19**), were active as catalysts in the polymerization of D,L-LA in solution while the metallodendrimers were found to be more efficient in bulk polymerization of the monomer. The substituents on the phenoxy moiety were varied in order to probe their influence on the polymerization process. The unsubstituted mononuclear complex, **C1** was established to be the most active catalyst achieving high monomer conversions at various metal concentrations. The polymerization rate constants (k_{app}) for catalyst **C1** at different Zn concentrations were established to be 2.63, 3.80 and $13.62 \times 10^{-2} \text{ h}^{-1}$ for $[\text{Zn}] = 0.01, 0.02$ and 0.04 M respectively. The study also revealed that the polymerization reactions followed 1st order kinetics with respect to the monomer. An induction period for the polymerization process was observed. Using **C3**, this induction period was found to be up to 10 h. The sterically bulky substituents on the phenoxy rings of **C3** resulted in a decrease in the rate of polymerization.

The above mentioned catalysts produced amorphous polylactides as evident from the FT-IR spectra. DSC analysis showed T_g values between 54 and 56 °C for the polymers produced.

The metallodendrimers exhibited very high activity in bulk polymerization reactions. However, the polymers produced were largely cyclic polylactides whose molecular weights (obtained from GPC) were lower than that predicted using ¹H-NMR spectroscopy. This indicates that intra-chain trans-esterification reactions were taking place. From the data

acquired it can be concluded that both the mononuclear and dendritic Zn(II) complexes are efficient in the polymerization of D,L-LA.

The palladium complexes, **C10** – **C14**, were evaluated as pre-catalysts, in the oligomerization of α -olefins using ethylaluminium dichloride (EtAlCl_2) as a co-catalyst. The mononuclear complexes were found to be active in the oligomerization of ethylene with activities of up to 920 kg product $(\text{mmol Pd})^{-1} \text{ h}^{-1}$ for **C11**. The dendrimer based pre-catalysts **C12** and **C13** showed no catalytic activity under the conditions employed.

Catalyst **C10**, **C11** and **C14** produced alkyl toluenes that were detected as uneven carbon numbered products after analysing the reaction mixture using GC. These Friedel-Crafts alkylation products are formed by the reaction of toluene with the C_4 and C_6 oligomers formed in the catalytic oligomerization process. The Friedel-Crafts alkylation is mediated by the co-catalyst, EtAlCl_2 and not by the metal complex. The transition metal complex does however seem to facilitate isomerisation of the α -olefins formed leading to the formation of alkyl toluenes with branched alkyl substituents. Long chain even carbon numbered oligomers were obtained after removal of all volatiles from the reaction mixture. The oligomers ranged from C_{20} to C_{64} and were isolated as viscous oils.

Attempts to oligomerize higher olefins such as 1-hexene were not successful instead Friedel-Crafts alkylation of toluene similar to that observed with the ethylene oligomers occurred. The palladium complexes also isomerized 1-hexene to the internal isomers. However the internal hexene isomers were also subsequently consumed in the alkylation leading to the formation of branched alkyl substituted toluenes.

Opsomming

In hierdie tesis word die sintese en katalitiese toepassing van nuwe enkelkernige en meerkernige metaal komplekse van salisielaldimien (N,O) en pirrolielaldimien (N,N) ligande beskryf. Die enkelkernige komplekse is gesintetiseer deur van enkelkernige ligande gebruik te maak, terwyl die meerkernige komplekse vanaf dendritiese ligande verkry is.

Die monofunksionele salisielaldimien ligande (**L1 – L3**) is gesintetiseer deur Schiff-basis kondensasie van *n*-propielamien met 'n geskikte aldehyd; 2-hidroksielbensaldehyd, 3-^tbutiel-2-hidroksielbensaldehyd en 3, 5-^tdi-butiel-2-hidroksielbensaldehyd onderskeidelik. Dendritiese eweknieë is verkry deur die oppervlakkige groepe van 'n eerste of tweede generasie poli(propileenimin) dendrimeer [(DAB-(NH₂)_n (n = 4 of 8)], wat kommersieël beskikbaar is met die voorafgenoemde aldehyde, te modifiseer om ligande (**L4 – L9**) te verkry. Sink komplekse (**C1 – C9**) en palladium komplekse (**C14 – C17**) is verkry deur elk van die ligande met onderskeidelik diëtielsink of palladiumasetaat te reageer.

Die pirrolielaldiminato Pd(II) komplekse is verkry deur van 'n soortgelyke protokol as die van salisielaldimien gebruik te maak. Die ligande is gesintetiseer deur die kondensasie van pirroliel-2-karboksialdehyd met onderskeidelik *n*-propielamien, 2, 6-dissopropielanalien of die eerste en tweede generasie DAB-(NH₂)_n dendrimere om ligande (**L10 – L13**) te verkry. Hierdie ligande is later met palladiumasetaat gereageer om komplekse **C10 – C13** op te lewer.

Die ligande en metaalkomplekse is volledig gekarakteriseer deur van verskeie analitiese tegnieke gebruik te maak. Dit sluit in KMR, FT-IR en ICP-AE spektroskopie, massa spektroskopie en mikroanaliese. Termiese analise (TGA en DSC) is uitgevoer om die termiese eienskappe van die metallodendrimere te bepaal. Enkelkristal X-straaldiffraksie analise van kompleks **C14** is uitgevoer om die molekulêre struktuur te bepaal. Die struktuur lewer 'n effens verwronge vierkantigvlakke geometrie rondom die metaalkern met die imino stikstowwe *trans* van mekaar geposisioneer.

Die Zn(II) komplekse is geëvalueer as katalisatore in die ring opening polimerisasie (ROP) van D,L-laktied (D, L-LA). Die reaksies is gevolg met ^1H -KMR en die polilaktiede wat verkry is, is gekarakteriseer deur van FT-IR en KMR-spektroskopie, GPC, SEM, TGA en DSC gebruik te maak.

Vyf enkelkernige komplekse (**C1** - **C3**, **C18** en **C19**), is aktief as katalisatore in die polimerisasie van D, L-LA in oplossing terwyl daar gevind is dat die metallodendrimere meer doeltreffend in grootmaat polimerisasie van die monomeer was. Die substituentte op die fenoksie eenheid is verander om die uitwerking daarvan op die polimerisasie te ondersoek. Die ongesubstitueerde enkelkernige kompleks **C1** is gevind om die mees aktief te wees deurdat dit hoë monomeer omskakeling by verskillende metaal konsentrasies getoon het. Die polimerisasiesnelheidskonstante (k_{app}) vir **C1** by verskillende Zn konsentrasies is gevind om 2.63, 3.80 en $13.62 \times 10^{-2} \text{ h}^{-1}$ te wees vir $[\text{Zn}] = 0.01, 0.02$ en 0.04 M onderskeidelik. Die studie het ook getoon dat die reaksies eerste orde kinetika volg ten opsigte van die monomeer. Induksie tydperk vir die polimerisasie is ook waargeneem. Vir kompleks **C3** is die induksie tydperk gevind om tot 10 ure te wees. Die steriese lywige substituentte op die fenoksie ringe van kompleks **C3** het 'n afname in die tempo van polimerisering getoon.

Die bogenoemde katalisator het amorf polilaktiedes geproduseer soos getoon deur FT-IR. DSC analise het getoon dat T_g waardes tussen 54 en 56 °C vir die polimere wat gevorm is.

Die metallodendrimere het baie hoë aktiwiteit getoon in grootmaat polimeriseringsreaksies. Hierdie polimere was egter grotendeels sikliese polilaktiedes met molekulêre massas (verkry vanaf GPC) laer as wat deur ^1H -KMR voorspel is. Dit het daarop gedui dat intra-ketting trans-esterifikasie reaksies plaasgevind het. Hierdie data het getoon dat beide die enkelkernige en dendritiese Zn(II) komplekse doeltreffende D,L-LA polimeriseringskatalisatore is.

Die palladium komplekse, **C10** - **C14**, is geëvalueer as pre-katalisatore in die oligomerisasie van α -olefiene deur etielaluminium dichloried (EtAlCl_2) as kokatalisator te gebruik. Die enkelkernige komplekse is gevind om aktief te wees in die oligomerisasie van etileen met aktiwiteit van tot 920 kg produk $(\text{mmol Pd})^{-1}\text{h}^{-1}$ vir **C11**. Die dendriemergebaseerde pre-katalisatore **C12** en **C13** toon egter geen katalitiese aktiwiteit onder hierdie reaksie kondisies nie.

Katalisatore **C10**, **C11** en **C14** het alkiel toluen produkte tot gevolg gehad. Hierdie produkte is waargeeem as onewe-koolstof genommerde produkte nadat die reaksiemengsel met GC geanaliseer is. Hierdie Friedel-Crafts alkilerings produkte word gevorm deur die reaksie van die toluen met die C_4 en C_6 oligomere wat gevorm word tydens die oligomerisasie proses. Die Friedel-Crafts alkilering word gemedieer deur die kokatalisator, EtAlCl_2 en nie deur die metaal kompleks self nie. Die oorgangsmetaal kompleks fasiliteer egter die isomerisasie van α -olefiene wat lei tot die vorming van alkiel toluen met vertakte alkielsubstituent. Lang ketting ewe-koolstof genommerde oligomere is verkry na die verwydering van alle vlugtige verbindings vanuit die reaksiemengsel. Die oligomere het gewissel van C_{20} tot C_{64} en is geïsoleer as viskose olies.

Pogings om hoër olefiene soos 1-hekseen te oligomeriseer was nie suksesvol nie. In plaas daarvan is Friedel-Crafts alkilering van toluen, soortgelyk aan wat waargeneem is met die etileen oligomere, gevind. Die palladium komplekse het ook 1-hekseen na interne isomere geïsoleer. Die interne hekseen isomere is egter daarna opgebruik in die alkilering wat gelei het tot die vorming van vertakte alkiel gesubstitueerde toluen.

Publications

Journal articles

1. **The Use of Cu and Zn Salicylaldimine Complexes as Catalysts Precursors in Ring Opening Polymerization of Lactides: Ligand Effect on Polymer Characteristics**
S. Bhunora, J. Mugo, A. Bhaw-Luximon, S. Mapolie, J. L. van Wyk, J. Darkwa, E. Nordlander, *Applied Organometallic Chemistry* **25** (2011) 133–145.

Conference presentations

1. **Pyrrole-imine and Salicylaldimine Pd(II) Complexes: α -Olefins Oligomerization and Transformation**
J. N. Mugo and S. F. Mapolie Catalysis Society of South Africa (CATSA), Johannesburg, South Africa, (2011).
2. **Ring Opening Polymerization of D,L - Lactide Using Novel Salicylaldiminato Zn(II) Complex**
J. N. Mugo and S. F. Mapolie, *South Africa Chemical Institute Young Scientist Symposium*, University of Cape Town, (2010).
3. **α -Olefin Transformation Catalyzed by Pyrrolylaldiminato Pd(II) and Cr(III) Complexes**
J. N. Mugo and S. F. Mapolie, *Catalysis Society of South Africa (CATSA)*, Bloemfontein, South Africa, (2010).
4. **α -Olefin Transformation Catalyzed by Pyrrolylaldiminato Pd(II) and Cr(III) complexes**
J. N. Mugo and S. F. Mapolie, *Catalysis Society of South Africa (CATSA)*, Cape Town, South Africa, (2009).

5. Oligomerization of 1-Hexene Catalyzed by Pyrrolylaldiminato Pd(II) and Cr(III) Complexes

J. N. Mugo and S. F. Mapolie, *Catalysis Society of South Africa (CATSA)*, Parys, South Africa, (2008).

Table of Contents

Declaration	i
Abstract.....	ii
Opsomming	v
Publications	viii
Table of Contents	x
List of Figures.....	xv
List of Tables.....	xxi
List of Schemes	xxiii
List of Abbreviations.....	xxv
Acknowledgement.....	xxix
Chapter 1 : Salicylaldimine and Pyrrole-imine Schiff Base Complexes as Catalyst with an Emphasis on Polymerization and Oligomerization.....	1
1.1: General.....	2
1.2: Salicylaldimine (N,O) ligands and their metal complexes	3
1.2.1: Catalytic applications of salicylaldiminato metal complexes	9
1.3: Pyrrolylaldiminato (N,N) ligands and their metal complexes	22
1.3.1: Catalytic applications of pyrrolylaldiminato metal complexes.....	24
1.4: (Salicylaldiminato) (pyrrolylaldiminato) metal complexes; mixed ligand complexes.....	33
1.5: Other Schiff base metal complexes employed in the polymerization of cyclic esters	35
1.6: α -olefin oligomerization and polymerization	39
1.7: Dendrimer supported Schiff base metal complexes as catalysts	41
1.8: Aim and scope of this thesis	46
1.9: References.....	49

Chapter 2 : Synthesis and Characterization of Salicylaldimine and Pyrrolyaldimine

Schiff Base Ligands.....56

2.1: Introduction.....57

2.2: Results and discussion59

2.2.1: Synthesis and characterization of the monofunctional aliphatic
salicylaldimine ligands, **L1 – L3**.....59

2.2.2: Synthesis and characterization of the multifunctional (dendrimeric)
salicylaldimine ligands, **L4 – L9**.....62

2.2.3: Synthesis and characterization of the monofunctional (aliphatic and aromatic)
pyrrole-imine ligands, **L10 and L11**76

2.2.4: Synthesis and characterization of multifunctional pyrrole-imine ligands,
L12 and L13.....79

2.3: Conclusions.....82

2.4: Experimental.....85

2.4.1: Materials and instrumentation85

2.4.2: Preparation of salicylaldimine ligands87

2.4.3: Preparation of pyrrole-imine ligands.....88

2.5: References..... 90

Chapter 3 : Synthesis and Characterization of Salicylaldiminato Zn(II) Complexes92

3.1: Introduction.....93

3.1.2: Dendritic salicylaldimine metal complexes95

3.2: Results and discussion96

3.2.1: Synthesis and characterization of the bis(N-n-propylsalicylaldiminato) Zn(II) complexes, C1 – C3	96
3.2.2: Synthesis and characterization of the 1 st generation Zn(II) metallodendrimers, C4 – C6	102
3.2.3: Synthesis and characterization of the 2 nd generation Zn(II) metallodendrimers, C7 – C9	114
3.3: Conclusions.....	119
3.4: Experimental.....	120
3.4.1: Materials and instrumentation	120
3.4.2: Preparation of salicylaldiminato Zn(II) complexes.....	122
3.5: References.....	123
Chapter 4 : Synthesis and Characterization of Pyrrolylaldiminato and Salicylaldiminato Pd(II) Complexes.....	127
4.1: Introduction.....	128
4.2: Results and discussion	129
4.2.1: Preparation of mononuclear pyrrolylaldiminato Pd(II) complexes, C10 and C11	129
4.2.2: Preparation of dendritic pyrrolylaldiminato Pd(II) complexes	136
4.2.3: Preparation of mononuclear salicylaldiminato Pd(II) complexes, C14 – C16	141
4.2.4: Preparation of the dendritic salicylaldiminato Pd(II) complex, C17	147
4.3: Conclusions.....	150
4.4: Experimental.....	152
4.4.1: Materials and instrumentation	152

4.4.2.: Synthesis and characterization of mononuclear bis-N-n-propyl pyrrolyaldiminato Pd(II) complexes, C10 and C11	153
4.4.3.: Synthesis and characterization of dendritic Pd(II) pyrrolyaldiminato complexes, C12 and C13	154
4.4.4.: Synthesis and characterization of mononuclear bis-N-n- propyl- salicylaldiminato Pd(II) complex, C14 – C16	155
4.4.5.: Synthesis and characterization of salicylaldiminato bi-nuclear Pd(II) complex, C17	155
4.5: References.....	156
Chapter 5 : Ring Opening Polymerization of D,L–Lactide using Salicylaldiminato Zn(II) Complexes	159
5.1: Introduction.....	160
5.1.1: Lactide ring opening polymerization (ROP)	160
5.1.2: D, L-lactide isomers	163
5.2: Results and discussions.....	167
5.2.1: Preliminary results on D, L-lactide polymerization	167
5.2.2: Kinetic studies	173
5.2.3: Characterization of polylactides produced	187
5.3: Conclusions.....	197
5.4: Experimental.....	198
5.4.1: Materials and instrumentation	198
5.5: References.....	200

Chapter 6 : Preliminary Evaluation of Pd(II) Complexes as Pre-catalysts for α-Olefin Transformation	204
6.1: Introduction.....	205
6.2: Results and discussion	207
6.2.1: Ethylene oligomerization	207
6.2.3: Characterization of the oligomers obtained using C10 , C11 and C14 pre-catalysts	214
6.3: Conclusions.....	223
6.4: Experimental.....	223
6.4.1: Materials and instrumentation	223
6.4: References.....	225
Chapter 7 : Summary and Future Work.....	227
7.1: Summary.....	228
7.2: Future work.....	229

List of Figures

Figure 1.1: General structure of a salicylaldiminato complex	3
Figure 1.2: General structure of a pyrrolylaldiminato complex.....	3
Figure 1.3: Bis(N-isopropylsalicylaldimine) metal complexes reported by Torzilli <i>et al.</i> ¹⁷	4
Figure 1.4: Mononuclear Zn(II) compound reported by Zhu <i>et al.</i> ¹⁹	5
Figure 1.5: Mono- and binuclear salicylaldiminato Al(III) complexes reported by Martínez <i>et al.</i> ²⁰	6
Figure 1.6: Binuclear salicylaldiminato complexes reported by Tas <i>et al.</i> ²⁰	7
Figure 1.7: Mononuclear salicylaldiminato Ni(II) complexes reported by Kasumov ²¹	7
Figure 1.8: Mononuclear salicylaldiminato Cu(II) complexes reported by Kasumov and Köksal ²³	8
Figure 1.9: Mono- and bis-ligated salicylaldiminato Ni(II) complexes reported by Kettunen <i>et al.</i> ²⁴	9
Figure 1.10: Mono-ligated salicylaldimine Pd(II) complexes reported by Li <i>et al.</i> ³²	10
Figure 1.11: Neutral Ni(II) salicylaldimine complexes	11
Figure 1.12: <i>Mono-</i> and <i>bis-</i> (salicylaldiminato) Ni(II) complexes reported by Lu <i>et al.</i> ³⁶	12
Figure 1.13: Mononuclear salicylaldiminato Al(III) complexes reported by Cameron <i>et al.</i> ³⁷	13
Figure 1.14: Co(II) salicylaldiminato complexes reported by Chandran <i>et al.</i> ³⁸	14
Figure 1.15: Dimethyl phenoxy-imine Al(III) complexes reported by Lui <i>et al.</i> ³⁹	15
Figure 1.16: Dimethylaluminum(III) complexes reported by Pappalardo <i>et al.</i> ⁴⁰	16
Figure 1.17: Mono chelate Sn(II) salicylaldiminato complexes reported by Nimitsiriwat <i>et al.</i> ⁴¹	18
Figure 1.18: Tridentate N, N, O Sn(II) dimeric complex reported by Nimitsiriwat <i>et al.</i> ⁴¹ ...	18
Figure 1.19: Bis chelate Sn(II) salicylaldiminato complexes reported by Nimitsiriwat and co-workers ⁴²	19

Figure 1.20: Bis chelate Zn(II) salicylaldiminato complexes reported by Darensbourg <i>et al.</i> ⁴³	20
Figure 1.21: Salicylaldimine ligands used in the synthesis of mono and tri-nuclear Zn(II) complexes reported by Jones <i>et al.</i> ⁴⁴	21
Figure 1.22: Salicylaldiminato Zn(II) complex immobilised on silica (SiO-AMPS) reported by Jones <i>et al.</i> ⁴⁴	21
Figure 1.23: Bonding mode for pyrrolylaldiminato metal complexes	22
Figure 1.24: Example of a Ru (II) pyrrole-imine complex	23
Figure 1.25: Co(II) pyrrole-imine complexes reported by Carabineiro and co-workers ^{46, 49}	23
Figure 1.26: Mono- and bis-pyrrolylaldiminato nickel (II) complexes reported by Pérez-Puente <i>et al.</i> ⁵⁰	24
Figure 1.27: Ti(IV) complex with pyrrolide-imine ligands reported by Yoshida <i>et al.</i> ⁵²	25
Figure 1.28: Dibenzyl Hf(IV) pyrrolylaldiminato complexes reported by Matsui <i>et al.</i> ⁵⁴	26
Figure 1.29: Dibenzyl Hf (IV) and Zr(IV) pyrrolylaldiminato complexes reported by Matsui <i>et al.</i> ⁵⁷	27
Figure 1.30: 2-(N-arylimino)pyrrolide Ni(II) complexes reported by Li and co-workers ⁶¹	28
Figure 1.31: Neutral Ni (II) complexes of pyrrole imine with other auxiliary ligands reported by Li <i>et al.</i> ⁵¹	29
Figure 1.32: Pyrrolylaldiminato Nickel complex reported by Bellabarba <i>et al.</i> ⁶²	30
Figure 1.33: Cr (II) pyrrolylaldiminato complex reported by Gibson <i>et al.</i> ⁶³	30
Figure 1.34: Neutral pyrrolylaldiminato Pd(II) complexes reported by Liang <i>et al.</i> ⁶⁴	31
Figure 1.35: Sm and Y pyrrole-imine complexes reported by Cui and co-workers ⁶⁵	32
Figure 1.36: V(III) complexes bearing iminopyrrolyl ligands reported by Mu <i>et al.</i> ⁶⁶	33

Figure 1.37: Ti(IV) (salicylaldiminato)(pyrrolyaldiminato) metal complex	34
Figure 1.38: Zr(IV) (salicylaldiminato) (pyrrolyaldiminato) metal complex reported by Pennington <i>et al.</i> ⁶⁷	35
Figure 1.39: Zn(II)Cl ₂ metal complex, Kang <i>et al.</i> ⁸⁰	36
Figure 1.40: Al(III) and Y(III) alkoxide, Ovitt and co-workers ⁸¹	37
Figure 1.41: Al(III) salen complexes containing both chiral and achiral ligands reported by Darensbourg <i>et al.</i> ⁸²	38
Figure 1.42: 2, 6-diisopropylphenyl substituted β -diimine (BDI) Z(II) complex reported by Cheng <i>et al.</i> ⁸³	39
Figure 1.43: Ni(II) complexes based on tridentate pyrazolyl ligands reported by Oliveira <i>et al.</i> ⁸⁶	41
Figure 1.44: Dendrimeric pyrrolyaldiminato complexes reported by Mugo <i>et al.</i> ⁵⁹	42
Figure 1.45: 1 st generation Ni(II) salicylaldimine metallodendrimer reported by Malgas-Enus <i>et al.</i> ^{105, 106}	43
Figure 1.46: 2 nd generation Ni(II) salicylaldimine metallodendrimer, published by Malgas-Enus <i>et al.</i> ^{105, 106}	44
Figure 1.47: Peripherally bound Pd(II) metallodendrimer reported by Smith <i>et al.</i> ¹⁰⁷	45
Figure 2.1: General structure of a dendrimer	57
Figure 2.2: 1 st Generation poly (propylene imine) dendrimer, DAB-PPI-(NH ₂) ₄	59
Figure 2.3: 2 nd Generation dendritic salicylaldimine ligand, L6 – L9	64
Figure 2.4: ESI mass spectrum of the L5 showing [M+H] ⁺ and [M+H] ²⁺	66
Figure 2.5: ESI mass spectrum of the L8 showing [M+H] ²⁺ , [M+H] ³⁺ and [M+H] ⁴⁺	67
Figure 2.6: The molecular structure of L5 with the atom-numbering scheme. Displacement ellipsoids are drawn at the 30% probability. H atoms omitted for clarity	69
Figure 2.7: 2, 6-di(propan-2-yl)-N-[(E)-1H-pyrrol-2-ylmethylidene]aniline ligand, L11	79

Figure 2.8: 2 nd Generation dendritic pyrrolyaldiminato ligand, L13	80
Figure 3.1: Various architectures of metallodendrimers with the metal centers on periphery (a), at the core (b), at branching points (c) and as encapsulated metal nanoparticles (d); adapted from Balzani <i>et al.</i> ³²	95
Figure 3.2: ESI-MS spectrum of bis(N-n-propyl)-3- ^t -butyl salicyaldiminato) Zn(II) complexes, C2	101
Figure 3.3: ESI-MS spectrum of G1, 3- ^t -butyl phenyl salicyaldiminato Zn(II) complex, C5	106
Figure 3.4: MALDI-TOF spectrum of G1, 3, 5 phenyl- ^t -butyl salicyaldiminato Zn(II) complex, C6	107
Figure 3.5: Thermogram obtained for C4	112
Figure 3.6: DSC plot for complex C4	114
Figure 3.7: 2 nd Generation (G2) salicyaldiminato Zn(II) metallodendrimer	115
Figure 3.8: Fragments obtained in the ESI-MS spectra for 2 nd generation- (phenyl- 3, 5 – ^t -butyl) salicyaldiminato Zn(II) complex C7	116
Figure 3.9: Thermogram obtained for C7	118
Figure 3.10: DSC profile for complexes C9	119
Figure 4.1: Structure of a neutral pyrrole-imine Pd(II) complex, C11	135
Figure 4.2: ESI-MS spectrum of C11	136
Figure 4.3: G1 Pyrrole-imine Pd(II) complex, C12	137
Figure 4.4: FT-IR (ATR) spectrum of complex C12	138
Figure 4.5: The thermogram obtained for C12	139
Figure 4.6: 2 nd generation pyrrole-imine Pd(II) complex, C13	140
Figure 4.7: ESI-MS spectrum of <i>bis</i> (N-n-propyl) 3- ^t -butly-salicyaldiminato) Pd(II) complex, C15	144

Figure 4.8: The molecular structure of C14 with the atom-numbering scheme. Displacement ellipsoids are drawn at the 30% probability. H atoms are omitted for clarity	145
Figure 4.9: The molecular structure of a binuclear Pd(II) complex, C11	148
Figure 4.10: An ¹ H-NMR array for the product formed from L5 and Pd(OAc) ₂ ·H ₂ O.....	151
Figure 5.1: Lactide enantiomers.....	163
Figure 5.2: Structure of mononuclear salicylaldiminato Zn(II), C1 – C3 , C18 and C19	165
Figure 5.3: 1 st generation (G1) dendritic salicylaldiminato Zn(II) complexes	165
Figure 5.4: 2 nd generation (G2) dendritic salicylaldiminato Zn(II) complexes	166
Figure 5.5: ¹ H-NMR spectra obtained for M:Zn = 1 for C1 in an NMR tube at time (t = 0, 24 and 120 h.	172
Figure 5.6: A plot of $\ln\{[M]_0/[M]_t\}$ vs time (h) for complexes C1 at M/Zn = 25, 50 and 100	176
Figure 5.7: A plot of $\ln\{[M]_0/[M]_t\}$ vs time (h) for the salicylaldiminato Zn(II) complexes, C1 - C3 , at M/Zn = 50	178
Figure 5.8: FT-IR (ATR) spectrum of D, L – Lactide	190
Figure 5.9: FT-IR spectra of polymer produced by C1 as catalyst at various times, M/Zn = 25	191
Figure 5.10: FT-IR spectra of polymer; M/Zn = 50, C1 and C2 at 72 h, and at 96 h for C3	192
Figure 5.11: FT-IR spectra of polymer of C5 , C6 and C18 at M/Zn = 50 after 72 h, C19 , M/Zn = 50 after 68 h.....	193
Figure 5.12: SEM images of PDLLA obtained using C1	194
Figure 5.13: SEM images of various PDL-LA obtained using C5 and C6 at M/Zn = 50, 72 h.	194

Figure 5.14: SEM images of various PDLA obtained using C18 and C19 at M/Zn = 25, 20 h.	195
Figure 5.15: Thermogram for polymer obtained from C18 , M/Zn = 50, 96 h	196
Figure 5.16: DSC plot for C18 , M/Zn = 50, 96 h; 1 st cycle of heating, 2 nd cycle of heating after cooling	197
Figure 6.1: Structure of mononuclear pyrrolyaldiminato Pd(II) complexes, C10 and C11	207
Figure 6.2: 1 st generation (G1) dendritic pyrrolyaldiminato Pd(II) complex, C12	207
Figure 6.3: 2 nd generation (G1) dendritic pyrrolyaldiminato Pd(II) complex, C13	208
Figure 6.4: FT-IR spectrum of oligomers obtained using C11 (1000:1, toluene, 25 °C, 20 bar)	215
Figure 6.5: APCI-mass spectrum obtained for C11 , Al:Pd (2000:1), 1 h, 25 °C in toluene.....	217
Figure 6.6: APCI-mass spectrum obtained for C10 , Al:Pd (2000:1) , 3 h, 30 °C in Hexane.	218
Figure 6.7: GC-MS chromatogram indicating Friedel-Craft alkylation of toluene with 1-hexene while using C10 and C14 as pre-catalysts	220
Figure 6.8: GC-MS spectra of the fractions with retention time of between 10.97 and 11.56 min for the products produced using C10 and 1-hexene	221

List of Tables

Table 2.1: ^1H -NMR ^a data for the salicylaldimine ligands ^a	70
Table 2.2: $\{^1\text{H}\}^{13}\text{C}$ -NMR shifts (δ in ppm) data for the salicylaldimine ligands ^a	72
Table 2.3: Salicylaldimine ligands analytical data.....	73
Table 2.4: Crystal structural data (collection, structure solution and refinement) for L5	74
Table 2.5: Selected bond lengths and bond angles for L5	75
Table 2.6: ^1H -NMR data of pyrrolylaldiminate ligands ^a	83
Table 2.7: Analytical data for pyrrolylaldiminate ligands	84
Table 2.8: Pyrrolylaldiminate ligands $\{^1\text{H}\}^{13}\text{C}$ -NMR data (CDCl_3) ^a	84
Table 3.1: Salicylaldiminato Zn(II) complexes characterization data	104
Table 3.2: ^1H -NMR data for the salicylaldiminato Zn(II) complexes ^a	108
Table 3.3: $\{^1\text{H}\}^{13}\text{C}$ -NMR shifts (δ in ppm) for the salicylaldiminato Zn(II) complexes ^a	110
Table 4.1: Characterization data for Pd(II) complexes of pyrrolylaldimine and salicylaldimine ligands.....	132
Table 4.2: $\{^1\text{H}\}^{13}\text{C}$ -NMR shifts (75 MHz in CDCl_3 δ in ppm) data for the mononuclear pyrrolylaldiminato and salicylaldiminato complexes ^a	132
Table 4.3: ^1H -NMR (300 MHz in CDCl_3 , δ in ppm) data for the pyrrolylaldiminato and salicylaldiminato Pd(II) complexes ^a	133
Table 4.4: Crystal structural data (collection, solution and refinement) for C14	146
Table 4.5: Selected bond distances and angles for C14	147
Table 5.1: Preliminary polymerization results using $[\text{M}]/[\text{Zn}] = 50$, $[\text{M}] = 1 \text{ M}$	168
Table 5.2: Polymerization of D, L-Lactide using complexes C1 at different M/Zn ratios ^a	174
Table 5.3: Lactide polymerization using mononuclear complexes C1 – C3 ^a	177

Table 5.4: Lactide polymerization using mononuclear complexes C18 and C19^a	181
Table 5.5: Solution polymerization of D, L-lactide using dendritic complexes C5 and C6 as catalyst ^a	182
Table 5.6: Effect of solvent and temperature in the polymerization of D, L-lactide using C1 at M/Zn = 25.....	184
Table 5.7: Polymerization of D, L-lactide using C4 – C9 under melt conditions	185
Table 5.8: Intensities of different tetrad stereo-sequences of the polymers from solution reactions calculated from the ¹³ C-NMR spectra. ^a	189
Table 5.9: Intensities of different tetrad stereo-sequences of the polymers calculated from the ¹³ C-NMR spectra of the polymers from melt reactions.	189
Table 6.1: Ethylene oligomerization data C11^a	209
Table 6.2: Ethylene oligomerization catalysed by C10, C11 and C14^a	213
Table 6.3: Selectivity of the Friedel-Craft alkylation products using C10 - C14^a	222

List of Schemes

Scheme 1.1: Inter-conversion of Zn(II) (N-Propylsalicylaldiminato) to dichlorobis (N-Propylsalicylaldiminato) Zn(II) complex reported by Torzilli <i>et al.</i> ¹⁸	5
Scheme 2.1: Synthetic route to the monofunctional salicylaldimine ligands, L1 – L3	60
Scheme 2.2: Synthetic route for 1 st generation dendrimeric salicylaldimine ligands, L4 – L6	63
Scheme 2.3: Significant fragment ion of L8 as inferred from ESI-MS	68
Scheme 2.4: Synthetic route to N-[(1E)-1H-pyrrol-2-ylmethylene]propan-1-amine, L10	76
Scheme 2.5: Fragmentation pattern for L10 as inferred from the GC-MS	78
Scheme 2.6: Synthetic route to G1 dendrimeric ligand, (DAB-PPI-(N=CH(C ₄ H ₃ NH) ₄), L12	79
Scheme 2.7: Fragmentation pattern for L13 deduced from the ESI-mass spectrum.....	82
Scheme 3.1: Mononuclear Zn(II) complexes, C1 – C3	97
Scheme 3.2: Fragmentation pattern and proposed aggregation structures for C1 as inferred from FAB-MS.	100
Scheme 3.3: Preparation of the 1 st generation (G1) salicylaldiminato Zn(II) complexes	102
Scheme 4.1: Synthetic route for pyrrole-imine Pd(II) complex, C10	130
Scheme 4.2: Fragmentation pattern and proposed aggregation structures inferred from ESI-MS spectrum of C10	134
Scheme 4.3: Mononuclear salicylaldiminato Pd(II) complexes, C14 – C16	141
Scheme 4.4: The proposed fragmentation pattern and aggregation structures inferred from ESI-MS spectrum of C14	143
Scheme 5.1: Mechanism for the coordination and insertion of the D, L – lactide into C1 's Zn-O bond	173

Scheme 5.2: Equations to determine the order of the polymerization reaction using of D, L-Lactide as monomer.	175
Scheme 5.3: Tetrads from the possible stereosequences of lactide polymers ¹³	188
Scheme 6.1: Proposed mechanism for the oligomerization of ethylene	211
Scheme 6.2: Two-stage process for ethylene oligomerization and subsequent alkylation of toluene	212

List of Abbreviations

Å	Ångstrom
AMPS	2-acrylamido-2-methyl-propane sulfonic acid
ICP-AES	Inductively coupled plasma-atomic emission spectroscopy
atm	atmosphere
(BD)	1,3-butadiene
br	broad
calcd.	calculated
(ϵ -CL)	ϵ -caprolactone
°C	degrees Celsius
COD	cyclooctadiene
C	complex
δ	chemical shift
d	doublet
<i>Da</i>	daltons
dd	doublet of doublets
DEAC	diethylaluminumchloride
DAB-PPI	diaminobutane-poly(propyleneimine)
D-LA	D-lactide
D,L-LA	D, L-Lactide
DME	1,2-dimethoxyethane
DMF	dimethylformamide
DMAP	4-dimethylaminopyridine
DMSO	dimethylsulfoxide
DSC	differential scanning calorimetry

EAS	ethylaluminum sesquichloride
EDG	Electron donating groups
ESI-MS	electrospray ionization mass spectrometry
eV	electron volt
EWG	electron withdrawing groups
FAB-MS	fast atom bombardment mass spectrometry
FDA	food and drug administration
FT-IR	Fourier transform infrared spectroscopy
g	gram(s)
G1	first generation
G2	second generation
GC	gas chromatography
GC-MS	gas chromatography mass spectrometry
h	hour(s)
Hz	hertz
ⁱ Pr	isopropyl
<i>i</i>	isotactic
J	coupling constant
L-LA	L-lactide
L	Ligand
m	multiplet
MALDI-TOF MS	matrix assisted laser desorption-ionization time of flight mass spectrometry
m. p	melting point
m/z	mass to charge ratio

MMA	methyl methacrylate
MAO	methylaluminoxane
MMAO	modified methylaluminoxane
MHz	megahertz
min	minute(s)
mL	millilitres
mmol	millimoles
mol	moles
M_n	number average molecular weight
M_w	weight average molecular weight
NMR	nuclear magnetic resonance
n.d.	not determined
PDI	polydispersity index
PCL	polycaprolactone
PE	polyethylene
PEG	polyethylene glycol
PGL	polyglycolide
PLA	polylactide
ppm	parts per million
PMMA	polymethyl methacrylate
PNBE	polynorbonene
ROP	ring opening polymerization
s	singlet
SEM	scanning electron microscopy
<i>s</i>	syndiotactic

SXRD	single crystal X-ray diffraction
t	triplet
^t butyl	tertiary butyl
TGA	thermogravimetric analysis
T _g	glass transition temperature
TLC	thin layer chromatography
THF	tetrahydrofuran
T _m	melting temperature
TOF	turn over frequency
TON	turn over number

Acknowledgement

I would like to express my sincere gratitude to the following:

- ◆ Professor Selwyn Mapolie for his invaluable support and guidance throughout my studies.
- ◆ Dr. Archana Blaw-Luximon for her guidance and input into the project
- ◆ Dr. Marietjie Stander and her team for the mass analysis. Elsa Malherbe for the NMR analysis and the useful suggestions.
- ◆ The support staff at Stellenbosch University in particular Sylette May, Phillip Allen Ursula Wanza and Johnny Smut. Thank you for all the assistance.
- ◆ To the current and past members of the organometallic research group at Stellenbosch University; Andrew Swarts, Angelique Viret, Corli Joubert, Danie van Niekerk, Derik Wilbers, Nomvano Mketso, Wallace Manning and Yolanda Tancu, thank you for the encouragement, support and your input into this research project. Rehana Malga-Enus you are more than a colleague. You have been a valuable friend. We shall forever be united by dendrimers. Hennie Kotze, I'm grateful for you always making time to fix up everything especially the glove box. Dr. Bagihalli thank you for making time to run my GPC analysis. Dr. Onyancha, thank you for the encouragement and assistance throughout this process.
- ◆ The *c change Centre of Excellence in Catalysis, the Department of Science and Technology (DST) and the National Research Foundation (NRF) for financial assistance.
- ◆ To my friends Snehta Gordur, Charles Nderitu and especially Glyn Chirwa; you are my family here in Capetown. You always knew what to say and in other time what not to say when things were tight.

- ◆ My immediate and extended family, particularly my mum Alice Mugo and my late dad Joseph Mugo. My brothers, Moses Gituru and Gordon Mutugi, my sisters Agatha Nyaguthii and Beatrice Wairiuko. You always encouraged me even when times were tough. My nephew Joe Mugo you have brought so much joy into our lives. Prof G. C. Mwangi and Prof. O. Yoshiko thank for you the financial support and your encouragement. (Ngai aromũrathima inyuothe).

- ◆ And most of all to God for making all things possible, (gutiri Ngai ũngĩ tawe).

A dedication to my late dad Joseph Mugo Gordon (ũro hurũka ũhoro)

**Chapter 1 : Salicylaldimine and Pyrrole-imine
Schiff Base Complexes as Catalyst with an
Emphasis on Polymerization and
Oligomerization**

1.1: General

Development of coordination chemistry has been greatly influenced by Schiff base ligands because they form stable transition metal complexes.¹ Schiff bases stabilise many metals in various oxidation states. These coordination compounds have been investigated for various applications including catalysis^{2,3} and bioinorganic chemistry.⁴⁻⁶ They are typically formed via the condensation of a primary amine and an aldehyde (ketones will also form imines of type $R_1R_2C=N-R_3$, but the reaction tends to occur less readily than with aldehydes).⁷ The resultant functional group $R_1HC=N-R_2$ is called an imine and is capable of binding metal ions via the N atom, especially when used in combination with one or more other donor atoms to form a chelating ligand.⁸ Introduction of various substituent groups, R including aryls or alkyls, allows for the tailoring of ligands with varied steric and electronic properties. In addition chiral aldehydes or amines can also be used. This facilitates control of the performance of the metal complexes in a variety of useful catalytic transformations. The transferred chirality may allow for the production of non-racemic products through a catalytic process.⁹

There are various types of Schiff base ligands with pyrrolylaldimine and salicylaldimine being two such examples. These two classes of ligands, pyrrolylaldimine and salicylaldimine, are closely related. Salicylaldimine Schiff base ligands are formed from 2-hydroxybenzaldehydes while pyrrolylaldiminato ligands are synthesized using pyrrole-2-carboxaldehydes. General structures of salicylaldimine and pyrrolylaldiminato Schiff base compounds are shown in Figures 1.1 and 1.2 respectively.¹⁰ The main difference between these two ligand systems is that salicylaldimine is an N,O chelate forming a six-membered ring with the metal ion while the pyrrolylaldiminato is an N,N chelate that yields a five-membered ring on coordination. These metal complexes exhibit specific chemical transformations in both a stoichiometric and a catalytic manner.

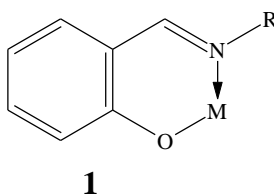
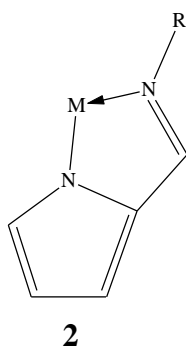


Figure 1.1: General structure of a salicylaldiminato complex



R = Aryl or alkyl

Figure 1.2: General structure of a pyrrolylaldiminato complex

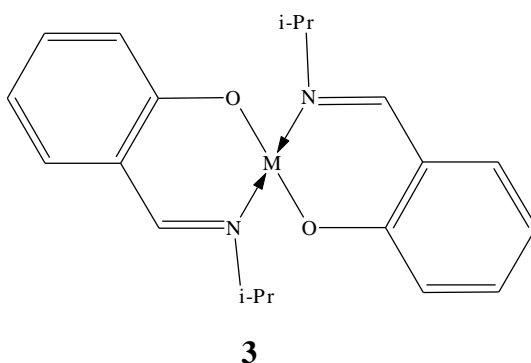
This chapter is a review of Schiff base transition metal complexes with a particular emphasis on the salicylaldimine and pyrrolylaldiminato system. Their applications in various catalytic processes especially olefin oligomerization or polymerization as well as the ring opening polymerization of cyclic esters. We also discuss dendrimer supported Schiff base metal complexes and their catalytic applications.

1.2: Salicylaldimine (N,O) ligands and their metal complexes

Salicylaldimines are an extensively studied class of chelating ligands in the coordination chemistry of main group and transition metals. Salicylaldiminato metal complexes can be obtained by the reaction of the salicylaldimine ligand with an appropriate metal salt. In some cases, a base is required to deprotonate the phenol-imine leading to the

formation of a bidentate mono-anionic N,O donor ligand. These complexes can either be *mono-* or *bis-* salicylaldiminato complexes depending on, the steric properties of the ligand, the nature of the metal salt used as well as the presence of other auxiliary ligands. Numerous salicylaldimine complexes have been reported, all in good yields.^{11-15, 16}

Torzilli *et al.*¹⁷ reported *bis*(N-isopropylsalicylaldimine) iron(II) and Zn(II) complexes, Figure 1.3. The Fe(II) complex, **3a**, also formed an oxo-bridged dinuclear Fe(III) complex on exposure to air.

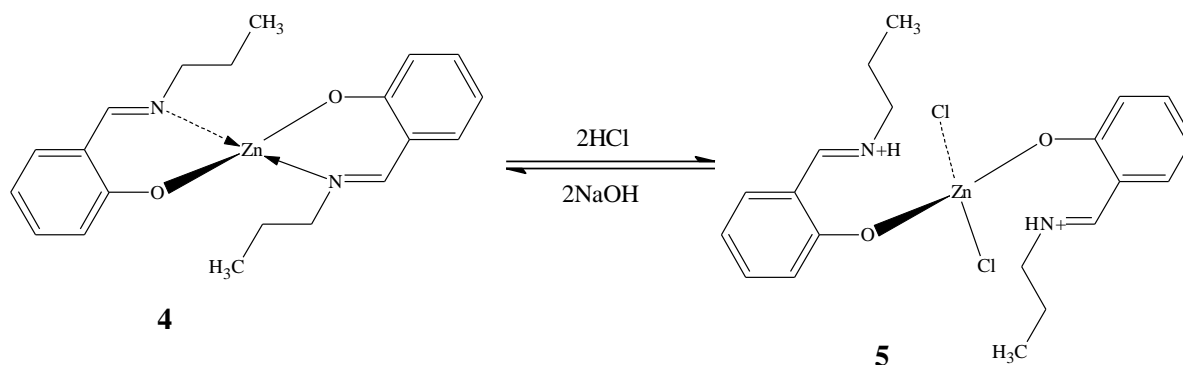


3a: M = Fe

3b: M = Zn

Figure 1.3: Bis(N-isopropylsalicylaldimine) metal complexes reported by Torzilli *et al.*¹⁷

Torzilli *et al.*¹⁸ also observed that Zn(II) *N*-propylsalicylaldiminato complex, Scheme 1.1, can be inter-conversion from *bis*(N-n-propylsalicylaldiminato) zinc(II) to dichloro-*bis*(N-n-propylsalicylaldiminato) zinc(II) by addition of either a base or acid. In the dichloro-*bis*(N-n-propylsalicylaldiminato) Zn(II) complex, the salicylaldimine ligands were deprotonated and bound to the zinc atom through the phenolic oxygen while the imino nitrogen was protonated and non-coordinating.



Scheme 1.1: Inter-conversion of Zn(II) (N-Propylsalicylaldiminato) to dichlorobis (N-Propylsalicylaldiminato) Zn(II) complex reported by Torzilli *et al.*¹⁸

Zhu *et al.*¹⁹ synthesised a mononuclear zinc(II) compound (**6**), Figure 1.4, derived from one zwitterionic form of the Schiff base (E)-2-[(3-dimethylaminopropylimino) methyl]-phenol and two iodide ligands, (compound **6**). The Zn(II) atom was four-coordinated with tetrahedral coordination geometry. In the solid state, intermolecular N—H····O hydrogen bonds give rise to the formation of chains running along the b axis.

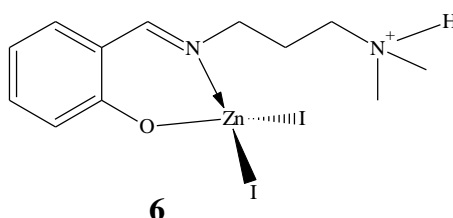
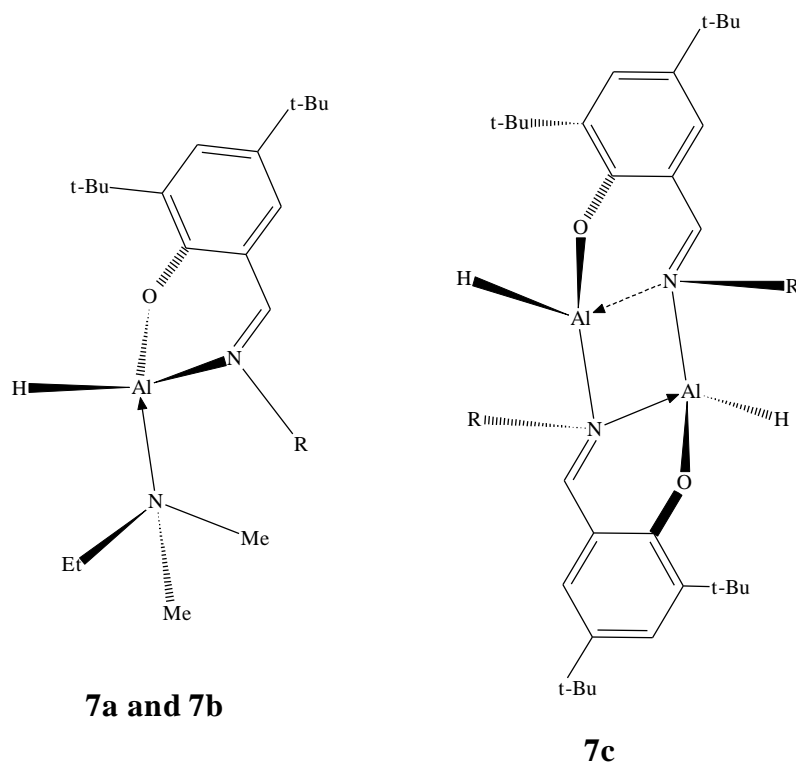


Figure 1.4: Mononuclear Zn(II) compound reported by Zhu *et al.*¹⁹

Mononuclear and binuclear aluminium hydride complexes were reported by Martínez and co-workers.²⁰ In these complexes, bulky substituents on the imino nitrogen determined the nature of the complex, Figure 1.5. An Al(III) dimer, **7c**, was obtained when the imino moiety was a *t*-butyl group. However, when the imino moiety was replaced with an aromatic group a mononuclear complexes, **7a** and **7b**, were obtained.

**7a:** R = 2, 6-Me₂C₆H₃**7b:** R = C₆F₅**7c:** R = ^tButyl**Figure 1.5:** Mono- and binuclear salicylaldiminato Al(III) complexes reported by Martínez *et al.*²⁰

Binuclear metal complexes can also be obtained when a tridentate ligand is used. Tas and co workers²⁰ reported Cu(II), Ni(II), V(IV) and Mn(II) metal complexes, **8a** – **8d**, with an N-(2-hydroxyphenyl)-3,5-^tbutylsalicylaldimine ligand, Figure 1.6.

Kasumov²¹ published a series of Ni(II) *bis*[N-(2,6-^tbutyl-1-hydroxyphenyl) salicylaldiminato] complexes bearing OH and MeO substituents on the salicylaldehyde moiety at various positions, Figure 1.7. In the solid state and in dioxane these complexes appeared to be tetrahedral in geometry while in non-donor solvents they were square planar. Another property observed was that in solution the OH-substituted complexes formed six-coordinate adducts with pyridine, DMF or DMSO, **9a**, **9c**, **9e**, **9g** and **9h**, unlike their MeO analogues.

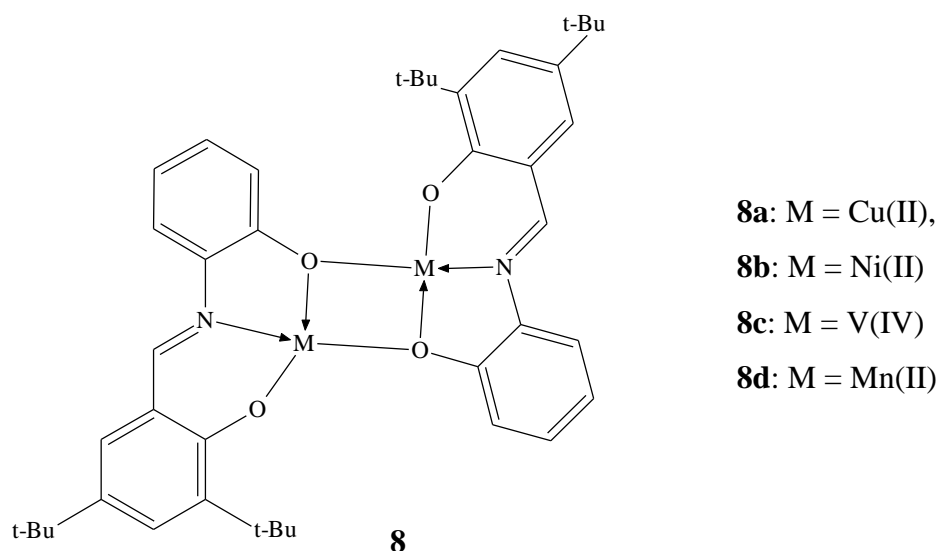


Figure 1.6: Binuclear salicylaldiminato complexes reported by Tas *et al.*²⁰

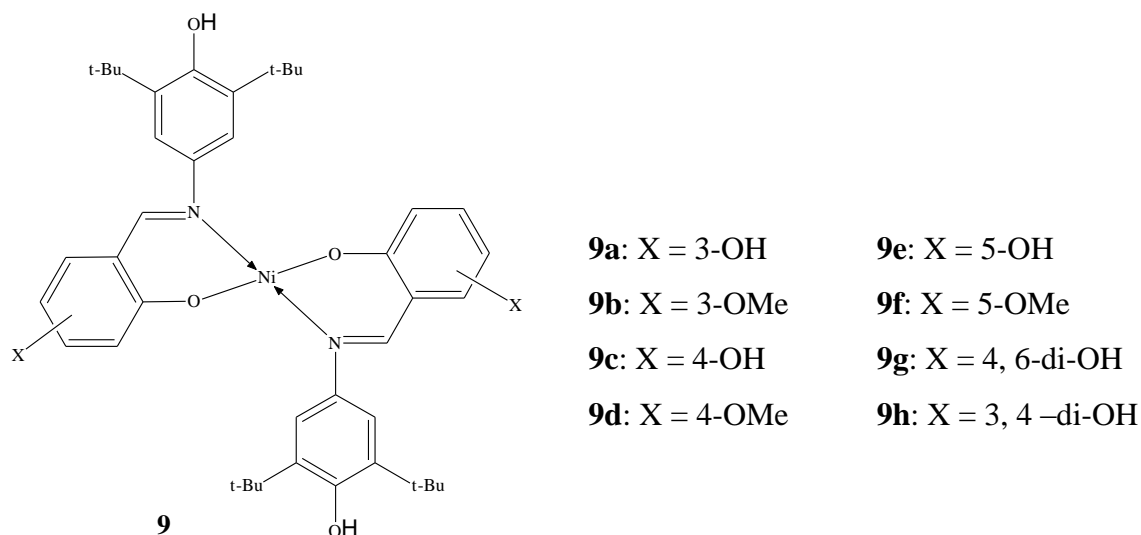


Figure 1.7: Mononuclear salicylaldiminato Ni(II) complexes reported by Kasumov²¹

Similar to the Ni(II) complexes above, Kasumov and Köksal²² also reported some Cu(II) analogues, **10a** and **10b**. These copper complexes have two (N-(2,6-*di*-phenyl-1-hydroxyphenyl) salicylaldimine ligands bearing either a hydrogen or bulky ^tbutyl substituent on the aniline ring, Figure 1.8.

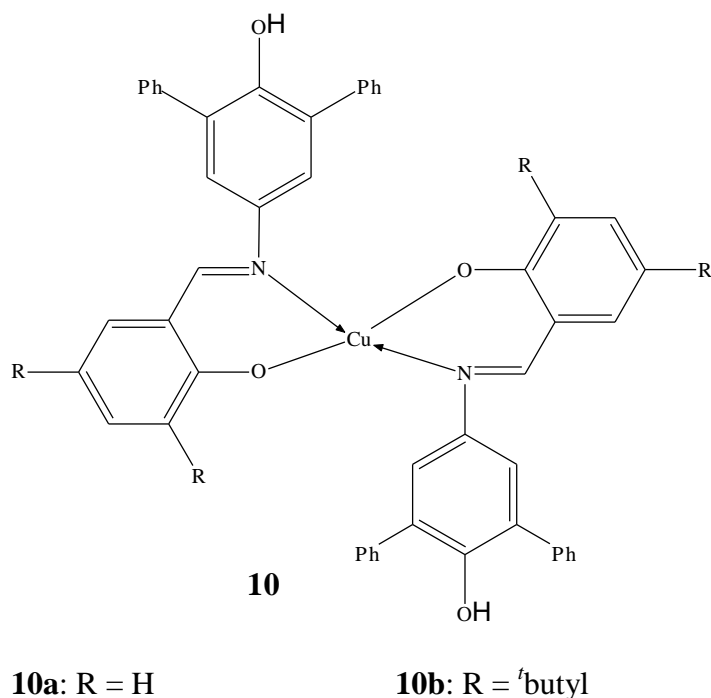


Figure 1.8: Mononuclear salicylaldiminato Cu(II) complexes reported by Kasumov and Köksal²³

Kettunen *et al.*²⁴ observed that the nature salicylketiminato Ni(II) complexes, Figure 1.9 was controlled by the substituent on the ketimine N as well as the reaction protocol. At an exact 1:2 mole ratio of *trans*-[(PPh₃)₂Ni((Ph)Cl)] to ligand, a mixture of *mono*- and *bis*-ligated salicylketiminato Ni(II) complexes were obtained. When a slight excess of sodium salt of the ligand was used in the reaction, the *bis*-ligated complexes are formed as the major product with only traces of **11a** and **11b**. Complex, **11e**, was readily formed due to the influence of the phenyl group on the ketimine carbon in the ligand. The phenyl group allows for faster dissociation of the second PPh₃ thus increasing the tendency to form a *bis*-ligated complex. These salicylketimine ligands were found to form *bis* Ni(II) complexes more readily than salicylaldimine ligands.

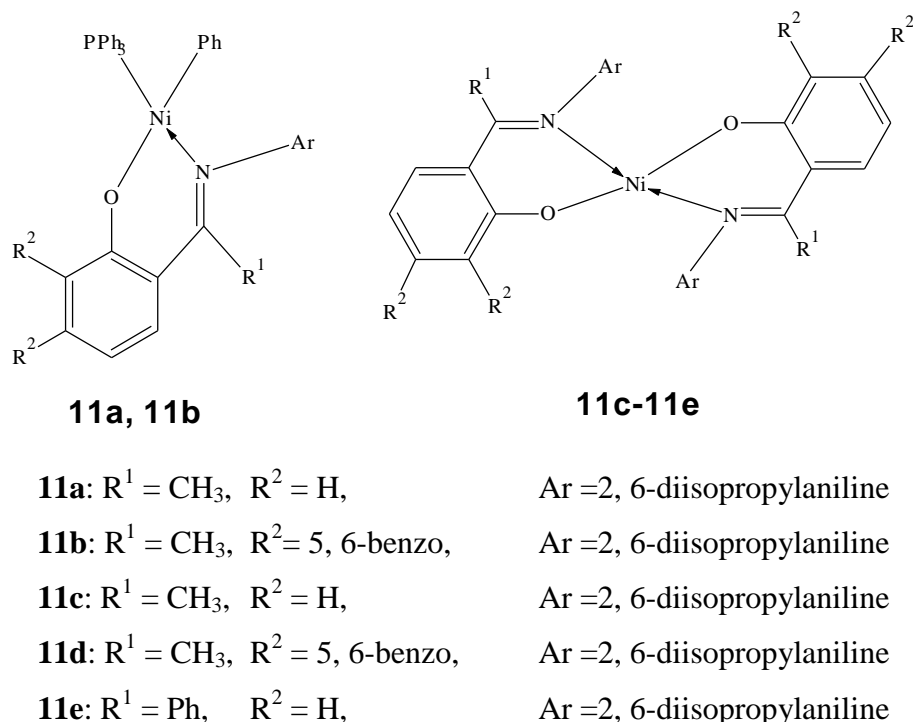


Figure 1.9: Mono- and bis-ligated salicylaldiminato Ni(II) complexes reported by Kettunen *et al.*²⁴

1.2.1: Catalytic applications of salicylaldiminato metal complexes

A wide range of salicylaldiminato complexes have been reported and evaluated for various catalytic processes such as ring opening polymerization processes of heterocyclic monomers and in olefins polymerization reactions.²⁵⁻³¹

Non-symmetric neutral salicylaldiminato Pd(II) complexes have been evaluated as norbornene polymerization catalysts, Figure 1.10. Catalyst activities and polymer yields were found to depend on reaction temperature, concentration of norbornene, and Al:Pd ratio. Activities of up to 8.52×10^6 g PNB (mol Pd)⁻¹ h⁻¹ for **12a** were obtained at the optimal reaction conditions of Al/Pd = 2000, norbornene/Pd = 5.2×10^4 , 30 °C after only 10 min of reaction time. The other two catalysts, **12b** and **12c**, gave lower activities of 5.64 and 3.21×10^6 g PNB (mol Pd)⁻¹ h⁻¹ respectively under similar condition as those used for **12a**. The reactivity of these Pd(II) systems was greatly influenced by the reaction temperature. At

temperatures either below or above 30 °C, polymer yield decreases by half for these three complexes. The decrease in activity was attributed to active species stability.³²

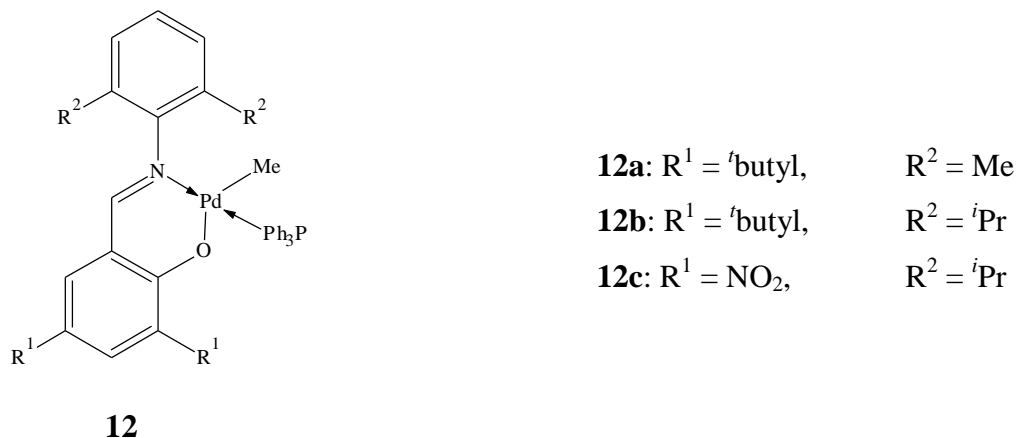
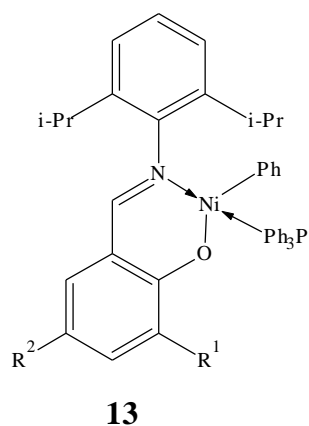


Figure 1.10: Mono-ligated salicylaldimine Pd(II) complexes reported by Li *et al.*³²

The neutral Ni(II) salicylaldimine complexes, Figure 1.11, have also been found to be active catalysts for the polymerization of ethylene under mild conditions in the presence of a phosphine scavenger such as Ni(COD)₂ or B(C₆F₅)₃. The most active catalyst was **13g** with a TOF of 2.53×10^5 g PE (mol Ni)⁻¹ h⁻¹, however under similar conditions **13a** gave a TOF of 2.67×10^4 g PE (mol Ni)⁻¹ h⁻¹. Increasing the bulkiness of R¹ resulted in increased polymerization activity. Activity followed the order of **13e** > **13d** > **13c** > **13b** > **13a**.

The electronic effects were investigated by attaching a substituent in the *para*-position relative to the phenoxyl group in the salicylaldimine ligand. Electron donating groups such as -OMe, **13f**, reduced the catalytic activity while electron withdrawing groups, **13g**, were found to greatly enhance the activity. These authors also reported a direct correlation between the TOF and the PDI. **13g** gave polymers with very high molecular weight distribution polymers with PDI values of 12.2.

An induction period was observed in compounds **13a**, **13f** and **13g** ranged from 5 to 20 min, typical of the SHOP system due to the slow insertion of ethylene into the Ni-Ph bond. Interestingly no induction period was observed for complexes **13b - 13e**.³³⁻³⁵

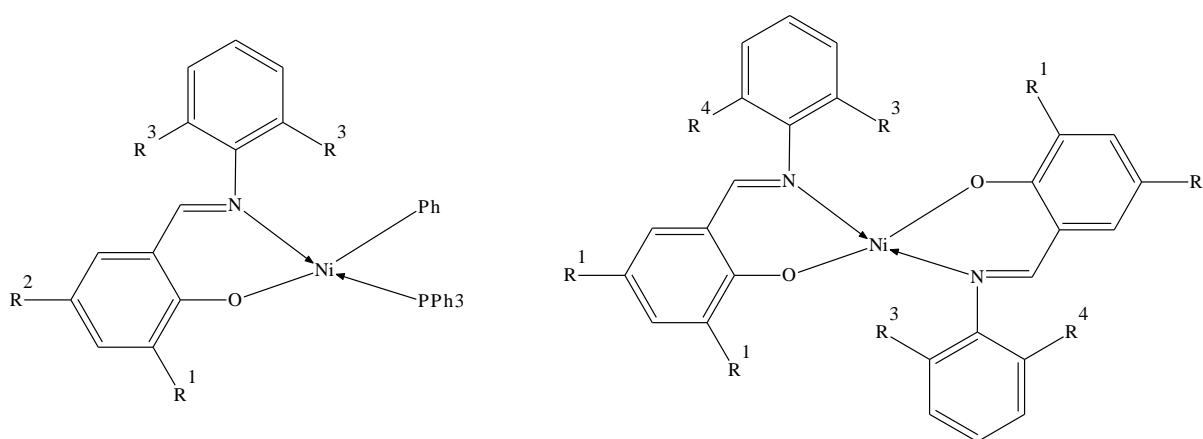


- 13a:** $R^1 = H,$ $R^2 = H$
13b: $R^1 = t\text{butyl}$ $R^2 = H$
13c: $R^1 = Ph,$ $R^2 = H$
13d: $R^1 = 9\text{-phenanthrenyl},$ $R^2 = H$
13e: $R^1 = 9\text{-anthracenyl},$ $R^2 = H$
13f: $R^1 = H,$ $R^2 = OMe$
13g: $R^1 = H,$ $R^2 = NO_2$

Figure 1.11: Neutral Ni(II) salicylaldimine complexes

Recently Lu *et al.*³⁶ reported *mono*- and *bis*(salicylaldiminato) Ni(II) complexes, Figure 1.12, that were active catalyst for the polymerization of MMA in the presences of MAO as co-catalyst. Both the *mono*- and *bis*(salicylaldiminato) Ni(II) complexes exhibited high activities. Compound **14e** was used for screening and optimization of the reactions conditions and the best parameters were selected based on the activity and the M_n of the polymer obtained. The optimal conditions were selected as Al/Ni ratio of 150 at 60 °C in toluene as solvent. However the highest activity was obtained as 2.9×10^4 g PMMA (mol Ni)⁻¹ h⁻¹ at an Al/Ni = 300 and the highest M_n of 1.26×10^6 at a lower Al/Ni = 100. Under the optimal conditions, reaction temperature variation showed that 40 °C produced the highest activity of 3.27×10^4 g PMMA (mol Ni)⁻¹ h⁻¹ and a M_n of 1.13×10^6 . At lower temperature of 20 °C a lower activity was obtained but with a slightly higher M_n . Longer reaction times beyond 0.5 hour only improved on the M_n but reduced the activity by almost

half. At 0.5 h an activity of 1.14×10^5 g PMMA (mol Ni) $^{-1}$ h $^{-1}$ was obtained, however after 1 h the activity had declined to 6.52×10^4 g PMMA (mol Ni) $^{-1}$ h $^{-1}$. This was attributed to catalyst stability and lifetime. The polymer molecular weight nevertheless increased to 9.13×10^5 from 7.6×10^5 . Solvent also played a vital role. CH₂Cl₂ was the best solvent in terms of both the activity and M_n . THF showed no activity. This was attributed to its stronger coordination to the metal as compared to the MMA.



14a: R¹ = R² = H, R³ = *i*Pr

14b: R¹ = R² = Br, R³ = *i*Pr

14c: R¹ = *t*butyl, R² = H, R³ = *i*Pr

14d: R¹ = R² = Br, R³ = R⁴ = *i*Pr

14e: R¹ = R² = Br, R³ = *o*-PhO, R⁴ = H

Figure 1.12: *Mono-* and *bis-*(salicylaldiminato) Ni(II) complexes reported by Lu *et al.*³⁶

At the optimal conditions of Al:Ni = 150, reaction temperature of 40 °C and 23.4 mmol MMA in CH₂Cl₂, all the other complexes were evaluated. The substituents on the phenoxy moiety of the salicylaldimine greatly influenced the rate of polymerization with the presence of bulky substituents resulted in lower activity. Compound **14a** which has the least steric interference of the three salicylaldiminato catalysts, **14a** - **14c**, showed the highest activity of 1.15×10^5 g PMMA (mol Ni) $^{-1}$ h $^{-1}$ as well as the highest M_n of 5.35×10^5 . A direct comparison of the *mono-* and *bis-*(salicylaldiminato) Ni(II) complexes showed that **14b** was

more active than **14d** with activities of 4.04 and 2.04×10^4 g PMMA (mol Ni)⁻¹ h⁻¹ respectively. They attributed this trend to the easier accessibility of the active metal site in **14b** as compared to **14d**. The highest activity as well as M_n was obtained with **14e**. In this complex the substituents in the N-aryl moiety produce less steric hindrance as compared to the iso-propyl in **14d** thus favouring the MMA insertion. The polymers produced by the catalyst systems showed very little differences in the microstructure.

Aluminium complexes as shown in Figure 1.13 were evaluated as catalysts in combination with 1 equiv. of B(C₆F₅)₃ as co-catalyst for ethylene polymerization. Only complexes **15a** and **15b** were active catalysts with **15b** being more active than **15a**. Under optimal conditions, an activity of 50 and 110 g PE (mol Al)⁻¹ h⁻¹ bar⁻¹ was obtained for **15a** and **15b** respectively.

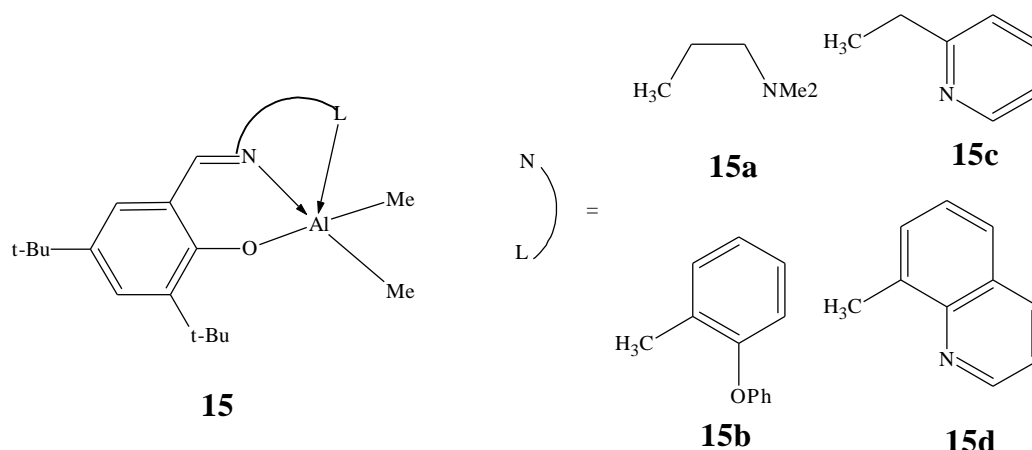


Figure 1.13: Mononuclear salicylaldiminato Al(III) complexes reported by Cameron *et al.*³⁷

An average molecular weight (M_w) of 1.72×10^5 and M_n of 2.4×10^3 was obtained for **15a** whilst **15b** gave M_w of 2.18×10^5 and M_n of 5.2×10^3 . The labile pendant donor arm in **15a** and **15b** is an important feature in the polymerization mechanism. The labile donor arm provides a pathway for ethylene to approach the aluminium centre. In contrast the N-heterocyclic based complexes, **15c** and **15d**, probably form cations with stronger donor to

metal bonds thereby reducing the propensity for dissociation of the coordinating arm to generate an active centre.

A series of Co(II) salicylaldiminato complexes, Figure 1.14, were reported by Chandran *et al.*³⁸ They were observed to be active catalysts for the polymerization of 1,3-butadiene (BD) in the presence of ethylaluminum sesquichloride (EAS). Moderate conversion ranging from 47 % to 57 % in 10 min with the order of conversion being **16a** > **16b** > **16c** > **16d** > **16e** > **16f** were reported.

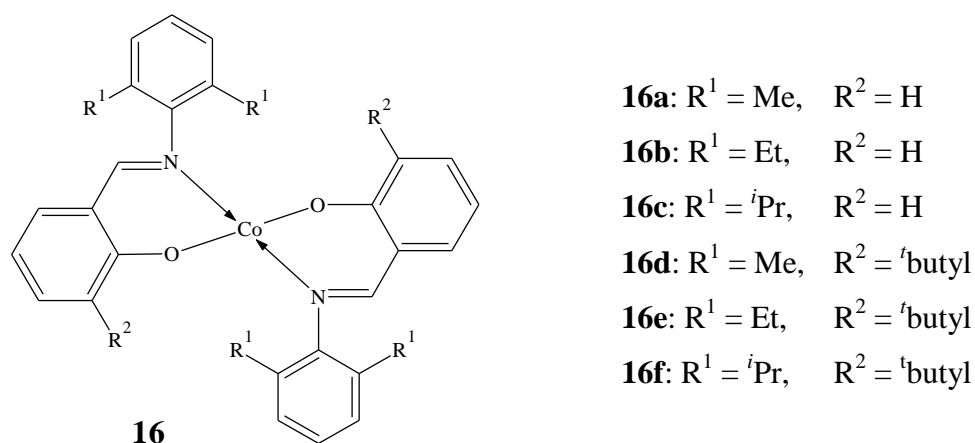
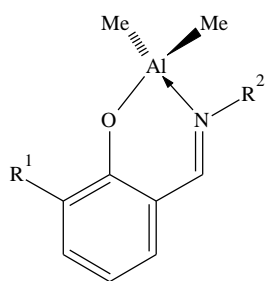


Figure 1.14: Co(II) salicylaldiminato complexes reported by Chandran *et al.*³⁸

The monomer concentration as well as temperature was observed to play a role in the rate of polymerization. Compound **16a** showed an increase in conversion from 29 to 57 % when the concentration of the BD was varied from 0.2 to 0.7 M at 30°C. Negligible activities were obtained at temperatures lower than 20 °C for **16a** and **16d**. At temperature above 30 °C, only a slight increase in conversion was recorded. Moderate molecular weights (M_w) of between 2.26 and 3.82×10^4 were obtained with PDI values ranging from 1.29 to 2.36. These catalysts were also highly selective for *cis*-1, 4-polybutadienes (94 %) with negligible amounts of 1, 4-*trans* (2.32 %) and 1, 2-addition products (3.37 %) in the reactions carried out at 30 °C

Phenoxy-imine Al(III) complexes, Figure 1.15, were synthesised and evaluated as catalyst precursors for ring opening polymerization (ROP) of ϵ -caprolactone (ϵ -CL) in the presence of *n*-BuOH (1.0 equiv. to Al) by Lui and co-workers.³⁹ These researchers observed that the catalytic activity of the complexes was highly influenced by the electronic and steric properties of the substituent on the imino nitrogen. At 60 °C the catalytic activity order was: **17i** > **17h** > **17a** > **17g** > **17e** > **17d** > **17f**. It was observed that the M_n of the polymer could be controlled by varying the CL:Al molar ratios.



17a- 17i

17a: $R^1 = \text{Me}$,	$R^2 = 2,6\text{-}^i\text{PrC}_6\text{H}_3$
17b: $R^1 = \text{Me}$,	$R^2 = \textit{t}\text{butyl}$
17c: $R^1 = \textit{t}\text{butyl}$,	$R^2 = 2,6\text{-}^i\text{PrC}_6\text{H}_3$
17d: $R^1 = \textit{t}\text{butyl}$,	$R^2 = \textit{t}\text{butyl}$
17e: $R^1 = \textit{t}\text{butyl}$,	$R^2 = \text{cyclohexyl}$
17f: $R^1 = \textit{t}\text{butyl}$,	$R^2 = \text{adamantyl}$
17g: $R^1 = \textit{t}\text{butyl}$,	$R^2 = \text{Ph}$
17h: $R^1 = \textit{t}\text{butyl}$,	$R^2 = 2,6\text{-Me}_2\text{C}_6\text{H}_3$
17i: $R^1 = \textit{t}\text{butyl}$,	$R^2 = \text{C}_6\text{F}_5$

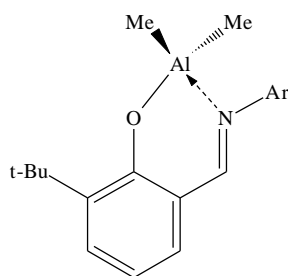
Figure 1.15: Dimethyl phenoxy-imine Al(III) complexes reported by Lui *et al.*³⁹

A linear relationship between the M_n and the turn over number (TON) values was reported. Complex **17i** was observed to be the best catalyst. Under diluted conditions a TON of 370 was obtained after 20 min and giving polycaprolactone with a low PDI of 1.19. Complex **17d** was significantly less active achieving 86 % monomer conversion after 48 h with TON of 215 and a slightly higher PDI of 1.72 for the polymer obtained. This suggests that trans-esterification may have taken place.

Pappalardo *et al.*⁴⁰ published another type of dimethylaluminum(III) compounds, Figure 1.16, and evaluated these as initiators in the ring opening polymerization (ROP) of ϵ -

caprolactone (ϵ -CL), L-lactide (L-LA) and D, L-Lactide (D,L-LA). These compounds were observed to be efficient initiators in both homo- and co- of these cyclic esters in the presence of MeOH at 70 °C. The catalytic activity followed the order: **18a**>**18b**>**18c**. These compounds showed poor activity at room temperature. At higher temperature, moderate to high conversions were obtained. Compound **18a** polymerized all the ϵ -CL in 2 h at a reaction temperature of 70 °C and a ϵ -CL:Al molar ratio of 360:1. A linear correlation between the polymer molecular weight and the conversion was observed. The PDI also remained narrow until nearly complete consumption of the monomer and broadens over longer reaction times with trans-esterification reactions becoming significant. A cationic analogue of **18c** generated *in-situ* by the abstraction of the methyl group in the presence of $B(C_6F_5)_3$ gave low conversion of 13 % even after 7 h at 70 °C with the polymer having a PDI of 1.66.

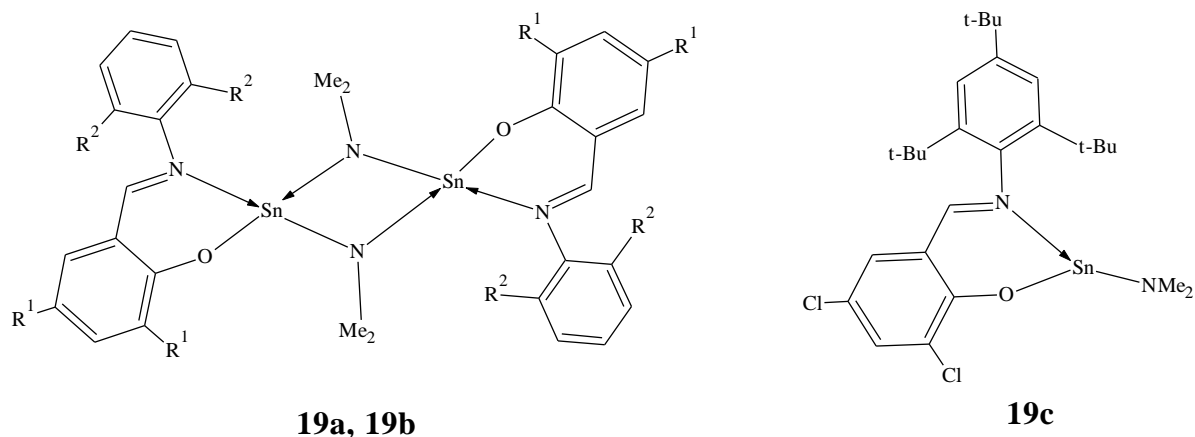
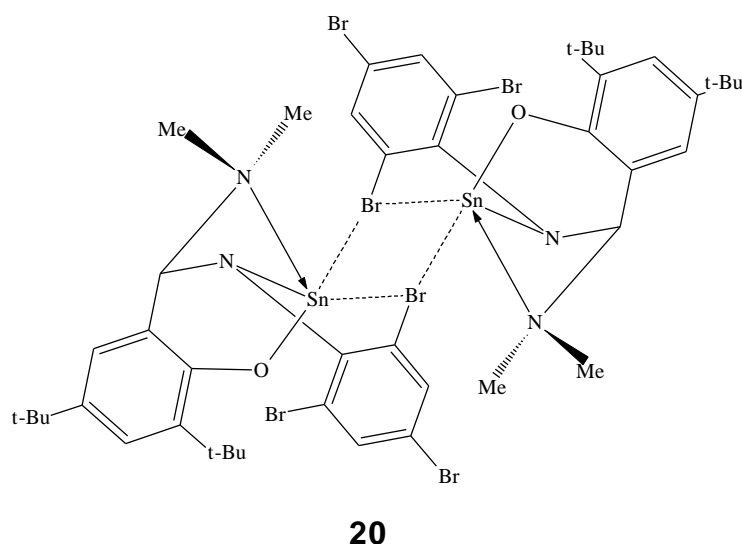
In lactide polymerization, these complexes behaved as single-site initiators giving rise to controlled polymerization with narrow molecular weight distributions. The three catalysts (Fig. 1.16) needed up to 96 h to achieve conversions >90 % for L-LA at a L-LA:Al molar ratio of 96:1 at 70 °C. Under the same conditions, the of D, L-Lactide progressed at similar rate except for **18a** which required up to 120 h for 85 % of the D, L-Lactide to be polymerized. Again low PDI's for the polylactides ranging from 1.0 to 1.3 were obtained.

**18****18a:** Ar = C₆H₅**18b:** Ar = 2,6-ⁱPrC₆H₃**18c:** Ar = C₆F₅**Figure 1.16:** Dimethylaluminum(III) complexes reported by Pappalardo *et al.*⁴⁰

Complex **18c** was also investigated for the random copolymerization of ϵ -CL/L-LA and ϵ -CL/D,L-LA. The copolymers were prepared by mixing in appropriate proportion of the two monomers in toluene, at 70 °C with 1 equiv of MeOH and a reaction time of 96 h. When ϵ -CL was added in equal molar proportion to any of the other two monomers, the percentage of the CL in the copolymer was less in comparison to the other monomer. This is in contrast to the homo-polymerization of CL and LA since CL polymerizes much faster than LA. In all cases, the obtained copolymers had random sequences, with percentage of heterodiads being higher than 50%. They attributed this phenomenon to the random ϵ -CL/LA co.

Nimitsiriwat *et al.*⁴¹ showed that the reaction of salicylaldehyde (*ortho*-iminophenol) with $\text{Sn}(\text{NMe}_2)_2$ yielded either *mono*- and *bi*-nuclear complexes, (**19a-19c**), Fig. 1.17. The nature of the product was determined by the steric and electronic characteristics of the N-substituent. Bulky substituent groups such as ^tbutyl on the N-aryl moiety gave a mixture of *mono*- and *bis*- ligated complexes.

However when bromine was introduced, the imino carbon is activated towards nucleophilic attack forming a tridentate dianionic aminoamidophenoxide ligand (**20**), Figure 1.18. Such carbon activation has not been reported before when the halo substituents are located on the phenolic ring only.

**19a:** $R^1 = \text{Cl}$; $R^2 = i\text{Pr}$ **19b:** $R^1 = \text{I}$; $R^2 = i\text{Pr}$ **Figure 1.17:** Mono chelate Sn(II) salicylaldiminato complexes reported by Nimitsiriwat *et al.*⁴¹**Figure 1.18:** Tridentate N, N, O Sn(II) dimeric complex reported by Nimitsiriwat *et al.*⁴¹

These complexes initiated ring-opening polymerization of D, L-lactide. Complexes **19a**, **19b** and **20** showed similar activities, but propagation with **19c** was at a slower rate. Compound **19a** was the most active with 92 % of the D, L-Lactide converted after 1 h in toluene at 60 °C and at $[\text{LA}]:[\text{Sn}] = 100$. However the polylactides had a high PDI value of 1.4 which was attributed to trans-esterification. Compounds **19b** and **20** had well-controlled chain growth processes, with linear relationships between M_n and monomer conversion.

Conversion of 92 % was obtained for **19b** and 93 % for **20** in 100 min. Compound **19c** showed an induction period of almost 5 h with 94 % conversion after 24 h.

Nimitsiriwat and co-workers⁴² also synthesised another type of Sn(II) complexes (**21a** - **21c**), Figure 1.19 that polymerized D, L-lactide. These complexes initiated polymerization at 60 °C, in toluene at LA/Sn = 100 affording polymers with well-controlled molecular weights. High conversions of 91 %, 95 % and 94% were obtained after 1 h for **21a**, **21b** and **21c** respectively. A linear relationship was also observed between the D, L-lactide:Sn ratio and M_n of the polymer obtained. These three complexes gave similar reaction rates (k_{app}) suggesting that the heteroatom had little effect on the polymerization reactions.

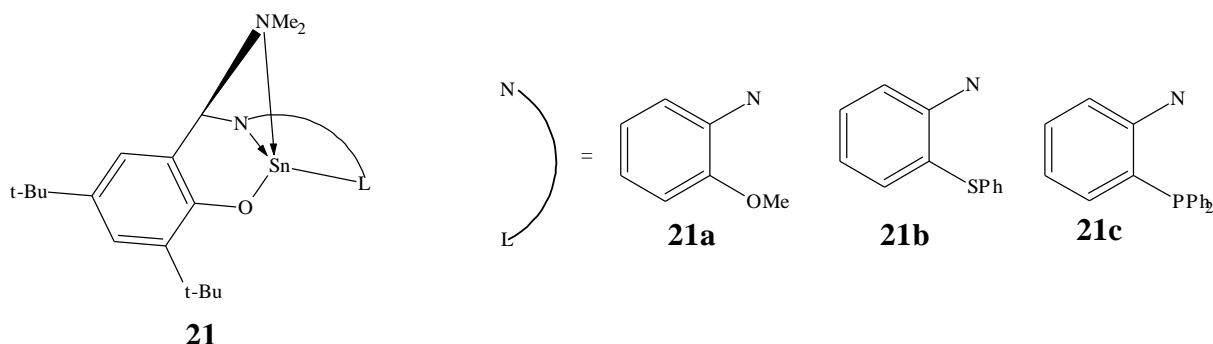
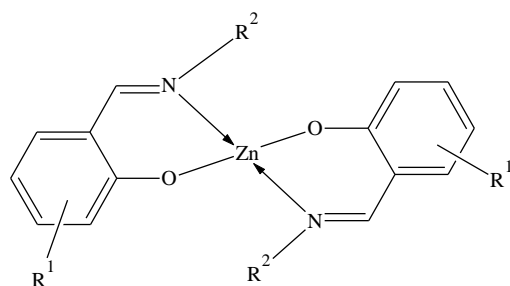


Figure 1.19: Bis chelate Sn(II) salicylaldiminato complexes reported by Nimitsiriwat and co-workers⁴²

Darensbourg *et al.*⁴³ reported a series of Zn(II) complexes based on salicylaldimine ligands, Figure 1.20. These Zn(II) complexes showed varying activities as catalyst precursors for the co-polymerization of CO₂ and cyclohexene oxide with activity of up to 16 g PC (mol Zn)⁻¹ h⁻¹ being obtained for **22a** at 80 °C and 55 bar. The polycarbonates obtained were of high molecular weight. The catalytic efficiency decreased in the order **22a** > **22e** > **22b** > **22d** with TOF values of 15 > 7.3 > 5.0 > 1.2 g PC (mol Zn)⁻¹ h⁻¹ respectively. Complex **22c** only gave traces of polymer. The difference in activity can be attributed to the

different steric and electronic effects provided by the substituents R^1 and R^2 on the various steps of the co-polymerization process. In **22a** and **22e** the methyl group displays an electron donating property as opposed to a steric one thus enabling CO_2 insertion.



22a: $R^1 = 3\text{-Me}$; $R^2 = 2, 6\text{-}^i\text{Pr}_2\text{C}_6\text{H}_3$

22b: $R^1 = 3, 5\text{-}^t\text{butyl}$; $R^2 = 2, 6\text{-}^i\text{Pr}_2\text{C}_6\text{H}_3$

22c: $R^1 = 3, 5\text{-Cl}$; $R^2 = 2, 6\text{-}^i\text{Pr}_2\text{C}_6\text{H}_3$

22d: $R^1 = 5\text{-OMe}$; $R^2 = 2, 6\text{-}^i\text{Pr}_2\text{C}_6\text{H}_3$

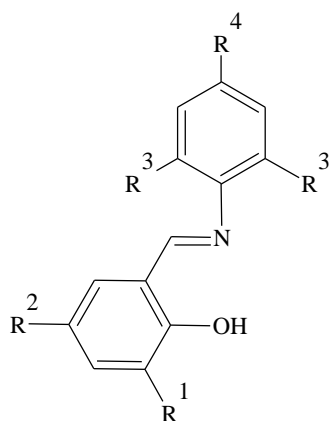
22e: $R^1 = 3\text{-Me}$; $R^2 = 3, 5\text{-}(\text{CF}_3)_2\text{C}_6\text{H}_3$

22a - 22e

Figure 1.20: Bis chelate Zn(II) salicylaldiminato complexes reported by Darenbourg *et al.*⁴³

Mononuclear and trinuclear Zn(II) metal complexes of ligands shown in Figure 1.21 were prepared by Jones *et al.*⁴⁴. The trimetallic complexes were obtained with ligands **23a** and **23b** only. These complexes comprised two ligands, three zinc atoms and four acetate groups. Mononuclear complexes were obtained for **23c** to **23g** even after the stoichiometric ratio of $Zn(OAc)_2 \cdot 2H_2O$: ligand was changed from 1:1 to 1:2. The presence substituents in either of the phenyl ring highly influenced the nature of the product.

These Zn(II) complexes polymerized D, L-lactide in melt conditions at 130 °C and a lactide:Zn:ratio of 300:1. They showed reasonable conversions over a period of time ranging from 30 minutes to two hours. The mononuclear complex **23f** was the best catalyst with 80 % conversion after 30 min. The least active complexes were those of **23d** and **23e** giving 10 and 20 % conversion respectively even after 2 hours. However, the trinuclear complexes gave polymers with high PDI values as compared to the mononuclear ones.



23a and 23g

23a: $R^1 = R^2 = R^3 = R^4 = H$

23b: $R^1 = R^2 = R^4 = H; R^3 = iPr$

23c: $R^1 = R^2 = H; R^3 = R^4 = Me$

23d: $R^1 = R^2 = Cl; R^3 = R^4 = H$

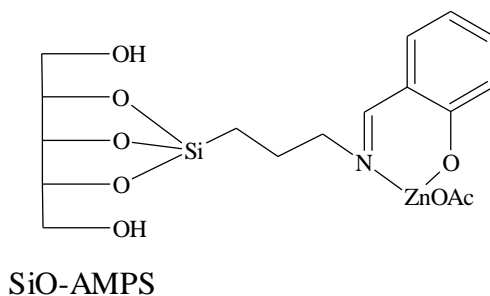
23e: $R^1 = R^2 = Cl; R^3 = R^4 = Me$

23f: $R^1 = R^2 = Cl; R^3 = iPr; R^4 = H$

23g: $R^1 = Me; R^2 = R^3 = R^4 = H$

Figure 1.21: Salicylaldimine ligands used in the synthesis of mono and tri-nuclear Zn(II) complexes reported by Jones *et al.*⁴⁴

A heterogeneous salicylaldiminato Zn(II) system (**24**), Figure 1.22, was shown to initiate the polymerization of lactide but with less efficiency compared to the homogeneous systems evaluated. After 24 h, the heterogeneous initiator showed 40 % conversion.



24

Figure 1.22: Salicylaldiminato Zn(II) complex immobilised on silica (SiO-AMPS) reported by Jones *et al.*⁴⁴

In the case of the Zn(II) complex for **23a**, higher M_n polymers were obtained over time as the % conversion increased. The M_n of the polymer obtained after 30 min was 2.16×10^4

as compared to 5.14×10^4 after 2 h. The PDI values of the polymers ranged from 1.34 to 1.85. Complex with the least steric hindrance gave polymers with the highest PDI values. The heterogeneous catalyst system gave polymers with the lowest values of 1.34.

1.3: Pyrrolyaldimine (N,N) ligands and their metal complexes

Metal complexes containing the pyrrolyl moiety (pyrrolyaldimine) have received much less attention as compared to salicylaldimino analogues. Reports have shown that they are excellent ligands for both transition and main group metals. These complexes have predominantly shown the type **I** bonding mode as shown in Figure 1.23^{10, 45, 46}. However, a few exceptions have been reported. Lewiński *et al.*⁴⁷ reported a pyrrolyaldimine bifunctional ligand that exhibited novel and diversity of bonding modes of type **II** and **III**, Figure 1.23 for Mg and Zn in the solid state. The magnesium complex was a centrosymmetric dimer with $(\mu\text{-N})_2$ bridges, type **II**. The zinc dimers were formed by intermolecular bonding of the unsaturated metal centres and the one of the carbon atoms of the pyrrole ring from the adjacent monomeric molecule reflecting the formation of the $\text{Zn}\dots\pi$ bonded dimer, type **III**.

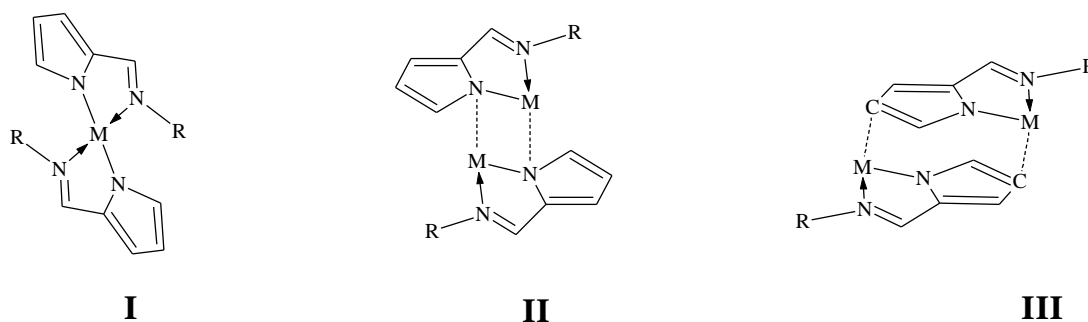


Figure 1.23: Bonding mode for pyrrolyaldimine metal complexes

Drouin *et al.*⁴⁵ published a pyrrole-imine Ru (II) complex of type **I** with other ancillary ligands attached to the metal center Ru (II) as shown in Figure 1.24.^{45, 48}

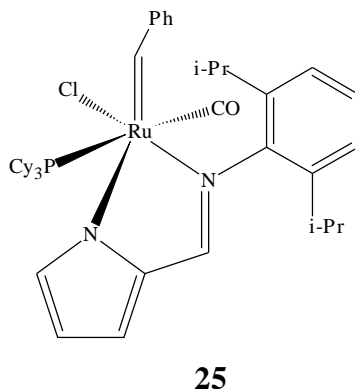
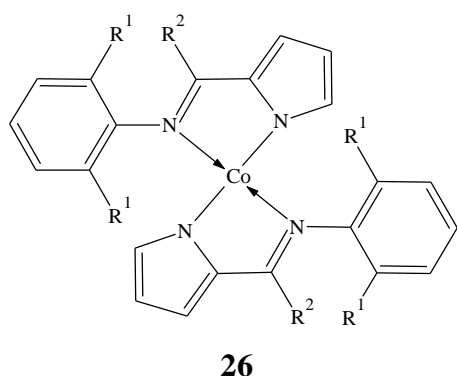


Figure 1.24: Example of a Ru (II) pyrrole-imine complex

A series of 2-iminopyrrole cobalt complexes were reported by Carabineiro and co-workers, Figure 1.25.^{46, 49} Complexes **26a** - **26e** displayed tetrahedral geometry which is the preferred geometry for four coordinate Co(II) compounds while **26f** revealed a square planar geometry. In the case of **26f**, the square planar geometry is slightly more stable than the tetrahedral geometry probably due to a combination of steric and electronic effects from the substituent groups R^1 and R^2 .



26a: $R^1 = R^2 = H$

26b: $R^1 = H; R^2 = Me$

26c: $R^1 = Me; R^2 = H$

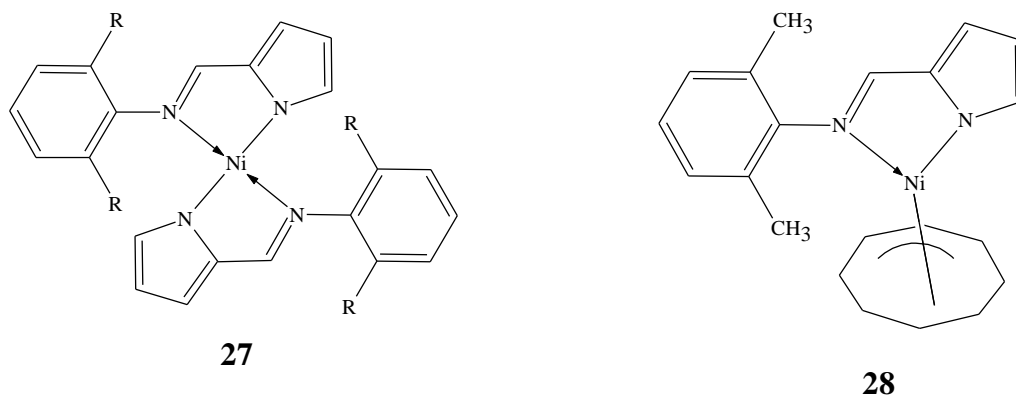
26d: $R^1 = R^2 = Me$

26e: $R^1 = iPr; R^2 = H$

26f: $R^1 = iPr; R^2 = Me$

Figure 1.25: Co(II) pyrrole-imine complexes reported by Carabineiro and co-workers^{46, 49}

Bis-pyrrolylaldiminato nickel (II) complexes, **27a** and **27b**, were isolated after the treatment of the sodium salt of the ligand with $\text{NiBr}_2(\text{DME})$ (DME = 1,2-dimethoxyethane), Figure 1.26, Pérez-Puente *et al*⁵⁰.



27a: R = Me

27b: R = *i*Pr

Figure 1.26: Mono- and bis-pyrrolylaldiminato nickel (II) complexes reported by Pérez-Puente *et al*.⁵⁰

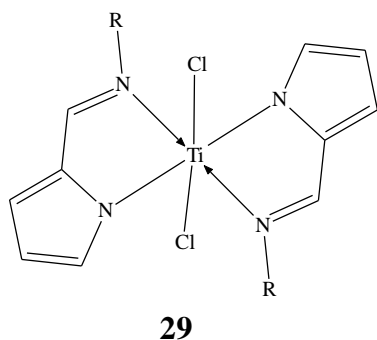
However, the use of a different nickel source, $\text{Ni}(\text{COD})_2$ (COD = 1,5-cyclooctadiene), resulted in compound **28** which is a mono- (iminomethylpyrrolide) Ni(II) complex where the coordinated COD undergoes isomerisation resulting in a cyclooctenyl ligand to give an η^3 -allyl-type organonickel complex.

1.3.1: Catalytic applications of pyrrolylaldiminato metal complexes

The main application for the published pyrrolylaldiminato metal complexes is in polymerization and oligomerization of α -olefins exhibiting moderate to high activities.⁵¹⁻⁵⁴ Ti(IV) *bis*(pyrrolylaldiminato) complexes have been reported as good catalysts for *homo*- as well as co-polymerization as of 1-alkenes as well as cyclic alkenes. Zr and Hf *bis*(pyrrolide-imine) complexes have also proved to be highly active catalysts for the polymerization of

ethylene.⁵⁵⁻⁵⁸ Other reported applications are cyclohexene oxidation as well as phenol hydroxylation.^{59, 60}

Yoshida *et al.*⁵² prepared a Ti(IV) complex having two bidentate pyrrolide-imine chelating ligands, Figure 1.27. These complexes were evaluated in the polymerization of ethylene with MAO as co-catalyst. They displayed very high activities and produced high molecular weight polyethylene. Activities of 1.4×10^7 g PE (mol Ti)⁻¹ h⁻¹ were obtained and these are comparable to what was obtained using Cp₂TiCl₂. The polyethylene had a M_w of up to 2.6×10^6 . Alternatively, using [Ph₃C]B(C₆F₅)₄/*i*-Bu₃Al as a co-catalyst yielded ultrahigh molecular weight polyethylene ($M_w > 4.0 \times 10^6$) and slightly lower activities of $1.5 - 2.0 \times 10^6$ g PE (mol Ti)⁻¹ h⁻¹. A PDI of the polyethylene was 2.21 typical of single-site titanium catalysts. Complexes **29b** and **29c** exhibited lower activities of 4.0×10^2 and 8.0×10^5 g PE (mol Ti)⁻¹ h⁻¹ with relatively high M_w values of 4.12×10^5 and 4.41×10^5 respectively. Complex **29d** showed very high activity of 1.4×10^7 kg PE (mol Ti)⁻¹ h⁻¹ with a very high M_w value of 2.6×10^6 . These are the highest activities reported for homogeneous titanium complexes which do not contain cyclopentadiene (Cp) ligands. It was observed that an increase in the bulkiness of the imino N substituent, (R) resulted in enhanced activity. This activity enhancement was attributed to the effective separation between the cationic active species and the anionic co-catalyst as a result of the attachment of bulkier alkyl substituents to the imino nitrogen.



- 29a:** R = Ph
29b: R = Et
29c: R = *n*-hexyl
29d: R = cyclohexyl

Figure 1.27: Ti(IV) complex with pyrrolide-imine ligands reported by Yoshida *et al.*⁵²

Dibenzyl hafnium (IV) complexes with pyrrolide-imine ligands, Figure 1.28, were synthesised by Matsui *et al.*⁵⁴ Complex **30c** showed activity of up to 2.2×10^6 g PE $(\text{mol Hf})^{-1} \text{h}^{-1} \text{bar}^{-1}$ with a M_w value of 8.8×10^4 in the presence of triisobutylaluminium ($i\text{-Bu}_3\text{Al}$) in ethylene polymerization.

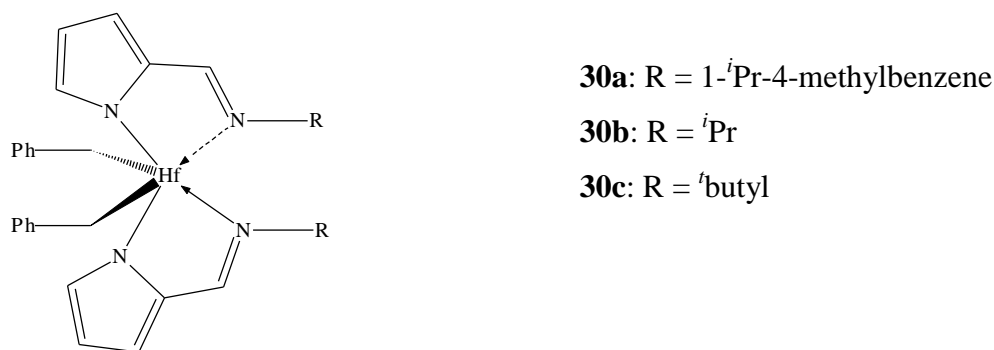
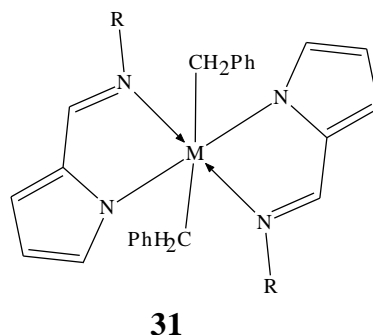


Figure 1.28: Dibenzyl Hf(IV) pyrrolyaldiminato complexes reported by Matsui *et al.*⁵⁴

When $[\text{Ph}_3\text{C}][\text{B}(\text{C}_6\text{F}_5)_4]$ was used as a co-catalyst in the presence of $i\text{Bu}_3\text{Al}$, a polymer with a PDI of 2.1 was obtained. This compares favourably with PDI values normally obtained for other single site catalysts. Complex **30c** in the presence of MAO as the co-catalyst showed activity of 1.2×10^6 g PE $(\text{mol Hf})^{-1} \text{h}^{-1} \text{bar}^{-1}$. This activity is in the same order of magnitude as that of titanium complexes with pyrrole-imine ligands under the similar polymerization conditions.

Zr(IV) analogues and other Hf(IV) pyrrole complexes were also prepared and evaluated for ethylene polymerization by Matsui *et al.*⁵⁷ The hafnium complexes with tertiary alkyl substituents, **31d** and **31e**, showed better activity compared to those with secondary alkyl groups, **31c**, Figure 1.29. Only traces of polyethylene were observed when complex **31c** was evaluated in the presence of $\text{B}(\text{C}_6\text{F}_5)_3/(i\text{Bu}_3\text{Al})$ or MAO as co-catalysts. Cationic complexes of **31d** and **31e** generated by the *in-situ* reaction with $\text{B}(\text{C}_6\text{F}_5)_3/i\text{Bu}_3\text{Al}$ showed high activity of 2.2 and 2.1×10^6 g PE $(\text{mol Hf})^{-1} \text{h}^{-1} \text{bar}^{-1}$ respectively. In the presence of MAO, again,

complexes **31d** and **31e** produced polyethylene at activities of 1.3 and 6.2×10^6 g PE (mol Hf)⁻¹ h⁻¹ bar⁻¹.



31a: R = 4-ⁱPrPh, M = Hf

31b: R = ⁱPr, M = Hf

31c: R = 4-^tbutyl-cyclohexyl, M = Hf

31d: R = ^tbutyl, M = Hf,

31e: R = 1-adamantyl, M = Hf

31f: R = 4-^tbutyl-cyclohexyl, M = Zr

31g: R = ^tbutyl, M = Zr

31h: R = 1-adamantyl, M = Zr

Figure 1.29: Dibenzyl Hf (IV) and Zr(IV) pyrrolylaldiminato complexes reported by Matsui *et al.*⁵⁷

These hafnium catalysts produced multimodal polyethylene with high PDIs, possibly caused by the gradual generation of the active species and/or isomerisation of the active species under the polymerization conditions. The zirconium complexes follow similar polymerization trends to that of the Hf, notably, complex **31f** displayed no activity. In the presence of MAO, complexes **31g** and **31h** showed higher activity than the Hf(IV) analogues giving TOF values of 1.8 and 2.3×10^7 g PE (mol Zr)⁻¹h⁻¹ bar⁻¹. However, when B(C₆F₅)₃/ⁱBu₃Al was employed as co-catalyst, lower activities of 7.46 and 17.6×10^5 g PE (mol Zr)⁻¹ h⁻¹ were obtained, such activities being lower than those of the Hf(IV) catalysts. The polymers produced had PDI values of between 2.05 and 2.25 , typical of single site catalysts.

Li and co-workers⁶¹ documented Ni(II) complexes with two pyrrolyaldimine ligands, Figure 1.30. However for complex **32**, the nickel atom is bound to one of the imino-pyrrolide ligand only *via* the N(imine) leaving the pyrrole nitrogen free. This allowed for the coordination of the bromide ligand. They found these complexes to be highly active catalysts in the polymerization of methyl methacrylate in the presence of MAO (Al:Ni = 12.5). These two complexes showed activity of 2.9 and 3.7×10^4 g PMMA (mol Ni)⁻¹ h⁻¹ for **32** and **33**, respectively at room temperature. The polymers obtained had a molecular weight of $M_w = 5.42$ to 6.66×10^4 g PMMA (mol Ni)⁻¹ h⁻¹ with narrow PDI of 1.3 – 1.4. At higher temperatures of 110 °C and 75 °C compound **32** displayed a higher activity of 8.4 and 4.4×10^4 g PMMA (mol Ni)⁻¹ h⁻¹ but at 0 °C, it was almost inactive. The % *rr* values of PMMA decreased from 72.1 to 58.2% with an increase in temperature, and a similar trend was observed for PDI (from 1.3 to 1.8).

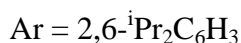
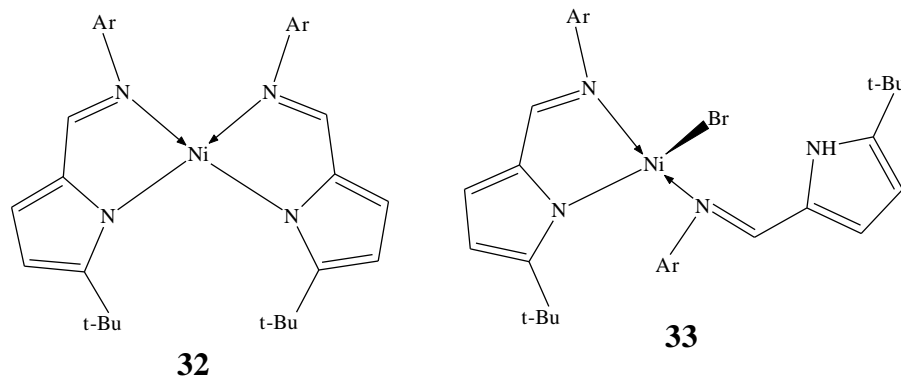
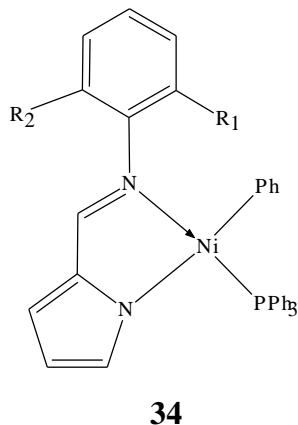


Figure 1.30: 2-(N-arylimino)pyrrolide Ni(II) complexes reported by Li and co-workers⁶¹

Neutral Ni(II) complexes, **34a** - **34d**, with only one pyrrole-imine and two other auxiliary ligands were reported by Li *et al.*⁵¹. These complexes exhibited high catalytic activities for the vinylic polymerization of norbornene in the presence of MAO. Variation of the Al:Ni molar ratios while using **34a** showed a considerable effect on the polymer yields as

well as the molecular weights. The activity ranged from 3.6×10^6 g PNB (mol Ni)⁻¹ h⁻¹ at Al:Ni ratio of 1000:1 to 8.8×10^6 g PNB (mol Ni)⁻¹ h⁻¹ at Al:Ni ratio of 2000:1.



34a: R¹ = R² = *i*Pr

34b: R¹ = *i*Pr; R² = Me

34c: R¹ = R² = Et

34d: R¹ = *t*butyl, R² = H

Figure 1.31: Neutral Ni (II) complexes of pyrrole imine with other auxiliary ligands reported by Li *et al.*⁵¹

Bulky substituents in the *ortho* position of the aromatic group attached to the imino nitrogen atom hindered the insertion of norbornene. Hence **34a** with two large substituents displays the lowest catalytic activity and produces polymers with the lowest molecular weight. **34d** with only one substituent displayed the highest catalytic activity of up to 1.3×10^6 (g PNB) (mol Ni)⁻¹ h⁻¹ and produced polymers with the highest molecular weight amongst the four catalysts.

Bellarbarba *et al.*⁶² also synthesised a Ni(II) pyrrolylaldiminato complex, **35**, and the preliminary catalytic ability in the oligomerization of ethylene in the presence of a phosphine scavenger as [Ni(COD)₂]. An activity at 25 °C was estimated to be 1.3×10^3 g oligomer (mol Ni)⁻¹ h⁻¹ bar⁻¹. This value corresponds to non-optimized oligomerization conditions.

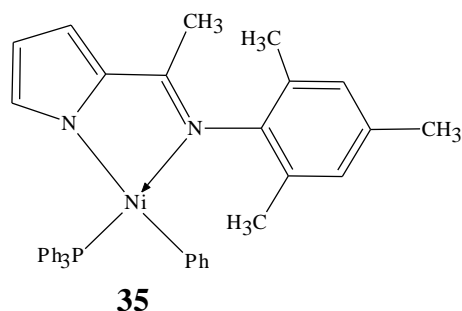


Figure 1.32: Pyrrolylaldiminato Nickel complex reported by Bellabarba *et al.*⁶²

Gibson *et al.*⁶³ reported a Cr(II) complex bearing two bulky N,N chelating mono anionic pyrrole-imine ligands, Figure 1.33. Activity of up to 1.2×10^5 (g PE) $(\text{mol Cr})^{-1} \text{h}^{-1} \text{bar}^{-1}$ in ethylene polymerization was obtained when **36** was evaluated in the presence of MAO.

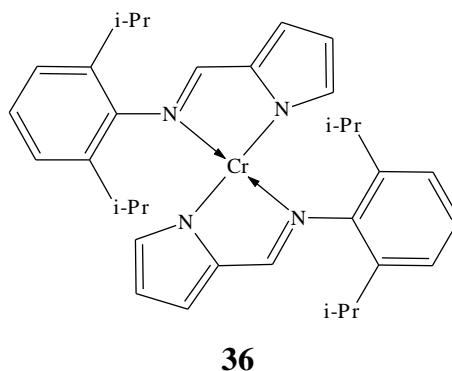


Figure 1.33: Cr (II) pyrrolylaldiminato complex reported by Gibson *et al.*⁶³

Asymmetric bi-dentate pyrrolylaldiminato Pd(II) complexes, Figure 1.34, were reported by Liang *et al.*⁶⁴ as highly active catalysts for the production of polynorbornenes when used in conjunction with modified methylaluminoxane (MMAO) as a co-catalyst. Activity between 1.68 and 3.84×10^6 g PNB $(\text{mol Pd})^{-1} \text{h}^{-1}$ was obtained at the optimal Al:Pd ratio of 2000:1.

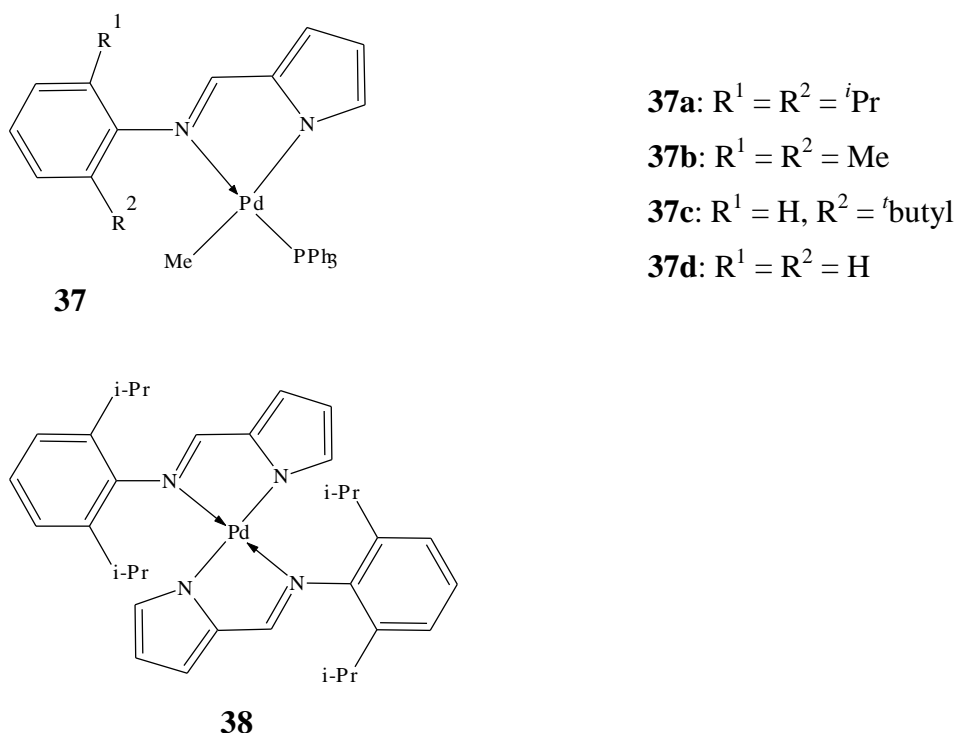
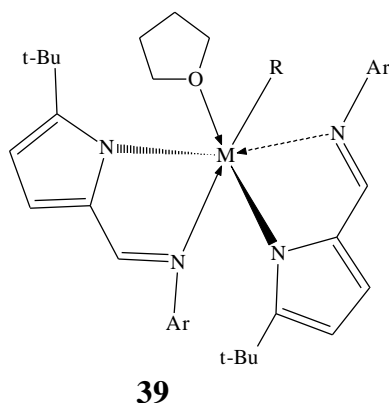


Figure 1.34: Neutral pyrrolylaldiminato Pd(II) complexes reported by Liang *et al.*⁶⁴

Cui and co-workers⁶⁵ prepared samarium and yttrium alkyl complexes with two pyrrolylaldiminato ligand together with other ligands, Figure 1.35. These compounds were found to be good catalysts for methyl methacrylate (MMA) polymerization. Compounds **39b** and **39c** were found to be highly active and isospecific for the polymerization of MMA. Compound **39b** differed from other known lanthanide catalysts showing excellent stereoregularity as well as very high molecular weight PMMA. The polymer produced had a *mm* triad content ranging from 91 to 98 % over a temperature range of -40 to +65 °C. Most reported lanthanide catalyst systems generate *syndio*-rich or *atactic* PMMA at ambient temperature. The yttrium complex **39c** showed narrow PDIs in the range of 1.24 - 1.98 but with relatively lower selectivity.



39a: M = Sm; R = Me; Ar = 2, 6-*i*Pr₂C₆H₃

39b: M = Sm; R = CH₂SiMe₃; Ar = 2, 6-*i*Pr₂C₆H₃

39c: M = Y; R = CH₂SiMe₃; Ar = 2, 6-*i*Pr₂C₆H₃

Figure 1.35: Sm and Y pyrrole-imine complexes reported by Cui and co-workers⁶⁵

Recently Mu *et al.*⁶⁶ published a *bis(imino) pyrrolyl* V(III) complex, Figure 1.36, which polymerized ethylene and 1-hexene in the presence of Et₂AlCl as cocatalyst. An activity of $1.26 \times \text{kg PE (mmol V)}^{-1} \text{ h}^{-1} \text{ bar}^{-1}$ was obtained in ethylene when **40** was evaluated in the presence of Et₂AlCl at 50 °C with a Al:V ratio of 500:1. The polymers obtained were of high molecular weight (6.23×10^4) with a PDI of 1.9, which value is typical of single site catalysts.

In ethylene and 1-hexene copolymerization, Et₂AlCl was used as a cocatalyst in conjunction with Cl₃CCOOEt (ETA) being a promoter. An activity of $2.40 \text{ kg PE (mmol V)}^{-1} \text{ h}^{-1} \text{ bar}^{-1}$ was obtained at 25 °C, and an Al:ETA:V ratio of 4000:500:1. The concentration of 1-hexene added was $2.0 \times 10^{-1} \text{ mol L}^{-1}$ and only 2 % was successively included onto the polymer. Copolymers obtained had a unimodal molecular weight distribution and M_w value of 4.35×10^4 .

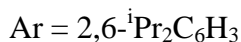
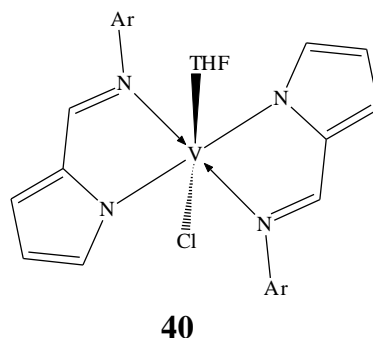


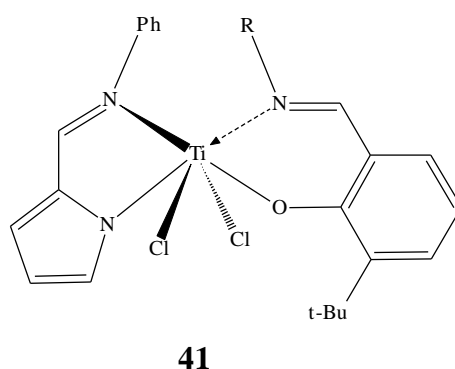
Figure 1.36: V(III) complexes bearing iminopyrrolyl ligands reported by Mu *et al.*⁶⁶

The microstructure analysis of these polymers was carried out using the ^{13}C -NMR spectroscopy. 90 % of the polymers obtained were derived purely from ethylene [EEE]. Polymers that possessed some extent of isolate 1-hexene units in a majorly ethylene polymer chain, [EEH], constituted 6.1 %. A small fraction of 2.7 % contained alternating sequence of ethylene and 1-hexene units, [EHE], with only 0.6 % assigned to two 1-hexene repeat unit, [EHH]. No polymers derived purely from 1-hexene [HHH] or of 1-hexene in alternating sequence spaced by an ethylene unit [HEH] were observed. The ^{13}C and ^1H NMR analysis of the low molecular weight copolymers did not reveal the signal of the chain-end double bonds. This observation reveals that under the conditions used, chain transfer to the aluminium was dominant.

1.4: (Salicylaldiminato) (pyrrolylaldiminato) metal complexes; mixed ligand complexes

Ti(III) (salicylaldiminato)(pyrrolylaldiminato) complexes were synthesised and observed to be good catalysts for olefin oligomerization and polymerization, Figure 1.37. These titanium mixed systems were found to be more effective catalysts for both ethylene *homo* and copolymerization with 1-hexene, norbornene, and cyclopentene than the *bis*(salicylaldiminato) or *bis*(pyrrolylaldiminato) systems.⁶⁷⁻⁷⁰

Linear polyethylenes of moderately to high M_w 's were obtained using complexes **41a** and **41b** after activation with MAO. **41a** showed a productivity of 5.6 g PE (mol Ti)⁻¹ h⁻¹ bar⁻¹ at 20 °C with 5000 equivalents of MAO. However, when the reaction temperature was increased to 50 °C a much lower activity of 2.3 g PE (mol Ti)⁻¹ h⁻¹ bar⁻¹ was obtained. Similarly, reduction in M_w and M_n are reported.



41a: R = C₆H₅

41b: R = C₆F₅

Figure 1.37: Ti(IV) (salicylaldiminato)(pyrrolylaldiminato) metal complex

41b proved to be a much better catalyst in terms of activity but displayed temperature intolerance. At 20 °C an activity of 89 g PE (mol Ti)⁻¹ h⁻¹ bar⁻¹ was obtained with a reduction to 38 g PE (mol Ti)⁻¹ h⁻¹ bar⁻¹ at 50 °C. Unlike **41a**, the M_w and M_n were not greatly affected.

Pennington *et al.*⁶⁷ also published the first example of a zirconium (salicylaldiminato)(pyrrolylaldiminato) complex, Figure 1.38. The zirconium systems also showed very high activity of up to 10⁸ g PE (mol Zr)⁻¹ h⁻¹ bar⁻¹ even at high dilution but very high Al/Zr ratios.

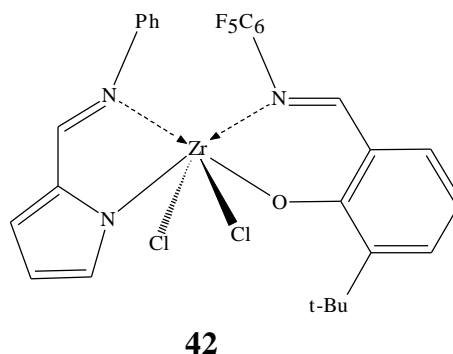


Figure 1.38: Zr(IV) (salicylaldiminato) (pyrrolylaldiminato) metal complex reported by Pennington *et al.*⁶⁷

1.5: Other Schiff base metal complexes employed in the polymerization of cyclic esters

Different types of catalyst/initiators have been employed in the polymerization of lactide ranging from main group elements to transition metals and numerous reviews on this topic have been written⁷¹⁻⁷⁷. Bulky substituents on the phenoxy donor can be used to significantly decrease side reactions. Electron withdrawing groups (EWG) have been reported to reduce both inter and intra-molecular trans-esterification reactions in the case of lactide.^{78, 79}

Kang *et al.*⁸⁰ recently reported an *in-situ* generated Zn (II) complex stabilised by N,N-bis[(3,5-dimethyl-1H-pyrazol-1-yl)methyl]-1-phenylethylamine (bdmppea) ligand, Figure 1.39. The complex $\text{ZnEt}_2(\text{bdmppea})$, **43**, polymerizes D, L-lactide at ambient temperature (25 °C) as well as at a very low temperature of -20 °C. At each temperature, the [M]/[I] ratio was varied from 50 to 200. At 25 °C, high activity was recorded after two hours with 93 % conversion being obtained at [M]/[I] = 50 while up to 84 % conversion was achieved at [M]/[I] = 200. However, PDI values of about 1.6 were recorded for the polymers in both cases. This indicated that the polymerization by *in-situ* prepared catalyst might involve other processes such as chain transfer or trans-esterification reactions. The presence of impurities may also facilitate earlier chain termination. At -20 °C a sharp decline in

activity was observed with only 52 % of the monomer being polymerized after 12 hours at $[M]/[I] = 50$. No improvement in the PDI was observed.

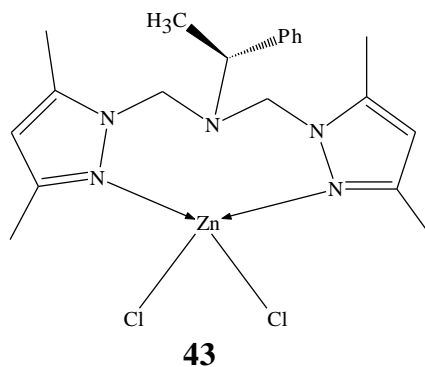
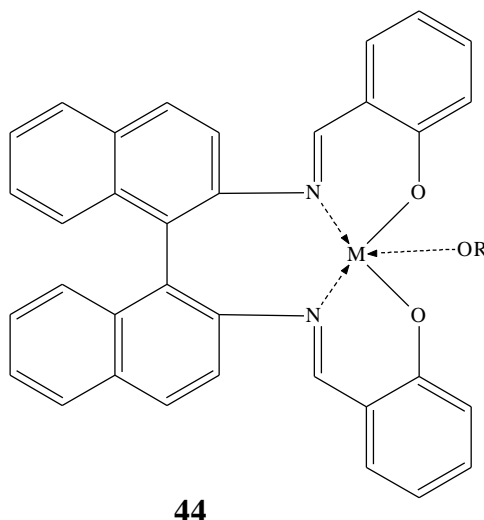


Figure 1.39: Zn(II)Cl₂ metal complex, Kang *et. al.*⁸⁰

Ovitt and co-workers⁸¹ observed similar lack of stereocontrol with an yttrium alkoxide, **44b**, during the polymerization of D, L-lactide. Compound **44b**, Figure 1.40, gave conversions of 97 % after 14 h while **44a** showed up to 94 % conversion after 40 h. The microstructure of the polymer produced by catalyst **44b** was shown to be atactic PDLLA. However, with **44a**, highly syndiotactic PLA was obtained with a PDI of 1.05 as determined from GPC analysis. Thus they concluded that this Al alkoxide behaved like a single site catalysts and followed a living polymerization mechanism.



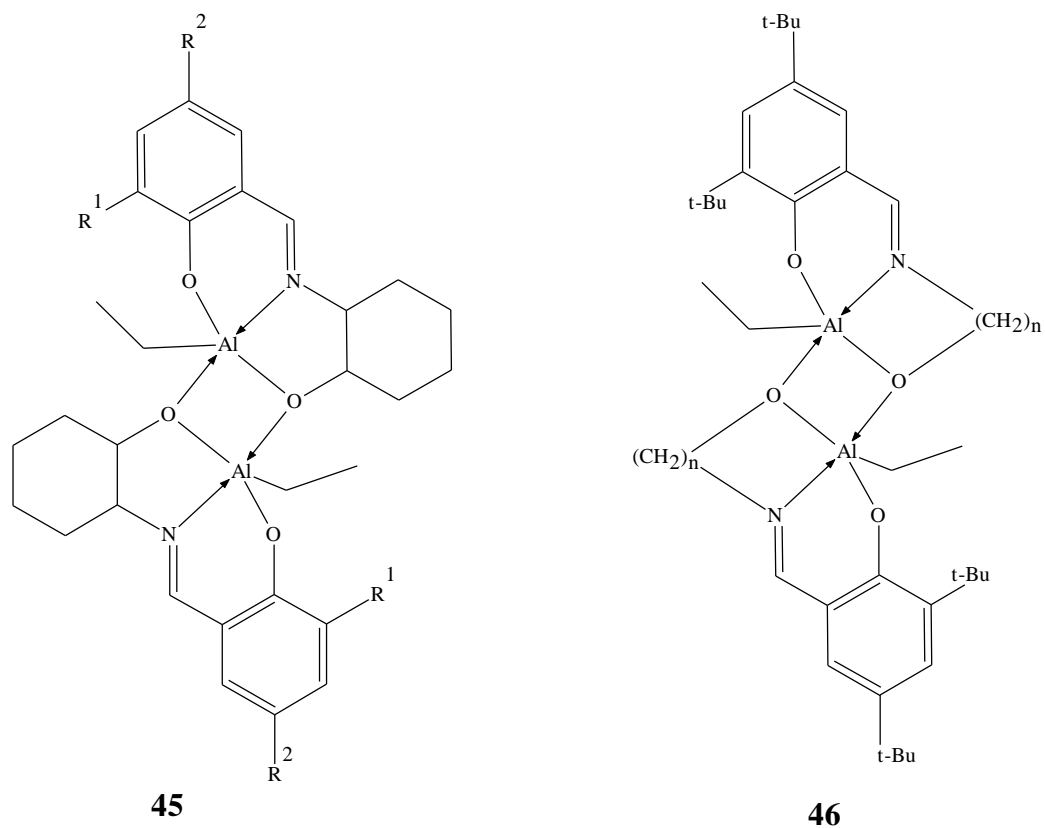
44a: M = Al; R = *i*Pr

44b: M = Y; R = (CH₂)₂NMe₂

Figure 1.40: Al(III) and Y(III) alkoxide, Ovitt and co-workers⁸¹

Darensbourg *et al.*⁸² published a series of both chiral and achiral aluminium salen based complexes, Figure 1.41, that initiated the polymerization of D, L-Lactide. These catalysts produced isotactic polylactides with narrow PDI and controlled molecular weights. Complexes **45a** – **45d** polymerized D, L-Lactide in toluene at 70 °C and [LA]/[Al] = 50. They showed a decrease in polymerization rate as the bulkiness of the substituents on the phenoxide increased. After 66 h, **45a** had converted 57% of the monomer to the moderately isotactic polylactide.

The complexes with an achiral aliphatic backbone, **46a**, **46c** and **46d**, were found to be better catalysts. High monomer conversion of up to 77 % in 15 h was recorded for **46a** under similar conditions as those of **45a**. The exception in this series was **46b** with 36 % monomer conversion after 76 h. The complexes derived from rac-amino acids, **47a** and **47b**, were found to also polymerize lactide. The polymer obtained were again isotactic with narrow PDI values.



45a; $R^1 = R^2 = t\text{butyl}$

45b; $R^1 = \text{H}, R^2 = \text{OMe}$

45c; $R^1 = \text{Me}, R^2 = \text{SiPh}_3$

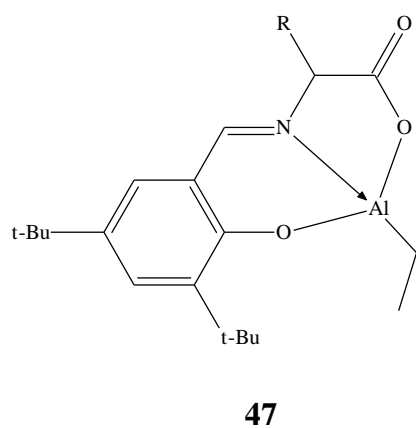
45d; $R^1 = \text{Me}, R^2 = \text{SiMe}_2 t\text{butyl}$

46a; $n = 2$

46b; $n = 3$

46c; $n = 4$

46d; $n = 5$

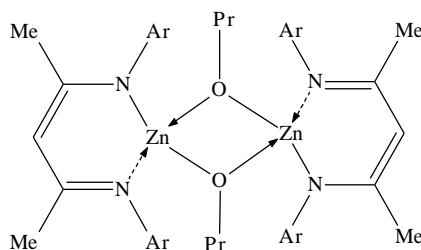


47a; $R = 2\text{-(methylthio)ethyl}$

47b; $R = \text{Benzyl}$

Figure 1.41: Al(III) salen complexes containing both chiral and achiral ligands reported by Darensbourg *et al.*⁸²

Cheng *et al.*⁸³ reported a very active 2,6-diisopropylphenyl substituted diimine zinc complex (BDIZnO^{*i*}Pr) complex (Figure 1.42) for the polymerization of D, L-Lactide. Compound **48** achieved 95 % conversion at a [M]/[I] ratio of 200 after 20 mins at a temperature of 20 °C. The GPC analysis of the polymers revealed a PDI of 1.10 and M_n of 3.8×10^4 g/mol. A highly tactic microstructure of the polymer was revealed by ¹H-NMR spectroscopy. Homonuclear decoupled ¹H-NMR spectroscopy of the methine region of heterotactic PLA showed two intense peaks at δ 5.22 and 5.14 ppm for the *rmr* and *mrm* tetrads respectively. On lowering the reaction temperature to 0 °C, stereoregularity of the polymers was enhanced but the rate of polymerization was lowered to 95% conversion after 2 h. The PDI and average molecular weight were not greatly affected by the change in reaction temperature.

**48**

Ar = 2, 6-^{*i*}Pr₂C₆H₃ reported by

Figure 1.42: 2, 6-diisopropylphenyl substituted β -diimine (BDI) Z(II) complex reported by Cheng *et al.*⁸³

1.6: α -olefin oligomerization and polymerization

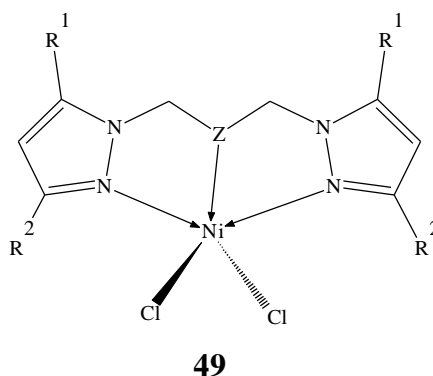
Olefins, particularly C₂-C₅ are easily available, cheap, reactive, and readily transformable into higher α -olefins, C₆-C₂₀, which are building blocks for a wide range of useful products e.g. biodegradable detergents, lubricants and other useful industrial chemicals. These higher α -olefins are obtained through the following processes: thermal and

catalytic cracking of paraffins, oligomerization of ethylene, dehydrogenation of paraffins, dimerization and metathesis of olefins as well as dehydration of alcohols.⁸⁴

Kissin *et al.*⁸⁵ published a kinetic study of 1-hexene oligomerization reaction with the Zr-MAO catalyst system. They used a commercially available (n-Bu-Cp)₂ZrCl₂ catalyst. The reactions were carried out at 1.4 atm and heated to 70 °C. After 5 h of reaction time, activity of up to 6×10^5 g oligomer (mol Zr)⁻¹ h⁻¹ was obtained producing dimer, C₁₂H₂₄, to the tetradecamer, C₈₄H₁₆₈. Kinetic modelling strongly supported the principal premise that the value of the chain propagation rate constant does not depend on the number of monomer units in the growing polymer chain.

Oliveira *et al.*⁸⁶ synthesised pyrazolyl nickel complexes, **49a** - **49d**, that were catalytically active in ethylene oligomerization reactions in the presence of both MAO and Et₂AlCl as co-catalysts. When MAO was used as co-catalyst at Al:Ni ratio of 250, **49a** displayed TOF values of 1.13×10^4 (mol C₂ consumed) (mol Ni)⁻¹ h⁻¹ while complex **49b** was less active giving a lower TOF value of 3.9×10^3 (mol C₂ consumed) (mol Ni)⁻¹ h⁻¹. Butene isomers were formed as major product with a small amount of C₆, (< 5 %). The selectivity for 1-butene was high. For example **49b** gave 94 % 1-butene of all the total amount of the C₄ formed in the oligomerization reactions. Increasing the temperature from 30 to 60 °C resulted in a notable decrease in TOF from 11.3 to 1.7×10^3 mol (C₂ consumed) (mol Ni)⁻¹ h⁻¹ for **49a**. However when the catalyst system with a sulphur-bridged ligand bearing methyl substituents was evaluated, i.e., **49c**, a very high TOF of 1.04×10^5 (mol C₂ consumed) (mol Ni)⁻¹ h⁻¹ was observed. Larger amounts of 2-butenes (ca. 26 % of the C₄ fraction) were also produced from **49c**.

Although Et₂AlCl proved to be a better co-catalyst with TOF values ranging from 3.4 to 9.1×10^4 mol (C₂ consumed) (mol Ni)⁻¹ h⁻¹, relatively poor selectivity for 1-butene was exhibited (72.0 – 81.3 %).



49a: Z = Benzylamine; R¹ = R² = Me

49b: Z = Butylamine ; R₁ = R² = Me

49c: Z = S; R₁ = R² = Me

49d: Z = S; R¹ = H; R² = Ph

Figure 1.43: Ni(II) complexes based on tridentate pyrazolyl ligands reported by Oliveira *et al.*⁸⁶

1.7: Dendrimer supported Schiff base metal complexes as catalysts

There has been enormous interest in supporting homogeneous Schiff base catalysts onto organic or inorganic supports. “Heterogenised” catalysts, in principle, combine the advantages of homogeneous and heterogeneous catalysts. These advantages are the high activity and selectivity of homogeneous catalysts and the simple extraction and recyclability of heterogeneous catalysts.

Silica is the most widely used inorganic support. Most of the complexes can be tethered onto silica surfaces through a ligand in the complex which has alkoxy - or chlorosilane functional groups (ion pair) that react with surface hydroxyl groups on the SiO₂ or by impregnating the homogeneous catalyst into a solid support. This may be achieved by using an ion-exchange resin to bind anionic catalysts, encapsulating inorganic complexes into pores of chemically modified silica such as MCM-22, MCM-41 and MCM-48 or zeolites, or covalently binding coordination complexes onto modified silica.⁸⁷⁻⁹² Metal complexes can also be supported on polymers.⁹³⁻⁹⁶ An alternative approach that is not widely explored is the

use of dendrimers.^{97, 98} A number of reviews on dendrimer and the application of their metal complexes have been written.⁹⁹⁻¹⁰⁴

We reported the preparation of new pyrrole-imine metallodendrimers of Co(II), Ni(II) and Cu(II), Figure 1.44.^{59, 60} These complexes were observed to act as catalysts in the oxidation cyclohexene and phenol. Metallodendrimers of copper, nickel and cobalt, **50a** - **50c** for example were found to be active in the oxidation of cyclohexene. **50a** was found to be more active than **50b** and **50c** with the highest TOF being 30.9, 27.1 and 22.0 mol (cyclohexene consumed) (mol metal)⁻¹ h⁻¹ respectively at a metal concentration of 3.0×10^{-3} molL⁻¹. A higher metal concentration of 1.2×10^{-2} molL⁻¹ leads to a reduction in activity attributed to catalyst deactivation by dimerization and aggregation of the metal centers with TOF of 6.5, 4.3 and 2.2 mol (cyclohexene consumed) (mol metal)⁻¹ h⁻¹ being obtained.

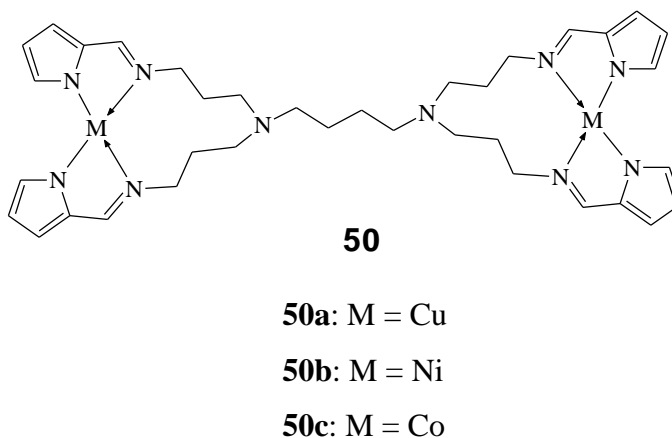
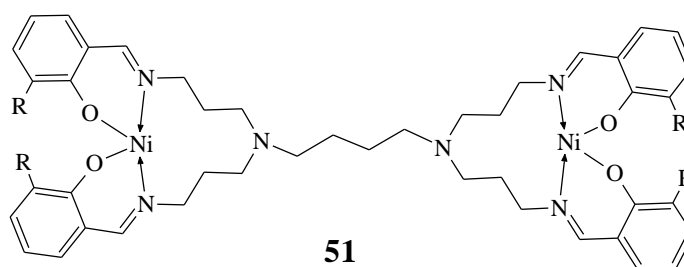


Figure 1.44: Dendrimeric pyrrolylaldiminato complexes reported by Mugo *et al.*⁵⁹

Under all the conditions investigated, the nickel catalysts were found to be more selective for the formation of cyclohexene oxide. At a metal concentration of 6×10^{-3} molL⁻¹ only **50b** gave the cyclohexene-oxide accounting for 47 % of the products. This was the highest selectivity to cyclohexene oxide using these dendrimeric catalysts.

Two dendritic complexes, **50a** and **50b**, also catalysed the hydroxylation of phenol in aqueous media over a pH range of 2 – 8 in the presence of H₂O₂ under oxygen atmosphere. Catechol and hydroquinone were obtained as the major products with only small amounts of *para*-benzoquinone being observed in both systems. The copper metallodendrimer (**50a**) was a better catalyst with TOF [moles (phenol consumed) (mol metal)⁻¹ h⁻¹] values of 6.6 - 10.8, as compared to the nickel analogous with 1.3 - 9.5. The solution pH impacted on both activity and selectivity of these metallodendrimers. Optimal conversion was obtained at pH 3 for **50a** (64.5 %) and at pH 8 for **50b** (56.9 %). However, the nickel complex proved to be more selective with up to 99 % selectivity for catechol at pH 6 while **50a** gave 63 % (catechol) under similar conditions.⁵⁹

Malgas-Enus *et al.*^{105, 106} synthesised Ni(II) complexes derived from 1st and 2nd generation poly(propyleneimine) dendrimeric salicylaldimine ligands, Figures 1.45 and 1.46. These complexes were found to be active catalysts in the polymerization of norbornene when used with MAO as co-catalyst. The polymers were found to have moderate M_w and low PDI values. The Ni(II) complex of the 2nd generation, (G2) **52a**, showed better activity than the G1 analogue, **51a**, over a range of Al:Ni ratios.



51a: R = H

51b: R = ^tbutyl

Figure 1.45: 1st generation Ni(II) salicylaldimine metallodendrimer reported by Malgas-Enus *et al.*^{105, 106}

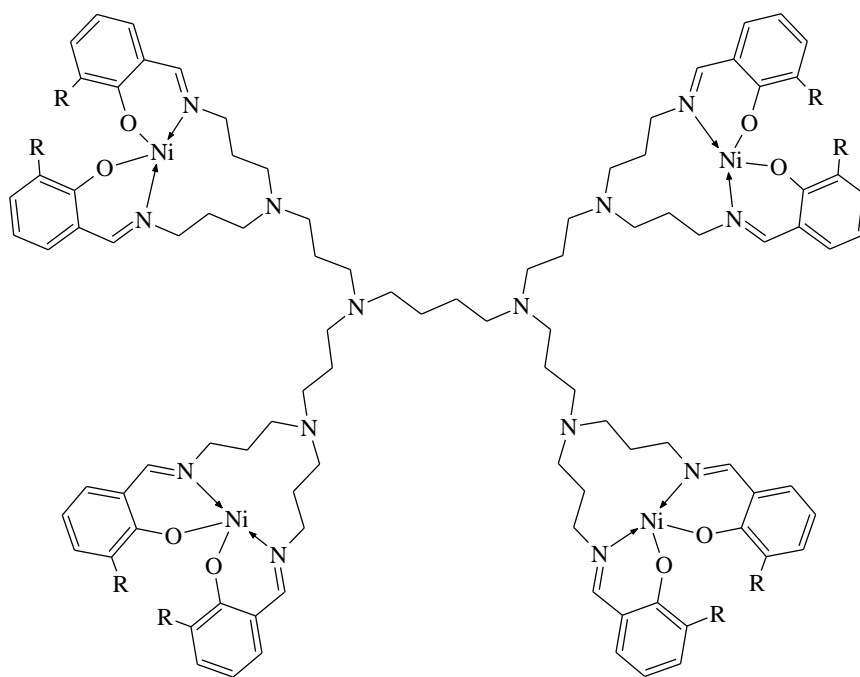
**52****52a:** R = H**52b:** R = ^tbutyl

Figure 1.46: 2nd generation Ni(II) salicylaldimine metallodendrimer, published by Malgas-Enus *et al.*^{105, 106}

The highest activity of 7.9×10^5 (g PNBE) (mol Ni)⁻¹ h⁻¹ for **52a** was obtained at Al:Ni ratio of 4500:1 whereas that of **51a** was 3.3×10^5 (g PNBE) (mol Ni)⁻¹ h⁻¹ at Al:Ni ratio of 4000:1.

51a and **52a** were also evaluated as ethylene oligomerization catalysts in the presence of EtAlCl₂ as co-catalyst. MAO and Et₂AlCl proved to be ineffective as co-catalysts for the oligomerization of ethylene. Reactions were performed over a range of Al:Ni ratios from 20:1 to 3000:1. **51a** Al:Ni = 500, 2.6×10^5 (g PE) (mol Ni)⁻¹ h⁻¹ **52a** Al:Ni = 1000, 2.6×10^5 (g PE) (mol Ni)⁻¹ h⁻¹ **52a** showed optimum catalyst activity of 2.6×10^5 (g PE) (mol Ni)⁻¹ h⁻¹ at an Al:Ni ratio of 500:1 while **52a** gave 2.6×10^5 (g PE) (mol Ni)⁻¹ h⁻¹ at 2000:1. The 2nd generation dendritic catalyst **52a**, showed significantly higher activity than the 1st generation catalyst, **51a**.

Previously a dendrimer with peripherally bound palladium containing four PdCl₂ moieties on the surface, Figure 1.47 were reported by Smith *et al.*¹⁰⁷ These palladium metallodendrimers, **53**, were shown to catalyse the polymerization of ethylene in the presence of MAO. Catalytic activity of up to 1.2×10^5 (g PE) (mol Pd)⁻¹ h⁻¹ was reported with moderate molecular weight polyethylene ($M_w = 1.4 \times 10^5$) being produced. This was found to be higher than the activities for analogous mononuclear and binuclear palladium diimine systems. The higher activity was attributed to the increased local concentration of catalytic sites within the multinuclear precursors.¹⁰⁷

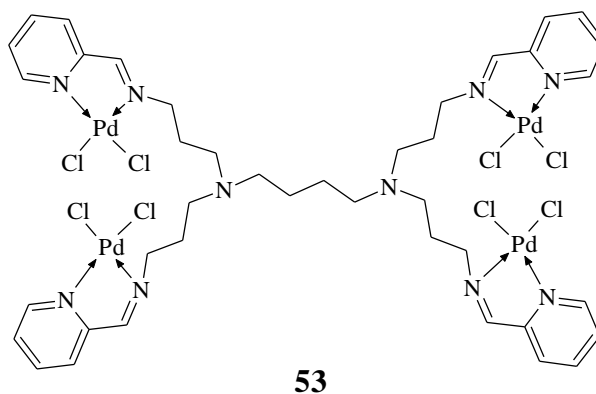


Figure 1.47: Peripherally bound Pd(II) metallodendrimer reported by Smith *et al.*¹⁰⁷

Marx *et al.*¹⁰⁸ reported 3rd generation metallodendrimers of Pd, Ir, Rh and Ni. They treated the DAB-PPI-(NH₂)₁₆ dendrimer with Ph₂PCH₂OH. The intermediate was then converted to the related metallodendrimers by treatment with [PdCl₂(PhCN)₂], [Pd(CH₃)₂(tmeda)], [Rh(COD)₂BF₄], and a 50:50 mixture of [Pd(CH₃)₂(tmeda)] and [Ni(CH₃)₂(tmeda)]. Amongst the complexes isolated was a Pd(II) metallodendrimer that catalyzes the Heck reaction of bromobenzene and styrene forming stilbene with 89 % conversion. The activity was significantly higher than that of the mononuclear palladium analogue possessing typical turnover numbers (TON) of 50 versus 16. The Rh (I)-

metallo-dendrimer gave a comparable TOF to that of the monomeric analogue for the hydroformylation of 1-octene.

1.8: Aim and scope of this thesis

In this thesis we set out to develop Schiff base transition metal complexes suitable as catalysts for ring opening polymerization of cyclic esters as well as α -olefin transformation. A summary of the various chapters in the thesis is given below.

Chapter 1: Literature review: Salicylaldimine and Pyrrole-imine Schiff Base Complexes as Catalyst with a Focus on Polymerization and Oligomerization

This chapter focuses on a brief review of Schiff base transition metal complexes with a particular emphasis on salicylaldimine and pyrrole-imine based systems. Reports of their application particularly in α -olefin polymerization and oligomerization as well as the ring opening polymerization of cyclic esters are reviewed.

Chapter 2: Synthesis and Characterization of Salicylaldimine and Pyrrolylaldiminato Schiff Base Ligands

This chapter deals with the synthesis and full characterization of salicylaldimine and pyrrolylaldiminato ligands. Monofunctional and multifunctional ligand systems were prepared via Schiff base condensation of appropriate amines and aldehydes. The multifunctional ligands were obtained by functionalising the peripheral groups of commercially available poly(propyleneimine) dendrimers with salicylaldimine and pyrrole-imine units. Characterizations of these ligands with a range of physical techniques which include NMR spectroscopy, FT-IR spectroscopy, elemental analysis, mass spectrometry as well as X-ray crystallography where appropriate are described.

Chapter 3: Synthesis and Characterization Salicylaldiminato Zn(II) Metal Complexes

This chapter covers the synthesis and characterization of Zn(II) complexes. Mono- and multi-nuclear metal complexes were prepared by the reaction of the salicylaldimine ligands discussed in Chapter 2 with diethyl zinc. Characterization techniques used include NMR and FT-IR spectroscopies, elemental analysis, mass spectrometry thermogravimetric analysis (TGA) as well as differential scanning calorimetry (DSC).

Chapter 4: Synthesis and Characterization Pd(II) Salicylaldiminato and Pyrrolylaldiminato Metal Complexes

The synthesis and characterization of palladium metal complexes is discussed in this Chapter. The complexes were prepared from palladium acetate with both the salicylaldimine and the pyrrole-imine ligands. Characterization techniques used include NMR, FT-IR and ICP-AE spectroscopies, elemental analysis, mass spectrometry and X-ray crystallography where suitable single crystals were obtained.

Chapter 5: Polymerization of Cyclic Esters using Mono- and Multi nuclear Salicylaldimine Zn(II) Complexes

This chapter discusses the catalytic evaluation of the zinc complexes prepared in Chapter 3 in the polymerization of D, L-Lactide. The complexes are evaluated at different monomer to zinc (M/Zn) ratio over time as well as different solvents and reaction temperature. We also discuss the use of the metallodendrimers in the melt. The reactions were monitored using ^1H -NMR spectroscopy. The polylactides obtained were characterized using ^{13}C -NMR and FT-IR spectroscopies, GPC, TGA, DSC and scanning electron microscopy (SEM).

Chapter 6: α -Olefin Transformation Catalysed by Pyrrolylaldiminato and Salicylaldiminato Pd(II) Complexes

Catalytic transformation of ethylene and 1-hexene with pyrrolylaldiminato and salicylaldiminato complexes in the presence of MAO, EtAlCl₂ and Et₂AlCl as co-catalysts is described in this chapter. Reaction parameters such as temperature, ethylene pressure and Al:Pd ratios were evaluated. The reactions were monitored using GC and the products obtained were characterized by APCI-MS and GC-MS.

Chapter 7 Summary and Future Work

This chapter covers a summary of the research work described in this thesis and gives some suggestions for further work.

1.9: References

1. H. Keypour, M. Shayesteh, A. Sharifi-Rad, S. Salehzadeh, H. Khavasi, L. Valencia, *J. Organomet. Chem.*, **693** (2008) 3179.
2. R. V. Heerbeek, P. C. J. Kamer, P. W. N. M. van Leeuwen, J. N. H. Reek, *Chem. Rev.*, **102** (2002) 3717.
3. C. Zhang, Z-X. Wang, *J. Organomet. Chem.*, **693** (2008) 3151.
4. P. K. Mascharak, *Coord. Chem. Rev.*, **225** (2002) 201.
5. S. Ilhan, H. Temel, I. Yilmaz, M. Sekerci, *J. Organomet. Chem.*, **692** (2007) 3855.
6. T. Ueno, T. Koshiyama, S. Abe, N. Yokoi, M. Ohashi, H. Nakajima, Y. Watanabe, *J. Organomet. Chem.*, **692** (2007) 142.
7. T. Katsuki, *Chem. Soc. Rev.*, **33** (2004) 437.
8. R. L. De, K. Samanta, K. Maiti, E. Keller, *Inorg. Chim. Acta*, **316** (2001) 113.
9. K. C. Gupta, A. K. Sutar, *Coordin. Chem. Rev.*, **252** (2008) 1420.
10. H. Hao, S. Bhandari, Y. Ding, H. W. Roesky, J. Magull, H. Schmidt, M Noltemeyer, C. Cui, *Eur. J. Inorg. Chem.*, (2002) 1060.
11. L. Tatar, D. Ulku, O. Atatkol, *Acta Crystallogr. Sect. C*, **55** (1999) 508.
12. H. Sakiyama, H. Okawa, N. Matsumoto, S. Kida, *Dalton Trans.*, (1990) 2935.
13. F. A. Bottino, P. Finocchiaro, E. J. Libertini, *Coord. Chem.*, **16** (1988) 341.
14. G. E. Batley, D. P. Graddon, *Aust. J. Chem.*, **20** (1967) 877.
15. P. L. Orioli, M. Di Vaira, L. Sacconi, *Inorg. Chem.*, **3** (1966) 400.
16. A. D. Garnovskii, A. S. Burlov, K. A. Lysenko, D. A. Garnovskii, I. G. Borodkina, A. G. Ponomarenko, G. G. Chigarenko, S. A. Nikolaevskii, V. I. Minkin, *Rus. J. Coord. Chem.*, **35** (2009) 120.
17. M. A. Torzilli, S. Colquhoun, J. Kim, R. H. Beer, *Polyhedron*, **21** (2002) 705.
18. M. A. Torzilli, S. Colquhoun, D. Doucet, R. H. Beer, *Polyhedron*, **21** (2002) 697.

19. X-W. Zhu, X. Z. Yang, *Acta Crystallogr.*, E, **64** (2008) m1090.
20. G. Martínez, J. Chirinos, M. E. G. Mosquera, T. Cuenca, E. Gómez, *Eur. J. Inorg. Chem.*, (2010) 1522.
21. E. Tas, V. T. Kasumov, O. Sahin and M. Ozdemir, *Trans. Met. Chem.*, **27** (2002) 442.
22. V. T. Kasumov, *Trans. Met. Chem.*, **27** (2002) 228.
23. V. T. Kasumov, F. Köksal, *Trans. Met. Chem.*, **28** (2003) 888.
24. M. Kettunen, A. S. Abu-Surrah, H. M. Abdel-Halim, T. Repo, M. Leskelä, M. Laine, I. Mutikainen, M. Ahlgren, *Polyhedron*, **23** (2004) 1649.
25. J. Liu, N. Iwasa, K. Nomura, *Dalton Trans.*, (2008) 3978.
26. P. A. Cameron, V. C. Gibson, C. Redshaw, J. A. Segal, M. D. Bruce, A. J. P. White, D. J. Williams, *Chem. Commun.*, (1999) 1883.
27. D. Pappalardo, C. Tedesco, C. Pellicchia, *Eur. J. Inorg. Chem.*, (2002) 621.
28. S. Matsui, M. Mitani, J. Saito, Y. Tohi, H. Makio, N. Matsukawa, Y. Takagi, K. Tsuru, M. Nitabaru, T. Nakano, H. Tanaka, N. Kashiwa, T. Fujita, *J. Am. Chem. Soc.*, **123** (2001) 6847.
29. J. Saito, M. Mitani, S. Matsui, Y. Tohi, H. Makio, T. Nakano, H. Tanaka, N. Kashiwa, T. Fujita, *Macromol. Chem. Phys.*, **203** (2002) 59.
30. M. Mitani, J. Mohri, Y. Yoshida, J. Saito, S. Ishii, K. Tsuru, S. Matsui, R. Furuyama, T. Nakano, H. Tanaka, S. Kojoh, T. Matsugi, N. Kashiwa, T. Fujita, *J. Am. Chem. Soc.*, **124** (2002) 3327.
31. M. Mitani, R. Furuyama, J. Mohri, S. Ishii, H. Terao, T. Nakano, H. Tanaka, T. Fujita, *J. Am. Chem. Soc.*, **125**, (2003) 4293.
32. Y-S. Li, Y-R. Li, X-F. Li, *J. Organomet. Chem.*, **667** (2003) 185.
33. C. Wang, S. Friedrich, T. R. Younkin, R. T. Li, R. H. Grubbs, D. A. Bansleben, M. W. Day, *Organometallics*, **17** (1998) 3149.

34. U. Klabunde, S. D. Ittel, *J. Mol. Catal.*, **41** (1987) 123.
35. U. Klabunde, R. Mulhaupt, T. Herskovitz, A. H. Janowicz, J. Calabrese, S. D. Ittel, *J. Polym. Sci., Part A: Polym. Chem.*, **25** (1987) 1989.
36. J. Lu, D. Zhang, Q. Chen, B. Yu, *Front. Chem. Sci. Eng.*, **5** (2011) 19.
37. P. A. Cameron, V. C. Gibson, C. Redshaw, J. A. Segal, M. D. Bruce, A. J. P. White, D. J. Williams, *Chem. Commun.*, (1999) 1883.
38. D. Chandran, C. H. Kwak, C-S. Ha, I. Kim, *Catal. Today*, **131** (2008) 505.
39. J. Liu, N. Iwasa, K. Nomura, *Dalton Trans.*, (2008), 3978.
40. D. Pappalardo, L. Annunziata, C. Pellicchia, *Macromolecules*, **42** (2009) 6056.
41. N. Nimitsiriwat, V. C. Gibson, E. L. Marshall, M. R. J. Elsegood, *Dalton Trans.*, (2009) 3710.
42. N. Nimitsiriwat, E. L. Marshall, V. C. Gibson, M. R. J. Elsegood, S. H. Dale, *J. Am. Chem. Soc.*, **126** (2004) 13598.
43. D. J. Darensbourg, P. Rainey, J. Yarbrough, *Inorg. Chem.*, **40** (2001) 986.
44. M. D. Jones, M. G. Davidson, C. G. Keir, L. M. Hughes, M. F. Mahon, D. C. Apperley, *Eur. J. Inorg. Chem.*, (2009) 635.
45. S. D. Drouin, H. M. Foucault, G. P.A. Yap. D. E. Fogg, *Can. J. Chem.*, **83** (2005) 748.
46. S. A. Carabineiro, R. M. Bellabarba, P. T. Gomes, S. I. Pascu, L. F. Veiros, C. Freire, L. C. J. Pereira, R. T. Henriques, M. C. Oliveira, and J. E. Warren, *Inorg. Chem.*, **47** (2008) 8896.
47. J. Lewiński, M. Dranka, I. Kraszewska, W. Sliwiński, I. Justyniak, *Chem. Commun.*, (2005) 4935.
48. H. M. Foucault, D. L. Bryce, D. E. Fogg, *Inorg. Chem.*, **45** (2006) 10293.
49. S. A. Carabineiro, L. C. Silva, P. T. Gomes, L. C. J. Pereira, L. F. Veiros, S. I. Pascu, M. T. Duarte, S. Namorado, R. T. Henriques, *Inorg. Chem.*, **46** (2007) 6880.

50. P. Pérez-Puente, E. de Jesús, J. C. Flores, P. Gómez-Sal, *J. Organomet. Chem.*, **693** (2008) 3902.
51. J. Li, H. Song, C. Cui, *Appl. Organomet. Chem.*, **24** (2010) 82.
52. Y. Yoshida, S. Matsui, Y. Takagi, M. Mitani, T. Nakano, H. Tanaka, N. Kashiwa, T. Fujita, *Organometallics*, **20** (2001) 4793.
53. Y. Yoshida, J. Saito, M. Mitani, Y. Takagi, S. Matsui, S. Ishii, T. Nakano, H. Tanaka, N. Kashiwa, T. Fujita, *Chem. Commun.*, (2002) 1298.
54. S. Matsui, T. P. Spaniol, Y. Takagi, Y. Yoshida, J. Okuda, *Dalton Trans.*, (2002) 4529.
55. Y. Yoshida, J. Mohri, S. Ishii, M. Mitani, J. Saito, S. Matsui, H. Makio, T. Nakano, H. Tanaka, M. Onda, Y. Yamamoto, A. Mizuno, T. Fujita, *J. Am. Chem. Soc.*, **126** (2004) 12023.
56. Y. Yoshida, S. Matsui, T. Fujita, *J. Organomet. Chem.*, **690** (2005) 4382.
57. S. Matsui, T.P. Spaniol, Y. Takagi, Y. Yoshida, J. Okuda, *Dalton Trans.*, (2002) 4017.
58. S. Matsui, T. P. Spaniol, Y. Yoshida, Y. Takagi, J. Okuda, *J. Organomet. Chem.*, **689** (2004) 1155.
59. Jane Ngima Mugo, MSc Thesis, *Mononuclear, Dendrimeric and MCM-41 Immobilized Pyrrole-Imine Complexes of Cu, Co and Ni as Catalytic Precursors in Oxidation Reactions*, University of the Western Cape 2007
60. J. N. Mugo, S. F. Mapolie, J. L. van Wyk, *Inorg. Chim. Acta.*, **363** (2010) 2643.
61. Y-S. Li, Y-R. Li, X-F. Li, *J. Organomet. Chem.*, **667** (2003) 185.
62. R. M. Bellabarba, P.T. Gomes, S. I. Pascu, *Dalton Trans.*, (2003) 4431.
63. V. C. Gibson, C. Newton, C. Redshaw, G. A. Solan, A. J. P. White, D. J. Williams, *Dalton Trans.*, (2002) 4017.
64. H. Liang, J. Liu, X. Li, Y. Li, *Polyhedron*, **23** (2004) 1619.
65. C. Cui, A. Shafir, C. L. Reeder, J. Arnold, *Organometallics*, **22** (2003) 3357.

66. J-S. Mu, Y-X. Wang, B-X. Lia, Y-S. Li, *Dalton Trans.*, **40** (2011) 3490.
67. D. A. Pennington, S. J. Coles, M. Hursthouse, M. Bochmann, S. J. Lancaster, *Chem. Commun.*, (2005) 3150.
68. A. F. Mason, G.W. Coates, *J. Am. Chem. Soc.*, **126** (2004) 10798.
69. Y. Suzuki, T. Oshiki, H. Tanaka, K. Takai, T. Fujita, *Chem. Lett.*, **34** (2005) 1458.
70. K. P. Bryliakov, E. A. Kravtsov, L. Broomfield, E. P. Talsi, M. Bochmann, *Organometallics*, **26** (2007) 288.
71. D. A. Pennington, S. J. Coles, M. B. Hursthouse, M. Bochmann, S. J. Lancaster, *Macromol. Rapid Commun.*, **27** (2006) 599.
72. B. J. O'Keefe, M. A. Hillmyer, W. B. Tolman, *Dalton Trans.*, (2001) 2215.
73. B. J. O'Keefe, S. M. Monnier, M. A. Hillmyer, W. B. Tolman, *J. Am. Chem. Soc.*, **123** (2001) 339.
74. J. Wu, T-L. Yu, C-T. Chen, C-C. Lin, *Coordin. Chem. Rev.*, **250** (2006) 602.
75. C. A. Caputo, N. D. Jones, *Dalton Trans.*, (2007) 4627.
76. M. H. Chisholm, Z. Zhou, *J. Mater. Chem.*, **14** (2004) 3081.
77. P. Dobrzynski, J. Kasperczyk, H. Janeczek, M. Bero, *Polymer*, **43** (2002) 2595.
78. X. Y. Wang, K. R. Liao, D. P. Quan, Q. Wu, *Macromolecules*, **38** (2005) 4611.
79. G. Montaudo, M. S. Montaudo, C. Puglisi, F. Samperi, N. Spassky, A. LeBorgne, M. Wisniewski, *Macromolecules*, **29** (1996) 6461.
80. Y. K. Kang, J. H. Jeong, N. Y. Lee, Y. T. Lee, H. Lee, *Polyhedron*, **29** (2010) 2404.
81. T. M. Ovitt, G. W. Coates, *J. Am. Chem. Soc.* **121** (1999) 4072.
82. D. J. Darensbourg, O. Karroonnirun, *Organometallics*, **29** (2010) 5627.
83. M. Cheng, A. B. Attygalle, E. B. Lobkovsky, G. W. Coates, *J. Am. Chem. Soc.*, **121** (1999) 11583.
84. J. Skupinska, *Chem. Rev.*, **91** (1991) 613.

85. Y. V. Kissin, *Macromol. Chem. Phys.*, **210** (2009) 1241.
86. L. L. de Oliveira, R. R. Campedelli, M. C. A. Kuhna, J-F. Carpentier, O. L. Casagrande Jr., *J. Mol. Catal. A: Chem.*, **288** (2008) 58.
87. H. Gao, R. J. Angelici, *J. Am. Chem.*, **119** (1997) 6937.
88. C. W. Jones, M. W. McKittick, J. V. Nguyen, K. Yu, *Top. Catal.*, **34** (2005) 67.
89. B. S. Lane, K. Burgess, *Chem. Rev.*, **103** (2003) 2457.
90. T. R. Gaydhankar, U. S. Taralkar, R. K. Jha. P. N. Joshi, R. Kumar, *Catal. Commun.*, **6** (2005) 361.
91. M. Salavati-Niasari, P. Salemi, F. Davar, *J. Mol Catal. A: Chem.*, **238** (2005) 215.
92. A. Caselli, E. Gallo, F. Ragaini, A. Oppezzo, S. Cenini, *J. Organomet. Chem.*, **690** (2005) 2142.
93. M. Frediani, D. Sémeril, D. Matt, L. Rosi, P. Frediani, F. Rizzolo, A. M. Papini, *Int. J. Polym. Sci.*, **2010** (2010) 490724.
94. M. Oshimura, A. Takasu, K. Nagata, *Macromolecules*, **42** (2009) 3086.
95. D. Liu, S. Lin, F. Zhu, H. Gao, Q. Wu, *Polym. Bul.*, **61** (2008) 71.
96. S. Nagayama, S. Kobayashi, *Angew. Chem., Int. Ed.*, **39** (2000) 567.
97. D. A. Tomalia, H. Baker, J. R. Dewald, M. Hall, G. Kallos, S. Martin, J. Roeck, J. Ryder, P. Smith, *Polym. J. (Tokyo)*, **17** (1985) 117.
98. D. A. Tomalia, H. Baker, J. R. Dewald, M. Hall, G. Kallos, S. Martin, J. Roeck, J. Ryder, P. Smith, *Macromolecule*, **19** (1986) 2466.
99. A. J. L. Villaraza, A. Bumb, M. W. Brechbiel, *Chem. Rev.*, **110** (2010) 2921.
100. S.-H. Hwang, C. D. Shreiner, C. N. Moorefield, G. R. Newkome, *New J. Chem.*, **31** (2007) 1192.
101. V. Balzani, G. Bergamini, P. Ceroni, F. Vögtle, *Coordin. Chem. Rev.*, **251** (2007) 525.
102. O. Bourrier, A. K. Kakkar, *Macromol. Symp.*, **209** (2004) 97.

103. R. van Heerbeek, P. C. J. Kamer, P. W. N. M. van Leeuwen, J. N. H. Reek, *Chem. Rev.*, **102** (2002) 3717.
104. A. W. Bosman, H. M. Janssen, and E. W. Meijer *Chem. Rev.*, **99** (1999) 166.
105. R. Malgas-Enus, S. F. Mapolie, G. S. Smith, *J. Organomet. Chem.*, **693** (2008) 2279.
106. R. Malgas, S. F. Mapolie, S. O. Ojwach, G. S. Smith, J. Darkwa, *Catal. Commun.*, **9** (2008) 1612.
107. G. Smith, R. Chen, S. Mapolie, *J. Organomet. Chem.*, **673** (2003) 111.
108. R. Marx, H.-W. Moulines, F. Wagner, T. Astruc, D. Hexaki. *Angew. Chem.: Int. Ed. Engl.*, **35** (1996) 1701.

Chapter 2 : Synthesis and Characterization of Salicylaldimine and Pyrrolyaldimine Schiff Base Ligands

2.1: Introduction

Schiff bases ligands have been extensively employed in the stabilization of transition metal complexes since the 19th century in coordination chemistry.^{1, 2} Salicylaldimine and pyrrole-imine are Schiff base type ligands with N,O and N,N donor atoms respectively.

Dendrimers are highly branched and well defined macromolecules. This class of macromolecules was developed independently by Tomalia *et al.*³ and Fréchet *et al.*⁴ The main structural regions of a dendrimer are the central core, the internal branching layers and the peripheral end groups, Figure 2.1. The core greatly impacts on the shape of dendrimers.

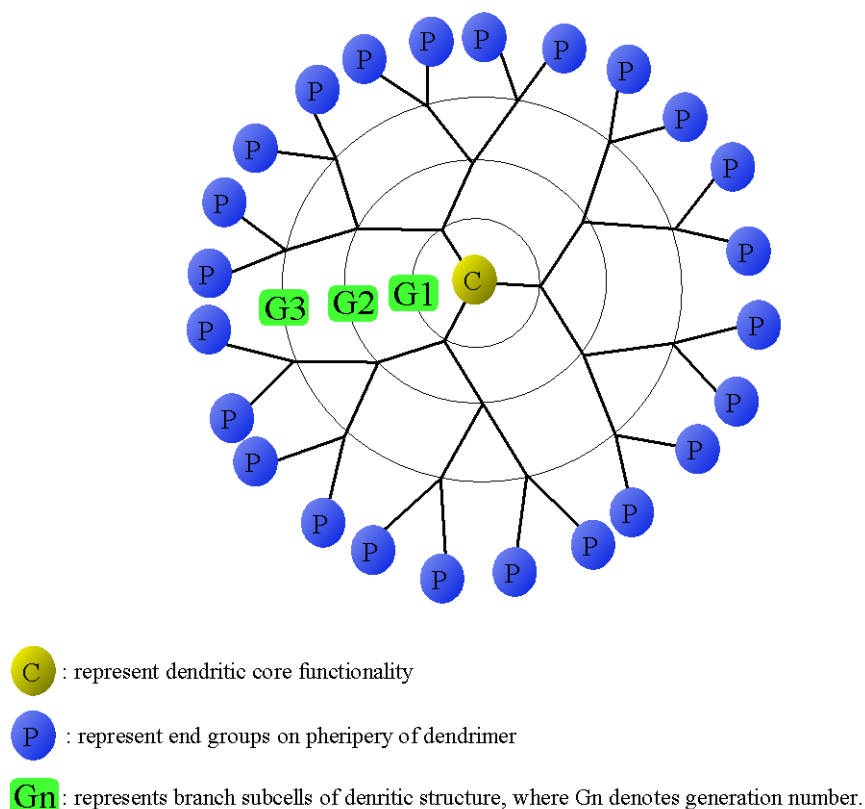


Figure 2.1: General structure of a dendrimer

Hecht and Fréchet outlined various dendrimer architectures, spheroid, ellipsoid or cylindrical, determined by the geometrical shape of the core.⁵ The repeat branching layers are regular and specific thus allowing for a globular and three-dimensional macromolecule.

These structural features impart the physical, chemical and electronic properties of the dendrimer which differ from those of the corresponding linear analogues.⁶⁻¹²

From on-going research into dendrimers and their applications in coordination chemistry, it has become clear that metallic moieties can be attached at various points in the dendrimer *viz* at the core, the branching points or on the periphery. This gives rise to metallodendrimers whose synthesis and applications have been growing in the recent years and a number of reviews on the subject have appeared.¹³ These materials show potential in a number of applications.^{14, 15}

Periphery (terminal)-functionalized, dendritic catalysts have their active sites located at the surface of the dendrimer supports, and these active sites are therefore directly available to the substrate. Several of these types of dendrimers have been reported. They have become popular in the recent years because they contain many coordination sites that can be used as catalysts, components of molecular electronic and photochemical devices and are thought to possess interesting electronic, magnetic, optical and catalytic properties.¹⁶

In Chapter 1 various methods used to heterogenise homogeneous catalysts were highlighted. Amalgamation of homogeneous and heterogeneous catalytic systems into a single system would be a gateway to greener chemistry which would incorporate the advantages of the two systems. These advantages are mainly the selectivity of the homogeneous catalyst and the easy separation of the heterogeneous analogues. It is hypothesized that dendrimers may be able to combine the advantages of these two catalytic systems into a single entity.

Diaminobutane-poly(propyleneimine) or (DAB-PPI-(NH₂)_n) dendrimers are commercially available up to several generations. The first generation [DAB-PPI-(NH₂)₄], Figure 2.2, has a diaminobutane core with 4 terminal amino, groups. These amino groups can be functionalized and subsequently converted to metallodendrimers using appropriate

metal precursors. Several of this type of nitrogen rich dendrimers have been prepared and characterized by various analytical methods.^{17,18}

In this chapter, we report the synthesis and characterization of monofunctional and multifunctional (dendritic) salicylaldimine and pyrrolylaldimine ligands. The monofunctional ligands are derived from monofunctional amines and have an aliphatic substituent on the imino nitrogen while the multifunctional ligands are based on 1st and 2nd generation poly(propyleneimine) dendrimers, DAB-PPI-(NH₂)_n (n = 4 or 8). The propyl functionality at the imino nitrogen was chosen in the mononuclear ligands because it corresponds to the branching unit in the dendrimer backbone. In addition, a pyrrole-imine ligand system with the aromatic substituent on the imino nitrogen is also reported in this chapter. These Schiff base ligands were characterized using NMR and FT-IR spectroscopy, ESI mass spectrometry and elemental analysis.

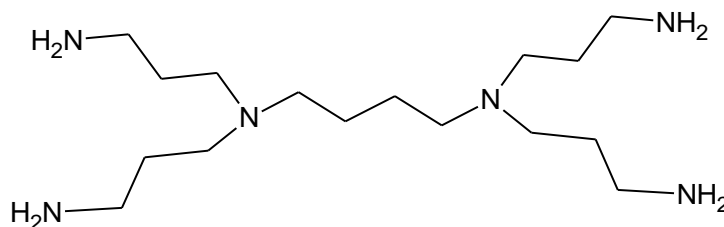


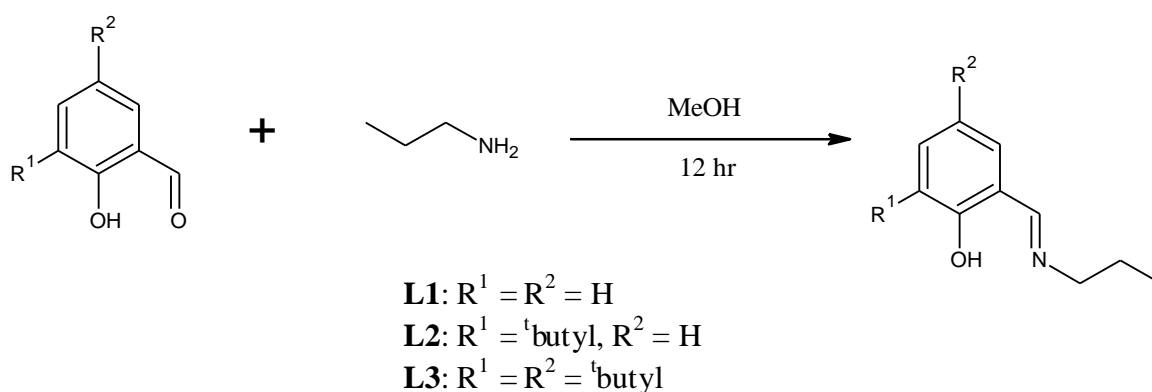
Figure 2.2: 1st Generation poly (propylene imine) dendrimer, DAB-PPI-(NH₂)₄

2.2: Results and discussion

2.2.1: *Synthesis and characterization of the monofunctional aliphatic salicylaldimine ligands, L1 – L3*

The monofunctional ligands were prepared using a published protocol for **L1** with slight modification, (Scheme 2.1).¹⁹ The ligands **L1** - **L3** were prepared by reacting propyl amine with the appropriate aldehyde; 2-hydroxybenzaldehyde, 3-^tbutyl-2-hydroxybenzaldehyde and 3, 5-^tbutyl-2-hydroxybenzaldehyde respectively in dry

methanol. A ratio of 1:1, amine to the aldehyde was used. These ligands were obtained in moderate to high yields (60 – 80 %) as yellow-orange oils with **L3** being the most viscous. These ligands were soluble in common organic solvents including pentane and hexane. They are stable even when stored at room temperature for prolonged time. The products were characterized by FT-IR and NMR spectroscopy, mass spectrometry and elemental analysis.



Scheme 2.1: Synthetic route to the monofunctional salicylaldehyde ligands, **L1 – L3**

FT-IR spectroscopy data for L1- L3

From the FT-IR (ATR) spectra obtained, it was clear that condensation had occurred due to the presence of the $\nu(\text{C}=\text{N})$ stretching vibration observed at 1630 cm^{-1} for **L1**, 1633 cm^{-1} for **L2** and 1630 cm^{-1} for **L3**. Another significant band was that of the $\nu(\text{C}-\text{O})$ at 1277 , 1266 , and 1253 cm^{-1} for **L1 – L3** respectively, Table 2.3. The values obtained for **L1** compare favourably with those reported in literature for the same compound.¹⁹

NMR spectroscopy data for L1 - L3

The most characteristic signal in the ^1H -NMR spectrum of **L1** was that of the imine ($\text{N}=\text{CH}$) proton observed at $\delta\ 8.23\text{ ppm}$. The other proton signals were at $\delta\ 0.96\text{ ppm}$ for the terminal CH_3 of the propyl chain, $\delta\ 1.66\text{ ppm}$ for the central CH_2 at the center and $\delta\ 3.47\text{ ppm}$

for the CH_2 adjacent to the imine. The signals of the aromatic protons were assigned as δ 7.27 ppm for the CH proton next to carbon containing the OH and δ 7.19 ppm for the CH next to the carbon bonded to the imine system. The other two aromatic protons are observed at δ 6.96 and δ 6.83 ppm while that of the OH was observed at δ 13.68 ppm. Characterization data is summarised in Table 2.1. This compares favourably with that of a similar compound reported by Torzilli *et al.*¹⁹

Similar spectra are obtained for the other two monofunctional ligands with the imine proton resonances, $\text{HC}=\text{N}$, at δ 8.38 and δ 8.37 ppm for **L2** and **L3** respectively. Additional peaks for the *ortho*-^tbutyl protons are observed at δ 1.53 ppm for **L2** while those of **L3** are observed at δ 1.49 ppm for the *ortho*-^tbutyl protons and δ 1.34 ppm for the *para*-^tbutyl. The phenolic OH group resonance appears at 14.29 ppm in **L2** and 14.02 ppm in **L3**. The downfield shift in **L2** can also be attributed to the intramolecular hydrogen bonding interaction that have been observed for other Schiff base ligands.²⁰

In the ^{13}C -NMR spectrum, the signal for the terminal $-\text{CH}_3$ carbon in the propyl chain is at δ 11.31 ppm for **L1**, δ 23.71 ppm for the CH_2 at the center and δ 60.71 ppm for the CH_2 adjacent to the imine. The imine carbon signal is observed at δ 164.30 ppm while the aromatic carbon signals are those at δ 161.20, 131.65, 130.85, 118.45, 117.96 and δ 116.62 ppm. The ^{13}C -NMR data for **L1**, **L2** and **L3** are summarised in Table 2.2. The ^{13}C -NMR data for **L2** and **L3** also illustrate the presence of ^tbutyl groups.

Electron spray ionisation mass spectrometry (ESI-MS) data for L1- L3

The molecular weight of these ligands was also confirmed by mass spectrometry and micro analysis, the data is summarised in Table 2.3. Singly charged molecular ion peak of the predicted compounds was observed for each of the ligands. Under the conditions used to record electron spray ionisation mass spectra (ESI-MS), very little fragmentation was

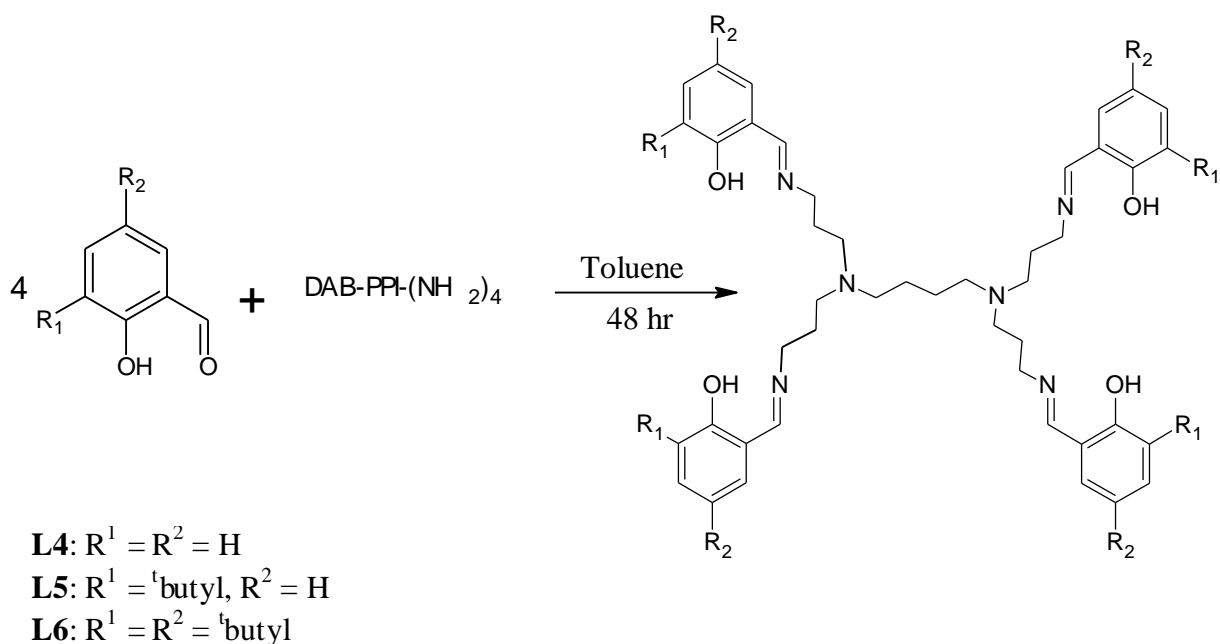
observed for these ligands. The purity was also confirmed by elemental analysis as well as TLC where only one spot was observed on the plate.

2.2.2: Synthesis and characterization of the multifunctional (dendrimeric) salicylaldimine ligands, L4 – L9

A series of dendritic salicylaldimine peripheral functionalized ligands were obtained by condensation of commercially available DAB-PPI-(NH₂)_n where n = 4 or 8 with the appropriate 2-hydroxybenzaldehyde, Scheme 2.2 and Figure 2.3. After purification and recrystallization, the 1st generation ligands, **L4 - L6**, were obtained as yellow solids while the 2nd generation analogues, **L7 - L9** were isolated as viscous yellow oils. These ligands are completely soluble in most organic solvents except hexane and pentane. The dendrimeric ligands were characterized using various analytical techniques such as NMR, FT-IR, mass spectrometry and micro analysis.

FT-IR spectroscopy data for L4 - L6

The FT-IR (ATR) spectra of all the dendritic ligands were acquired under similar conditions and the main peaks are summarized in Table 2.3. The spectra showed a strong band between 1630 - 1632 cm⁻¹ unambiguously assignable to the $\nu(\text{C}=\text{N})$ stretching vibration band. The presence of this band clearly signifies that condensation had occurred. These spectra are similar to those previously reported for **L4** and **L6**.^{21, 22}



Scheme 2.2: Synthetic route for 1st generation dendrimeric salicylaldehyde ligands, **L4 – L6**

NMR spectroscopy data for L4 - L6

The ¹H-NMR spectra of these dendrimeric ligands were acquired in CDCl₃ and the data are summarized in Table 2.1. This ¹H-NMR data complements the FT-IR results obtained. The spectrum of **L4** exhibits a singlet at δ 8.32 ppm for the imine (HC=N) proton and a broad peak for the phenolic OH proton at δ 13.57 ppm. Another very significant peak that confirmed condensation was that of the methylene protons adjacent to the imine. These protons resonated at δ 3.61 as compared to δ 2.61 ppm for the CH₂ next to the NH₂ in the starting DAB-PPI-(NH₂)₄. The dendrimer core protons resonate at δ 1.40 ppm (-NCH₂CH₂-), while the central methylene protons in the 1st tier branches are observed at δ 1.81 ppm (-NCH₂CH₂-). The signals at δ 2.40 and δ 2.50 ppm can be assigned to the core and 1st tier branching methylene protons next to the nitrogens in the dendrimer, (-NCH₂CH₂-). The broadening of the peaks is due to overlapping of a number of protons that are chemically equivalent and also due to the restricted mobility of the dendrimer scaffold. Similar observations were made by Haba *et al.*²³ regarding signal broadening of the proton signals of

the interior segment of periphery modified methacroyl PAMAM dendrimers. In the aromatic region, four signals are observed and are discussed herein with reference to the OH group. The proton in the *ortho* position resonates at δ 7.21 ppm, that in the *meta* position at δ 6.95 ppm while that in the *para* position is at δ 6.85 ppm. The other peak at δ 7.29 ppm is that of the proton attached to the imino moiety. In some cases, long range coupling is also evident, Table 2.1.

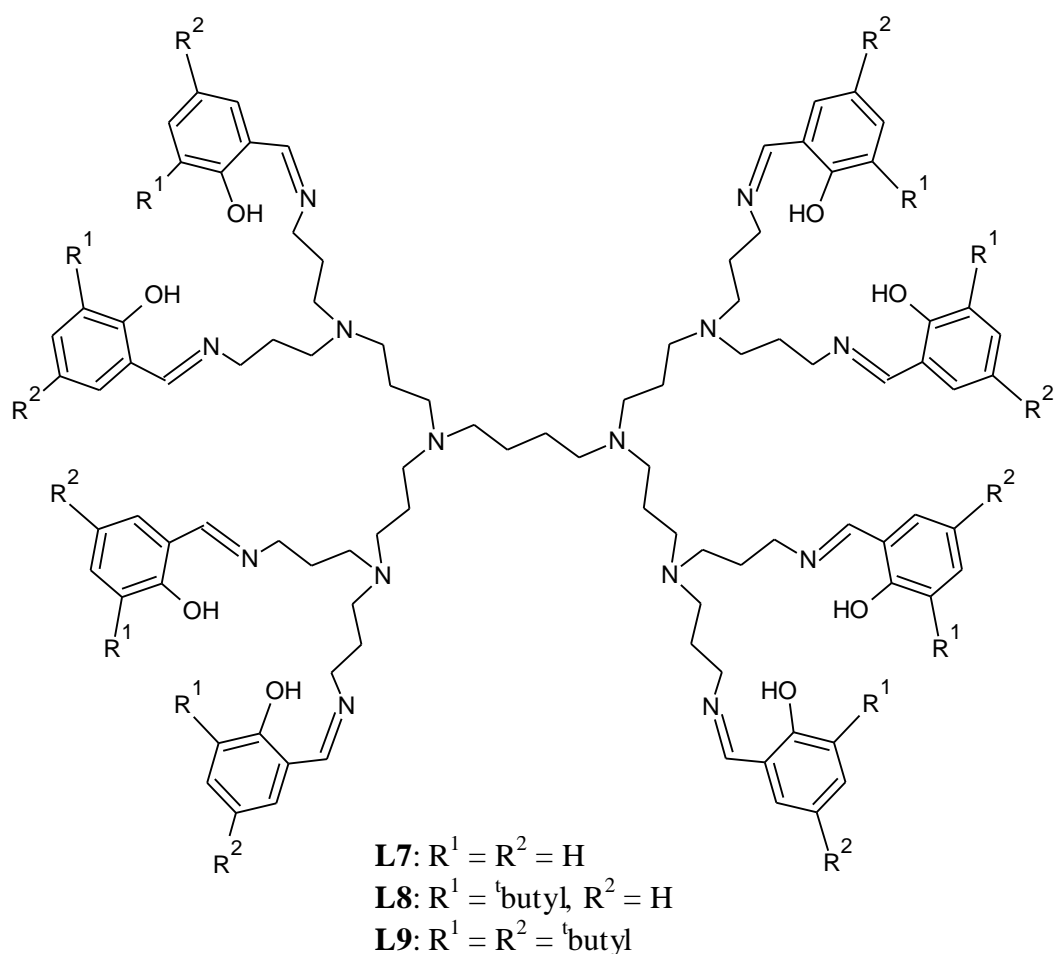


Figure 2.3: 2nd Generation dendritic salicylaldimine ligand, **L6 – L9**

The other two G1 dendritic ligands gave similar spectra to that of **L4** exhibiting singlets between δ 8.29 and 8.38 ppm for the imine proton. The phenolic OH proton resonance appeared at δ 14.17 ppm in **L5** and δ 13.93 ppm in **L6**. The presence of this signal in the spectra of all three ligands indicates the phenol-imine tautomer is dominant for the dendritic

ligands. The difference in appearance of the signal can be attributed to the electron donating ability of the ^tbutyl groups as well as the presence of intramolecular hydrogen bonding.²⁴ Thus **L5** signal for the phenolic OH proton appears more deshielded than in the other two ligands.

In addition **L5** showed a singlet at δ 1.45 ppm for the ^tbutyl methyl protons while **L6** showed two singlets at δ 1.48 and 1.34 ppm for the ^tbutyl methyl protons at positions 3 and 5.

Similar data was obtained for the 2nd generation analogues, **L7 – L9**, and ¹H-NMR data is summarised in Table 2.1. The imine proton resonated at between δ 8.29 – 8.38 ppm while that of the phenolic proton was observed at between δ 13.5 – 14.2 ppm. The spectrum for **L8** showed a singlet at δ 1.48 ppm for the ^tbutyl methyl protons while that for **L9** gave two singlets for the ^tbutyl methyl protons at δ 1.48 and 1.34 ppm. These spectra also showed that these ligands are symmetrical.

In the ¹³C- NMR spectra, the carbon signal of the imine (HC=N) appears between δ 164.81 and 165.79 ppm while that of the carbon bonded to the phenolic group is between δ 158.2 to 161.2 ppm in the 1st and 2nd generation salicylaldimine dendritic ligands. The other aromatic carbon signals appear in the range δ 116 - 139 ppm for the six ligands. The dendritic framework carbon signals appear in between δ 24.5 and 57.3 ppm.²⁵

Mass spectrometry data for L4 – L9

The dendritic ligands were investigated using ESI-MS as well as Matrix-assisted laser desorption ionisation time of flight mass spectrometry (MALDI-TOF) to establish their molecular weights. It must be noted that the analysis for the 1st and 2nd generation ligands was done under similar conditions.

The ESI-MS spectra obtained confirmed the molecular weight of some of the dendritic ligands with a molecular weight < 2000 Da. The ESI-MS spectra for **L5** and **L8** shown in Figure 2.4 and 2.5 are given as examples. 1st generation ligands, **L4** - **L6**, gave singly charged parent ions corresponding to the expected molecular weights of the ligands.

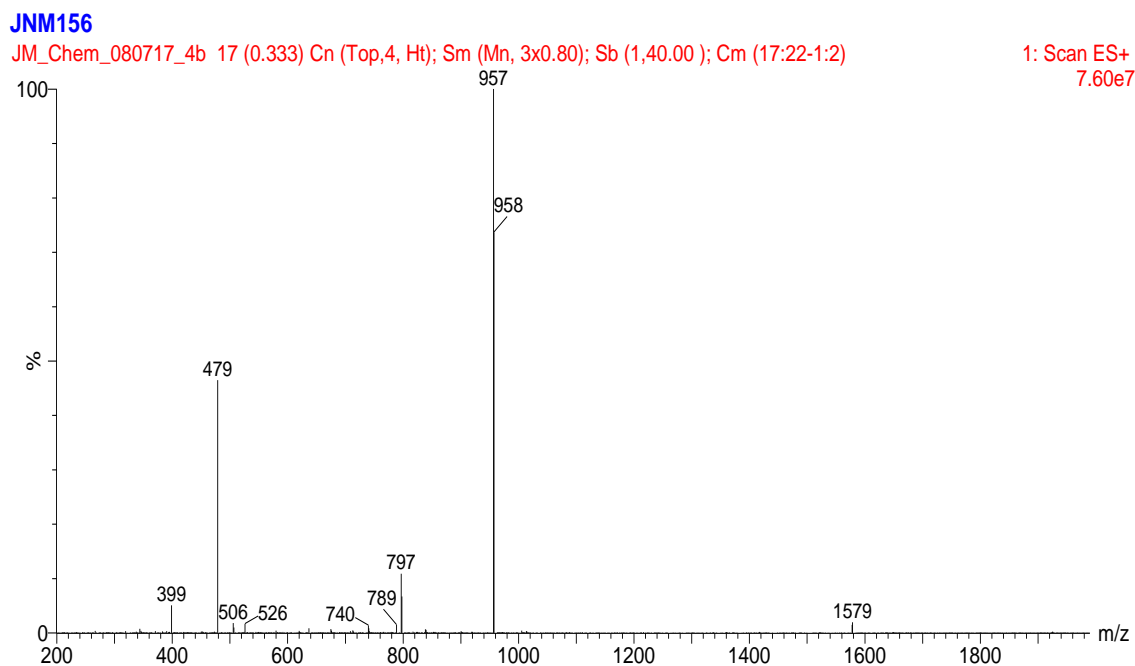


Figure 2.4: ESI mass spectrum of the **L5** showing $[M+H]^+$ and $[M+H]^{2+}$

These ligands also showed fragments due to the hydrolysis of the imine bond of one of the salicylaldimine units as well as a multiply doubly charged ions. For example in Figure 2.4, a singly charged parent ion of **L5** was obtained at m/z 957, doubly charged ion at m/z 479 and a fragment due to the loss of one salicylaldimine unit at m/z 797.

In the 2nd generation ligands, **L7** – **L9**, only multiply charged ions (m/z where $z = 2, 3 - 4$) and daughter ions arising from the ligand molecular ions were obtained where the molecular weight exceeded m/z 2000. The base peak was that of the doubly charged ion. Other ions observed were the quaternary ammonium ions formed after cleavage at one of the dendrimer scaffold nitrogen followed by cyclization of the *n*-butyl to form a pyrrolidinium

group. In Figure 2.5 multiply charged ions are observed at m/z 1027, 685, 514 and 411 where $z = 2, 3, 4$ and 5 respectively. The quaternary ammonium ion was also observed at m/z 1054. A proposed fragmentation pattern is shown in Scheme 2.3.

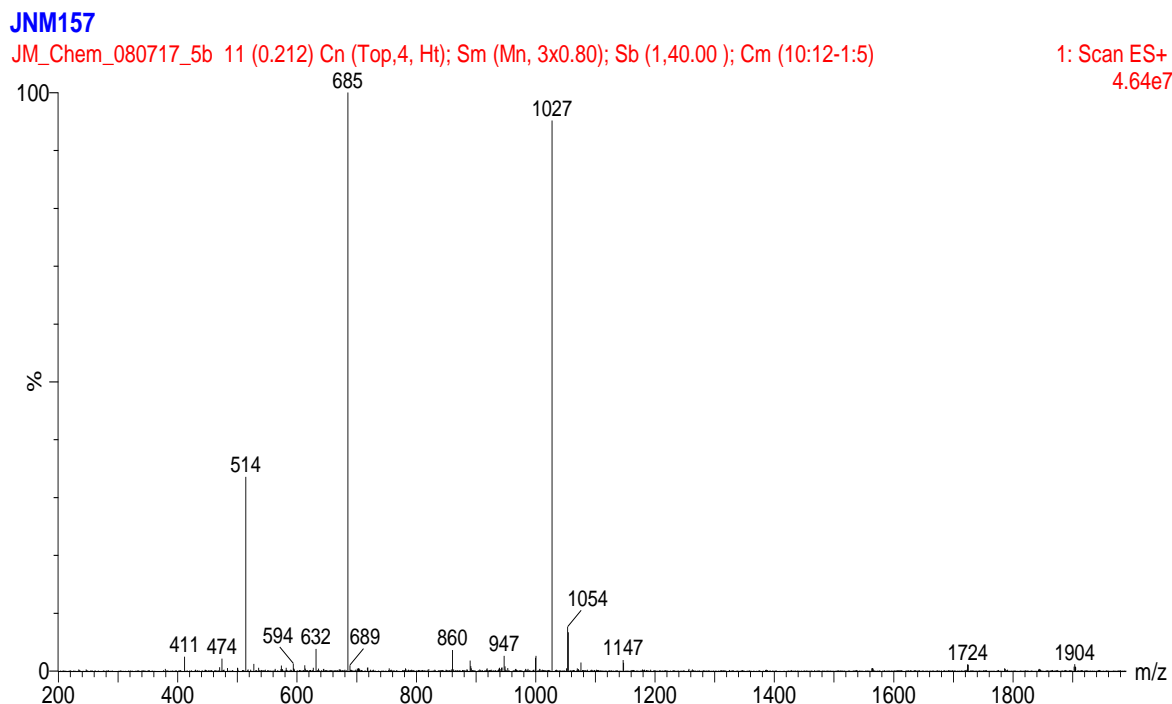
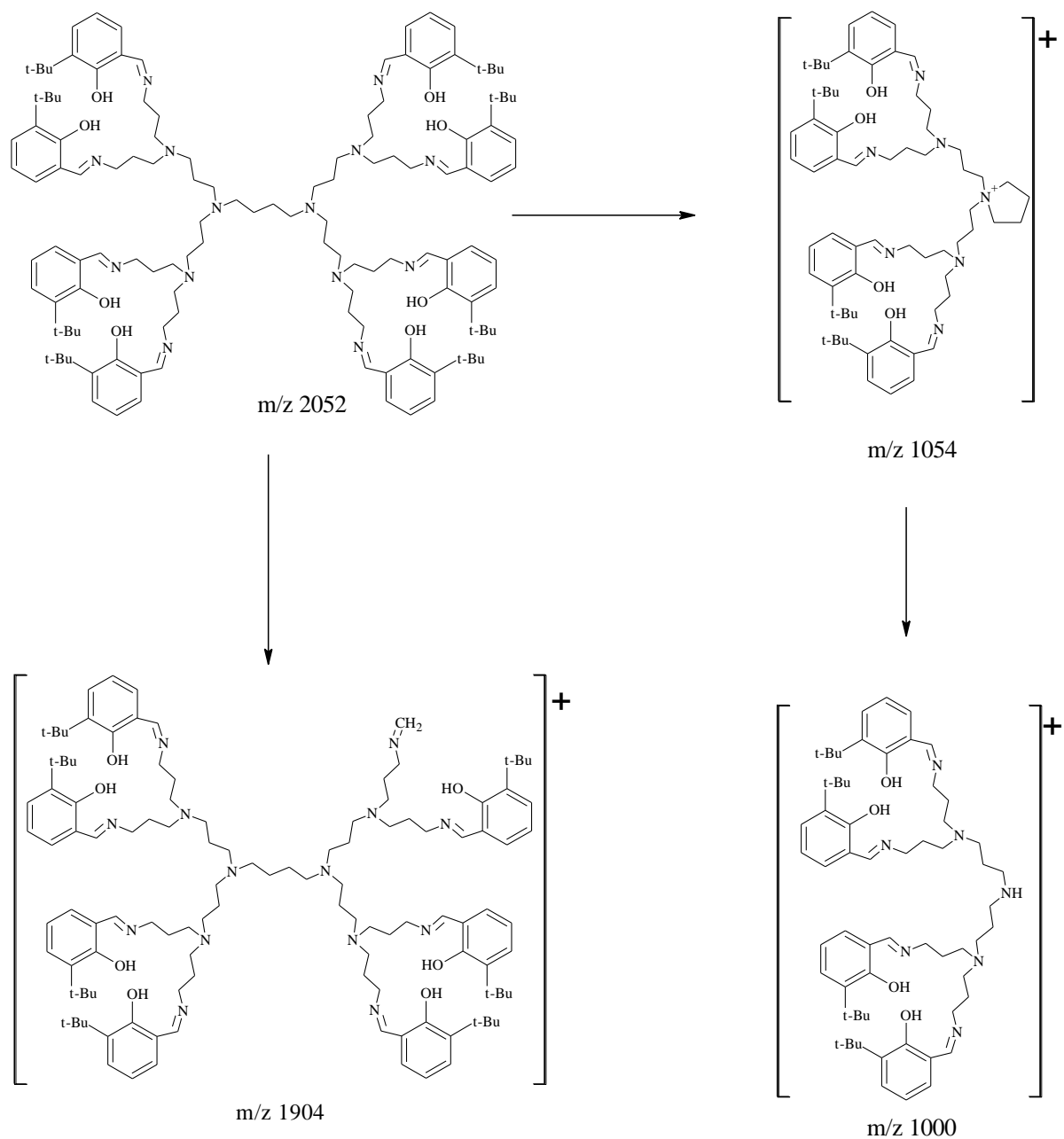


Figure 2.5: ESI mass spectrum of the **L8** showing $[M+H]^{2+}$, $[M+H]^{3+}$ and $[M+H]^{4+}$

The molecular weight of these dendritic ligands was also confirmed by MALDI-TOF. In the spectra obtained, the base peak was that of the expected 1st generation ligands and a doubly charged species for the 2nd generation ones. The main advantage of the MALDI-TOF spectra was that for the 2nd generation dendritic ligands, a peak for the single charged ion was observed irrespective of the ligands molecular weight. Elemental analysis data obtained for these ligand systems were in agreement with proposed formulations as shown in Scheme 2.2 and Figure 2.3.^{26,27}



Scheme 2.3: Significant fragment ion of **L8** as inferred from ESI-MS

Single crystal diffraction (SXR)

After recrystallization **L5** gave analytically pure yellow single crystals good for single crystal X-ray diffraction (SXR). The crystal structure of **L5** is shown in Figure 2.6. The ligand crystallizes in the triclinic space group *P*-1 ($Z = 4$) with a twofold center of inversion at the two C16 center. The bond distance of the C=N bond of 1.2752(17) Å is similar to

those of published monofunctional Schiff base salicylaldehyde ligands (1.281 Å).²⁸ Hydrogen bonding between the imino nitrogen and the phenolic hydrogen is observed, N1·····H1-O1 and O2-H3·····N3. The presence of hydrogen bonding is further supported by the other characterization data. **L5** a higher melting point of 95-97 °C as compared to the other G1 ligands and from the ¹H-NMR data, the phenolic OH peak was slightly deshielded as compared to the other two ligands **L4** and **L6**.

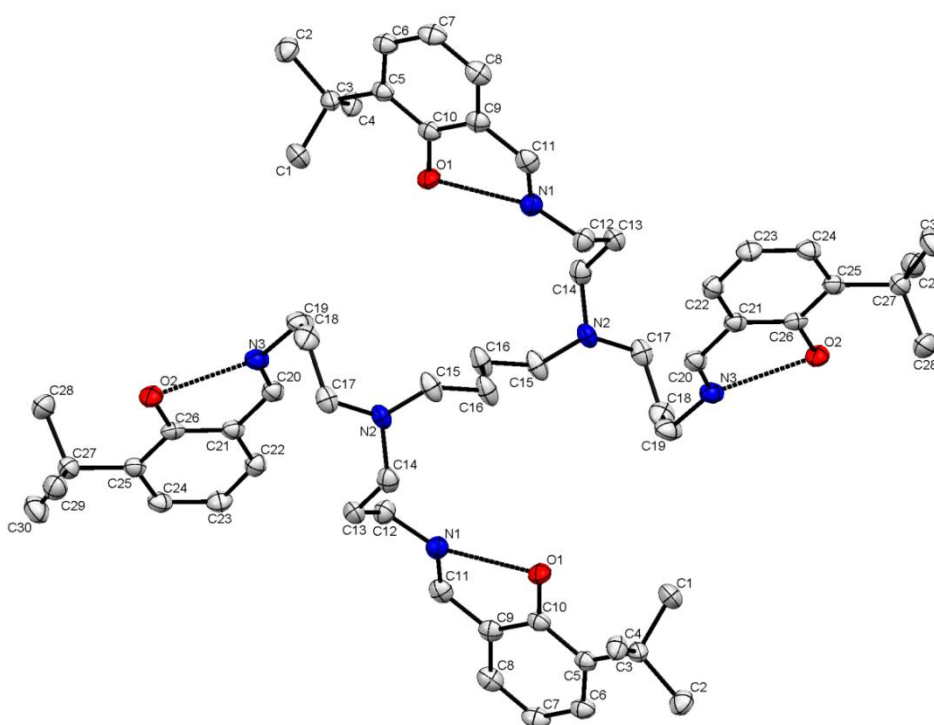


Figure 2.6: The molecular structure of **L5** with the atom-numbering scheme. Displacement ellipsoids are drawn at the 30% probability. H atoms omitted for clarity

A thermal ellipsoid diagram of the ligand is shown in Figure 2.6. Crystal structural data and structure refinement parameters are shown in Table 2.4 while selected bond lengths and angles are shown in Table 2.5.

Table 2.1: $^1\text{H-NMR}^a$ data for the salicylaldehyde ligands^a

Ligand	<u>OH</u>	<u>HC=N</u>	<u>Ar-H</u>	<u>HC=NCH₂</u>	<u>CH₂</u>	<u>CH₃</u>	<u>C(CH₃)₃</u>
L1^b	13.68 (br s, 1H)	8.23 (s, 1H)	7.27 (dt, 1H, $^3J_{\text{HH}} = 7.2$ Hz) 7.19 (dd, 1H, $^3J_{\text{HH}} = 7.6$ Hz) 6.96 (d, 1H, $^3J_{\text{HH}} = 7.4$ Hz) 6.83 (dt, 1H, $^3J_{\text{HH}} = 7.5$ Hz)	3.47 (dt, 2H, $^3J_{\text{HH}} = 7.4$ Hz)	1.66 (m, 2H, $^3J_{\text{HH}} = 7.2$ Hz)	0.96 (t, 3H, $^3J_{\text{HH}} = 7.5$ Hz)	-
L2^b	14.29 (br s, 1H)	8.38 (s, 1H)	7.39 (dd, 1H, $^3J_{\text{HH}} = 7.8$ Hz) 7.15 (dd, 1H, $^3J_{\text{HH}} = 7.6$ Hz) 6.87 (t, 1H, $^3J_{\text{HH}} = 7.4$ Hz)	3.60 (dt, 2H, $^3J_{\text{HH}} = 7.5$ Hz)	1.80 (m, 2H, $^3J_{\text{HH}} = 7.2$ Hz)	1.06 (t, 3H, $^3J_{\text{HH}} = 7.4$ Hz)	1.53 (br s, 9H)
L3^b	14.02 (br s, 1H)	8.37 (s, 1H)	7.40 (d, 1H, $^4J_{\text{HH}} = 4.0$ Hz) 7.11 (d, 1H, $^4J_{\text{HH}} = 4.0$ Hz)	3.57 (dt, 2H, $^3J_{\text{HH}} = 7.4$ Hz)	1.76 (m, 2H, $^3J_{\text{HH}} = 7.2$ Hz)	1.01 (t, 3H, $^3J_{\text{HH}} = 7.4$ Hz)	1.49 (br s, 9H) 1.34 (br s, 9H)
L4	13.58 (br s, 4H)	8.32 (s, 4H)	7.29 (dt, 4H, $^3J_{\text{HH}} = 7.2$ Hz) 7.21 (dd, 4H, $^3J_{\text{HH}} = 7.6$ Hz) 6.95 (d, 4H, $^3J_{\text{HH}} = 7.2$ Hz) 6.85 (dt, 4H, $^3J_{\text{HH}} = 7.4$ Hz)	3.61 (t, 8H, $^3J_{\text{HH}} = 6.3$ Hz)	2.50 (t, 8H, $^3J_{\text{HH}} = 7.0$ Hz) 2.40 (br s, 4H) 1.81 (m, 8H, $^3J_{\text{HH}} = 6.9$ Hz) 1.40 (br s, 4H)	-	-
L5	14.17 (br s, 4H)	8.33 (s, 4H)	7.32 (d, 4H, $^3J_{\text{HH}} = 7.8$ Hz) 7.08 (d, 4H, $^3J_{\text{HH}} = 7.4$ Hz) 6.80 (dt, 4H, $^3J_{\text{HH}} = 7.4$ Hz)	3.62 (t, 8H, $^3J_{\text{HH}} = 6.7$ Hz)	2.54 (t, 8H, $^3J_{\text{HH}} = 6.9$ Hz) 2.44 (br s, 4H) 1.84 (m, 8H, $^3J_{\text{HH}} = 6.8$ Hz) 1.45 (br s, 4H)	-	1.45 (br s, 36H)

Table 2.1: continued

L6	13.93 (br s, 4H)	8.35 (s, 4H)	7.37 (d, 4H, $^4J_{\text{HH}} = 4.0$ Hz)	3.60 (t, 8H, $^3J_{\text{HH}} = 6.5$ Hz)	2.53 (t, 8H, $^3J_{\text{HH}} = 7.0$ Hz)	1.45 (br s, 36H)	
			7.07 (d, 4H, $^4J_{\text{HH}} = 4.0$ Hz)		2.43 (br s, 4H)		1.34 (br s, 36H)
					1.83 (m, 8H, $^3J_{\text{HH}} = 7.0$ Hz)		
					1.45 (br s, 4H)		
L7	13.57 (br s, 8H)	8.29 (s, 8H)	7.27 (dt, 8H, $^3J_{\text{HH}} = 7.1$ Hz)	3.58 (t, 16H, $^3J_{\text{HH}} = 6.6$ Hz)	2.50 (t, 16H, $^3J_{\text{HH}} = 7.0$ Hz)		
			7.20 (dd, 8H, $^3J_{\text{HH}} = 7.7$ Hz)		2.45 (br m, 20H)		
			6.95 (d, 8H, $^3J_{\text{HH}} = 7.8$ Hz)		1.80 (br m, 16H)		
			6.83 (dt, 8H, $^3J_{\text{HH}} = 7.4$ Hz)		1.57 (br m, 8H); 1.40 (br s, 4H)		
L8	14.18 (br s, 8H)	8.34 (s, 8H)	7.34 (d, 8H, $^3J_{\text{HH}} = 7.8$ Hz)	3.63 (t, 16H, $^3J_{\text{HH}} = 6.5$ Hz)	2.57 (t, 16H, $^3J_{\text{HH}} = 6.8$ Hz)	1.48 (br s, 72H)	
			7.09 (d, 8H, $^3J_{\text{HH}} = 7.8$ Hz)		2.49 (br m, 20H)		
			6.82 (t, 8H, $^3J_{\text{HH}} = 7.7$ Hz)		1.87 (br m, 16H)		
					1.64 (br, 8H)		
					1.48 (br s, 4H)		
L9	13.94 (br s, 8H)	8.38 (s, 8H)	7.41 (d, 8H, $^4J_{\text{HH}} = 4.0$ Hz)	3.62 (t, 16H, $^3J_{\text{HH}} = 6.6$ Hz)	2.57 (t, 16H, $^3J_{\text{HH}} = 7.0$ Hz)	1.48 (br s, 72H)	
			7.10 (d, 8H, $^4J_{\text{HH}} = 4.0$ Hz)		2.47 (br m, 20H)		1.34 (br s, 72H)
					1.86 (br m, 16H)		
					1.63 (br, 8H); 1.48 (br s, 4H)		

^a 300 MHz (CDCl₃, δ in ppm), ^b 400 MHz (CDCl₃, δ in ppm), s = singlet, d = doublet, dd = doublet of doublets, t = triplet, dt = doublet of triplets, m = multiplet, br = broad

Table 2.2: $\{^1\text{H}\}^{13}\text{C}$ -NMR shifts (δ in ppm) data for the salicylaldehyde ligands^a

Ligand	<u>HC=N</u>	<u>C-OH</u>	<u>Ar-C</u>	<u>HC=NCH₂</u>	<u>CH₂</u>	<u>CH₃</u>	<u>C and (CH₃)₃</u>
L1^b	164.30	161.20	131.65, 130.85, 118.45, 117.96, 116.62	60.71	23.71	11.31	-
L2^b	165.20	160.65	137.38, 129.42, 129.08, 118.65, 117.56	61.22	24.10	11.79	34.80, 29.33
L3^b	165.55	158.25	139.79, 136.65, 126.62, 125.64, 117.85	61.29	24.14	11.78	34.74, 34.28, 31.51, 29.31
L4	164.81	161.27	132.01, 131.08, 118.74, 118.37, 116.95	57.36	53.93, 51.38, 28.44, 25.12	-	-
L5	165.47	160.56	137.32, 129.45, 129.12, 118.62, 117.61	57.33	54.03, 51.39, 28.48, 25.23	-	34.79, 29.33
L6	165.75	158.14	139.74, 136.55, 126.57, 125.61, 117.81	57.45	53.99, 51.43, 28.50, 25.12	-	34.96, 34.03 31.34, 29.40
L7	165.79	158.21	139.82, 136.64, 126.62, 125.65, 117.89	57.50	54.10, 51.55, 28.64, 25.22	-	-
L8	165.48	160.51	137.28, 129.47, 129.13, 118.59, 117.63	57.40	52.25, 52.17, 51.46, 28.50, 25.19, 24.60	-	34.78, 29.33
L9	165.73	158.15	139.81, 136.59, 126.63, 125.67, 117.84	57.60	54.19, 52.22, 51.57, 28.56, 24.62, 24.54	-	34.98, 34.08, 31.32, 29.45

^a75 MHz (CDCl₃, δ in ppm), ^b 100 MHz (CDCl₃, δ in ppm),

Table 2.3: Salicylaldehyde ligands analytical data

Ligand	Yield (%)	M.p (°C) ^a	Formula	ES-MS m/z = [M+H] Found (Calcd.)	FT-IR (cm ⁻¹)		Anal Found (Calcd.)		
					ν(C=N)	ν(C-O)	C	H	N
L2	61	oil	C ₁₄ H ₂₁ N O•0.5 CH ₃ OH	220 (219)	1633	1266	74.20 (74.00)	9.67 (9.34)	4.51 (5.95)
L3	70	oil	C ₁₈ H ₂₉ N O	276 (275)	1630	1272	78.99 (78.49)	10.30 (10.61)	4.78 (5.09)
L4	61	48-51	C ₄₄ H ₅₆ N ₆ O ₄ •0.25CH ₂ Cl ₂	733 (732)	1630	1281	71.01 (70.47)	7.37 (7.55)	11.17 (11.14)
L5	83	95-98	C ₆₀ H ₈₈ N ₆ O ₄	957 (956)	1632	1264	75.49 (75.27)	7.78 (9.26)	8.85 (8.78)
L6	68	66-69	C ₇₆ H ₁₂₀ N ₆ O ₄	1181 (1180)	1631	1272	77.24 (77.23)	8.35 (10.23)	6.79 (7.11)
L7	72	oil	C ₉₆ H ₁₂₈ N ₁₄ O ₈ •0.5CH ₂ Cl ₂	1605 (1604)	1630	1277	70.74 (71.05)	7.97 (8.00)	10.84 (12.02)
^b L8	77	oil	C ₁₂₈ H ₁₉₂ N ₁₄ O ₈ •0.5CH ₂ Cl ₂	1027 (2052)	1631	1271	73.27 (73.59)	9.15 (9.34)	8.67 (9.31)
^b L9	80	oil	C ₁₆₀ H ₂₅₆ N ₁₄ O ₈ •0.5CH ₂ Cl ₂	1251 (2500)	1630	1277	75.66 (75.55)	10.10 (9.80)	7.67 (6.57)

^a Uncorrected melting points, ^bDoubly charged ion, n. d. = not determined

Table 2.4: Crystal structural data (collection, structure solution and refinement) for **L5**

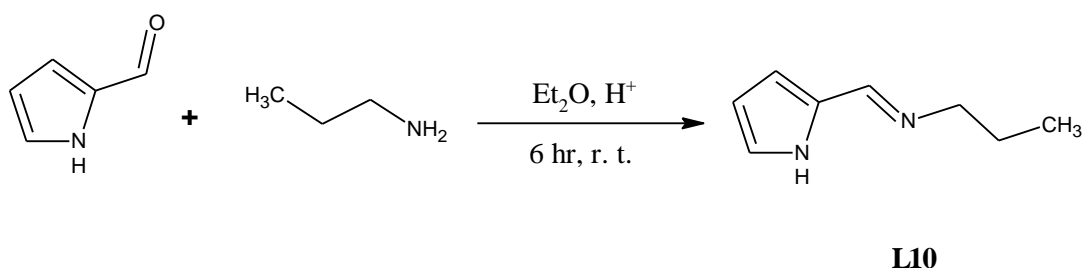
Empirical formula	$C_{60}H_{88}N_6O_4$	
Formula weight	957.36	
Crystal system	triclinic	
Space group	$P-1$	
Crystal size (mm^3)	0.55 x 0.41 x 0.37	
Z	1	
Unit cell dimensions (\AA , $^\circ$)	$a = 10.4099(7)$	$\alpha = 94.7070(10)$
	$b = 10.5303(8)$	$\beta = 99.5130(10)$
	$c = 13.5072(10)$	$\gamma = 106.5280(10)$
Volume (\AA^3)	1386.84(17)	
Absorption coefficient (mm^{-1})	0.072	
Calculated density (g cm^{-3})	1.146	
F_{000}	522	
Temperature (K)	100(2)	
Wavelength	0.71073	
θ range for data collection ($^\circ$)	1.54 to 26.43	
Miller index ranges	$-13 \leq h \leq 13, -13 \leq k \leq 13, -16 \leq l \leq 16$	
Reflections collected	15010	
Independent reflections	5659 [$R_{\text{int}} = 0.0196$]	
Completeness to theta (%)	99.3	
Max. and min. transmission	0.9737 and 0.9617	
Refinement method	Full-matrix least-squares on F^2	
Data / restraints / parameters	5659 / 0 / 322	
Goodness-of-fit on F^2	1.053	
Final R indices [F^2 for $I \geq 2\sigma$]	$R1 = 0.0444, wR2 = 0.1170$	
R indices (all data)	$R1 = 0.0496, wR2 = 0.1218$	
Largest diff. peak and hole (e \AA^{-3})	0.342 and -0.156	

Table 2.5: Selected bond lengths and bond angles for **L5**

Bond lengths [Å]		Bond Angles [°]	
O(1)-C(10)	1.3519(15)	C(11)-N(1)-C(12)	118.87(11)
O(2)-C(26)	1.3517(14)	N(1)-C(11)-C(9)	122.72(12)
N(1)-C(11)	1.2752(17)	N(1)-C(12)-C(13)	110.37(10)
N(1)-C(12)	1.4558(17)	C(15)-N(2)-C(14)	110.74(10)
N(2)-C(14)	1.4712(17)	C(15)-N(2)-C(17)	109.88(10)
N(2)-C(15)	1.4668(15)	C(14)-N(2)-C(17)	108.57(10)
N(2)-C(17)	1.4729(16)	N(2)-C(14)-C(13)	112.75(10)
N(3)-C(19)	1.4578(16)	N(2)-C(17)-C(18)	115.30(11)
N(3)-C(20)	1.2725(17)	N(2)-C(15)-C(16)	113.74(11)
C(12)-C(13)	1.5210(18)	N(3)-C(19)-C(18)	110.80(12)
C(13)-C(14)	1.5240(18)	N(3)-C(20)-C(21)	122.89(12)
C(15)-C(16)	1.5229(19)	O(1)-C(10)-C(5)	119.66(11)
C(17)-C(18)	1.5190(18)	O(1)-C(10)-C(9)	119.53(11)
C(18)-C(19)	1.5210(2)	O(2)-C(26)-C(21)	119.73(11)
		O(2)-C(26)-C(25)	119.66(11)
		C(6)-C(5)-C(10)	116.80(12)
		C(6)-C(5)-C(3)	121.63(11)
		C(10)-C(5)-C(3)	121.56(10)
		C(8)-C(9)-C(10)	119.64(12)
		C(8)-C(9)-C(11)	119.37(12)

2.2.3: Synthesis and characterization of the monofunctional (aliphatic and aromatic) pyrrole-imine ligands, **L10** and **L11**

The pyrrolylaldimine ligands were prepared by Schiff base condensation of pyrrole-2-carboxyaldehyde with the appropriate amine following a method we have reported previously.²⁹ **L10** was obtained in moderate yield (56 %) after condensation of pyrrole-2-carboxyaldehyde with one equivalent of propyl amine. The ligand showed good solubility in common organic solvents such as dichloromethane, diethyl ether, chloroform, tetrahydrofuran, acetonitrile as well as in toluene. Characterization was done using NMR and FT-IR spectroscopies, mass spectrometry and elemental analysis. **L10** is relatively stable and does not decompose on exposure to air even when in solution for prolonged periods.



Scheme 2.4: Synthetic route to N-[(1E)-1H-pyrrol-2-ylmethylene]propan-1-amine, **L10**

FT-IR spectroscopy data for **L10**

The FT-IR spectrum shows a characteristic band at 1636 cm^{-1} for the $\nu(\text{C}=\text{N})$ band as a sharp peak and at *ca.* 3100 cm^{-1} for the $\nu(\text{N}-\text{H})$ band, Table 2.7. The broadness of the latter peak can be attributed to intermolecular hydrogen bonding of the NH groups.³⁰

NMR spectroscopy data for **L10**

The ^1H -NMR spectrum of **L10** summarized in Table 2.6, showed signals at δ 0.92 ppm for the terminal CH_3 of the propyl chain, δ 1.68 ppm for the CH_2 at the center and δ 3.50 ppm

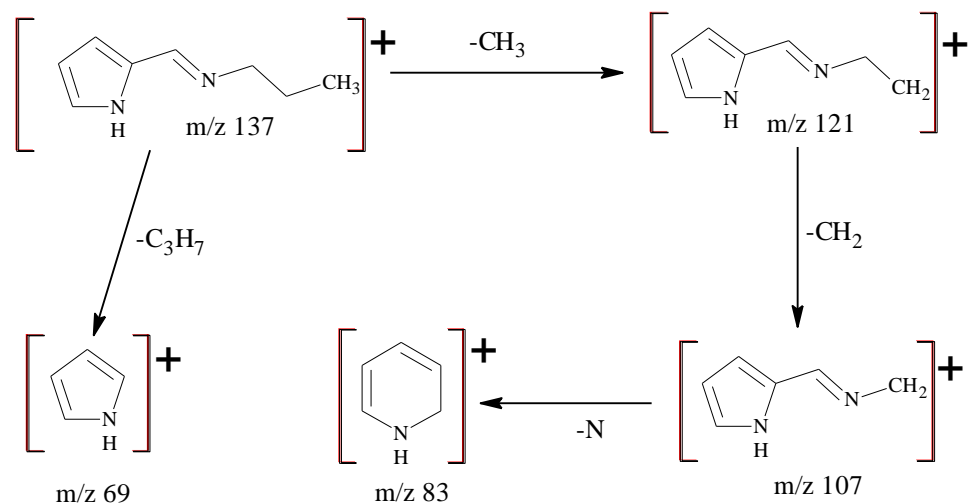
for the CH_2 adjacent to the imine functionality. The imine, $\text{N}=\text{CH}$, proton was observed at δ 8.04 ppm while those of the pyrrole ring can be assigned as δ 6.9 ppm for the CH proton next to NH , δ 6.2 ppm for the CH next to the carbon bonded to the imine system and δ 6.5 ppm for the CH in between. The NH proton signal was not observed in the spectrum. This may be due to the fact that the proton is exchangeable and thus may not be observed in the deuterated solvent.

In the ^{13}C -NMR spectrum, the terminal propyl chain's methyl carbon resonated at δ 11.7 ppm while that of the methylene to the imine bonded carbon at δ 62.7 ppm and the CH_2 carbon central at δ 24.3 ppm. The signals of the pyrrole ring carbons were observed at δ 121.4, 109.5, 113.7 and δ 130.1 ppm while that of the imino group was observed at δ 151.4 ppm.

Mass spectrometry and micro analysis data for L10

The elemental analysis data obtained agrees with that calculated % composition for the proposed structure of **L10** associated with 0.25 H_2O as shown in Table 2.7.

Electron impact mass spectrometry was used to characterize **L10** to establish the molecular weight. The spectrum obtained exhibited the fragmentation pattern shown in Scheme 2.4. A singly charged ion at m/z 137 corresponds to the molecular ion of **L10**. The fragmentation pattern shows the initial stepwise loss of the propyl chain followed by imino nitrogen forming a dihydropyridine ion, m/z 83. The base peak was observed at m/z 69 corresponding to pyrrole group formed after the loss *n*-propyl chain and the imine group.²⁷



Scheme 2.5: Fragmentation pattern for **L10** as inferred from the GC-MS

L11, Figure 2.8, is a previously reported compound and was obtained as a cream coloured crystalline solid from the Schiff base condensation of pyrrole -2-carboxyaldehyde with 2, 6-diiisopropyyl aniline in a 1:1 ratio in diethyl ether. This synthetic protocol was adopted from literature.^{29, 31}

FT-IR spectroscopy, ESI mass spectrometry and microanalysis data for L11

The FT-IR (ATR) spectrum obtained shows a sharp band at 1626 cm^{-1} for the $\nu(\text{C}=\text{N})$ stretching frequency confirming that the condensation had occurred. The data obtained from ESI-MS shows a singly charged parent ion at $m/z \text{ 255}$. Under the conditions used to record the mass spectrum, there is very little fragmentation of the compound. The microanalysis confirms the purity and product composition.

NMR spectroscopy data for L11

The $^1\text{H-NMR}$ data, Table 2.6, obtained exhibit a resonance at $\delta \text{ 8.05 ppm}$ for the imine $\text{HC}=\text{N}$ proton, $\delta \text{ 1.21 ppm}$ for the isopropyl CH_3 , $\delta \text{ 3.20 ppm}$ for the isopropyl CH , while the pyrrole ring protons between $\delta \text{ 6.14 - 6.68 ppm}$ and the phenyl ring proton at $\delta \text{ 7.27 ppm}$.

The ^{13}C -NMR data, Table 2.8, shows signals at δ 27.90 and δ 23.56 ppm that can be assigned to the isopropyl carbons. The aromatic carbon signals for the pyrrole ring were observed at δ 109.89, 116.86, 123.20 and δ 129.77 ppm while those of the phenyl ring were at δ 124.32, 124.57, 139.03 and δ 148.29. The imine carbon ($\text{HC}=\text{N}$) resonates at δ 152.72 ppm.

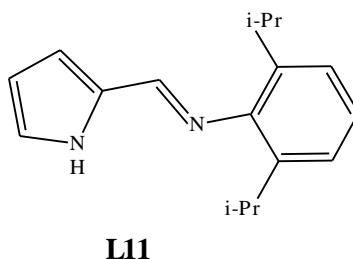
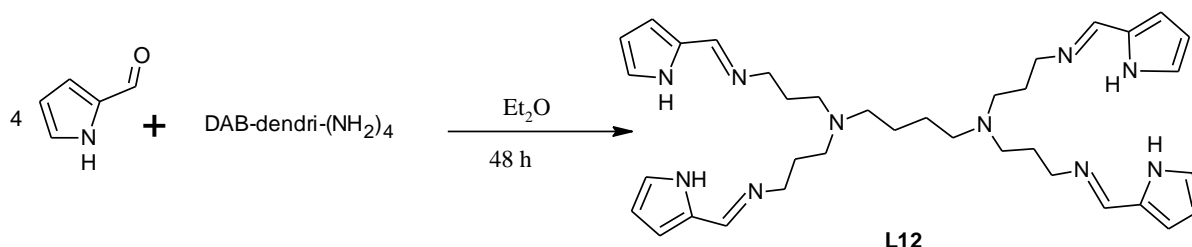


Figure 2.7: 2, 6-di(propan-2-yl)-*N*-[(*E*)-1*H*-pyrrol-2-ylmethylidene]aniline ligand, **L11**

2.2.4: Synthesis and characterization of multifunctional pyrrole-imine ligands, **L12** and **L13**

The dendrimeric ligands **L12** and **L13** were prepared and purified in a similar way as **L10**. The 1st and 2nd generation poly(propylene imine) DAB-PPI-(NH_2)_n were used in place of propyl amine. We previously reported the synthesis and characterization of **L12**, Scheme 2.6.²⁹ Both ligands were isolated as orange oils in fairly good yields and were fully characterized by a range of techniques. The full characterization data of these ligands are summarised in Tables 2.6 - 2.8.



Scheme 2.6: Synthetic route to G1 dendrimeric ligand, (DAB-PPI-($\text{N}=\text{CH}(\text{C}_4\text{H}_3\text{NH})_4$), **L12**

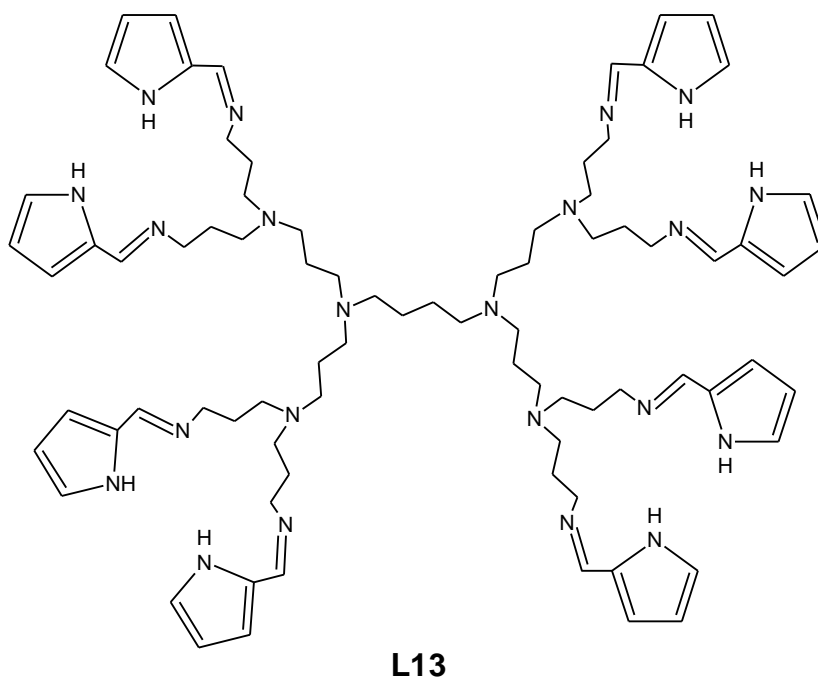


Figure 2.8: 2nd Generation dendritic pyrrolylaldimine ligand, **L13**

FT-IR spectroscopy for L12 and L13

FT-IR (ATR) spectra of both ligands showed the expected functionalities. These include a $\nu(\text{C}=\text{N})$ stretching band at 1636 cm^{-1} , $\nu(\text{N}-\text{H})$ at 3152 cm^{-1} and the $\nu(\text{C}-\text{H})$ between $2972\text{-}2884\text{ cm}^{-1}$.

NMR spectroscopy data for L12 and L13

The $^1\text{H-NMR}$ spectrum of **L12** showed clear evidence of the condensation, Table 2.6. The CH_2 signal adjacent to the imino group is observed to shift down field from the signal of the CH_2 next to NH_2 of the starting dendrimeric amine. Another characteristic peak is that of the $\text{N}=\text{CH}$ proton observed at $\delta\ 8.03\text{ ppm}$. The dendrimer backbone proton signals are observed between $\delta\ 1.4\text{ to }3.6\text{ ppm}$. The CH_2 protons next to the imine moiety resonate at $\delta\ 3.60\text{ ppm}$. The peaks at $\delta\ 2.4$ and $\delta\ 2.33$ can be assigned to the protons of the methylene groups adjacent to nitrogen in the dendrimer framework. The signal of the central CH_2 in the

dendron appeared at δ 1.7 ppm while that in the core is observed at δ 1.37 ppm. The pyrrole ring protons were observed between δ 6.2 - 6.9 ppm. Again broadening of the dendrimer scaffold protons was observed.

The ^1H -NMR spectrum of the 2nd generation pyrrole imine ligand, **L13**, (Figure 2.9) is similar to that of the 1st generation ligand. The proton signals of the dendrimer framework are observed between δ 1.3 and δ 3.5 ppm. These resonances are similar to those of the salicylaldimine ligands discussed earlier. The pyrrole ring proton peaks are between δ 6.21 and δ 6.84 ppm while the imino proton resonates at δ 8.05 ppm.

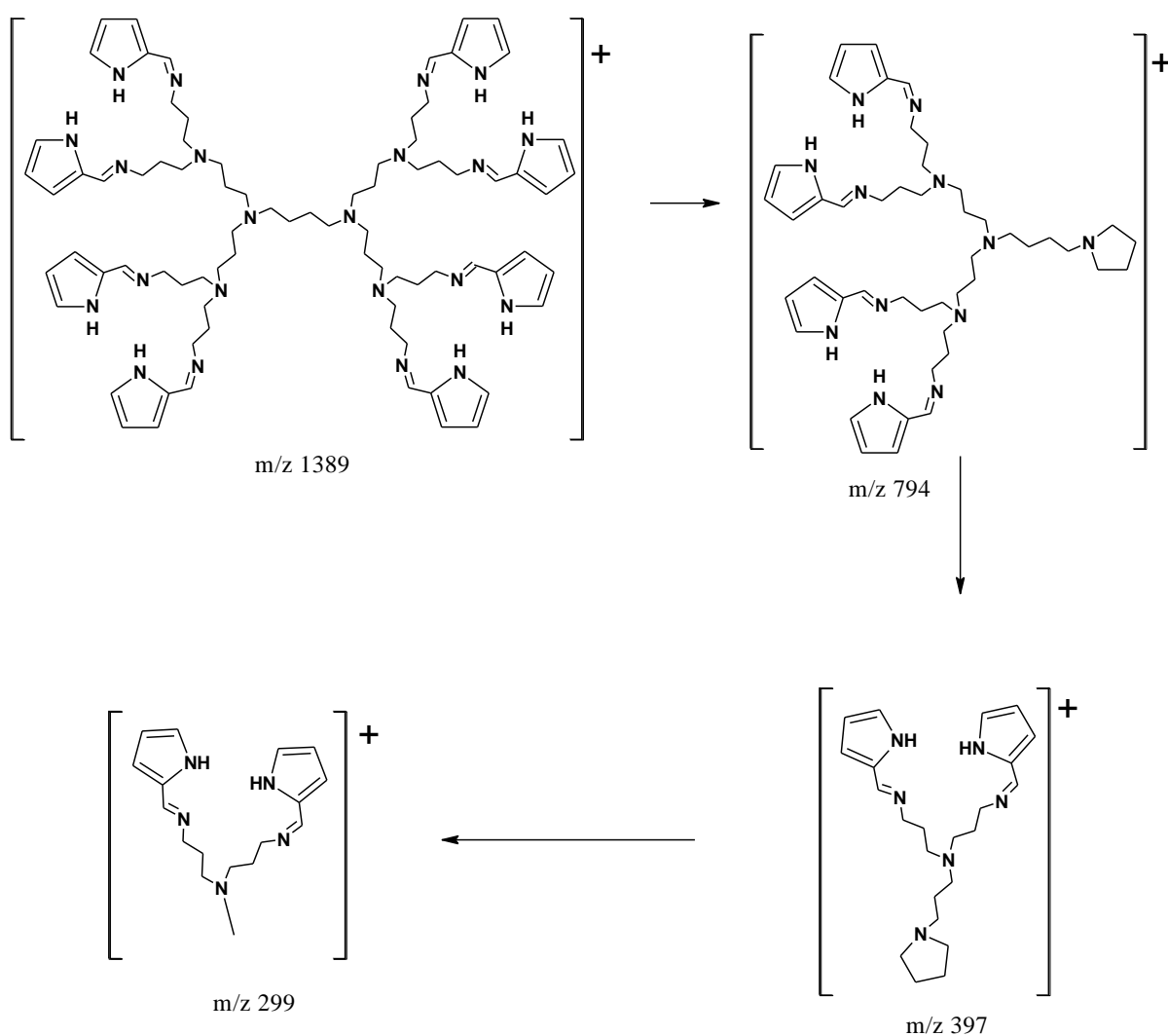
The ^{13}C spectrum of **L12** shows signals at δ 152.1 ppm for the $\text{N}=\underline{\text{C}}\text{H}$, δ 130.1, 121.9, 114.3 and δ 109.5 ppm for the pyrrole ring. The dendrimeric framework $\underline{\text{C}}\text{H}_2$ carbons are observed between δ 58.8 and δ 25.0 ppm. Similar ^{13}C data is obtained for the 2nd generation ligand, **L13**, Table 2.8.

ESI mass spectrometry data for L12 and L13

The ESI-MS mass spectrum of **L12** showed a molecular ion peak at m/z 779. This corresponds to the calculated molecular weight of 625 with four potassium ions associated with each of the pyrrole groups on the periphery of the dendrimeric ligand. **L13** gave an ESI-MS spectrum similar to that of the G2 salicylaldimine systems. Singly charged as well as multiply charged molecular ions are observed. The peak at $m/z = 1389$ matches the expected weight of a singly charged ion of the ligand. Sodium adducts of the ligand are also observed as was the case with **L12**. In addition **L13** forms other ions species observed at m/z 794 and $m/z = 397$ with a pyrrolidine group forming after cleavage at the dendrimer nitrogen groups as shown in Scheme 2.7. The data obtained from micro analysis agrees with the calculated molecular weight and $1/2 \text{CH}_2\text{Cl}_2$ associated with the ligands as shown in Table 2.7.

2.3: Conclusions

Monofunctional as well as multifunctional salicylaldimine and pyrrolylaldimine ligands were successfully prepared. All the ligands were obtained in moderate yields and fully characterized using a range of analytical techniques. The 1st generation multifunctional ligands have four peripheral N, O or N, N chelating units while 2nd generation analogues have eight.



Scheme 2.7: Fragmentation pattern for **L13** deduced from the ESI-mass spectrum

Table 2.6: ¹H-NMR data of pyrrolylaldiminato ligands^a

Ligand	<u>H</u>C=N	Ar-<u>H</u>	HC=N<u>CH</u>₂	<u>CH</u>₂	<u>CH</u>₃ and <u>CH</u>(<u>CH</u>₃)₂
L10	8.04 (s, 1H)	6.91 (br s, 1H) 6.56 (dd, 1H, ³ J _{HH} = 3.0 Hz) 6.29 (t, 1H, ³ J _{HH} = 3.0 Hz)	3.59 (dt, 2H, ³ J _{HH} = 7.0 Hz)	1.73 (m, 2H, ³ J _{HH} = 7.0 Hz)	0.98 (t, 3H, ³ J _{HH} = 9.0 Hz)
^bL11	8.05 (s, 1H)	7.27 (br s, 3H) 6.68 (d, 1H, ³ J _{HH} = 3.6 Hz) 6.19 (t, 1H, ³ J _{HH} = 2.9 Hz) 6.14 (s, 1H)			3.20 (m, 1H, ³ J _{HH} = 6.8 Hz) 1.21 (d, 12H, ³ J _{HH} = 6.9 Hz)
L12	8.06 (s, 4H)	6.86 (s, 4H) 6.49 (dd, 4H, ³ J _{HH} = 3.4 Hz) 6.27 (t, 4H, ³ J _{HH} = 3.0 Hz)	3.56 (t, 8H, ³ J _{HH} = 6.1 Hz)	2.44 (t, 8H, ³ J _{HH} = 6.7 Hz) 2.35 (br 4H) 1.75 (q, 8H, ³ J _{HH} = 7.0 Hz) 1.35 (br s, 4H)	
L13	8.04 (s, 8H)	6.83 (s, 8H) 6.49 (dd, 8H, ³ J _{HH} = 3.4 Hz) 6.22 (t, 8H, ³ J _{HH} = 3.1 Hz)	3.53 (t, 16H, ³ J = 6.4 Hz)	2.42 (t, 16H, ³ J _{HH} = 7.0 Hz) 2.36 (br, 20H) 1.73 (br m, 16H) 1.51 (br, 8H); 1.37 (s, 4H)	-

^a 300 MHz (CDCl₃, δ in ppm), ^b 300 MHz (CD₂Cl₂, δ in ppm), s = singlet, d = doublet, dd = doublet of doublets, t = triplet, dt = doublet of triplets, m = multiplet, br = broad

Table 2.7: Analytical data for pyrrolylaldiminate ligands

Ligand	Yield (%)	M. p (°C)	Formula	ES-MS m/z = [M+H] ⁺	FT-IR (cm ⁻¹)	Anal Found (Calcd.)		
				Found (Calcd.)	v(C=N)	C	H	N
^a L10	56	-	C ₈ H ₁₂ N ₂ ·0.25 H ₂ O	137 (136)	1636	68.11 (68.29)	8.48 (8.95)	19.31(19.91)
L11	85	142.3 - 143.1	C ₁₇ H ₂₂ N ₂	255 (254)	1626	80.24 (80.27)	8.75 (8.72)	10.80 (11.01)
L12	51	-	C ₃₆ H ₅₂ N ₁₀ ·0.5 CH ₂ Cl ₂	625 (624)	1636	65.02 (65.69)	7.84 (8.01)	19.80 (20.90)
L13	52	-	C ₈₀ H ₁₂₀ N ₂₂ ·0.5 CH ₂ Cl ₂	1389 (1388)	1635	67.71 (67.50)	8.89 (8.51)	22.24 (21.51)

^aGC-MS m/z**Table 2.8:** Pyrrolylaldiminate ligands {¹H} ¹³C-NMR data (CDCl₃)^a

Ligand	HC=N	Pyrrole-C	Ar-C	HC=NCH ₂	CH ₂	CH ₃	(CH ₃) ₃
L10	151.4	129.8, 121.4, 113.7, 109.5		62.7	62.7, 24.3	11.7	
L11	152.7	129.8, 123.2, 116.9, 109.9	148.3, 139.0, 124.6, 124.3				23.56, 27.90
L12	152.1	130.1, 121.9, 114.3, 109.5		58.8	53.8, 51.4, 28.3, 25.0		-
L13	153.1	130.3, 122.3, 114.7, 109.7		59.2	54.2, 51.6, 28.5, 25.1		-

^a 75.4 MHz (CDCl₃, δ in ppm)

2.4: Experimental

2.4.1: Materials and instrumentation

Ligands were synthesized using standard Schlenk techniques under nitrogen employing a dual vacuum/nitrogen line. All solvents used were of analytical grade and were dried and distilled prior to use. Tetrahydrofuran (THF), hexane and diethyl ether were dried and distilled from sodium/benzophenone, methanol from magnesium turnings/iodine and dichloromethane over phosphorous pentoxide. Propylamine, 2, 6-diisopropylaniline, pyrrole-2-carboxyaldehyde, 2-hydroxybenzaldehyde, 3-*t*-butyl-2-hydroxybenzaldehyde, 3, 5-di-*t*-butyl-2-hydroxybenzaldehyde were purchased from Sigma-Aldrich Ltd. Poly (propyleneimine) DAB-dendr-(NH₂)₄ and poly (propylene imine) DAB-dendr-(NH₂)₈ were obtained from Symo-Chem, Netherlands. All starting materials were used without further purification.

The NMR spectra were recorded on a Varian 300 VNMRS spectrometer (¹H at 300 MHz, ¹³C at 75.4 MHz) at room temperature using tetramethylsilane as an internal standard. The chemical shifts are reported in δ (ppm) and referenced to the signal for the residual proton in CDCl₃ the NMR solvent. Infrared spectra were recorded on a Nicolet Avatar 330 FT-IR spectrophotometer using ATR accessory. ESI-MS data were obtained on a Waters API Q-TOF Ultima spectrometer calibrated with NaF. GC-MS analysis was performed using a Finnigan-Matt GCQ-Gas Chromatograph equipped with an electron impact ionization source at 70 eV and a 30 m HP-MS capillary column with a stationary phase based on 5% phenyl-methylpolysiloxane at the University of the Western Cape. Microanalyses were performed at the micro analytical laboratory of the University of Cape Town. Melting points were determined on a Stuart Scientific melting point apparatus (SMP3) at heating rate of 0.5 °C/m.

2.4.1.1: General method for the MALDI-TOF MS spectrometry

The MALDI-TOF MS spectra for **L4** – **L9** were recorded on a Voyager DE STR MALDI-TOF spectrometer equipped with 2 m linear and 3 m reflector flight tube and a 337 nm nitrogen laser. All spectra were obtained with an acceleration potential of 20 kV in the positive ion mode in ACTH linear and reflector mode. Dithranol was used as matrix (40 mg/mL in THF), sodium trifluoroacetate was used as the ionizing salt (1 mg/mL in THF) and the ligands (10 mg/mL in THF). The three solutions were then mixed at volume ratio of 10:5:1 for matrix:ligand:NaTFA. The solution mixture was then spotted on a steel plate and air dried. Calibration was done using Peg 1000Na. All the data was processed using data explorer

2.4.1.2: Molecular structure determination of single crystal by X-ray analysis, data collection

A yellow crystal with approximate dimensions $0.55 \times 0.41 \times 0.37 \text{ mm}^3$ was selected under oil under ambient conditions and attached to the tip of a nylon loop. The crystal was mounted in a stream of cold nitrogen at 100(2) K and centered in the X-ray beam by using a video camera. The crystal evaluation and data collection was performed on a Bruker CCD-1000 diffractometer with Mo K_{α} ($\lambda = 0.71073 \text{ \AA}$) radiation and the diffractometer to crystal distance of 4.9 cm. The initial cell constants were obtained from three series of ω scans at different starting angles. A total of 5659 reflections were obtained. The reflections were successfully indexed by an automated indexing routine built in the SMART (Bruker 2002) program.

2.4.1.3: Molecular structure determination of single crystal by X-ray analysis, structure solution and refinement

The systematic absences in the diffraction data were uniquely consistent for the space group *P1* that yielded chemically reasonable and computationally stable results of refinement.

A successful solution by the direct methods provided most non-hydrogen atoms from the *E*-map. The remaining non-hydrogen atoms were located in an alternating series of least-squares cycles and difference Fourier maps. All non-hydrogen atoms were refined with anisotropic displacement coefficients. All hydrogen atoms were included in the structure factor calculation at idealized positions and were allowed to ride on the neighbouring atoms with relative isotropic displacement coefficients.

2.4.2: Preparation of salicylaldimine ligands

2.4.2.1: General procedure for the synthesis of aliphatic salicylaldimine ligand; L1 - L3

The ligands were prepared by Schiff base condensation of *n*-propyl amine with the appropriate benzaldehyde, namely 2-hydroxybenzaldehyde for **L1**, 3-^tbutyl-2-hydroxybenzaldehyde for **L2** and 3, 5-^tbutyl-2-hydroxybenzaldehyde for **L3**. The synthesis of **L1** is used to illustrate.

A yellow solution of 2-hydroxybenzaldehyde (1.0 g, 1.8 mL, 8.19 mmol) and propyl amine (0.8 mL, 9.81 mmol) in 20 mL methanol was stirred for 12 h at room temperature under nitrogen. The yellow colour was retained throughout the reaction time. After 12 h, the methanol was removed and a yellow-orange oil obtained. The oil was dissolved in CH₂Cl₂ (25 mL) and washed with water (4 × 20 mL). The organic layer was collected, dried over anhydrous MgSO₄ and filtered by gravity. Upon removal of all volatiles from the filtrate, a yellow oil was obtained. The ligands were obtained as yellow oils in moderate to good yields of 60 – 80 %.

2.4.2.2: General procedure for the synthesis of 1st and 2nd generation periphery functionalised salicylaldimine ligand; **L4 - L9**

1st or 2nd generation polypropylenimine, DAB-(NH₂)_n (n = 4 or 8) was reacted with the appropriate 2-hydroxybenzaldehyde as was the case for the aliphatic ligands. The synthesis of **L4** is used as an example to illustrate.

A yellow solution of 1st generation polypropylenimine, DAB-(NH₂)₄ (0.4 g, 1.264 mmol) and salicylaldehyde (0.55 mL, 5.25 mmol) in 20 mL toluene was stirred at room temperature for 72 h under nitrogen. After the 72 h, the toluene was removed giving a yellow oil. The oil was dissolved in CH₂Cl₂ (25 mL) and washed with water (4 × 25 mL). The organic layer was collected, dried over anhydrous MgSO₄ and filtered by gravity. The filtrate was concentrated to about 5 mL and the product was crystallized by slow diffusion of pentane (10 mL) giving a yellow solid.

However **L5** was crystallized by slow diffusion of methanol into a solution of the compound in CH₂Cl₂. **L8** was purified in a same protocol as **L5**. The 1st generation salicylaldimine ligands were obtained as yellow solids while the 2nd generation analogues were viscous yellow oils. All the ligands were obtained in moderate to good yields of 60 – 85 %. The first generation salicylaldimine ligands were obtained as yellow oils while the second generation analogues were viscous yellow oils.

2.4.3: Preparation of pyrrole-imine ligands

2.4.3.1: Synthesis of (propyl-(1-H pyrrol-2-ylmethylene) imine; **L10**

To a yellow solution of pyrrole-2-carboxylaldehyde (1 g, 10.53 mmol) in dry diethyl ether (20 mL) propyl amine (0.86 mL, 10.53 mmol) was added via a syringed. A Few drops of glacial acetic acid were added as a catalyst. The solution was stirred at room temperature for 6 h. The solvent was then removed from the reaction solution by rotary evaporation

giving an orange oil. The product was purified by dissolving in CH_2Cl_2 (25 mL) and washing with water (5×25 mL). The organic layer was collected, dried over anhydrous MgSO_4 and filtered by gravity. Removal of the CH_2Cl_2 yielded an orange oil.

2.4.3.2: *Synthesis of N-(2,6-diisopropylphenyl)-N-[1-H-pyrrol-2-ylmethylene] imine; L11*

To a stirring yellow solution of pyrrole-2-carboxylaldehyde (3.0 g, 31.55 mmol) in dry diethyl ether (30 mL), 2, 6-diisopropylaniline (5.6 g, 31.55 mmol) was added. The solution had a few drops of formic acid added, as a catalyst, and stirred at r. t. for 24 h. After the reaction time, diethyl ether was removed by rotary evaporation giving a cream white solid that was recrystallized from methanol by slow evaporation to giving **L11** as white crystals. This method was adapted from reported procedures with slight modification.²⁷

2.4.3.3.: *General procedure for the synthesis of 1st and 2nd generation periphery functionalised pyrrolylaldiminate ligand; L12 and L13*

First and the second generation polypropylenimine, $\text{DAB}-(\text{NH}_2)_n$ ($n = 4$ or 8) was reacted with pyrrole-2-carboxylaldehyde. The preparation of **L12** is used as an illustration. These pyrrole-imine ligands were obtained as orange oils.

Into a Schlenk tube containing dry diethyl ether (20 mL) and anhydrous MgSO_4 (*ca* 2 g) pyrrole-2-carboxylaldehyde (0.48 g, 5.05 mmol) was added yielding an orange-yellow mixture. $\text{DAB}(\text{NH}_2)_4$ (0.4 g, 1.26 mmol) dissolved in dry diethyl ether (5 mL) was added drop-wise over 2 minutes. A catalytic amount of glacial acetic acid was added and the mixture stirred at r. t. for 2 days. The Et_2O was then removed from reaction mixture giving an orange oil.

The oil was dissolved in CH_2Cl_2 (25 mL) and washed with water (5×25 mL). The organic layer was collected, dried over anhydrous MgSO_4 and filtered by gravity. Removal

of CH₂Cl₂ yielded an orange oil. The ligands were obtained in yields of 51 and 52 % for **L12** and **L13** respectively.

2.5: References

1. H. Schiff, *Annalen.*, **131** (1864) 118.
2. A. Combes, *C. R. Acad. Fr.*, **108** (1889) 1251.
3. D. A. Tomalia, A. M. Naylor, W. A. Goddard, *Angew. Chem., Int. Ed. Engl.*, **29** (1990) 138.
4. D.A. Tomalia, D. M. Hedstrand, M. S. Ferrito, *Macromolecules*, **24** (1991) 1435.
5. S. Hecht, J. M. J. Fréchet, *Angew. Chem. Int. Ed.*, **40** (2001) 74.
6. C. J. Hawker, J. M. J. Fréchet, *J. Am. Chem. Soc.*, **112** (1990) 7638.
7. A. W. Bosman, H. M. Janssen, E. W. Meijer, *Chem. Rev.*, **99** (1999) 1665.
8. M. Fischer and F. Vögtle, *Angew. Chem., Int. Ed.*, **38** (1999) 884.
9. O. A. Mathews, A. N. Shipway, J. F. Stoddart, *Prog. Polym. Sci.*, **231** (1998).
10. F. Zeng, S. C. Zimmerman, *Chem. Rev.* (1997) **97** 1681.
11. M. Kimura, T. Shiba, T. Muto, K. Hanabusa, H. Shirai, *J. Chem. Soc. Chem. Commun.*, (2000) 11.
12. N. R. Luman, T. Kim, and M. W. Grinstaff, *Pure and Applied Chem.*, **76** (2004) 1375.
13. A. J. L. Villaraza, A. Bumb, M. W. Brechbiel, *Chem. Rev.*, **110** (2010) 2921.
14. R. Meijboom, M. J. Overett, J. R. Moss, *J. Organomet. Chem.*, **689** (2004) 987.
15. G. R. Newkome, E. He, C. N. Moorefield, *Chem. Rev.*, **99** (1999) 1689.
16. N. E. Domracheva, A. Mirea, M. Schwoerer, L. Torre-Lorente, G. Lattermann, *Physics of the Solid State*, **49** (2007) 1392.
17. G J. M. Koper, M. H. P. van Genderen, C. E. Roman, M. W. P. L. Baars, M. Borkovec, *J. Am. Chem. Soc.*, **119** (1997) 6512

18. R. Velarde-Ortiz, G. Larsen, *Chem. Mater.*, **14** (2002) 858.
19. M. A. Torzilli, S. Colquhoun, D. Doucet, R. H. Beer, *Polyhedron*, **21** (2002) 697.
20. A. Blagus, D. Cinčić, T. Friščić, B. Kaitner, V. Stilinović, *Maced. J. Chem. Chem. Eng.* **29** (2010) 117.
21. J. L. van Wyk, Ph.D. Thesis title, “*Mononuclear and Multinuclear Salicylaldimine Metal Complexes as Catalysts Precursors in the Oxidation of Phenol and Cyclohexene*” University of the Western Cape, 2008.
22. R. Malgas, S. F. Mapolie, S. O. Ojwach, G. S. Smith, J. Darkwa, *Catal. Commun.*, **9** (2008) 1612.
23. Y. Haba, A. Harada, T. Takagishi, K. Kono, *Polymer*, **46** (2005) 1813
24. William Kemp, *Organic Spectroscopy*, Third Edition 1991, Macmillan Press Limited, page 132-135.
25. W. Schilf, B. Kolodziej, E. Grech, *J. Mol. Struct.*, **791** (2006) 93.
26. J–W. Weener, J. L. J. van Dongen, E. W. Meijer, *J. Am. Chem. Soc.* **121** (1999) 10346.
27. B. Baytekin, N. Werner, F. Luppertz, M. Engeser, J. Brüggemann, S. Bitter, R. Henkel, T. Felder, C. A. Schalley, *Int. J. Mass Spectrom.*, **249** (2006) 138.
28. D. J. Darensbourg, P. Rainey, J. Yarbrough, *Inorg. Chem.*, **40** (2001) 986.
29. J. N. Mugo, S. F. Mapolie, J. L. van Wyk, *Inorg. Chim. Acta*, **363** (2010) 2643.
30. H. Günzeler and H.-U. Gremlich, *An Introduction to IR Spectroscopy*, Translated by M.-J. Blümich, 2002, WILEY-VCH Verlag GmbH, 69469 Weinheim (Federal Republic of Germany) pages 176-246.
31. V. C. Gibson, C. Newton, C. Redshaw, G. A. Solan, A. J. P. White, D. J. Williams, *Dalton Trans.*, (2002) 4017.
32. Y-S. Li, Y-R. Li, X-F. Li, *J. Organomet. Chem.*, **667** (2003) 185.

Chapter 3 : Synthesis and Characterization of Salicylaldiminato Zn(II) Complexes

3.1: Introduction

Salicylaldiminato Schiff base metal complexes can be readily obtained by the reaction of the ligand with a suitable metal salt. The synthesis by prior formation of the imine ligand appears to be most favoured because it allows the development of well-defined catalysts especially where the presence of ancillary ligands is necessary such as those reported for Sn¹ and Al^{2,3}. This approach can also produce bis-ligated metal complexes for example those of Ni⁴, Fe⁵, and Co⁶, Zn⁷. The presence of a base to deprotonate the ligand is crucial in some cases. Whether to use a base or not is determined by several factors. These include the nature of the metal precursor used, the stability of intermediate species as well as the acidity of the OH proton. The acidity of the phenoxy OH is influenced by the substituent groups on the phenoxy ring. The presence of these substituent groups on the phenoxy ring as well as the imino moieties also controls the steric and electronic properties of the ligand and subsequent reactivity of the metal complexes formed. This versatility in return allows metal complex fine-tuning for various applications.⁸ Another approach for the formation of the salicylaldimine metal complexes is the *in-situ* formation of the imine and the concomitant complexation to the metal center via a template-type synthesis. This synthetic protocol is suitable where one of the intermediates may be chemically unstable.⁹

Salicylaldiminato metal complexes have in the past been applied in numerous catalytic processes, including olefin oligomerization, as well as epoxidation and ring opening.¹⁰⁻¹³

We recently reported a series of Cu(II) and Zn(II) bis-salicylaldimine metal complexes.¹⁴ The Cu(II) complexes were readily obtained by the reaction of the salicylaldimine ligands with copper acetate monohydrate. In the zinc analogues the presence of *t*-butyl groups on the phenoxy ring hindered complex formation. Thus the use of sodium hydride was required in the preparation of the *bis*[N-(2,6-diisopropylphenyl)-3-*t*-butyl-

salicylaldiminato]Zn(II) complex as opposed to *bis*[N-(2,6-diisopropylphenyl)-salicylaldiminato]Zn(II) which was formed without prior deprotonation of the ligand.

A series of mono and *bis*(N-(aryl)salicylaldiminato) zinc complexes were previously reported by Darensbourg *et al.*¹⁵ These researchers observed that the nature and the relative amounts of the zinc precursor used determined the type of complexes that were obtained. Reacting the ligands with $\text{Zn}\{\text{N}[\text{Si}(\text{CH}_3)_3]_2\}_2$ in a stoichiometric ratio of 1:1 (Zn precursor:ligand) yielded a mono(salicylaldiminato) zinc complex. When this ratio was changed to 1:2, (Zn precursor:ligand) a *bis*(salicylaldiminato) Zn(II) complex was obtained. In the case where $\text{Zn}(\text{C}_2\text{H}_5)_2$ was used, only a mono(salicylaldiminato) zinc complex was obtained even when large excess of diethyl zinc was added. Other metal salts such as ZnCl_2 , $\text{Zn}(\text{OTf})_2$, $\text{Zn}(\text{OAc})_2 \cdot 2\text{H}_2\text{O}$ and $[\text{Zn}(\text{CH}_3\text{CN})_4](\text{BF}_4)_2$ gave only *bis*(salicylaldiminato) complexes. However, in these cases prior deprotonation of the ligands with NaH or BuLi was necessary.

A number of Cu(II) salicylaldimine complexes have also been reported in the literature. In most Cu(II) systems ligand deprotonation is not essential when $\text{Cu}(\text{OAc})_2 \cdot \text{H}_2\text{O}$ was used as metal precursor.¹⁶⁻¹⁸ Salicylaldiminato complexes of nickel are also readily formed from $\text{Ni}(\text{OAc})_2 \cdot 4\text{H}_2\text{O}$ and $\text{NiCl}_2 \cdot 6\text{H}_2\text{O}$ without prior ligand deprotonation.¹⁹ Metal complexes of aluminium are also readily formed in the presence of $\text{Al}(\text{CH}_3)_3$ without ligand deprotonation.²⁰ In the case of cobalt complexes, van Wyk *et al.*²¹ observed that complex formation only occurred when the salicylaldimine ligand was deprotonated *in-situ* with sodium hydroxide in the presence of cobalt acetate. Prior preparation of the sodium salt of the ligand using sodium hydride and subsequent complexation did not yield any cobalt complex. Chandran *et al.*²² also reported Co(II) complexes that were prepared in a one-pot reaction of salicylaldehyde or its derivatives with 2,6-dialkyl substituted anilines in the presence of $\text{Co}(\text{OAc})_2 \cdot 4\text{H}_2\text{O}$. In this case no deprotonating agent was required.

3.1.2: Dendritic salicylaldimine metal complexes

Various ways of immobilizing metal catalysts onto supports were introduced in Chapter 1. Several researchers have developed Schiff base metal complexes anchored on dendritic scaffolds.²³ Due to the hyper branched nature of dendrimers a number of coordination sites can be found in a single molecule. Metals can be introduced into the system via these coordination sites, Figure 3.1, and these compounds are referred to as metallodendrimers.

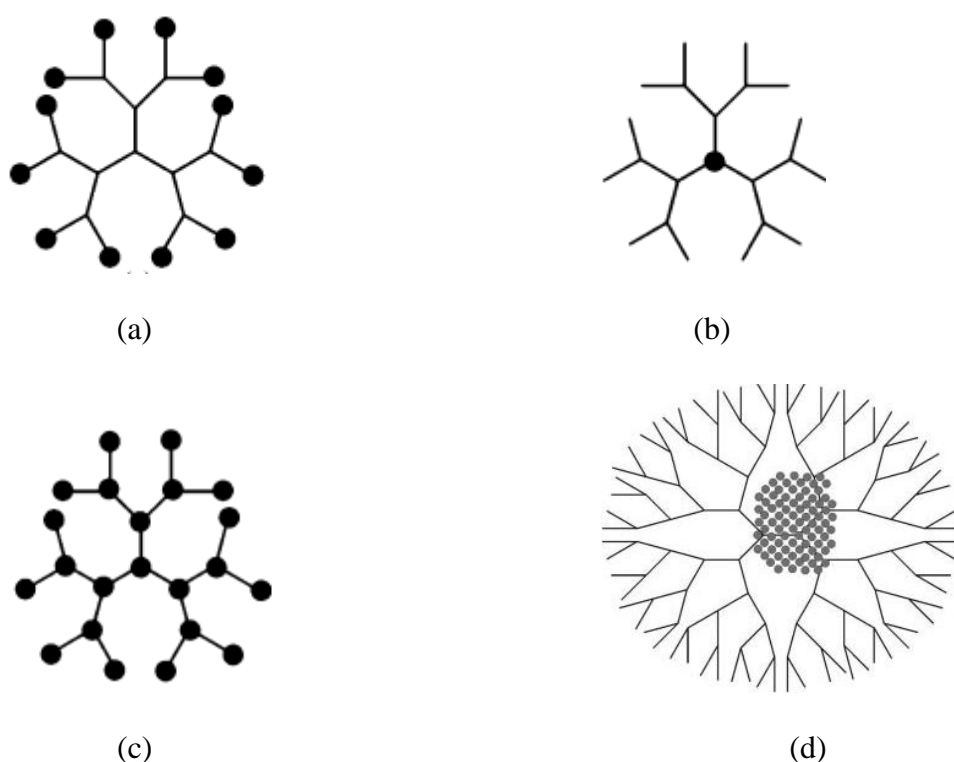


Figure 3.1: Various architectures of metallodendrimers with the metal centers on periphery (a), at the core (b), at the branching points (c) and as encapsulated metal nanoparticles (d); adapted from Balzani *et al.*³²

The metal sites may be on the periphery as shown in (a), at the core (b), at the branching points (c), or in the cavities as encapsulated nanoparticles (d). The resulting metallodendrimers have found application in different fields such as medicine for drug

delivery^{24, 25} and catalysis.²⁶⁻²⁸ Other applications are light and energy harvesting materials.²⁹⁻³¹

Metallodendrimers based on periphery modified polypropylene imine (PPI) scaffolds have extensively been explored.^{33, 34} Our group has published dendritic salicylaldimine complexes of Ni(II), Co(II), Ru(II) and Cu(II) based on the PPI scaffold. Malgas-Enus *et al.* observed that similar to the mononuclear Ni(II) complexes, 1st and 2nd generation Ni(II) salicylaldiminato complexes can be obtained by reacting the dendritic ligands with nickel acetate.^{35, 36} Copper complexes have also been readily formed from Cu(OAc)₂·H₂O without ligand deprotonation.³⁷ However in the case of the cobalt and ruthenium metallodendrimers ligand deprotonation was required.³⁸

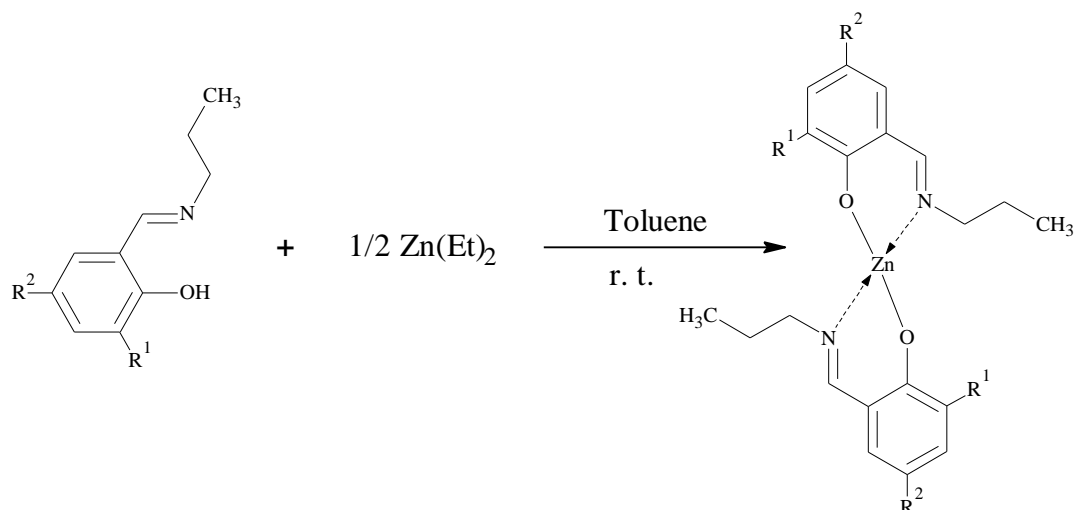
In this chapter we discuss the synthesis and characterization of mononuclear and multinuclear salicylaldiminato Zn(II) complexes. These complexes were prepared from diethyl zinc using either the monofunctional or the multifunctional salicylaldimine ligands whose synthesis was described in Chapter 2. The complexes were characterized using a range of analytical techniques such as NMR and FT-IR spectroscopies, mass spectrometry and elemental analysis.

3.2: Results and discussion

3.2.1: *Synthesis and characterization of the bis(N-n-propylsalicylaldiminato) Zn(II) complexes, C1 – C3*

The synthesis of the mononuclear Zn(II) complexes was achieved by the reaction of the monofunctional ligand with diethyl zinc using a mole ratio of 2:1 (ligand: ZnEt₂ in toluene, Scheme 3.1. ZnCl₂ and Zn(OAc)₂·2H₂O were also evaluated as metal precursors. ZnEt₂ was selected as the best precursor because it afforded the highest yields and purer products since ethane was the only by-product. Another advantage was that ligand deprotonation was not

necessary unlike in the case for zinc acetate and zinc chloride. After recrystallization, yields of 60 - 70 % were recorded for **C1** – **C3**. **C2** and **C3** were recrystallized by slow diffusion of methanol into a solution of the complex in CH₂Cl₂ at a ratio of 2:5 (MeOH:CH₂Cl₂) at -4°C while **C1** was recrystallized from hexane at -78 °C.



Scheme 3.1: Mononuclear Zn(II) complexes, **C1** – **C3**

These complexes were obtained as a cream solid for **C1**, a light yellow solid for **C2** and a lime green solid for **C3**. These products were observed to be soluble in all common organic solvents.

FT-IR spectroscopy data for complexes C1 – C3

The main stretching frequency bands monitored in the IR spectra were those of the $\nu(\text{C}=\text{N})$ and $\nu(\text{C}-\text{O})$ bands. From the FT-IR data, (Table 3.1), it was observed that these complexes showed a shift of the $\nu(\text{C}=\text{N})$ peak from around 1630 cm^{-1} in the free ligands to 1622 , 1616 , and 1611 cm^{-1} for **C1**, **C2** and **C3** respectively. The shift of the imine $\nu(\text{C}=\text{N})$ stretching frequency to lower wave numbers suggests the involvement of the nitrogen atom in

the coordination to the zinc center. Moreover, the strong bands associated with the $\nu(\text{C-O})$ stretch shifted from around 1270 to 1326, 1321, and 1324 cm^{-1} in **C1**, **C2** and **C3** respectively. This suggested that the oxygen was also involved in complex formation.³⁹ The values obtained for **C1** are also similar to those reported by Torzilli *et al.*⁷ for the same compound.

NMR spectroscopy data for C1 – C3

¹H-NMR data (Table 3.1) show that complex **C1** exhibited the imine proton peak at δ 8.17 ppm as compared to δ 8.30 ppm for the free ligand. The upfield shift results from the shielding of the imine proton as the nitrogen coordinates to the zinc center. The phenolic proton signal was also no longer present signifying the deprotonation of this group and subsequent coordination to the metal center. Another observation is that the signal for the methylene protons, CH_2 , adjacent to the imino group shifts downfield. There is also an increase in the separation between signals of the aromatic protons when going from the free ligand to the Zn(II) complex. This data compares favourably to that reported for the same compound by Torzilli *et al.*⁷

Similar observations were made for the ¹H-NMR spectra obtained for complexes **C2** and **C3**. In the spectrum of **C2** the imino proton signal shifted from δ 8.36 in the ligand to δ 8.20 ppm while that of **C3** shifted from δ 8.37 ppm in the ligand to δ 8.22 ppm in the complex. This fully supports the notion that the ligand coordinates to the metal center. The signal of the ^tbutyl group at position 3 was observed to be more affected by coordination to the metal than the ^tbutyl group that at position 5. In complexes **C2** and **C3** this signal for the ^tbutyl group at position 3 shifted upfield by 0.11 and 0.07 ppm respectively. However, only a slight upfield shift of 0.01 ppm is recorded for the protons of the ^tbutyl group at position 5 in **C3**.

The ^{13}C -NMR data for **C1** – **C3** is summarised in Table 3.3. There was a clear shift of the carbon signals compared to those of the free ligand. The coordination of the ligand to the metal produced a downfield shift of imino carbon ($\underline{\text{C}}=\text{N}$) as well as the aromatic carbon bonded to the phenolic oxygen ($\underline{\text{C}}-\text{O}$). There was also a slight downfield shift of the other carbon signals.

Mass spectral data for C1 – C3

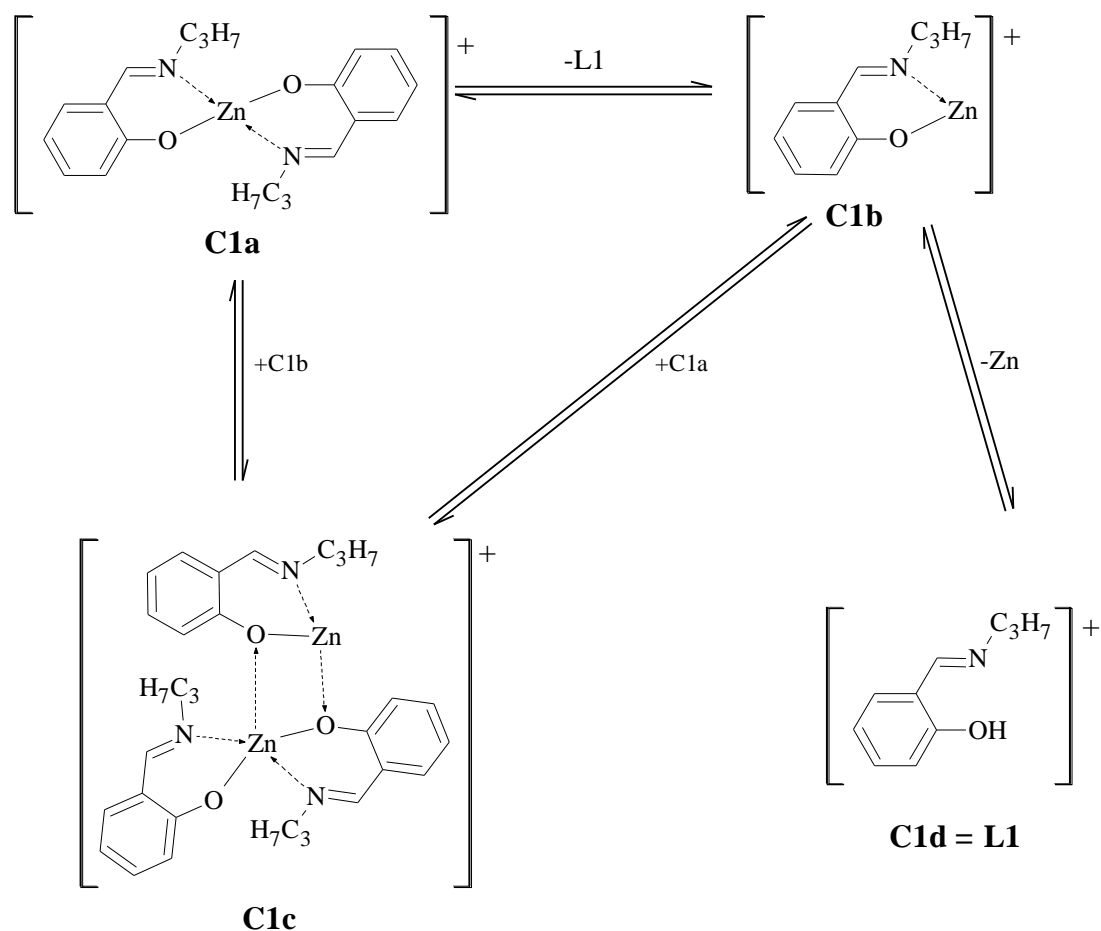
In the mass spectrometry analysis of **C1** – **C3**, ESI-MS and FAB-MS were used. ESI-MS data for **C1** has been previously reported.⁷ The FAB-MS spectrum obtained showed peak clusters centered at m/z 614.6, 389.3, 226.1 and 164 (Da). The cluster of peaks is due to the five stable zinc isotopes, the ^{14}N and ^{15}N isotopes as well $[\text{M}+\text{H}]^+$ and $[\text{M}]^+$ ions. The Zn isotopes are ^{64}Zn , ^{65}Zn , ^{67}Zn , ^{68}Zn and ^{70}Zn with average abundances of 48.63%, 27.90%, 4.10%, 18.75%, and 0.62%, respectively.⁴⁰ In the FAB-MS two ionisation processes occur, protonation and simple electron loss giving rise to the ions $[\text{M}+\text{H}]^+$ and $[\text{M}]^+$ respectively.

A proposed fragmentation pattern for **C1** is shown in Scheme 3.2. The ion at m/z 389 (**C1a**) is that of the monomeric complex. The loss of one ligand gives a fragment at m/z 226 (**C1b**). Under the mass spectral conditions used, there was association of **C1a** and **C1b** giving an ion at m/z 614 (**C1c**). This type of aggregation was also reported by Arockiasamy *et al.*⁴¹ for *bis*(N-R-salicylaldimine)nickel(II) (where R was methyl, ethyl, n-propyl, n-butyl and n-pentyl). These researchers reported that where R was methyl, aggregates of up to 5 metal centers were detected. In the case where R was ethyl to n-pentyl, aggregates with only two metal centers were formed. The loss of the sole Zn metal from **C1b** formed a fragment ion at m/z 164 (Scheme 3.2, **C1d**). This fragment ion represents the free ligand, **L1**.

C2 was also analysed by ESI-MS and FAB-MS. The data acquired using the two ionization techniques showed a singly charged Zn(II) bis-ligated mononuclear isotopomeric

cluster of ions centered at m/z 500. In the FAB-MS spectrum, the base peak was that of the bis-chelate mononuclear singly charged ion of the complex shown in Scheme 3.1 with no peaks associated with higher molecular mass ions.

However in the ESI-MS, the base peak was that of the bis-chelate unsubstituted mononuclear, **C1**, at m/z 391, Figure 3.2. It can be concluded that under the ESI-MS conditions used, the most stable ion was formed after the loss of the 'butyl groups at position 3.



Scheme 3.2: Fragmentation pattern and proposed aggregation structures for **C1** as inferred from FAB-MS.

Other significant clusters of peaks were observed at m/z 423, 722 and 826 and these formed after fragmentation and aggregation. The peak at m/z 423 can be attributed to an ion

formed after the loss of some of the methyl groups of the ^tbutyl substituent. The ion at *m/z* 826 was formed after aggregation of two metal centers with three ligands which was subsequently transferred into the gas phase and detected as discussed for **C1**, while that at *m/z* 722 was formed after the loss of one of the zinc metals from the aforementioned fragment. Since there was no evidence of dimers in the ¹H and ¹³C NMR spectra, it can thus be concluded that the aggregation only occurs when these complexes are ionized under the mass spectral conditions.

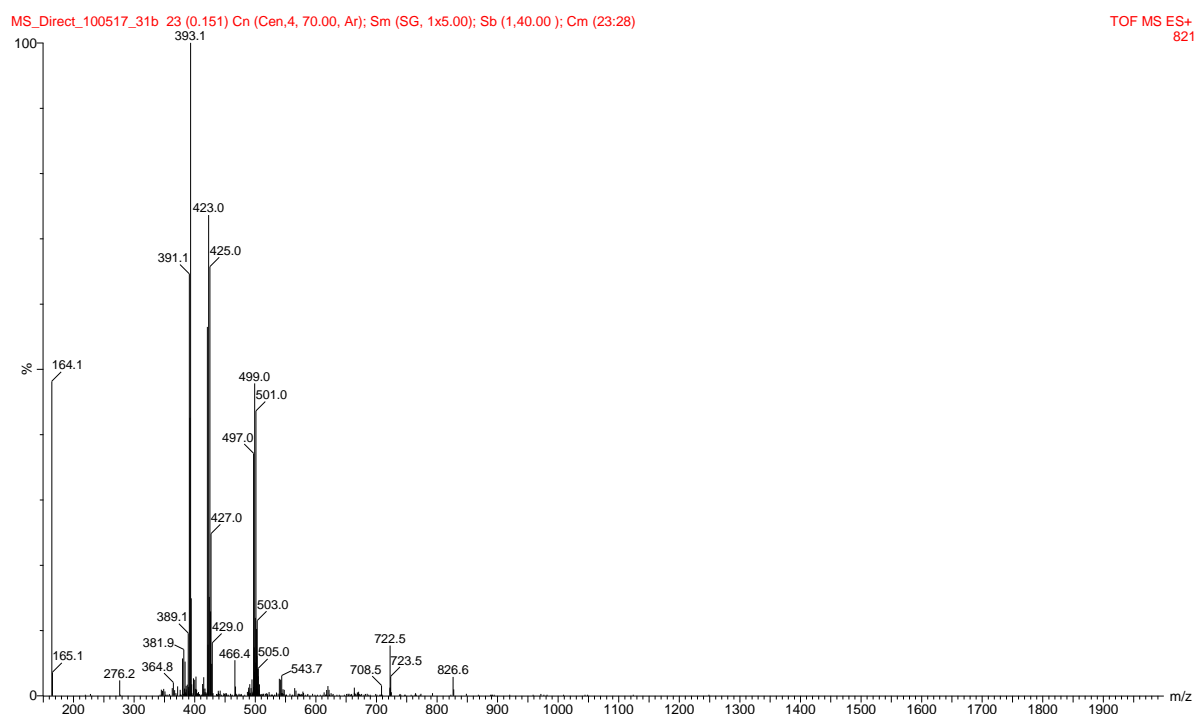
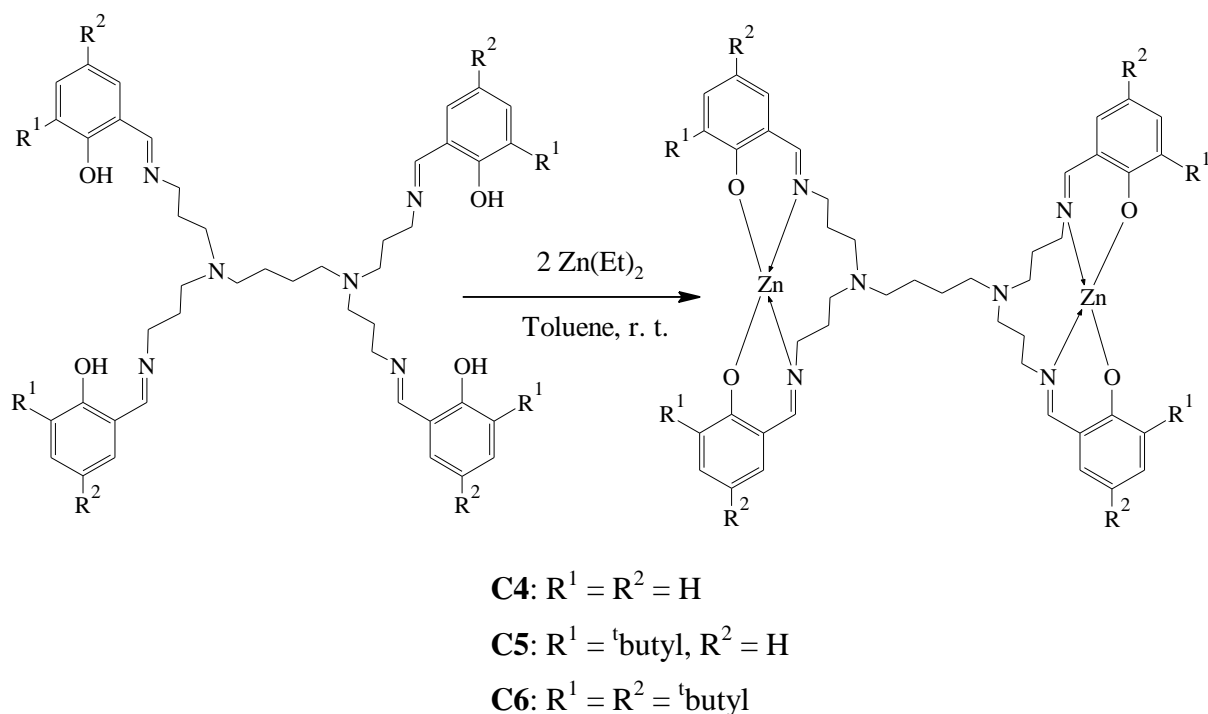


Figure 3.2: ESI-MS spectrum of bis(N-n-propyl)-3-^tbutyl salicylaldiminato Zn(II) complexes, **C2**

C3 was also analysed by ESI mass spectrometry. A number of ions were observed in the spectrum obtained. The base peak was that of the free ligand at *m/z* 276 and a singly charged ion of the expected zinc complex was observed at *m/z* 614. Similar to **C2**, aggregation of ions also occurred. A peak at *m/z* 955 corresponding to a fragment of two metals associated with three ligands was observed in the spectrum.

3.2.2: Synthesis and characterization of the 1st generation Zn(II) metallodendrimers, C4 – C6

The synthesis of the metallodendrimers was carried out following a similar protocol to that used for the mononuclear complexes. The (G1) dendritic ligands were reacted with two equivalents of diethyl zinc in toluene, Scheme 3.3.



Scheme 3.3: Preparation of the 1st generation (G1) salicylaldiminato Zn(II) complexes

The reaction mixture was stirred at room temperature for the appropriate amount of time. These complexes, **C4** – **C6**, were obtained in good yields as yellow solids of varying intensities with complex **C6** showing the most intense colour. The solubility of these complexes follows the order **C4**<**C5**<**C6**. **C4** was only slightly soluble in CH₂Cl₂ and CHCl₃ while **C6** was completely soluble in common organic solvents such as CH₂Cl₂, CHCl₃ and methanol and partially soluble in toluene. The presence of ^tbutyl groups on the phenoxy ring of **C6** enhanced its solubility dramatically.

FT-IR spectroscopy data for C4 - C6

From the infrared spectral data, Table 3.1, it was observed that there was a shift of the imine bands to lower frequency in the complexes as compared to that of the free ligands. This band appeared around 1630 cm^{-1} in the ligand while it occurred at 1621, 1618 and 1617 cm^{-1} for **C4**, **C5** and **C6** respectively. The bands associated with the $\nu(\text{C-O})$ also shifted from around 1270 to 1324, 1326, and 1327 cm^{-1} in **C4**, **C5** and **C6** respectively.

NMR spectroscopy data for C4 – C6

The $^1\text{H-NMR}$ data is summarised in Table 3.2. The imine proton resonance in **C4** shifted from $\delta\ 8.34$ ppm in the ligand to $\delta\ 8.07$ ppm. The phenolic proton was not observed signifying the deprotonation of the OH group. This is similar to what was observed for the mononuclear complexes. The remaining protons of the dendrimer framework showed broad peaks with a slight downfield shift. The broadness of these peaks is characteristic of dendritic systems due to the difference in the relaxation time of chemically equivalent protons. Another unique observation was that the signal for the methylene proton, CH_2 , adjacent to the imino group in the dendrimer frame work was split into two broad peaks at 3.36 and 4.32 ppm.

Table 3.1: Salicylaldiminato Zn(II) complexes characterization data

Complex	Yield (%)	M.p (°C)	Formula	Molecular mass ^a	FT-IR (ATR) (cm ⁻¹)		Anal Found (Calcd.)		
				Found (Calcd.)	$\nu(\text{C}=\text{N})$	$\nu(\text{C}-\text{O})$	C	H	N
C1	73	122 – 123	C ₂₀ H ₂₄ N ₂ O ₂ Zn	^b 389 (389)	1622	1321	61.52 (61.62)	6.23 (6.21)	7.22 (7.19)
C2	69	126 - 128	C ₂₈ H ₄₀ N ₂ O ₂ Zn	^b 500 (501)	1616	1321	66.72 (66.99)	7.90 (8.03)	5.26 (5.58)
C3	62	134 - 136	C ₃₆ H ₅₆ N ₂ O ₂ Zn	614 (613)	1611	1327	70.09 (70.39)	8.71 (9.19)	4.26 (4.56)
C4	78	^g 350	C ₄₄ H ₅₂ N ₆ O ₄ Zn ₂ •0.75 PhMe	^{d, e} 859 (858)	1621	1324	63.63 (63.18)	6.15 (6.68)	8.95 (9.08)
C5	82	^g 350	C ₆₀ H ₈₄ N ₆ O ₄ Zn ₂ •0.5 CH ₂ Cl ₂	^{b, e} 1083 (1082)	1618	1320	64.47 (64.63)	7.82 (7.85)	6.40 (7.41)
C6	89	^g 350	C ₇₆ H ₁₁₆ N ₆ O ₄ Zn ₂ •PhMe	^{b, e} 1309 (1306)	1614	1327	68.21 (68.01)	8.35 (8.73)	5.64 (6.22)
C7	77	^g 370	C ₉₆ H ₁₂₀ N ₁₄ O ₈ Zn ₂ •PhMe	^{d, e} 2182 (1860)	1615	1319	62.29 (62.01)	6.37 (6.50)	10.21 (10.54)
C8	81	^g 320	C ₁₂₈ H ₁₈₄ N ₁₄ O ₈ Zn ₄ •PhMe	^{b, e} 2628 (2304)	1617	1321	64.62 (64.63)	7.83 (7.85)	6.96 (7.41)
C9	85	^g 365	C ₁₆₀ H ₂₄₈ N ₁₄ O ₈ Zn ₄ •PhMe	^e 2985 (2752)	1612	1325	70.02 (70.24)	8.97 (9.25)	6.23 (6.87)

^aValues reported are those obtained from ESI-MS except in **C7-C9**, ^bMass also determined by FAB-MS, ^cReported values obtained using MALDI-TOF **C6-C9** and were observed as sodium adducts, ^dDecomposition temperature as determined using TGA

In the $^1\text{H-NMR}$ spectra of the other two 1st generation zinc complexes, similar observations to those for **C4** were made. In **C5**, the imino proton was observed at 8.07 ppm, while that in **C6** was at δ 8.11 ppm. The imino proton in complex **C6** was more shielded than that of **C5** because of the presence of the two electron donating ^tbutyl groups on the aromatic ring.

In the $^{13}\text{C-NMR}$ spectra broad carbon resonances were observed, Table 3.3. This is a common phenomenon for these dendritic systems. When the data was compared to that of the free ligands, a significant downfield shift of the imino carbon ($\underline{\text{C}}=\text{N}$) and the aromatic carbon containing the O atom ($\underline{\text{C}}-\text{O}$) is observed. There is also a slight downfield shift of the other carbon signals.

Mass spectral data for C4 – C6

These 1st generation Zn(II) salicylaldiminato complexes undergo fragmentation upon ionization under the ESI-MS conditions used. The ESI-MS data obtained for **C4** showed a singly charged molecular ion of the expected complex but with very low abundance (below 5 %). The base peak was that of a triply charged molecular ion of the free ligand at m/z 246. The other significant peaks are those of multiply charged ions of the free ligand, **L4**. In fact, the spectrum looks very similar to that of the free ligand, **L4**, obtained under similar conditions. The only difference is a number of ion peaks with very low abundance (below 5 %) that can be assigned to a doubly charged molecular ion of **C4** as well as ions resulting from fragmentation of the molecular ion of the complex. PPI and PAMAM dendrimers have previously been shown to form multiply charged species when analysed by ESI-MS.⁴²

In the case of **C5**, the higher abundance peaks are those of the singly, doubly and triply charged molecular ions of the free ligand, **L5**, at m/z 958, 480 and 320 respectively, Figure 3.3. Other peaks are observed but with relatively low abundance. The peak at m/z 1183 can

be assigned to a sodium adduct of the singly charged molecular ion of **C5** containing 4 Na ions. Similar observations are made for **C6**. Again the peaks with high abundance corresponded to the free ligand, **L6**, as well as the doubly and triply charged ions of the ligand.

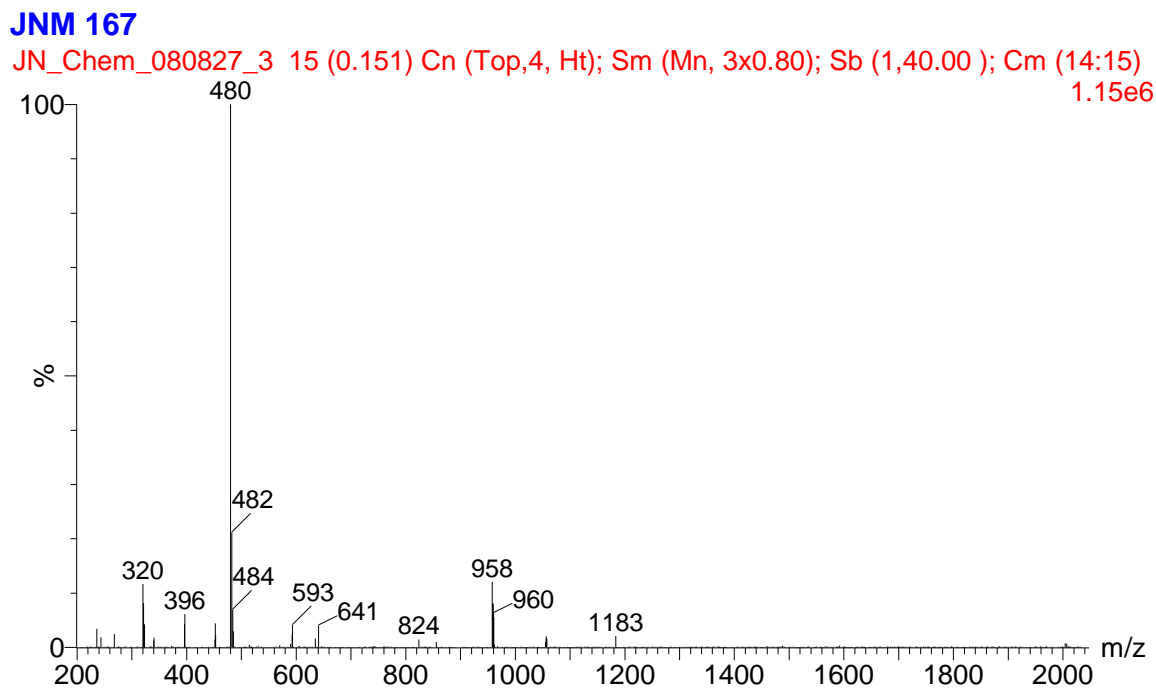


Figure 3.3: ESI-MS spectrum of G1, 3-^tbutyl phenyl salicylaldiminato Zn(II) complex, **C5**

Due to the high fragmentation observed in the ESI-MS spectra, matrix-assisted laser desorption-ionization time-of-flight) mass spectrometry (MALDI-TOF MS) was used to determine the molecular mass of these complexes. The use of a matrix renders this a softer ionization technique thus reducing the fragmentation of the analyte. In the spectra obtained, singly charged ions at m/z 859, 1082 and 1309 were obtained for **C4**, **C5** and **C6** respectively. These m/z values correspond to the expected molecular weight for the G1 dendritic salicylalimine ligand with two zinc metals centers. The base peaks for the three

compounds were obtained as sodium adducts of the doubly charged molecular ion of the metal complexes. The spectrum for **C6** is shown as an example, Figure 3.4.

In addition **C5** was also analysed by FAB-MS. Similar to the MALDI-TOF results, a singly charged molecular ion of the expected complex was observed at m/z 1084. Other ions observed in the spectrum are those of the singly charged ion of the free ligand at m/z 958, as well as that of a cyclic quaternary ammonium ion species observed at m/z 571 which are similar to those for the ligands as discussed in Chapter 2.

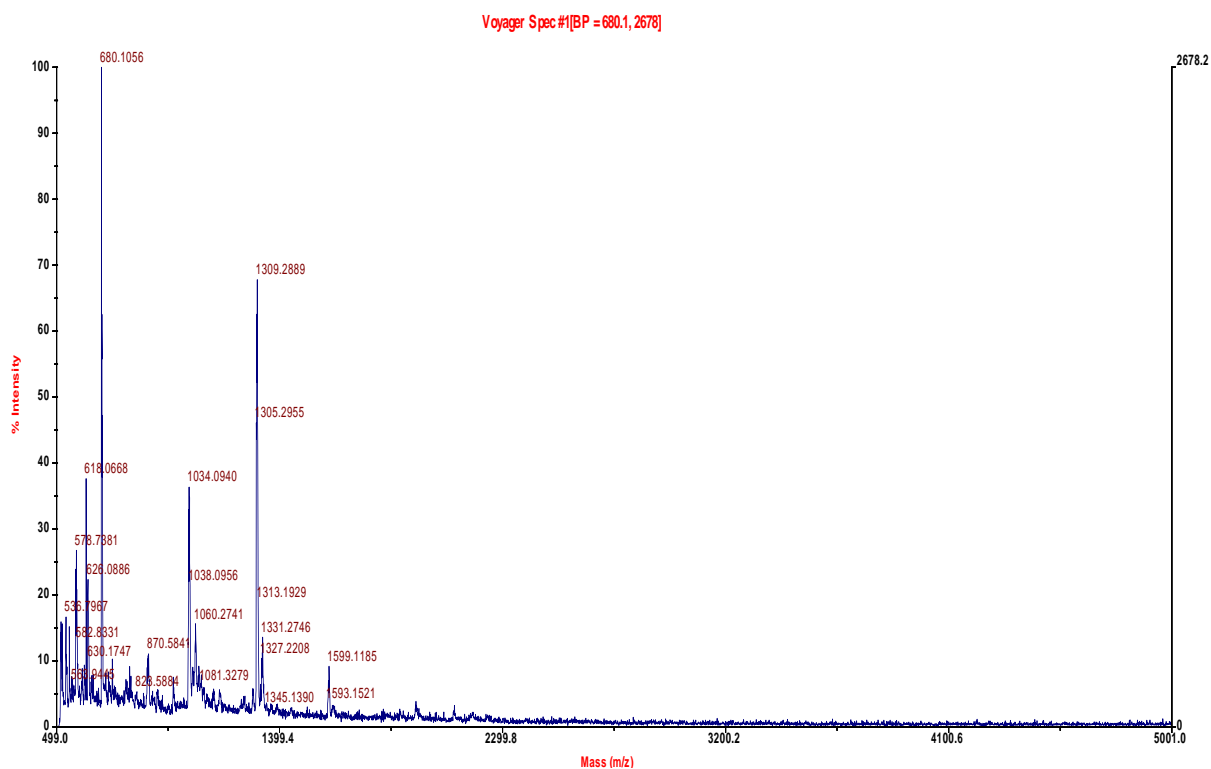


Figure 3.4: MALDI-TOF spectrum of G1, 3, 5 phenyl-^tbutyl salicylaldiminato Zn(II) complex, **C6**

Table 3.2: ^1H -NMR data for the salicylaldiminato Zn(II) complexes^a

Complex	$\underline{\text{HC}}=\text{N}$	$\text{Ar}-\underline{\text{H}}$	$\text{HC}=\text{N}\underline{\text{CH}}_2$	$\underline{\text{CH}}_2$	$\underline{\text{CH}}_3$	$\text{C}(\underline{\text{CH}}_3)_3$
C1	8.17 (s, 2H)	7.30 (t, 2H, $^3J_{\text{HH}} = 8.4$ Hz) 7.11 (d, 2H, $^3J_{\text{HH}} = 7.9$ Hz) 6.85 (d, 2H, $^3J_{\text{HH}} = 8.5$ Hz) 6.61 (t, 2H, $^3J_{\text{HH}} = 7.9$ Hz)	3.52 (t, 4H, $^3J_{\text{HH}} = 7.2$ Hz)	1.63 (m, 4H)	0.89 (t, 6H, $^3J_{\text{HH}} = 7.4$ Hz)	-
C2	8.20 (s, 2H)	7.37 (d, 2H, $^3J_{\text{HH}} = 7.5$ Hz) 7.03 (d, 2H, $^3J_{\text{HH}} = 7.7$ Hz) 6.57 (t, 2H, $^3J_{\text{HH}} = 7.7$ Hz)	3.49 (t, 4H, $^3J_{\text{HH}} = 7.2$ Hz)	1.63 (br m, 4H)	0.88 (t, 6H, $^3J_{\text{HH}} = 7.4$ Hz)	1.42 (br s, 18H)
C3	8.22 (s, 2H)	7.47 (d, 2H, $^4J_{\text{HH}} = 2.8$ Hz) 6.97 (d, 2H, $^4J_{\text{HH}} = 2.8$ Hz)	3.51 (t, 4H, $^3J_{\text{HH}} = 8.0$ Hz)	1.68 (br m, 4H)	0.89 (t, 6H, $^3J_{\text{HH}} = 8.0$ Hz)	1.42 (br s, 18H) 1.35 (br s, 18H)
^b C4	8.07 (s, 4H)	7.20 (t, 4H, $^3J_{\text{HH}} = 6.8$ Hz) 7.06 (d, 4H, $^3J_{\text{HH}} = 7.7$ Hz) 6.77 (t, 4H, $^3J_{\text{HH}} = 7.6$ Hz) 6.51 (t, 4H, $^3J_{\text{HH}} = 7.0$ Hz)	4.32 (br m, 4H) 3.36 (br t, 4H)	2.58 – 2.46 (br signal, 12H) 1.78 – 1.68 (br signal, 8H) 1.12 (br signal, 4H)		
C5	8.06 (s, 4H)	7.23 (d, 4H, $^3J_{\text{HH}} = 7.5$ Hz) 6.94 (d, 4H, $^3J_{\text{HH}} = 7.7$ Hz) 6.42 (t, 4H, $^3J_{\text{HH}} = 7.5$ Hz)	4.46 (br signal, 4H) 3.35 (br signal, 4H)	2.74 - 2.69 (br signal, 12H) 1.87 - 1.73 (br signal, 8H) 1.22 (br signal, 4H)		1.36 (br s, 36H)
C6	8.11 (s, 4H)	7.35 (br t, 4H) 6.92 (d, 4H, $^3J_{\text{HH}} = 7.8$ Hz)	4.53 br signal, 4H 3.38 (br signal, 4H)	2.75 (br signal, 12H) 1.87 - 1.77 (br signal, , 8H) 1.57 (br s, 2H)		1.43 (br s, 36H) 1.34 (br s, 36H)

Table 3.2: continued...

C7	8.09 (s, 8H)	7.17 (t, 8H, $^3J_{HH} = 8.2$ Hz)	4.35 (br signal, 8H)	2.66 – 2.55 (br signal, 24H)	
		7.04 (d, 8H, $^3J_{HH} = 7.8$ Hz)	3.44 (br signal, 8H)	2.09 (br signal, 16H)	
		6.75 (t, 8H, $^3J_{HH} = 8.4$ Hz)		1.92 (br signal, 8H)	
		6.48 (t, 8H, $^3J_{HH} = 7.3$ Hz)		1.80 (br signal, 8H)	
			1.32 (br signal, 8H)		
			1.10 (br signal, 4H)		
C8	8.09 (s, 8H)	7.30 (br d, 8H)	4.51 (br signal, 8H)	2.75 (br signal, 24H)	1.29 (br s, 72H)
		6.76 (br d, 8H)	3.37 (br signal, 8H)	2.19 (br signal, 12H)	
		6.49 (br t, 8H)		1.94 (br signal, 8H)	
			1.83 (br signal, 8H)		
C9	8.07 (s, 8H)	7.32 (br t, 8H)	4.51 (br signal, 8H)	2.75 (br signal, 24H)	1.38 (br s, 72H)
		6.86 (br d, 8H)	3.37 (br signal, 8H)	1.94 (br signal, 8H)	1.27 (br s, 72H)
				1.84 (br signal, 8H)	

^a300 MHz (CDCl₃, δ in ppm), ^b400 MHz (DMSO, δ in ppm), br = broad, s = singlet, d = doublet, t = triplet, m = multiplet

Table 3.3: $\{^1\text{H}\}$ ^{13}C -NMR shifts (δ in ppm) for the salicylaldiminato Zn(II) complexes^a

Complex	<u>HC=N</u>	<u>C-OH</u>	<u>Ar-C</u>	<u>HC=NCH₂</u>	<u>CH₂</u>	<u>CH₃</u>	<u>C and (CH₃)₃</u>
C1	171.34	169.42	139.63, 132.76, 122.54, 117.98, 114.11	62.86	23.05	10.93	
C2	171.44	170.43	142.14, 134.15, 131.18, 118.02, 113.21	63.16	23.79	11.38	35.28, 29.23
C3	171.76	168.59	141.52, 134.80, 129.46, 129.35, 116.69	63.15	23.92	11.39	35.51, 34.11, 31.41, 29.31
^b C4	171.55	168.54	134.80, 133.45, 123.04, 118.75, 113.11	57.33	52.09, 47.59, 46.98, 26.02, 18.28, 17.68		
C5	171.67	168.51	134.87, 133.38, 126.07, 119.30, 112.85	57.36	52.29, 51.57, 46.95, 45.75, 26.14, 18.03, 16.87		31.45, 26.13
C6	170.60	168.28	140.80, 133.53, 128.48, 128.12, 117.68	57.24	52.47, 51.76, 47.31, 47.09, 26.20, 17.57, 17.00		35.19, 33.88, 31.72, 29.67
C7	171.59	168.67	134.82, 133.56, 123.07, 118.69, 113.14	57.48	53.71, 52.21, 51.57, 46.25, 26.13, 24.95, 18.15		
C8	171.62	168.75	134.85, 133.66, 123.13, 118.73, 113.24	57.43	52.27, 51.64, 46.15, 28.52, 26.02, 25.00, 18.22		31.55, 26.18
C9	171.35	168.58	137.83, 133.48, 123.09, 127.67, 116.89	57.34	52.98, 52.07, 47.33, 28.64, 26.19, 24.95, 18.17		35.35, 34.01, 31.77, 29.53,

^a50 MHz (CDCl₃, δ in ppm), ^b75 MHz (DMSO, δ in ppm)

Elemental analysis data and other analytical data for C4 – C6

The micro analysis data obtained for the 1st generation Zn(II) salicylaldiminato complexes are shown in Table 3.1 and explicitly confirmed the molecular formulae as proposed in Scheme 3.3. The data also suggest solvent molecule inclusion within the cavities of the dendrimers. This is typical of these dendritic compounds.

Thermal gravimetric analysis (TGA) for C4 – C6

Thermogravimetric analysis (TGA) was performed on compounds **C4** – **C6**. The thermogram obtained for **C6** is given as an example, Figure 3.5. The decomposition profiles obtained for these metallodendrimers were similar and compare favourably to those of analogous Cu(II) and Co(II) complexes reported by Van Wyk.³⁷ There is an initial mass loss of 3 % between 100 and 150°C. This can be attributed to the loss of residual toluene encapsulated in the cavities of the dendrimer. The presence of toluene was observed in the NMR spectrum and can also be accounted for on closer inspection of the micro analysis results, Table 3.1. It should be noted that toluene was the solvent employed in the synthesis and proved difficult to remove even after prolonged drying at elevated temperature under vacuum.

There is minimal decomposition up to 320 °C. The major and last stage of the decomposition occurred as a single step between 350 to 400°C and reflected a mass loss of approximately 57 % relative to the initial mass. This can be attributed to the loss the phenolic rings. El-Said *et al.*⁴³ proposed that the phenolic rings of similar systems are lost first as free radicals.

C4 and **C5** showed similar decomposition profiles. Trapped toluene that represents about 5 % of the total mass was lost at around 120 °C. The major mass loss of about 50 % occurred between 320 and 400 °C. The remaining mass loss after heating to 600 °C was

slightly higher than 40 %. The presence of ^tbutyl substituent groups does not seem to greatly influence the thermal stability of these G1 Zn(II) metallodendrimers. van Wyk *et al.*³⁷ similarly reported that the presence of ^tbutyl groups did not affect thermal stability of Cu(II) and Co(II) metallodendrimers for the same dendrimer scaffold.

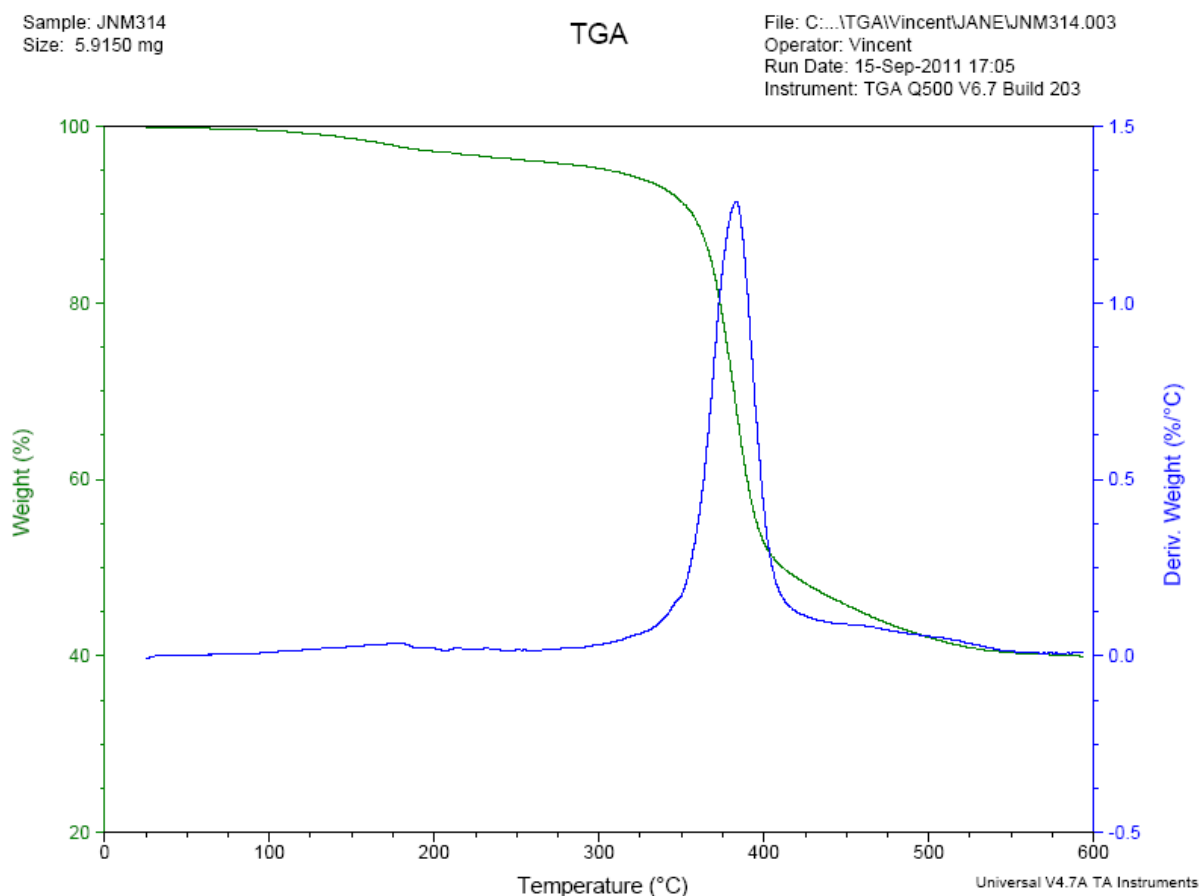


Figure 3.5: Thermogram obtained for **C4**

Differential scanning calorimetry (DSC) for complexes C4 - C6

The zinc metallodendrimers were subjected to DSC analysis over the temperature range of -20 to 210 °C. The DSC experiment entailed heating the sample at a rate of 10 °C/min then cooling followed by a second heating cycle. In all cases two thermal transitions were noted viz. a T_g and a melting endotherm. The T_g for these complexes appeared in the range

of 75 - 90 °C while the broad T_m endotherm was observed at around 180 °C. The thermograms obtained for the first generation **C4** is given as an example.

The T_g of the first generation dendrimers (**C4-C6**) were relatively weaker in intensity while the T_m were relatively broad but becomes sharper with increasing number of *t*-butyl substituents on the aromatic ring. **C6**, the system which is *di*-substituted, showed two endothermic events at *ca.* 161 and 175 °C both of which can be associated with melting. It would appear that **C6** has two different phases in the solid state. Further investigation however is required to confirm this. Ropponet *et al.*⁴⁴ reported similar broadening of the melting endotherm for aliphatic polyester dendrimers.

The lack of a T_m in the second heating cycle would seem to indicate that these compounds are not able to recrystallize from the melt. This was confirmed by the absence of any crystallization exotherm during the cooling cycle. It would thus appear that for these complexes there was loss of thermal memory during the cooling cycle. Such observations have been made for other dendritic systems. Emran and coworkers reported that amide based dendrimers lost their thermal memory after the 1st heating cycle with no exothermic event on cooling even after using a slower cooling rate of -3 °C/min.⁴⁵ Loss of thermal memory could also be due to vitrification as proposed by Wooley *et al.*⁴⁶ This however was not the case in our complexes.

There was also a gradual endothermic desolvation of the complexes between 50 – 90 °C which concurs with similar characterization on other reported Schiff base metal complexes.⁴⁷

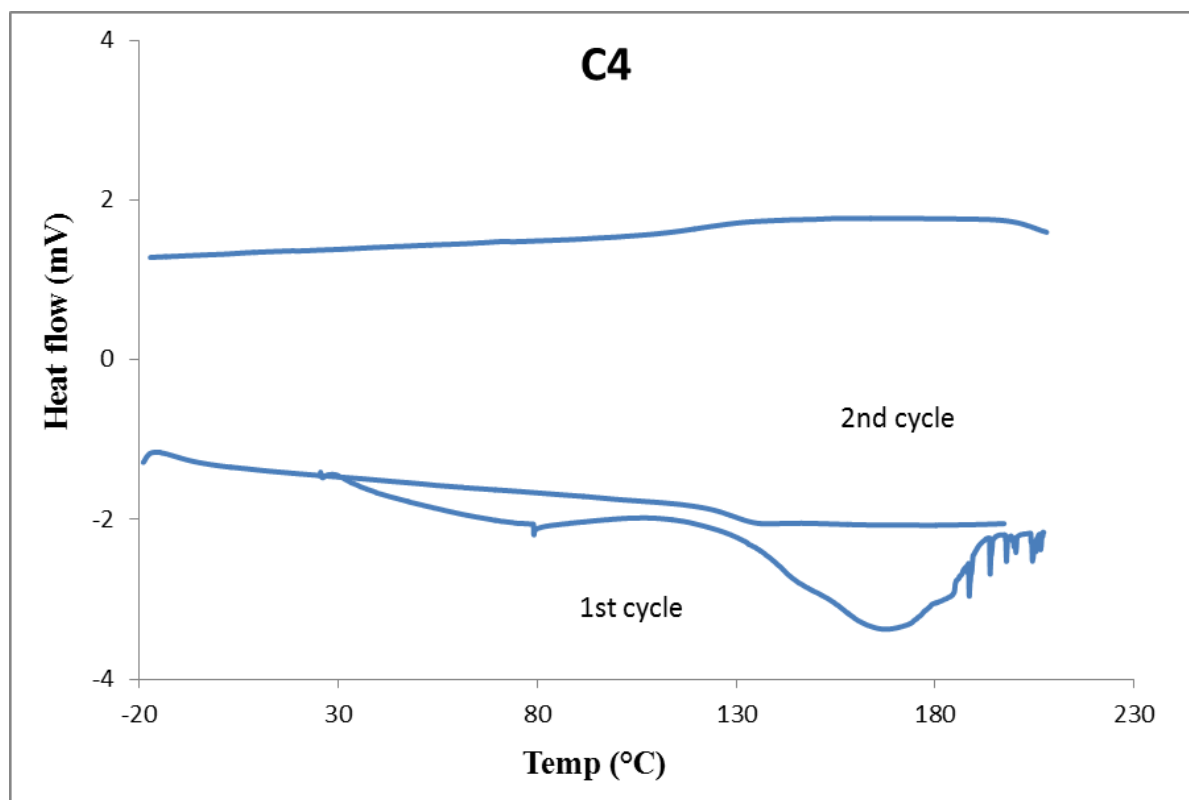
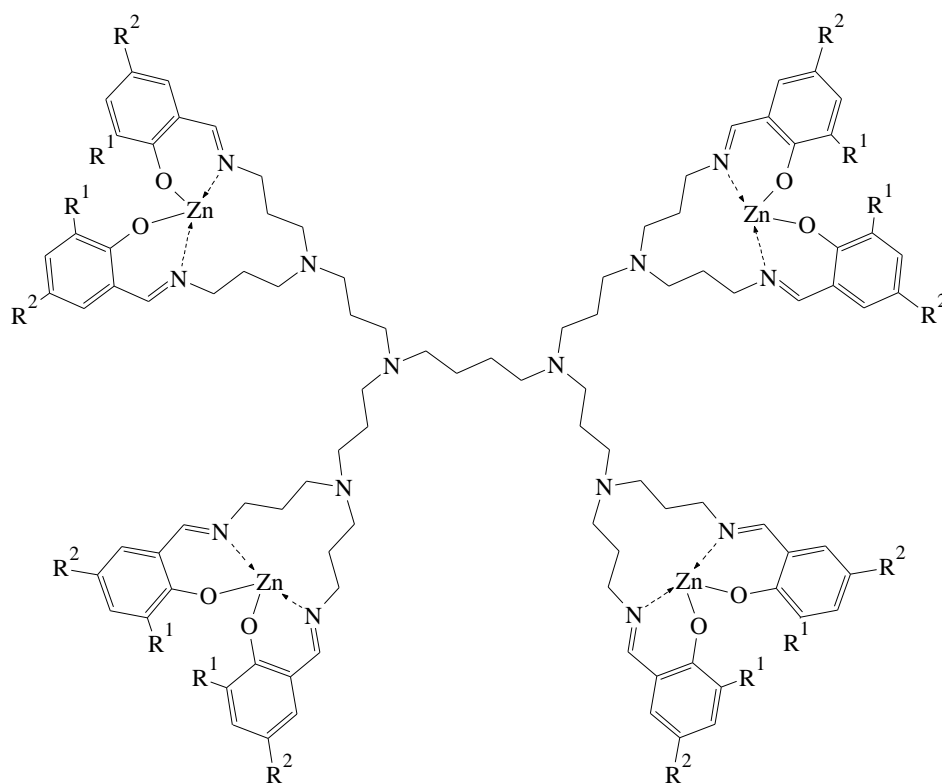


Figure 3.6: DSC plot for complex **C4**

3.2.3: Synthesis and characterization of the 2nd generation Zn(II) metallodendrimers, **C7 – C9**

The 2nd generation metallodendrimers were synthesised using a similar protocol to that of the mononuclear complexes. The G2 dendritic ligands, **L7 – L9**, were reacted with four mole equivalents of diethyl zinc in toluene. The reaction mixture was stirred at room temperature for the appropriate amount of time. Complexes **C7 – C9**, Figure 3.7, were obtained as yellow solids in good yields. These complexes were completely soluble in CH₂Cl₂, CHCl₃, and partially soluble in toluene and acetone.



C7: $R^1 = R^2 = H$

C8: $R^1 = t\text{butyl}, R^2 = H$

C9: $R^1 = R^2 = t\text{butyl}$

Figure 3.7: 2nd Generation (G2) salicylaldiminato Zn(II) metallodendrimer

FT-IR spectroscopy data for C7 – C9

The infrared spectral data is summarized in Table 3.1. Similar to the 1st generation metallodendrimers, the imine band was observed at lower wave numbers of 1615, 1617 and 1612 cm^{-1} for **C7**, **C8** and **C9** respectively.

NMR spectroscopy, C7 – C9

The ^1H -NMR data obtained for these complexes is similar to that of the G1 analogues (Table 3.2). The imine proton resonance shifted from around δ 8.30 ppm in the ligands to δ 8.07 ppm in **C9** and 8.09 ppm in both **C7** and **C8**. Again the phenolic proton was also absent. There was also a downfield shift of the aromatic proton peaks as well as those of the

dendrimer framework protons. However, the shift was greater for the aromatic proton as compared to those of the dendrimer scaffold. Broad peaks were obtained for the protons of the dendritic scaffold due to differences in relaxation time of chemically equivalent protons.⁴⁷

Similar to the ¹³C-NMR data obtained for G1 analogues, the G2 complexes also gave broad carbon resonances, Table 3.3. There was also a significant downfield shift of the signals of imino carbon (C=N) and the aromatic carbon with oxygen bonded to it (C-O) was observed.

Mass spectrometry data, C7 – C9

In the ESI mass spectrum obtained for C7 no singly or doubly charged molecular ions are observed. The expected molecular weight was 1860. The highest molecular mass peak was that of a singly charged ion corresponding to the ligand, [L7 + H]⁺ (m/z 1607). The base peak was that of the doubly charged ion of the ligand at m/z 804. Other observed ions are shown in Figure 3.8.

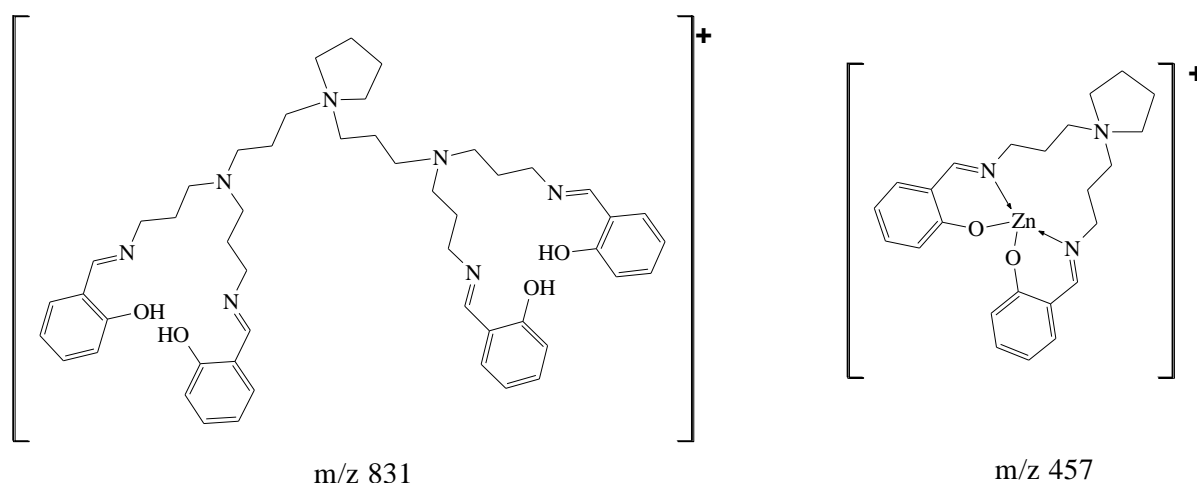


Figure 3.8: Fragments obtained in the ESI-MS spectra for 2nd generation- (phenyl- 3, 5 – *t*-butyl) salicylaldiminato Zn(II) complex C7

It should be noted that although the molecular ions of the dendritic complexes were not observed, daughter ions arising from the complex molecular ions were detected as shown in Figure. 3.8.

Similar ESI-MS data were obtained for **C8** and **C9**. The highest mass peak observed is that of the molecular ion of the ligands, **L8** and **L9**. Suitable mass spectrometry data for the 2nd generation dendrimer complexes using FAB-MS could also not be obtained. Other researchers have reported that classical mass spectrometry techniques can only be used for the characterization of small dendrimers whose molecular mass is < 3000. ESI –MS is mainly used where the dendrimers are able to form multiply charged ion species.⁵⁰

Thermal analysis (TGA) for C7 – C9

Thermogravimetric analysis (TGA) was performed on complexes **C7** – **C9**. The thermogram obtained for **C7** is given as an example, Figure 3.9. Similar to the 1st generation complexes, there was an initial mass loss of approximately 5 % which occurred between 100 and 150 °C. This loss was ascribed to the release of the encapsulated toluene. The presence of toluene can also be accounted for from the micro analysis whose data is shown in Table 3.1.

The next stage of the decomposition occurs as a single step with approximately 50% mass loss for **C7** between 350 to 400 °C. Once again this was as a result of loss the phenolic rings. However **C8** and **C9** showed slightly different decomposition profiles around this temperature. Two distinct decomposition steps are observed at *ca* 320 and 450 °C. This could be as a result of the initial loss of the ^tbutyl substituent groups followed by the phenolic rings. The presence of ^tbutyl substituent groups seems to increase the thermal stability of these G2 Zn(II) metallodendrimers. These bulky ^tbutyl groups may be involved in

intermolecular interactions with the phenol moiety and in return enhancing the thermal stability of these complexes similar to the G1 analogues **C4** - **C6**.

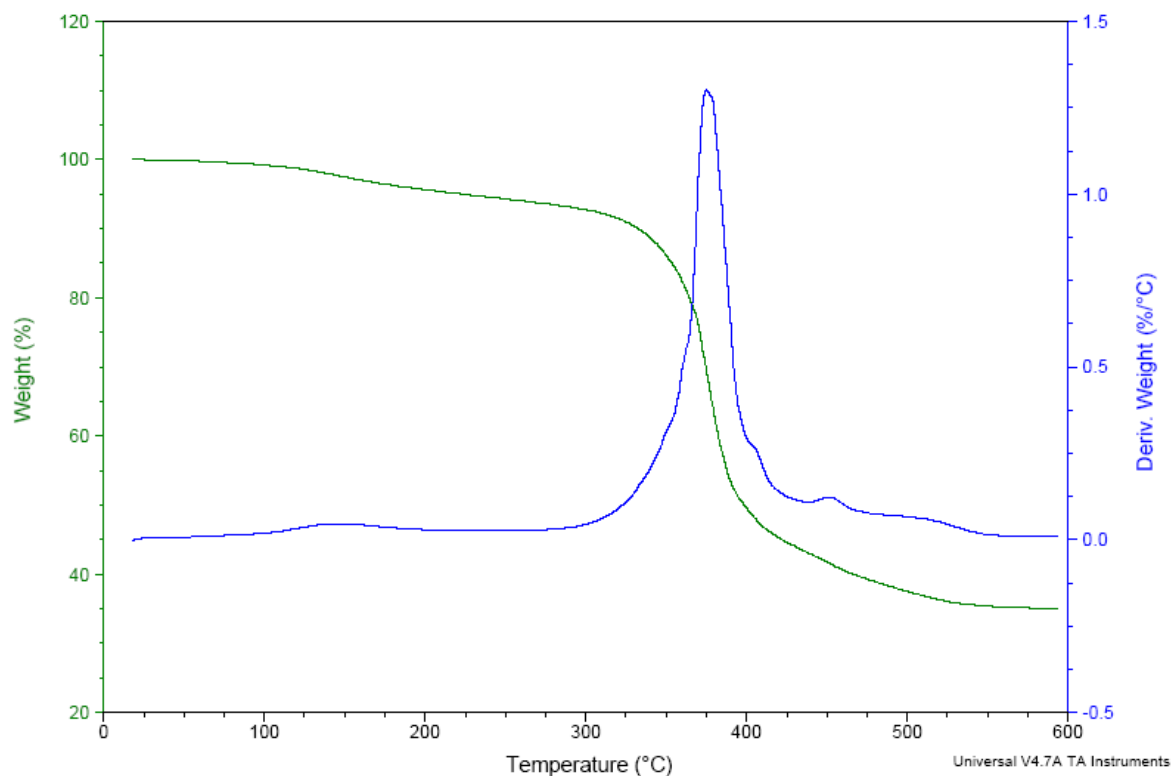


Figure 3.9: Thermogram obtained for **C7**

Differential scanning calorimetry (DSC) for complexes C7 – C9

The second generation complexes showed a similar trend with regard to the melting transition. However the T_g of these second generation analogues (**C7-C9**) were more intense than those of the first generation dendrimers (**C4-C6**). The thermogram obtained for **C9** is given as an illustration, Figure 3.10. Once again the unsubstituted analogue (**C7**) showed a very broad T_m endotherm. This endotherm becomes sharper with increasing the number of the substituents on the aromatic ring. The 3, 5-*t*-butyl substituted complex **C9** showed a very sharp melting endotherm at *ca.* 155 °C. This appears to be lower than the other two

analogues in the 2nd generation series. The alkyl substituents possibly affect intermolecular interactions leading to lowering of the melting point.

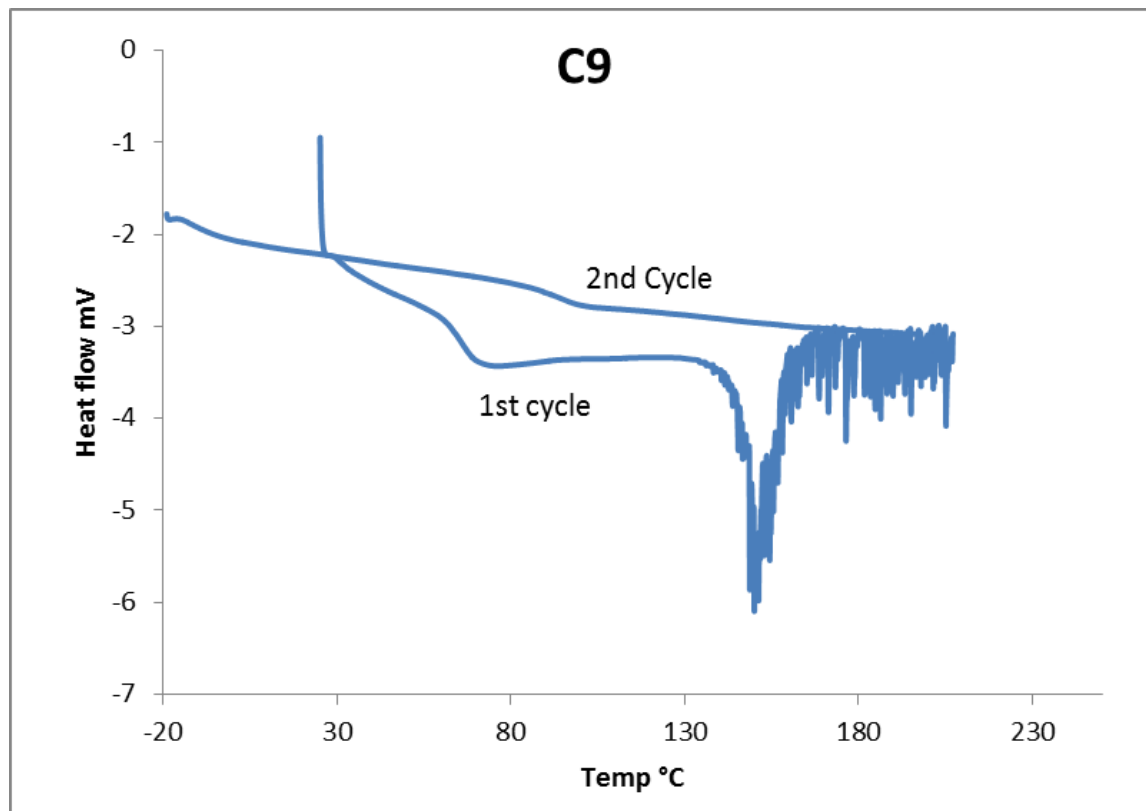


Figure 3.10: DSC profile for complexes **C9**

3.3: Conclusions

Mononuclear and multinuclear salicylaldiminato complexes were successfully prepared by the reaction of the various ligands with diethyl zinc. The complexes were fully characterized using a range of analytical techniques namely NMR and FT-IR spectroscopy, elemental analysis, mass spectrometry and thermal analysis (TGA and DSC).

The mononuclear complexes **C1** - **C3** were observed to form dimeric aggregates when ionized during the mass spectrometry analyses. The G1 complexes, **C4** - **C6**, formed complexes with two metal centers while the G2 analogues, **C7** - **C9**, had 4 metal centers.

These dendritic complexes were observed to be stable up to 300 °C, after which decomposition sets in.

3.4: Experimental

3.4.1: *Materials and instrumentation*

All manipulations were carried out on a double manifold Schlenk vacuum line under an atmosphere of nitrogen. All solvents used were of analytical grade and were dried and distilled prior to use. Toluene, hexane, and pentane were distilled from sodium/benzophenone, methanol from magnesium turnings/iodine and dichloromethane over phosphorous pentoxide. Diethyl zinc (1.1 M solution in toluene), ZnCl₂ and Zn(OCH₃)₂·2H₂O were obtained from Sigma-Aldrich Ltd. All starting reagents were used without further purification.

The NMR spectra were recorded on a Varian 300 VNMRS spectrometer (¹H at 300 MHz, ¹³C{¹H} at 75.4 MHz) or (¹H at 400 MHz, ¹³C{¹H} at 100 MHz) at room temperature using tetramethylsilane as an internal standard. The chemical shifts are reported in δ (ppm) and referenced relative to the NMR solvent.

ESI-MS spectra were obtained on a Waters API Q-TOF Ultima spectrometer calibrated with NaF at the University of Stellenbosch. Fast atom bombardment mass spectrometry (FAB-MS) was performed on a VG70SE using an 8kV argon atom source and 3-nitrobenzyl alcohol matrix at the University of the Witwatersrand. MALDI-TOF mass spectrometry was carried out on a Voyager DE STR MALDI-TOF spectrometer at the University of Stellenbosch.

Micro analyses were performed at the University of Cape Town micro analytical Laboratory. Infrared spectra were recorded on a Nicolet Avatar 330 FT-IR spectrophotometer using an ATR accessory.

Melting points were determined on a Stuart Scientific melting point apparatus (SMP3) at heating rate of 0.5 °C/min. Thermogravimetric analyses (TGA) were done on a TGA Q500 V6.7 modulus coupled with a thermal analyser. The differential scanning calorimetric (DSC) curves were recorded in a closed system on a DSC Q100 V9.9 Build 303 modulus. An aluminum pan was loaded with *ca.* 5 mg of sample and heating ramped at 10 °C/min under a nitrogen atmosphere at a flow rate of (50 ml/min). A pinhole on the lid was made to prevent pressure build up due to gaseous products. The thermal analytical data was collected between 20 to 598°C while DSC was from -20 to 200 °C.

3.4.1.1: General method for the MALDI-TOF MS spectrometry

The MALDI-TOF MS spectra for **C5 - C9** were recorded on a Voyager DE STR MALDI-TOF spectrometer equipped with a 2 m linear and a 3 m reflector flight tube and a 337 nm nitrogen laser. All spectra were obtained with an acceleration potential of 20 kV in the positive ion mode in ACTH linear and reflector mode. Dithranol was used as matrix (40 mg/mL in THF) sodium trifluoroacetate was used as the ionizing salt (1 mg/mL in THF) and the ligands (10 mg/mL in THF). The three solutions were then mixed at a volume ratio of 10:5:1 for matrix:ligand:NaTFA. The solution mixture was then spotted on a steel plate and air dried. In the case of **C4**, 20 mg of appropriate matrix, 10 mg of the sample and 5 mg NaTFA were ground together. The sample was then mounted by smearing the mixture on a sample plate using a microspatula. A drop of THF (less than 0.5 µl) was added to have better adhesion of the sample on the plate. The sample was left to dry in air. Calibration was done using a polyethylene glycol (PEG) 1000 (*Da*) sample. All the data were processed using the Voyager data processing software.

3.4.2: Preparation of salicylaldiminato Zn(II) complexes

3.4.2.1: General procedure for the synthesis of mononuclear Zn(II) complexes; **C1** – **C3**

The complexes were prepared by the reaction of diethyl zinc with two mole equivalents of ligands; **L1** – **L3**. The synthesis of **C1** is used to illustrate this.

In a Schlenk tube, a degassed yellow solution of n-propyl-salicylaldimine ligand; **L1** (0.3 g, 1.8 mmols) in dry toluene (10 mL) was mixed with diethyl zinc (1.0 mL, 1.0 mmols). The yellow mixture was stirred at room temperature for 2 h. No visible changes were observed over the reaction time. After 2 h, all volatiles were removed yielding a cream-yellow solid. The solid was dissolved in CH₂Cl₂, air filtered and all volatiles removed. A white crystalline product was obtained after recrystallization from hexane (3 mL) at -78 °C. **C2** and **C3** were recrystallized by slow diffusion of ethanol into a solution of the complex in dichloromethane at a volume ratio of 2:5. The complexes were obtained in moderate to good yields between 62 -75 %. **C1** was cream in colour, **C2** was light yellow while **C3** was yellow-green (lime) in colour.

3.4.2.2: General procedure for the synthesis of 1st and 2nd generation salicylaldimine metallodendrimers **C4** - **C9**

1st or 2nd generation salicylaldimine ligands; **L4** – **L9** were reacted with appropriate amounts of Zn(C₂H₅)₂. All the complexes were obtained as light yellow solids. The synthesis of **C5** is used as an example.

In a Schlenk tube a degassed solution of **L5**, (0.3 g, 0.313 mmol) in dry toluene (10 mL) had Zn(C₂H₅)₂ (0.9 mL, 0.9 mmols) added. The solution was then stirred at room temperature. After 20 minutes, the solution went cloudy and a precipitate began to form after about 40 minutes. The mixture was stirred for a further 1 h. No further changes were observed. After the reaction, toluene was removed giving a light yellow solid. The product

was insoluble in most common solvents except for CH₂Cl₂, THF and CHCl₃ in which it was partially soluble irrespective of the solution temperature.

A similar protocol was used for the synthesis of **C4** and **C6**; however longer reaction times (up to 6 h) are required to achieve appreciable yields. Yields 80 – 96 %.

3.5: References

1. N. Nimitsiriwat, V. C. Gibson, E. L. Marshall, M. R. J. Elsegood, *Dalton Trans.*, (2009) 3710.
2. J. Liu, N. Iwasa, K. Nomura, *Dalton Trans.*, (2008) 3978.
3. P. A. Cameron, V. C. Gibson, C. Redshaw, J. A. Segal, M. D. Bruce, A. J. P. White, D. J. Williams, *Chem. Commun.*, (1999) 1883.
4. L. Benisvy, R. Kannappan, Y.-F. Song, S. Milikisyants, M. Huber, I. Mutikainen, U. Turpeinen, P. Gamez, L. Bernasconi, E. Jan Baerends, F. Hartl, J. Reedijk, *Eur. J. Inorg. Chem.*, (2007) 637.
5. M. A. Torzilli, S. Colquhoun, J. Kim, R. H. Beer, *Polyhedron*, **21** (2002) 705.
6. J. L. van Wyk, S. F. Mapolie, A. Lennartson, M. Håkansson, S. Jagner, *Naturforschung*, **62b** (2007) 331.
7. M. A. Torzilli, S. Colquhoun, D. Doucet, R. H. Beer, *Polyhedron*, **21** (2002) 697.
8. J. Lewiński, J. Zachara, I. Justyniak, M. Dranka, *Coord. Chem. Rev.*, **249** (2005) 1185.
9. D. Chandran, C. H. Kwak, C.-S. Ha, I. Kim, *Catal. Today*, **131** (2008) 505.
10. N. Poulter, M. Donaldson, G. Mulley, L. Duque, N. Waterfield, A. G. Shard, S. Spencer, A. T. A. Jenkins, A. L. Johnson, *New J. Chem.*, **35** (2011) 1477.
11. D. Aiello, L. Malfatti, T. Kidchob, R. Aiello, F. Testa, I. Aiello, M. Ghedini, M. L. Deda, T. Martino, M. Casula, P. Innocenzi, *J. Sol-Gel Sci. Technol.*, **47** (2008) 283.
12. Q. Su, Q.-L. Wu, G.-H. Li, Y. Mu, *Polyhedron*, **26** (2007) 5053.

13. G. A. Morris, H. Zhou, C. L. Stern, S. T. Nguyen, *Inorg. Chem.*, **40** (2001) 3222.
14. S. Bhunora, J. Mugo, A. Bhaw-Luximon, S. Mapolie, J. L. van Wyk, J. Darkwa, E. Nordlander, *Appl. Organometal. Chem.*, **25** (2011) 133–145.
15. J. Darensbourg, P. Rainey, J. Yarbrough, *Inorg. Chem.*, **40** (2001) 986.
16. V. T. Kasumov, F. Köksal, Y. Zeren, *Spectrochimica Acta Part A*, **63** (2006) 330.
17. I. Yilmaz, *Trans. Met. Chem.*, **33** (2008) 259.
18. V. T. Kasumov, *Trans. Met. Chem.*, **28** (2003) 888.
19. M. Kettunen, A. S. Abu-Surrah, H. M. Abdel-Halim, T. Repo, M. Leskela, M. Laine, I. Mutikainen, M. Ahlgren; *Polyhedron*, **23** (2004) 1649
20. J. Liu, N. Iwasa, K. Nomura, *Dalton Trans.*, (2008) 3978
21. J. L. van Wyk, S. F. Mapolie, A. Lennartson, M. Håkansson, S. Jagner, *Inorg. Chim. Acta*, **361** (2008) 2094.
22. D. Chandran, C. H. Kwak, C.-S. Ha, I. Kim, *Catal. Today*, **131** (2008) 505
23. A. J. L. Villaraza, A. Bumb, M. W. Brechbiel, *Chem. Rev.*, **110** (2010) 2921.
24. P. Kumar, K. P. Meena, P. Kumar, C. Choudhary, D. S. Thakur, P. Bajpayee, *JITPS*, **1** (6) (2010) 252.
25. B. Helms, E. W. Meijer, *Science*, **313** (2006) 929.
26. S. Hecht, J. M. J. Fréchet, *Angew. Chem. Int. Ed.*, **40** (2001) 74.
27. R. Meijboom, M. J. Overett, J. R. Moss, *J. Organomet. Chem.*, **689** (2004) 987.
28. S–H. Hwang, C. D. Shreiner, C. N. Moorefield, G. R. Newkome, *New J. Chem.*, **131** (2007) 1192.
29. V. Balzani, P. Ceroni, M. Maestri, V. Vicinelli, *Current Opinion in Chem. Bio.*, **7** (2003) 657.
30. F. Vögtle, M. Gorke, R. Hesse, P. Ceroni, M. Maestri, V. Balzani, *Photochem. Photobiol. Sci.*, **1** (2002) 45.

31. B. Jan Ravoo, *Dalton Trans.*, (2008) 1533.
32. V. Balzani, G. Bergamini, P. Ceroni, F. Vögtle, *Coord. Chem. Rev.*, **251** (2007) 525.
33. N. E. Domracheva, V. I. Morozov, M. S. Gruzdev, R. A. Manapov, A. V. Pyataev, G. Lattermann, *Macromol. Chem. Phys.*, **211** (2010) 791.
34. M. T. Kaczmarek, M. Kubicki, and W. Radecka-Paryzek, *Monatshefte für Chemie*, **137** (2006) 997.
35. R. Malgas-Enus, S. F. Mapolie, G. S. Smith, *J. Organomet. Chem.*, **693** (2008) 2279.
36. R. Malgas, S. F. Mapolie, S. O. Ojwach, G. S. Smith, J. Darkwa, *Catal. Commun.*, **9** (2008) 1612.
37. J. L. van Wyk, Ph.D. Thesis title, “*Mononuclear and Multinuclear Salicylaldimine Metal Complexes as Catalysts Precursors in the Oxidation of Phenol and Cyclohexene*”, University of the Western Cape, 2008.
38. Y. Tancu, MSc. Thesis title, “*Monofunctional and Dendritic Schiff base (N, N’) Ruthenium Carbene Complexes and (N, O) Related Ruthenium Complexes: Synthesis, Characterization, and their Catalytic activity in Olefin Metathesis Reactions*” Stellenbosch University, 2010.
39. M. M. Campos-Vallette, K. A. Figueroa, R. Latorre, V. Manriquez, G. Diaz, J. Costamagna, M. Otero, *Vib. Spectrosc.*, **4** (1992) 77.
40. K. J. Rosman, *Geochim. Cosmochim. Acta*, **36** (1972) 801.
41. S. Arockiasamy, M. G. Johnson, C. Mallika, O.M. Sreedharan, K.S. Nagaraj, *Mater. Chem. Phys.*, **114** (2009) 456.
42. J. C. Hummelen, J. L. J. van Dongen, E. W. Meijer, *Chem. Eur. J.*, **3** (1997) 1489.
43. A. I. El-Said, *J. Therm. Anal. Cal.*, **68** (2002) 917.
44. J. Roppenen, T. Tuuttila, M. Lahtinen, S. Nummelin, K. Rissanen, *J. Polym. Sci. Part A: Polym. Chem.*, **42** (2004) 5574.

45. S. K. Emran, G. R. Newkome, C. D. Weis, J. P. Harmon, *J. Polym. Sci., Part B: Polym. Phys.*, **37** (1999) 2025.
46. K. L. Wooley, C. J. Hawker, J. M. Pochan, J. M. J. Frécher, *Macromolecules*, **26** (1993) 1514.
47. É. T. G Cavalheiro, F. C. D. Lemons, J. Zukerman, E. R. Dockal, *Thermochimica Acta*, **370** (2001) 129.
48. A. Kriza, M. L. Dianu, C. Andronescu, A. E. Rogozea, A. M. Musuc, *J. Therm. Anal. Cal.*, **100** (2010) 929.
49. G. R. Newkome, K. S. Yoo, S. Hwang, C. N. Moorefield, *Tetrahedron*, **58** (2003) 3955.
50. J. Peterson, V. Allikmaa, J. Subbi, T. Pehk, M. Lopp., *Eur. Polym. J.*, **39** (2003) 33.

Chapter 4 : Synthesis and Characterization of Pyrrolylaldiminato and Salicylaldiminato Pd(II) Complexes

4.1: Introduction

Salicylaldiminato and pyrrolyaldiminato palladium complexes have previously been applied as catalyst precursors in various processes. Metal complexes stabilized by anionic bidentate chelating pyrrolyaldimine ligands were first reported in the 1960's by Holm *et al.*¹ and Yen *et al.*² However until they were reported as catalysts by Brookhart and Gibson in the 1990's they had not received much attention as compared to other types of Schiff base ligands e.g. salicylaldimines.^{3, 4} Since then, several researchers have evaluated these complexes as catalyst precursors. Metal complexes of these N, N bidentate ligands include those of Ti(IV)^{5, 6}, Zr(IV) and Hf(IV)⁷, Pt(II)⁸, Cr(III)^{9, 10}, Ru(II)^{11, 12}, Ni(II)¹³⁻¹⁵, Cu(II)¹⁶, Co(II) and (III)^{17, 18}, Pd(II)¹⁹⁻²¹, Y(III)^{22, 23}, Sm(III)²⁴, Zn(II) and Mg(II)²⁵, Al(III)²⁶, Ln²⁷, and V(III)²⁸. Most of the pyrrole-imine complexes have been used in the oligomerization and of olefins.²⁹ We have previously synthesised and applied Cu(II), Ni(II) Co(II) and Co(III) pyrrolyaldiminato complexes as catalysts in the oxidation of phenol and cyclohexene.^{15, 29} Another application has been as lactide polymerization catalysts.^{23, 31}

The preparation of these complexes is similar to that of other Schiff base metal complexes. As with the salicylaldimine systems discussed in Chapter 3, the synthetic route to pyrrolyaldiminato metal complexes is dependent on the target molecule. The most favoured approach is the preparation of the ligand salt followed by complexation with the metal precursor. This protocol allows for the development of metal compounds with ancillary ligands where necessary as in the case with Ru(II)¹¹ and Ni (II)^{16, 32}. The template-type synthesis favours bis-ligated metal complexes and is best suited when one of the intermediates is chemically unstable as reported for a Co(II) complex by Chandran *et al.*³³

In this Chapter we report on the synthesis and characterization of mononuclear and multinuclear of Pd(II) complexes derived from pyrrole-imine and salicylaldimine ligands. Palladium acetate was reacted with some of the ligands discussed in Chapter 2. These

complexes were characterized using a range of analytical techniques such as NMR and FT-IR spectroscopy, mass spectrometry and micro analysis. The molecular structure of **C14** was also determined using single crystal X-ray diffraction (SXRDR).

4.2: Results and discussion

4.2.1: Preparation of mononuclear pyrrolylaldiminato Pd(II) complexes, **C10** and **C11**

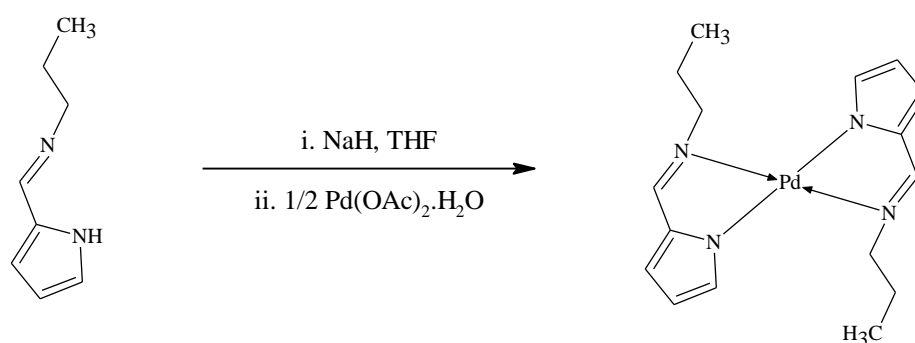
4.2.1.1: Preparation and characterization of the mononuclear pyrrolylaldiminato Pd(II) complexes, **C10**

The mononuclear pyrrolylaldiminato Pd(II) complex was prepared by first deprotonating the pyrrole-imine ligands with sodium hydride in stoichiometric amounts. The deprotonation proceeded cleanly affording a pink solution of the ligand salt. After filtration of unreacted NaH under nitrogen, the sodium salt of the ligand was then reacted with Pd(OAc)₂·H₂O in a mole ratio of 2:1 respectively, Scheme 4.1. On adding the acetate, the pink solution gradually turned orange. After 6 hours all volatiles were removed. The synthetic protocol is similar to that reported for Cu(II) analogues but with slight modification.¹⁵ An analytically pure orange crystalline product was obtained after recrystallization by slow evaporation from hexane giving a 78 % yield. Complex formation can also be achieved without the deprotonation of the ligand but with lower yields and requiring longer reaction time.

These complexes are stable at room temperature and can be stored without apparent decomposition in the solid state. Some palladium black was formed after prolonged time in CHCl₃ or CH₃OH solutions.

FT-IR spectroscopy data for C10

The FT-IR spectrum obtained for **C10** showed a shift to lower frequency by about 36 cm^{-1} to 1600 cm^{-1} for the $\nu(\text{C}=\text{N})$ stretching band in the complex, Table 4.1. This shift signifies the coordination of the ligand to the palladium through the imino nitrogen. The absence of the broad band at *ca.* $3200\text{-}3084\text{ cm}^{-1}$ was indicative of deprotonation of the pyrrole nitrogen. The shift is similar to that of the Cu(II) system previously reported.¹⁶



Scheme 4.1: Synthetic route for pyrrole-imine Pd(II) complex, **C10**

NMR spectroscopy data for C10

The ¹H-NMR spectrum of complex **C10** exhibits the imine proton peak at δ 7.42 ppm compared to δ 8.04 ppm for the free ligand. Coordination of the ligand to the palladium resulted in an upfield shift of the imine proton resonance. The resonance of the methylene protons, CH_2 , adjacent to the imino group ($\text{C}=\text{NCH}_2$) also shifted upfield by about 0.03 ppm. The central CH_2 of the propyl group showed a downfield shift of 0.09 ppm while the terminal CH_3 showed a downfield shift of only 0.01 ppm. In the pyrrole ring, the proton at position 5 showed a slight downfield shift of 0.06 ppm compared to that of the free ligand to δ 6.97 ppm in the complex. However the resonance of the proton at position 3 gave an upfield shift of the same magnitude to δ 6.22 ppm. A greater downfield shift of 0.16 ppm was recorded for

the proton at position 4 resonating at δ 6.72 ppm. The complete ^1H -NMR data is summarized in Table 4.3.

In the ^{13}C -NMR data, Table 4.2, there is a clear shift of the carbon signals when compared to those of the free ligand. The coordination of the ligand to the metal produces a downfield shift of the imino carbon ($\text{C}=\text{N}$) resonance by 10 ppm to δ 161.73 ppm as compared to the ligand's free ligand. The resonances of the pyrrole carbon also shift downfield. However, the propyl carbons show a slight upfield shift

Mass spectrometry data for C10

ESI-MS was used in the mass spectrometry analysis of **C10**. The data obtained concur with a *bis*(pyrrolide-imine) Pd(II) complex. An isotopomeric cluster of singly charged molecular ions centered at $m/z = 377$ for $[\text{M}+\text{H}]^+$ was observed. Palladium has six isotopes ^{102}Pd , ^{104}Pd , ^{105}Pd , ^{106}Pd , ^{108}Pd , and ^{110}Pd with percentage abundance of 1.02, 11.14, 22.33, 27.33, 26.46 and 11.72 respectively. Dimerization after ionization similar to that of the mononuclear zinc complexes, discussed in Chapter 3 was also observed for this palladium complex.³⁴ Scheme 4.2 shows the fragmentation and aggregation. The NMR spectral data (Table 4.3) as well as the elemental analysis (Table 4.1) agreed with the calculated values showing that **C10** is a *bis*(pyrrolide-imine) complex.

Table 4.1: Characterization data for Pd(II) complexes of pyrrolyaldimine and salicyaldimine ligands

	Yield (%)	M.p (°C)	Formula	ESI-MS m/z [M+H] ⁺ Found (Calcd)	FT-IR (cm ⁻¹)		Anal Found (Calcd.)		
					$\nu(\text{C}=\text{N})$	$\nu(\text{C}-\text{O})$	C	H	N
C10	78	199-201	C ₁₆ H ₂₂ N ₄ Pd	378 (377)	1600		50.90 (51.0)	5.99 (5.89)	14.52 (14.87)
C11	70	270-272	C ₃₄ H ₄₂ N ₄ Pd	614 (613)	1591		66.30 (66.60)	6.85 (6.90)	9.27 (9.14)
^{a, b} C12	52	150-280	C ₄₄ H ₆₀ N ₁₀ O ₈ Pd ₄ ·THF	-	1582		43.59 (42.30)	5.77 (5.62)	12.69 (10.28)
^{a, b} C13	53	120-320	C ₉₆ H ₁₃₆ N ₂₂ O ₁₆ Pd ₈ ·4THF	-	1583		44.40 (44.93)	6.64 (5.68)	12.6 (10.69)
C14	67	191-193	C ₂₀ H ₂₄ N ₂ O ₂ Pd	431 (430)	1614	1318	55.62 (55.76)	5.82 (5.61)	6.26 (6.50)
C15	65	153-155	C ₂₈ H ₄₀ N ₂ O ₂ Pd	543 (542)	1607	1305	61.72(61.93)	7.02 (7.42)	4.86 (5.16)
C16	70	179-181	C ₃₆ H ₅₆ N ₂ O ₂ Pd	655 (654)	1610	1307	65.84 (65.99)	8.17 (8.61)	3.60 (4.28)
^{a, b} C17	85	300-400	C ₄₄ H ₅₂ N ₆ O ₄ Pd ₂ ·0.5H ₂ O	-	1620	1319	55.44 (55.58)	5.48 (5.62)	8.73 (8.73)

^aDecomposition temperature range as determined using TGA, ^bMass spectra not recorded for **C12**, **C13** and **C17** due to their insolubility

Table 4.2: {¹H}¹³C-NMR shifts (75 MHz in CDCl₃ δ in ppm) data for the mononuclear pyrrolyaldiminato and salicyaldiminato complexes^a

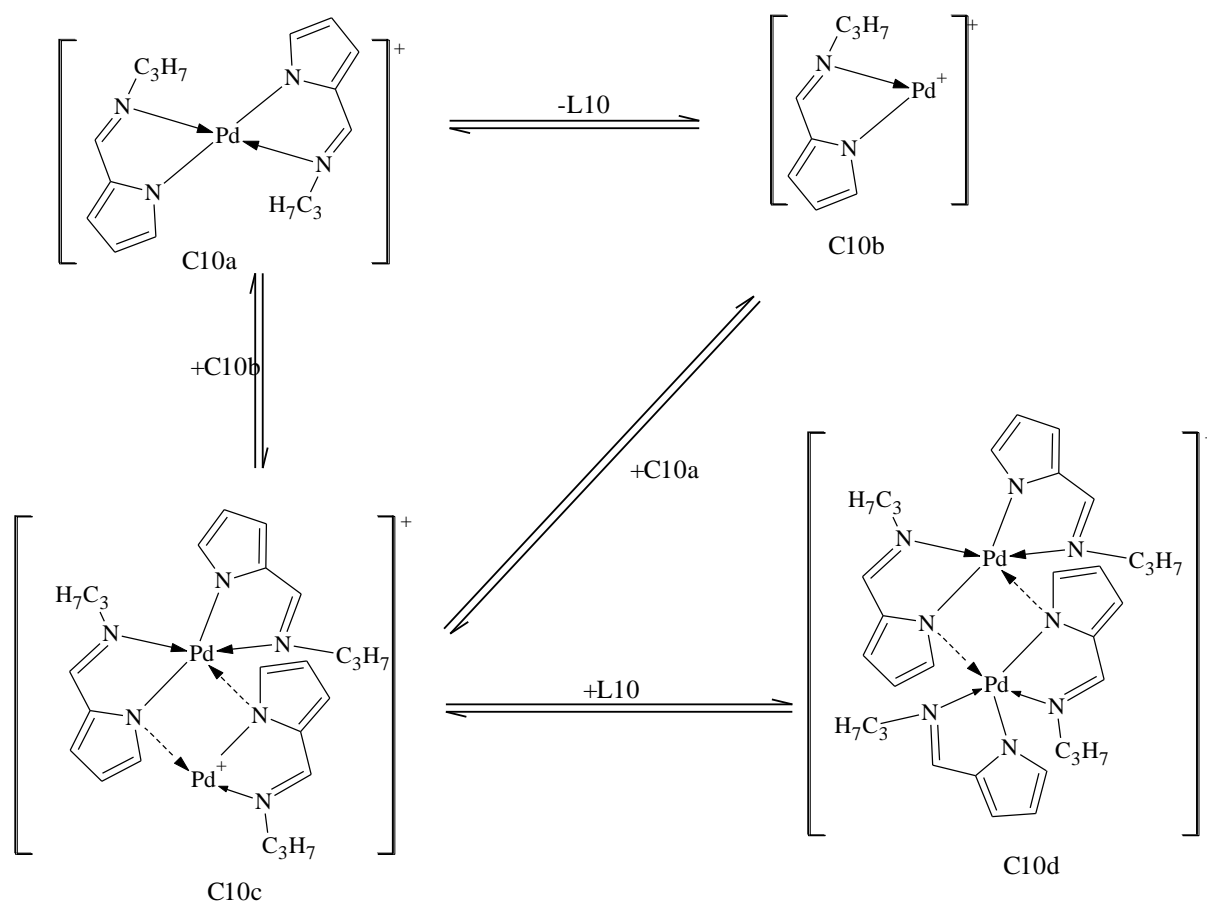
	<u>HC=N</u>	<u>Ar-C-X</u>	<u>Ar-C</u>	<u>HC=NCH₂</u>	<u>-CH₂-</u>	<u>-CH₃</u>	^t Butyl-(<u>C</u> and <u>CH₃</u>)	ⁱ Pr-(<u>CH</u> and <u>CH₃</u>)
C10	161.73		139.93, 135.61, 117.13, 110.66	60.19	24.10	10.55		
C11	164.3	160.9	146.9, 142.9, 139.2, 137.3, 135.8, 127.5, 126.4, 118.1, 118.3,					28.1, 28.0, 25.7, 24.4, 22.7, 22.3
C14	164.46	161.52	134.35, 133.99, 120.29, 120.14, 114.80	60.13	25.39	11.31		
C15	164.28	162.02	139.47, 132.49, 131.19, 122.30, 114.38	60.68	25.85	11.24	35.18, 29.21	
C16	162.42	162.23	138.71, 136.08, 129.35, 127.82, 121.23	60.64	25.82	11.24	35.42, 33.29, 31.34, 29.28	

^a**C12**, **C13** and **C17** are insoluble in all organic solvents thus no solution NMR could be acquired

Table 4.3: $^1\text{H-NMR}$ (300 MHz in CDCl_3 , δ in ppm) data for the pyrrolylaldiminato and salicylaldiminato Pd(II) complexes^a

	<u>HC=N</u>	<u>Ar-H</u>	<u>HC=NCH₂</u>	<u>CH₂</u>	<u>CH₃</u>	<u>Butyl-(CH₃)</u>	<u>Pr-(CH, CH₃)</u>
C10	7.42 (s, 2H)	6.97 (br s, 2H) 6.72 (dd, 2H, $^3J_{\text{HH}} = 4.8$ Hz) 6.22 (dd, 2H, $^3J_{\text{HH}} = 5.4$ Hz)	3.56 (t, 4H, $^3J_{\text{HH}} = 7.2$ Hz)	1.82 (m, 4H, $^3J_{\text{HH}} = 7.4$ Hz)	0.99 (t, 6H, $^3J_{\text{HH}} = 7.4$ Hz)		
C11	7.39 (s, 2H)	7.06(m, 3H, Ph-H) 6.92 (m, 3H) 6.81 (d, 2H, $^4J_{\text{HH}} = 2.3$ Hz) 6.38 (dd, 2H, $^4J_{\text{HH}} = 1.9$ Hz)					0.96 (m, 24H) 3.33 (m, 4H)
C14	7.62 (s, 2H)	7.25 (dt, 2H, $^3J_{\text{HH}} = 8.2$ Hz) 7.20 (dd, 2H, $^3J_{\text{HH}} = 7.8$ Hz) 6.87 (d, 2H, $^3J_{\text{HH}} = 8.4$ Hz) 6.58 (dd, 2H, $^3J_{\text{HH}} = 7.9$ Hz)	3.69 (t, 4H, $^3J_{\text{HH}} = 7.4$ Hz)	1.84 (m, 4H, $^3J_{\text{HH}} = 7.4$ Hz)	1.00 (t, 6H, $^3J_{\text{HH}} = 7.4$ Hz)		
C15	7.48 (s, 2H)	7.26 (dd, 2H, $^3J_{\text{HH}} = 7.5$ Hz) 7.04 (dd, 2H, $^3J_{\text{HH}} = 7.8$ Hz) 6.53 (t, 2H, $^3J_{\text{HH}} = 7.6$ Hz)	3.86 (t, 4H, $^3J_{\text{HH}} = 7.2$ Hz)	2.12 (m, 4H, $^3J_{\text{HH}} = 7.2$ Hz)	1.12 (t, 6H, $^3J_{\text{HH}} = 7.4$ Hz)	1.39 (br s, 18H)	
C16	7.48 (s, 2H)	7.33 (d, 2H, $^4J_{\text{HH}} = 2.7$ Hz) 6.97 (d, 2H, $^4J_{\text{HH}} = 2.7$ Hz)	3.84 (t, 4H, $^3J_{\text{HH}} = 7.1$ Hz)	2.08 (m, 4H, $^3J_{\text{HH}} = 7.3$ Hz)	1.10 (t, 6H, $^3J_{\text{HH}} = 7.3$ Hz)	1.38 (br s, 18H) 1.27 (br s, 18H)	

^a**C12**, **C13** and **C17** are insoluble in all organic solvents thus no solution NMR could be acquired.



Scheme 4.2: Fragmentation pattern and proposed aggregation structures inferred from ESI-MS spectrum of **C10**.

4.2.1.2: Synthesis and characterization of the mononuclear pyrrolylaldiminato Pd(II) complexes, **C11**

The neutral Pd(II) complex, **C11**, was obtained as an orange crystalline product from the reaction of the sodium salt of **L11** with palladium acetate in 2:1 mole ratio respectively, Figure 4.1. Analytically pure orange crystalline material was obtained after recrystallization by slow diffusion of hexane into a solution of the compound in CH₂Cl₂. Although this is a previously reported compound, we used a different synthetic protocol. The complex was obtained in good yield and the characterization data obtained from NMR and FT-IR spectroscopy, ESI-MS and micro analysis compared favourably with that of the same

complex reported by Liang *et al.*²⁰ **C11** was soluble in most organic solvents except hexane and pentane.

NMR spectroscopy data for C11

From the ¹H-NMR data obtained, the imino proton resonance signal was observed at δ 7.39 ppm as compared to δ 8.02 ppm in the free ligand, Table 4.3. The peak of the NH proton at 11.33 ppm in the free ligand was also missing suggesting that the pyrrole nitrogen was deprotonated and subsequently coordinated to the palladium metal.

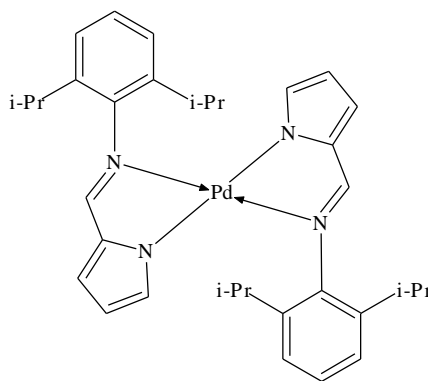


Figure 4.1: Structure of a neutral pyrrole-imine Pd(II) complex, **C11**.

Other characterization data for C11

The ESI-mass spectrum obtained showed a weak peak at m/z 654 that was assigned to a sodium adduct of a singly charged molecular ion, Figure 4.2. The base peak is that of the singly charged ligand ion which was obtained after the demetallation. Unlike in the case of aliphatic analogue **C10**, no dimers were observed. This may be attributed to the steric influence of the aromatic group. Minimal fragmentation was observed. This suggests that under the conditions employed, **C11** was relatively stable. The micro analysis is also consistent with a *bis*(pyrrolide-imine) Pd(II) complex.

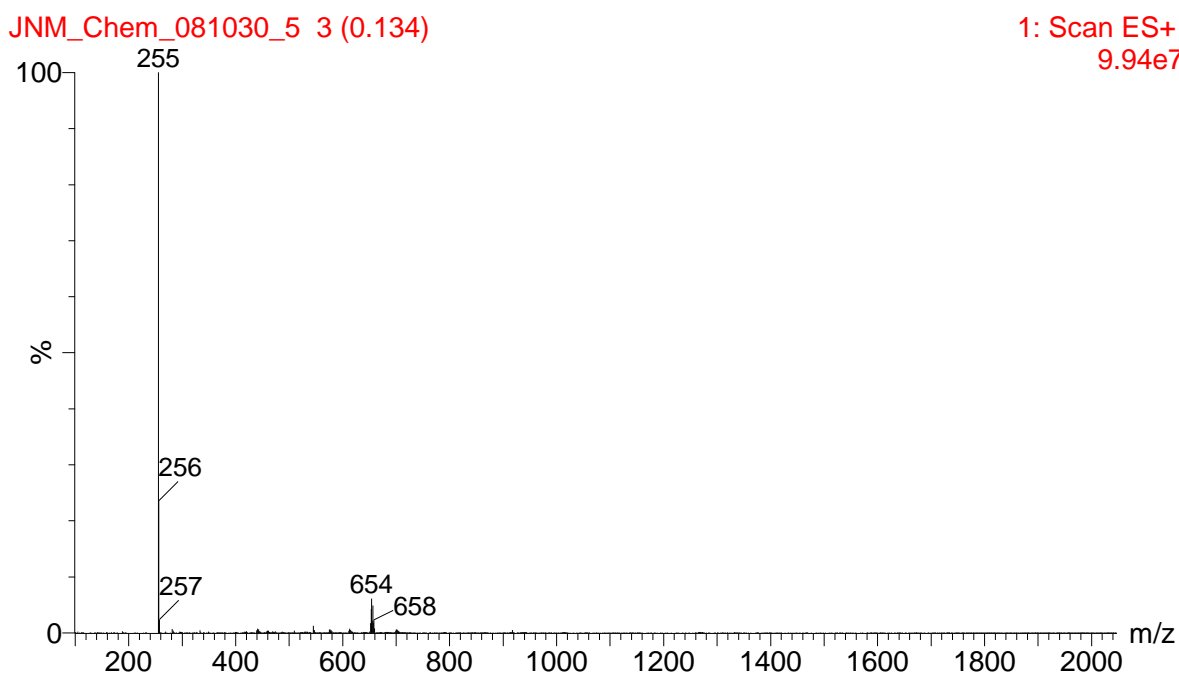


Figure 4.2: ESI-MS spectrum of **C11**

4.2.2: Preparation of dendritic pyrrolyaldiminato Pd(II) complexes

4.2.2.1: Preparation and characterization of the G1 dendritic pyrrolyaldiminato Pd(II) complex, **C12**

A similar protocol to that of the mononuclear complexes was employed in the preparation of the G1 dendritic Pd(II) complex. The sodium salt of **L12** was reacted with Pd(OAc)₂·H₂O. An orange material precipitated out. Due to the insolubility of the material in most organic solvents including DMSO, the work up included washing with water to remove the NaOAc produced as a by-product.

The FT-IR (ATR) spectrum obtained for the material after drying it under vacuum at elevated temperature showed a significant shift of the imine band from 1639 to 1583 cm⁻¹. However there was a broad band between 3380 – 3000 cm⁻¹ that was attributed to the presence of water in the compound. The water proved difficult to remove even after attempts to dry the sample for longer periods. The water may have been encapsulated within the cavities of the metallodendrimer.

In a 2nd attempt, the G1 pyrrolyaldimine ligand (**L12**) was reacted directly with Pd(OAc)₂·H₂O using a mole ratio of 1:2. As the acetate dissolved into the already orange solution of the ligand, a brown solid began to precipitate out of solution after about 10 min. After 1 h reaction time, the orange-brown solid was isolated by suction filtration, washed with copious amount of cold THF and dried under vacuum. This product was also insoluble in all common organic solvents including DMSO and H₂O. The complex showed no decomposition when stored as a solid at room temperature in a desiccator for prolonged time.

Due to the limited solubility this compound, characterization data was acquired from FT-IR and ICP-AES spectroscopy coupled with micro analysis and thermal analysis (TGA).

FT-IR spectroscopy data for C12

The infrared spectrum (Figure 4.4) obtained showed a shift of the imine absorption band to 1582 cm⁻¹ as compared to that of the free ligand 1636 cm⁻¹. However there was a broad band of weak intensity between 3300 and 3000 cm⁻¹. This band was observed even after extra precaution was taken to remove any water produced by adding 4 Å molecular sieves during the reaction.

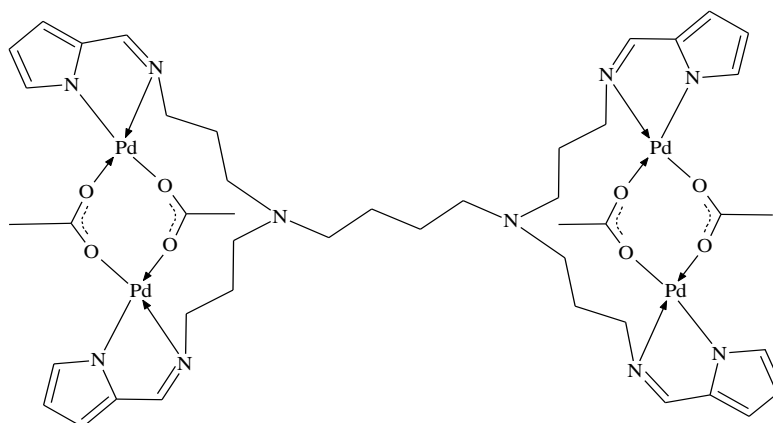


Figure 4.3: G1 Pyrrole-imine Pd(II) complex, **C12**

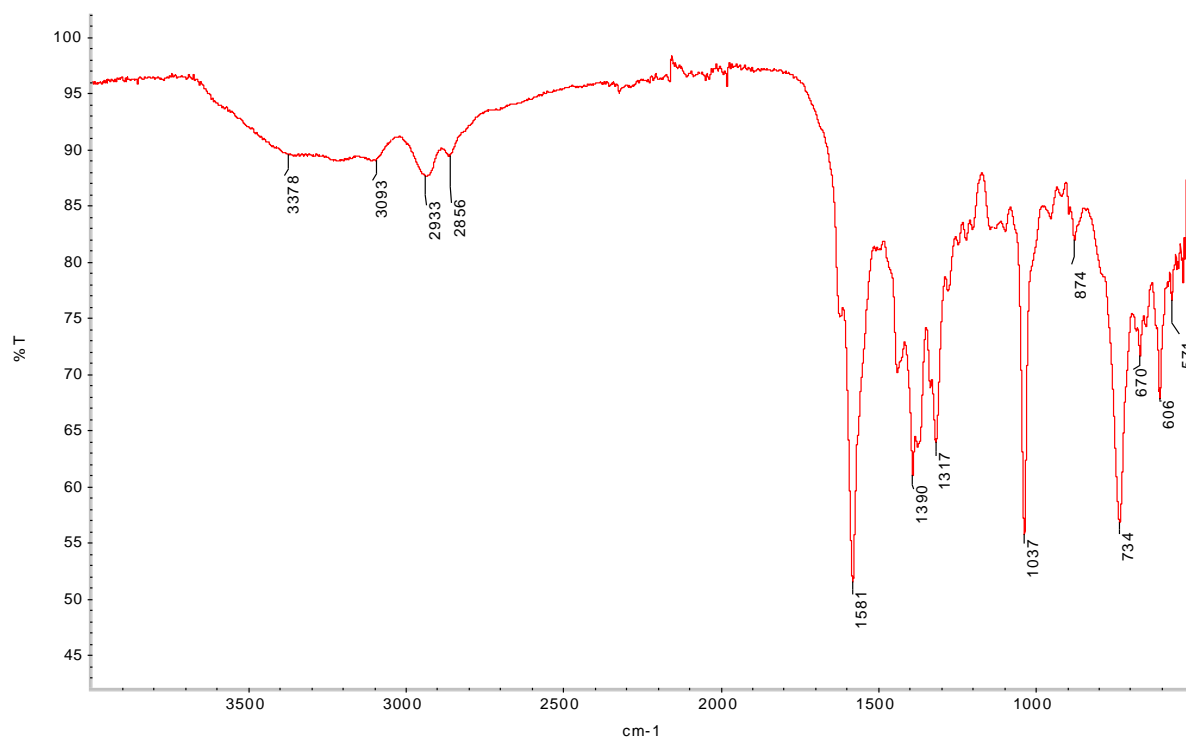


Figure 4.4: FT-IR (ATR) spectrum of complex **C12**

Thermogravimetric analysis (TGA) for C12

The thermogram obtained for metallodendrimer **C12** (Figure 4.5) revealed a profile with four decomposition steps within the temperature ranges of 50 - 80, 120 – 180, 230 – 250 and 260 – 290 °C. The first step that accounts for ~2 % mass loss may be attributed to the loss of THF encapsulated in the metallodendrimer. It should be noted that THF was the solvent used during synthesis. This is similar to the salicylaldiminato metallodendrimers discussed in Chapter 3. The next two stages of decomposition occur gradually with about 15 % mass loss. This may be due to the loss of the acetate ligands. The last stage may be due to the loss of the pyrrole rings that accounts for about 21 % of the total mass.

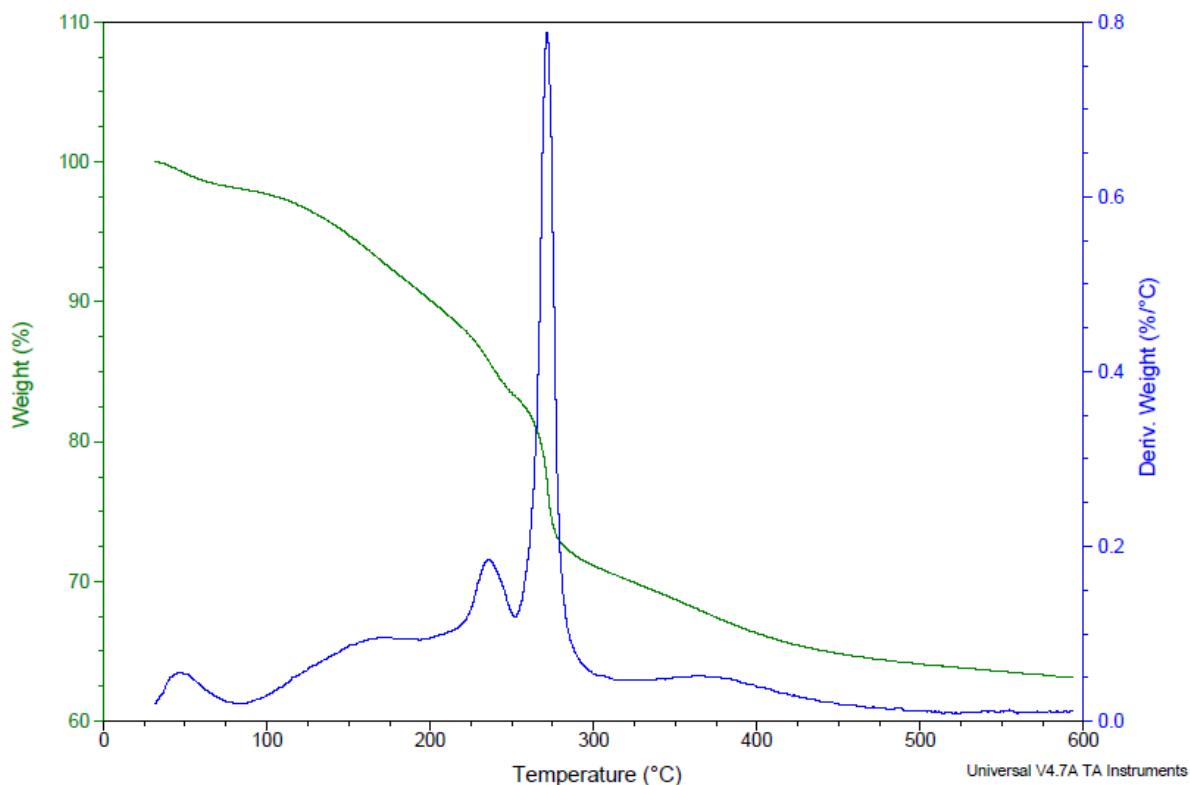


Figure 4.5: The thermogram obtained for **C12**

Other characterization data for complex C12

The micro analysis indicates that the complex has 4 palladium metal centers. It was also observed that some THF was encapsulated inside the cavities of the metallodendrimer complex similar to what was observed for the salicyaldiminato complexes discussed in Chapter 3. The palladium content of **C12** was established to be 30 % by ICP-AES. The metal content corresponds to the calculated values based on 4 metal centers and correlates with the C, H, N microanalysis obtained.

4.2.2.2: Preparation and characterization of the G2 dendritic pyrrolyaldiminato Pd(II) complex, C13

The 2nd generation complex was prepared using a similar method to that employed for **C12**. Ligand **L13** was reacted with Pd(OAc)₂·H₂O at a mole ratio of 1:4 respectively. A

brown solid that precipitated out of solution was washed repeatedly with THF and then dried under vacuum. The solid product was insoluble in all common organic solvents. A 53 % yield was obtained.

FT-IR spectroscopy data for C13

The FT-IR (ATR) spectrum obtained showed a shift of the imine absorption band to 1583 cm^{-1} as compared to 1639 cm^{-1} of the free ligand. Similar to the spectrum of **C12**, a broad band of weak intensity was observed between 3300 and 3000 cm^{-1} .

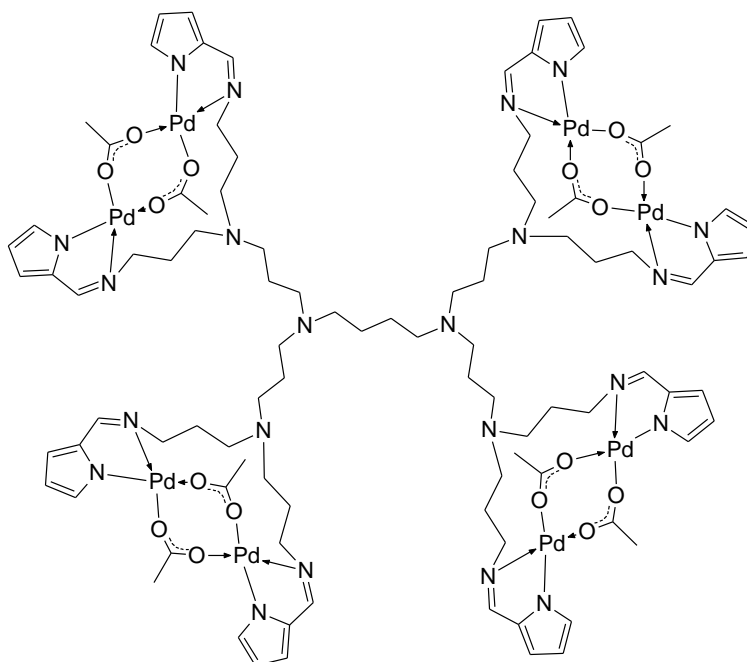


Figure 4.6: 2nd generation pyrrole-imine Pd(II) complex, **C13**

Other characterization data for C13

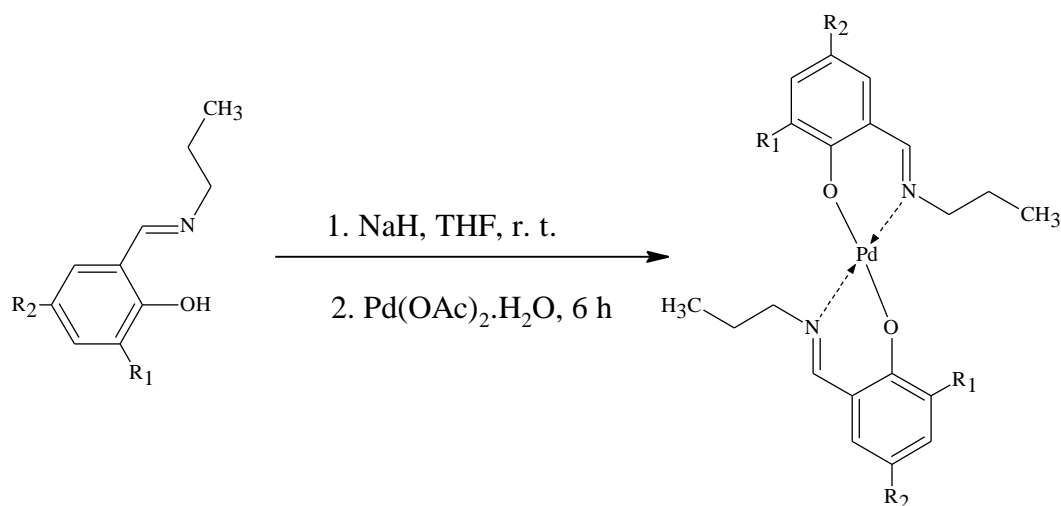
The micro analysis and ICP-EAS results confirmed the % composition for **C13** as shown in Figure 4.6. A palladium content of 28.2 % was obtained which correlated with the calculated values based on 8 Pd centers.

The thermogram obtained for this 2nd generation metallodendrimer is similar to that obtained for the 1st generation analogue. However, the last stage occurs between 280- 320 °C with a mass loss of about 20 %. **C13** is slightly more thermally stable than **C12**.

4.2.3: Preparation of mononuclear salicylaldiminato Pd(II) complexes, **C14** – **C16**

4.2.3.1: Synthesis and characterization of the mononuclear bis(*N*-*n*-propylsalicylaldiminato Pd(II) complexes, **C14** - **C16**

These mononuclear Pd(II) complexes were prepared by reacting the sodium salt of the ligands with Pd(OAc)₂·H₂O in a mole ratio of 2:1 in THF, Scheme 4.3. **C14** was obtained as an orange solid in 67 % yield after recrystallization by slow diffusion of hexane into a solution of the compound in CH₂Cl₂ at a ratio of 2:5 at -4 °C. **C15** and **C16** were also obtained as orange solids after purification by column chromatography in 65 and 70 % yields. These complexes were completely soluble in all common organic solvents except hexane and pentane.



C14: R¹ = R² = H

C15: R¹ = ^tbutyl, R² = H

C16: R¹ = R² = ^tbutyl

Scheme 4.3: Mononuclear salicylaldiminato Pd(II) complexes, **C14** – **C16**

FT-IR spectroscopy data for C14 – C16

The FT-IR data, (Table 4.1), showed a shift of the $\nu(\text{C}=\text{N})$ peak from around 1630 cm^{-1} in the free ligands to 1612 , 1607 and 1610 cm^{-1} for **C14**, **C15** and **C16** respectively. These shifts are similar to those of the Zn(II) analogues discussed in Chapter 3. Moreover, the strong bands associated with the $\nu(\text{C}-\text{O})$, shifted from around 1270 to 1314 , 1305 and 1307 cm^{-1} in **C14**, **C15** and **C16** respectively. Thus it can be inferred that the phenolic oxygen is also involved in the complex formation.

NMR spectroscopy data for C14 – C16

^1H -NMR data (Table 4.3) obtained for **C14** exhibit the imine proton resonance at δ 7.62 ppm as compared to δ 8.30 ppm for the free ligand. Similar to the Zn(II) analogues, the phenolic proton signal is not observed. The signal for the methylene proton, CH_2 , adjacent to the imino group shifts downfield to δ 3.69 ppm from δ 3.47 ppm in the free ligand.

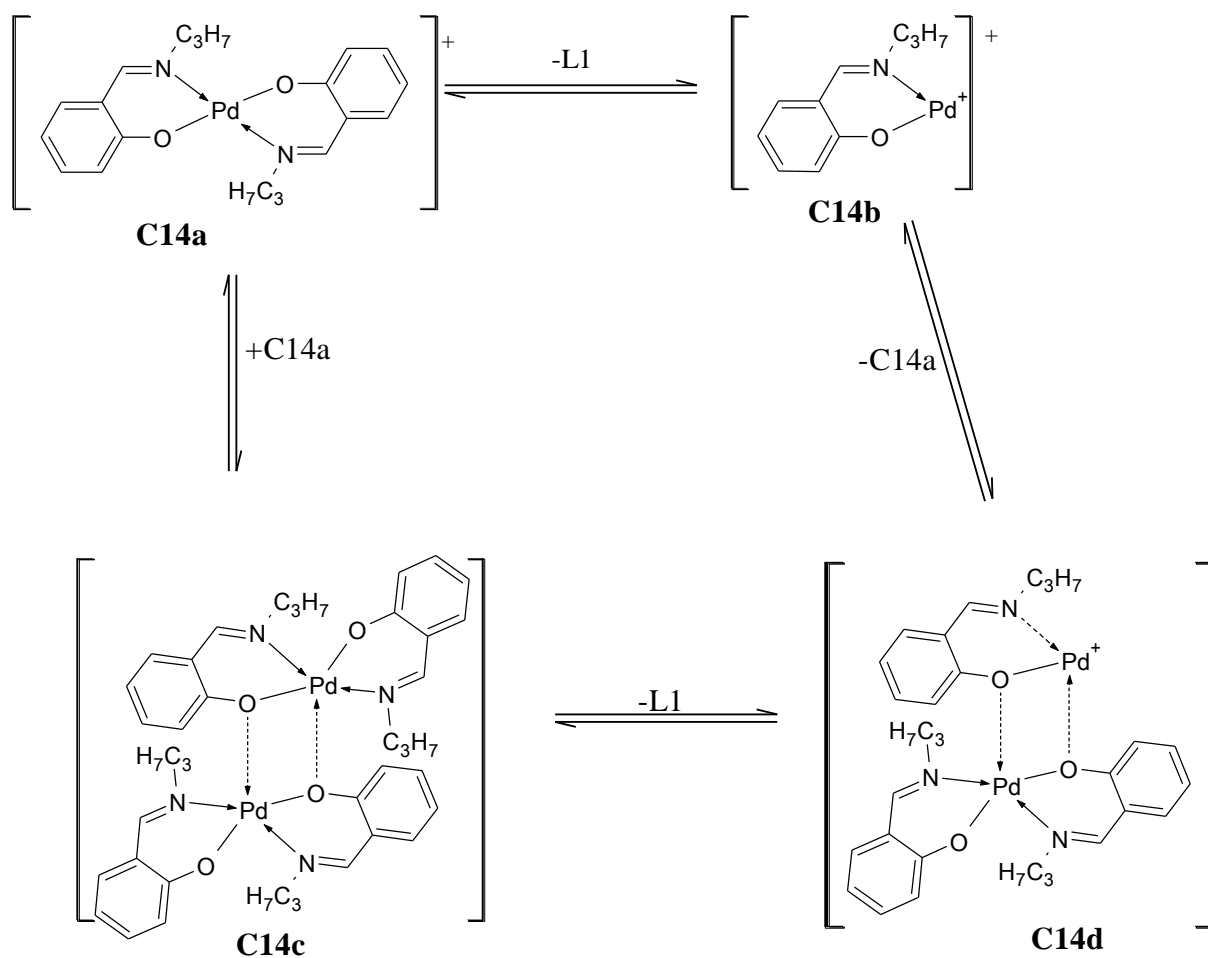
Similar observations were made for the ^1H -NMR spectra obtained for complexes **C15** and **C16**. The imino proton signal was observed at δ 7.48 ppm for both complexes. The methylene protons for the CH_2 adjacent to the imino group were observed at 3.86 and 3.84 for **C15** and **C16** respectively.

The ^{13}C -NMR data for **C14 – C16**, Table 4.2, showed there is a clear shift of the carbon signals as compared to those of the free ligand. The coordination of the ligand to the metal produces a downfield shift of the imino carbon ($\text{C}=\text{N}$) and the aromatic carbon bonded to the phenolic oxygen ($\text{C}-\text{O}$).

ESI-MS results for complexes C14 – C16

ESI-mass spectrometry analysis was carried out for **C14 – C16**. The data obtained for **C14** showed an isotopomeric cluster of peaks centered at m/z 431 as the base peak. The

peaks at m/z 1343 and 885 are those of sodium adducts of the trinuclear and binuclear compounds formed after aggregation which occurs during the ESI-MS analysis. The aggregation detected was similar to that observed for the Zn(II) analogues **C1** – **C3** as well as for **C10**. Other significant ion clusters observed at m/z 863, 700, 270 and 164 were formed after fragmentation of ions of the metal aggregates and as well as the parent ion. A proposed aggregation and fragmentation pattern is shown in Scheme 4.4.



Scheme 4.4: The proposed fragmentation pattern and aggregation structures inferred from ESI-MS spectrum of **C14**.

The mononuclear complex ion (**C14a**) is observed at m/z 431 while the binuclear aggregate ion cluster (**C14c**) is observed at m/z 863. The loss on one ligand from **C14c** gives a fragment at m/z 700 (**C14d**). The loss of the Pd metal from **C14b** formed a fragment ion at m/z 164 that represents the free ligand, **L1**.

Complex **C15** was also analysed by ESI-MS. The base peak was that of a singly charged Pd(II) *bis*-ligated mononuclear isotopomeric cluster of ions centered at m/z 544 as shown in Figure 4.7. A binuclear ion was observed at m/z 1094 while a trinuclear ion was observed at m/z 1629. Molecular ions associated with the sodium adducts of mononuclear as well as the binuclear and trinuclear complexes aggregates were also observed.

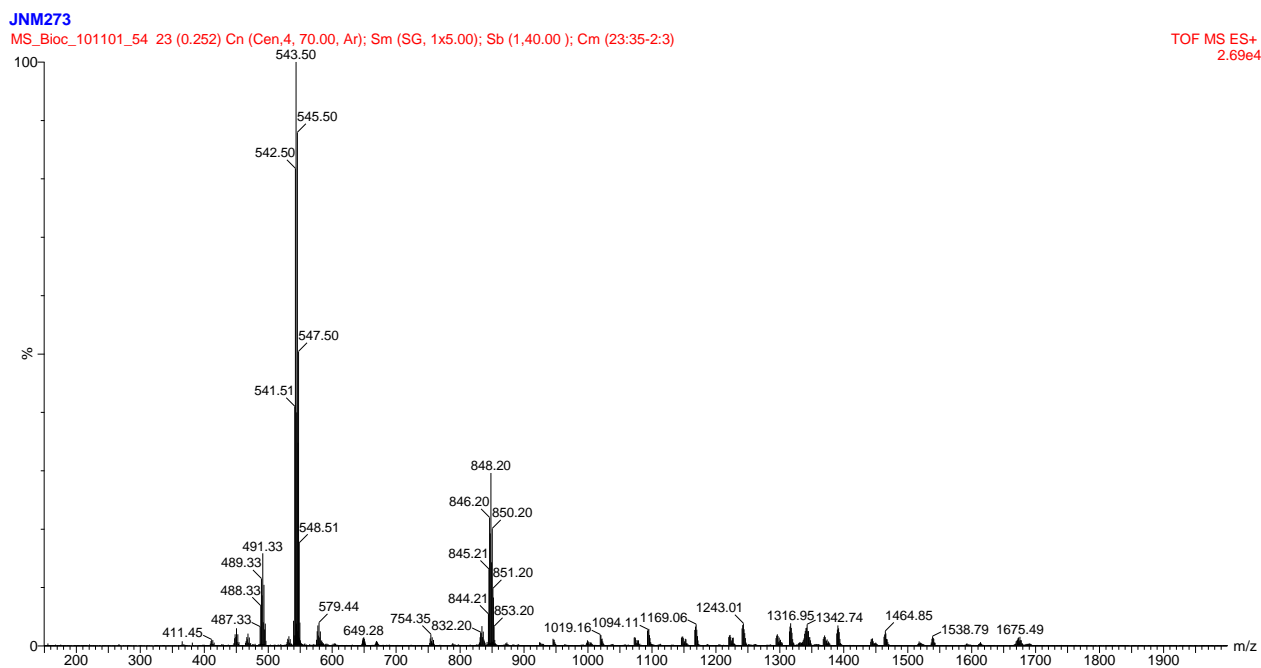


Figure 4.7: ESI-MS spectrum of *bis*(N-n-propyl) 3-*t*-butyl-salicylaldiminato Pd(II) complex, **C15**

Other significant clusters of peaks were observed at m/z 491 and 848. The peak at m/z 491 was attributed to an ion formed after the loss of some of the *t*-butyl substituents in the parent ion. The ion at m/z 848 was formed after the loss of one *t*-butyl group from an aggregate of two metal centers with three ligands. Ions between m/z 900-1700 (Da) are due

to binuclear and trinuclear aggregate ions. In addition to the aforementioned species, daughter ions of these aggregates were also observed as a result of fragmentation.

Similarly, **C16** was also analysed by ESI mass spectrometry and gave a number of peaks. The base peak was that of the mononuclear complex at m/z 655. A peak at m/z 955 corresponds to a fragment of two metals associated with three ligands. A peak associated with the binuclear aggregate was also observed but with very low intensity.

Single crystal X-ray diffraction (SXR) for C14

Orange crystals suitable for X-ray diffraction analysis were obtained after recrystallization from CH_2Cl_2 /hexane (1:3) at -4 °C. The molecular structure of **C14** is shown in Figure 4.8. A summary of the crystal data collection, structure solution and refinement is shown in Table 4.4. Selected bond angles and distances are shown in Table 4.5.

Complex **C14** was obtained as cube shaped crystals with approximate dimensions of $0.52 \times 0.42 \times 0.31$ mm. Refinement of 116 parameters based on all 1927 reflections yielded $R_1 = 0.0199$ and $wR_2 = 0.0889$ for $I > 2\sigma(I)$ (5133 reflections) for all reflections; maximum and minimum residual electron density $0.37; -0.80 \text{ e}\text{\AA}^{-3}$.

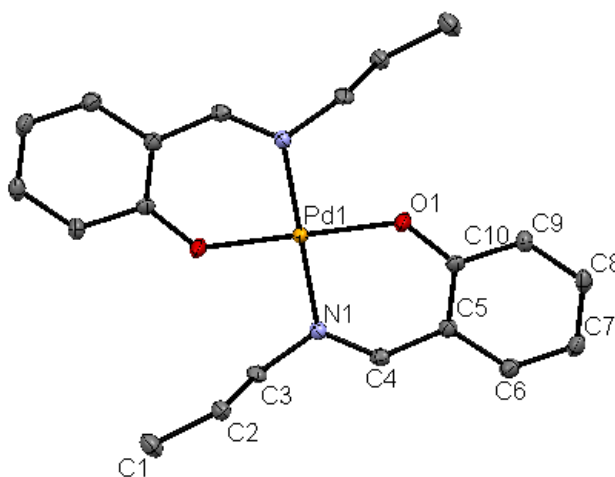


Figure 4.8: The molecular structure of **C14** with the atom-numbering scheme. Displacement ellipsoids are drawn at the 30% probability. H atoms are omitted for clarity

Table 4.4: Crystal structural data (collection, solution and refinement) for **C14**

Empirical formula	C ₂₀ H ₂₄ N ₂ O ₂ Pd	
Formula weight	537.21	
Crystal system	monoclinic	
Space group	P2 ₁ /C	
Crystal size (mm ³)	0.52 x 0.42 x 0.31	
Z	2	
Unit cell dimensions (Å, °)	a = 10.0344 (10)	α = 90.00
	b = 10.0807 (10)	β = 102.41
	c = 8.9849 (9)	γ = 190.00
Volume (Å ³)	887.62 (15)	
Absorption coefficient (mm ⁻¹)	2.043	
Calculated density (g cm ⁻³)	2.010	
F ₀₀₀	532	
Temperature (K)	100(2)	
Wavelength (Å)	0.71073	
2θ max (°)	55.9	
Miller index ranges	-8 ≤ h ≤ 13, -12 ≤ k ≤ 11, -11 ≤ l ≤ 11	
Reflections collected	5133	
Independent reflections	1927 [R _{int} = 0.0156]	
Refinement method	Full-matrix least square on F ²	
Data / restraints / parameters	1927/0/166	
Goodness-of-fit on F ²	0.845	
Final R indices [F ₂ for I ≥ 2σ]	0.0932	
R indices (all data)	R1 = 0.0199, wR2 = 0.0882	
Largest diff. peak and hole (e Å ⁻³)	0.371 and -0.80	

The molecule shows an inversion center at the palladium. The coordination at the metal center is almost perfectly square planar with a N1-Pd-O1 angle of 92°, O1-Pd-O angle of 180° and a N1-Pd-N angle of 88°. The bond distances around the coordination sphere were 1.9881(1) and 2.0333(10) Å for Pd - O and Pd - N respectively. These bond angles and lengths are similar to those reported in the literature for other salicylaldimine palladium complexes.³⁵

Table 4.5: Selected bond distances and angles for **C14**

Bond lengths [Å]		Bond angles [°]	
Pd-O1	1.9830(1)	O1-Pd-N1	87.96 (5)
Pd-N1	2.0333(10)	O1-Pd-O1'	180.0
C10-O1	1.312(2)	O1-Pd-N1	92.04(5)
C3-N1	1.4813(15)	N1-Pd-N1'	180.0
C4-N1	1.2855(16)	C10-O1-Pd	127.25 (11)

4.2.4: Preparation of the dendritic salicylaldiminato Pd(II) complex, **C17**

4.2.4.1: Preparation and characterization of the G1 dendritic salicylaldiminato Pd(II) complex, **C17**

The 1st generation dendritic Pd(II) complex of the unsubstituted salicylaldimine ligand, **L4**, was prepared using a similar method employed for mononuclear complexes. The sodium salt of the ligand, **L4**, was reacted with Pd(OAc)₂·H₂O in a mole ratio of 1:2 at room temperature. During the reaction, a brown solid precipitated out. To remove the NaOAc produced as a by-product, the material was washed with copious amounts of water followed by acetone. The product was then dried at an elevated temperature under reduced pressure for 24 h. A number of analytical techniques were employed in the characterization of the compound obtained.

FT-IR spectroscopy data for **C17**

The FT-IR spectrum obtained showed a shift of the imine absorption band by 10 cm⁻¹ to 1620 cm⁻¹. The ν(C-O) absorption band also shifted to 1319 cm⁻¹. These values are similar to those obtained for the mononuclear complex, **C14**.

Solid state ^{13}C (CP-MAS) NMR spectroscopy for C17

C17 was characterized by solid state NMR spectroscopy. In the spectrum, the dendritic scaffold carbons are observed as two very broad and unresolved peaks centered at δ 25.61 and 55.78 ppm. These peaks can be assigned to $\text{CH}_2\text{-}\underline{\text{C}}\text{H}_2\text{-CH}_2$ and $\underline{\text{C}}\text{H}_2\text{-N}$ carbons respectively. The aromatic and the imino peaks were more resolved and are observed at δ 113.68, 119.45, 134.32, 161.16, 163.60 and 171.7 ppm.

Other analytical data for C17

The micro analyses of **C17** agreed with the calculated values of the structure shown in Figure 4.9. The ICP results confirmed that the salicylaldiminato was formed with two metal centers unlike the pyrrolylaldiminato analogues that formed 4 metal centers.

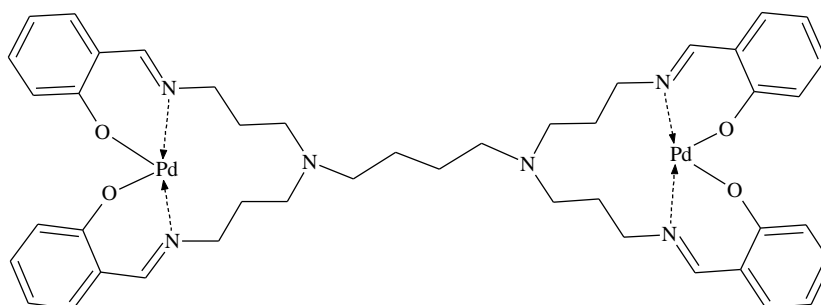


Figure 4.9: The molecular structure of a binuclear Pd(II) complex, **C11**.

4.2.4.2.: Other G1 dendritic salicylaldiminato Pd(II) complex,

Two attempts were made to prepare the palladium complex of **L5**. In the 1st attempt the ligand salt was reacted with $\text{Pd}(\text{OAc})_2$. No precipitation occurred during the reaction. After the reaction time all volatiles were removed giving an orange solid which was dissolved in CH_2Cl_2 , and then filtered. After removal of all volatiles from the filtrate the orange product was characterized by FT-IR. From the spectrum, it was evident that a mixture of compounds

was obtained. This method proved to be unsuccessful in that we were unable to separate a pure product.

In the 2nd attempt, the ligand was reacted directly with the Pd(OAc)₂. On addition of Pd(OAc)₂, an orange colour was observed and all the palladium salt dissolves in about 5 min. The orange solution was stirred at room temperature for 2 hours. No precipitate formation was observed. After the reaction time, all volatiles were removed and the product stored at room temperature in a desiccator with no additional work up until further use.

Attempted purification and characterization

An FT-IR (ATR) spectrum was acquired of the crude material. A broad band for the imine functionally was observed at 1610 cm⁻¹. This represented a shift of 22 cm⁻¹ in comparison to the free ligand. However the ν(C-O) bands showed only a slight shift of 2 cm⁻¹ to 1263 cm⁻¹.

The sample was dissolved in pre-dried CDCl₃ and a ¹H-NMR spectrum acquired immediately. The number of peaks observed was more than those expected. This suggested that there was a mixture of unreacted ligand and another compound. For example there were two peaks in the imine region at δ 8.30 and 8.42 ppm.

Attempts were made to separate the two components by recrystallization using various solvent systems and at different temperatures. In one case, a solution of the crude product in CH₂Cl₂ was layered with hexane and the allowed to stand at 4 °C (in the fridge) until a solid came out of solution. The orange mother liquor was syringed off and all volatiles were removed. The precipitate was also dried. Both products were orange in colour.

The FT-IR (ATR) spectra obtained for the two fractions showed new peaks at 1710 and 1766 cm⁻¹ in addition to those previously observed in the crude material. These wave

numbers are typical of $\nu(\text{C}=\text{O})$ of aldehyde suggesting hydrolysis of the imine bond had occurred.

Attempts to purify the material by column chromatography were futile. TLC in polar solvents such as ether as well as in non polar solvents such as CH_2Cl_2 and hexane showed no mobility of the compounds. The analyte remained immobilized on the TLC plate.

In a quest to understand the decomposition process, the sample used to record the above $^1\text{H-NMR}$ spectrum was left standing in the fridge and spectra acquired at 2, 6, 24 and 168 h, Figure 4.10. After 2 hrs in addition to all other peaks observed previously, a peak of low intensity is observed at δ 9.86 ppm. This peak signifies the presence of the aldehydic proton ($\text{H-C}=\text{O}$). In the commercially available 3-*t*-Butyl 2-hydroxyl-benzaldehyde, the $\text{H-C}=\text{O}$ proton signal was observed at 9.89. The intensity of this peak grew over time as those at δ 8.30 and 8.42 ppm start disappearing. After 7 days none of the peaks at δ 8.30 and 8.42 ppm were present. An array for the $^1\text{H-NMR}$ spectra acquired at $t = 0, 2, 24$ and 168 h is shown in Figure 4.10. No palladium black formation during the process was observed. This indicates that simple complex decomposition was not occurring. However based on the $^1\text{H-NMR}$, it may be concluded that the hydrolysis of the imine in the complex and in the ligand had been occurring. No such hydrolysis is observed in solid state.

4.3: Conclusions

Pd(II) complexes of some of the ligands discussed in Chapter 2 were successfully prepared. The complexes of both the pyrrole-imine, **C10**, **C11**, and salicylaldehyde ligands, **C14-C17**, were prepared by first deprotonating the ligand using NaH. The dendritic pyrrole-imine complexes were obtained by reacting the ligands directly with palladium acetate. Complexes **C12**, **C13** and **C17** were insoluble in most organic solvents.

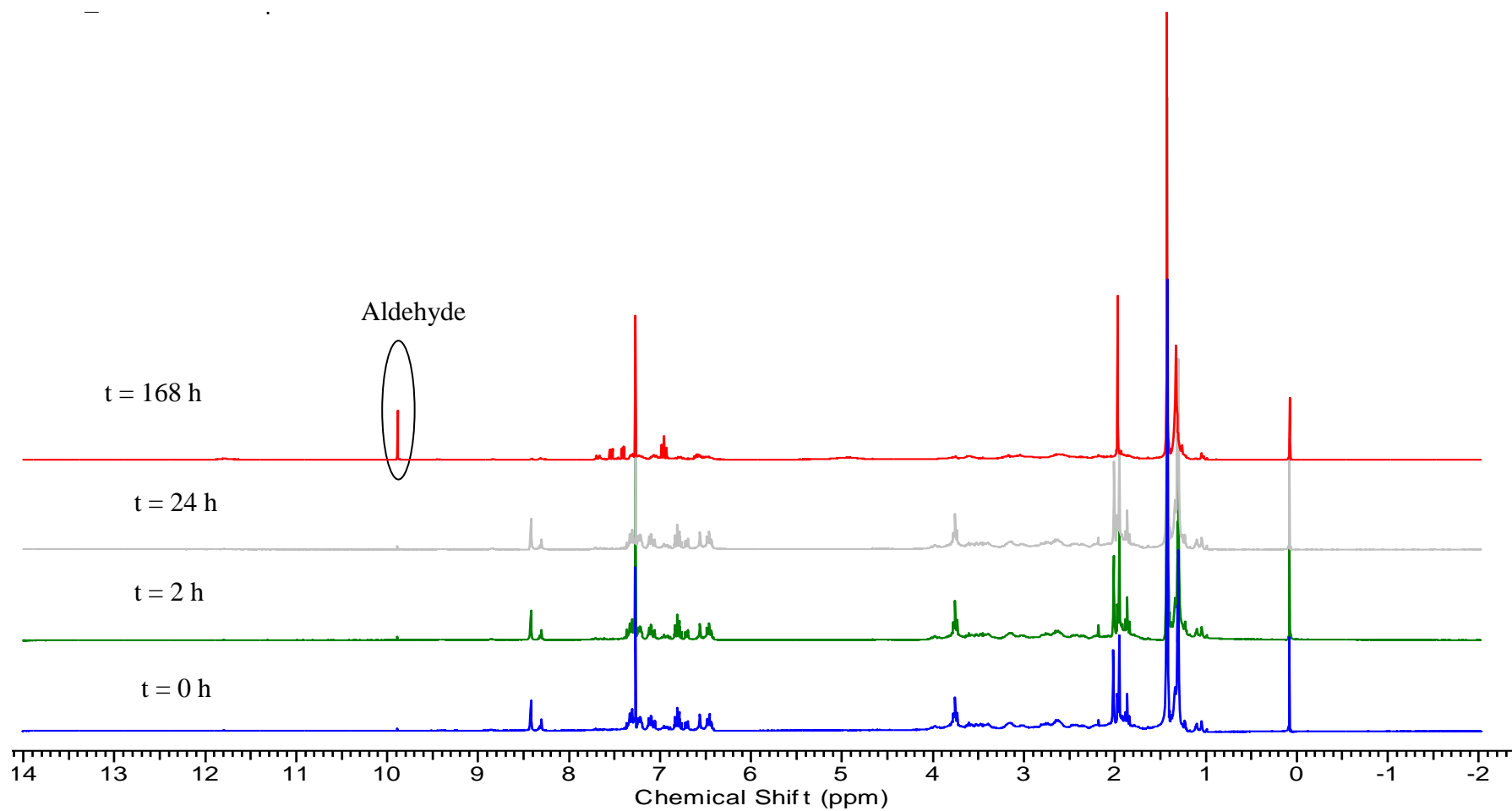


Figure 4.10: An $^1\text{H-NMR}$ array for the product formed from **L5** and $\text{Pd}(\text{OAc})_2 \cdot \text{H}_2\text{O}$

All complexes were fully characterized using a range of analytical techniques namely NMR and FT-IR spectroscopies, elemental analyses, mass spectrometry and thermal analysis (TGA).

The mononuclear complexes with aliphatic moiety on the imino nitrogen form binuclear and trinuclear aggregates when ionized during the ESI-mass spectrometry analysis. The pyrrole-imine complexes **C12** and **C13** contained 4 and 8 metal centers respectively. The G1 salicylaldiminato complex, **C17**, formed a binuclear complex.

4.4: Experimental

4.4.1: Materials and instrumentation

All synthetic manipulations were carried out using a double manifold Schlenk vacuum/nitrogen line. All solvents used were of analytical grade and were dried and distilled prior to use. Tetrahydrofuran (THF), hexane pentane and toluene were dried and distilled from sodium/benzophenone, ethanol from magnesium turnings/iodine and dichloromethane over phosphorous pentoxide. All solvents used for the synthesis and work up of the metallodendrimers were also allowed to stand over 4 Å molecular sieves for 24 h after drying over sodium/benzophenone before use. Williams and Lawton reported that the solvents dried over 3 Å molecular sieves had lower water content.³⁶ Sodium hydride; silica gel and palladium acetate were purchased from Sigma-Aldrich Ltd. All starting materials were used without further purification.

Solution NMR spectra were recorded on a Varian 300 VNMRS spectrometer (¹H at 300 MHz, ¹³C at 75.4 MHz) at room temperature using tetramethylsilane as an internal standard unless otherwise stated. The chemical shifts are reported in δ (ppm) and referenced to the signal for the residual proton in CDCl₃.

The solid state NMR spectra were acquired on a Varian spectrometer (VNMRS Wide Bore 500 solids) static magnetic field strength: 11.7 T (corresponding to a proton Larmor frequency of 500 MHz) two-channel spectrometer using 4 mm zirconia rotors and a 4 mm ChemagneticsTM T3 HX MAS probe. All cross-polarization (CP) MAS spectra were recorded at ambient temperature with proton decoupling, a 2.75 μs ^{13}C 90° pulse and a recycle delay of 2s. The power parameters were optimised for the Hartmann-Hahn match; the radio frequency fields were $\gamma_{\text{C}}\text{B}_{1\text{C}} = \gamma_{\text{H}}\text{B}_{1\text{H}} \approx 79$ kHz. The contact time for cross-polarization was 1.5 ms after optimization with a variable contact time experiment and the spin field was locked at 56 kHz. The data was processed using the programme SpinWorks[®].³⁷

Infrared spectra were recorded on a Nicolet Avatar 330 FT-IR spectrophotometer using an ATR accessory. ESI-mass spectra were obtained on a Waters API Q-TOF Ultima spectrometer calibrated with NaF. Microanalyses were performed at the micro analytical laboratory of the University of Cape Town. Melting points were determined on a Stuart Scientific melting point apparatus (SMP3) at a heating rate of 0.5 °C/min.

Thermogravimetric analyses (TGA) were done on a TGA Q500 V6.7 modulus coupled with a thermal analyser. An aluminum pan was loaded with *ca.* 2 - 5 mg of sample and heating ramped at 10 °C/min under a nitrogen atmosphere at a flow rate of (50.0 ml/min). The thermal analytical data were collected between 20 to 598 °C.

ICP-AES analysis was done on the Pd(II) metallodendrimer to quantify the amount of palladium metal using a Varian ICP-AES.

4.4.2.: Synthesis and characterization of mononuclear bis-N-n-propyl pyrrolylaldiminato)

Pd(II) complexes, C10 and C11

In a Schlenk tube NaH (0.025 g, 1.04 mmol) was suspended in freshly dried THF (5 mL) and a solution of **L10** (0.12 g, 0.882 mmols) in THF (5 mL) was added to it.

Immediate effervescence was observed and the solution acquired a pink colour. The mixture was stirred at room temperature for 2 h with no further observable changes. The solution was then filtered through celite under nitrogen into another Schlenk tube. To the solution of the sodium salt of the ligand, Pd(OAc)₂ (0.1 g, (0.45 mmols) was added and mixture stirred at room temperature for 4 h. The reaction mixture gradually acquired a yellow-orange colour. After the reaction time, all volatiles were removed. The orange solid was dissolved in CH₂Cl₂ and the resulting mixture filtered by suction filtration. The filtrate was concentrated by vacuum to ca. 3 mL. Recrystallization of the compound was effected by slow diffusion of hexane into the CH₂Cl₂ solution at -4 °C. A yellow-orange crystalline material was isolated by suction filtration and washed with cold hexane.

C11 was prepared from **L11** using a similar protocol to that employed for **C10**. The product was obtained as an orange crystalline material.

4.4.3.: Synthesis and characterization of dendritic Pd(II) pyrrolylaldiminato complexes, C12 and C13

A solution of **L12** (0.117g, 0.1875 mmols) in freshly dried THF (10 mL) in a Schlenk tube was degassed and Pd(OAc)₂·H₂O (0.09g, 0.401 mmols) added. A few pellets of 0.4 Å molecular sieves were added to absorb any water in the reaction mixture. As the acetate dissolves into the already orange solution, a brownish-orange solid begins precipitating out of solution after 10 min. After 1 h of stirring at room temperature, the orange brown solid was isolated by suction filtration and washed repeatedly with copious amounts of cold THF.

C13 was prepared from **L13** using a similar protocol to that employed for **C12**. The product was obtained as an orange-brown amorphous solid.

4.4.4.: Synthesis and characterization of mononuclear bis-N-n- propyl-salicylaldiminato Pd(II) complex, C14 – C16.

To a solution of **L1** (0.118 g, 0.87 mmol) in freshly dried THF (10 mL) NaH (0.022 g, 0.92 mmol) was added. Immediate effervescence is observed. The mixture was stirred at room temperature for 2 h during which the NaH gradually dissolved. No colour changes to the solution were observed. After 2 h the solution was filtered under nitrogen into another Schlenk tube and Pd(OAc)₂·H₂O (0.173 g, 0.77 mmol) was added. The yellow solution acquired a brownish colour. The mixture was stirred at room temperature for 6 h and gradually acquired an orange – yellow colour. After 6 h all volatiles were removed giving an orange solid. This crude product was dissolved in CH₂Cl₂, and suction filtered. The filtrate was concentrated to *ca.* 2 mL. Crystallization was induced by slow diffusion of hexane into the CH₂Cl₂ solution at -4 °C using a 1:3 solvent system. An orange crystalline material was isolated by suction filtration and washed with cold hexane.

C15 and **C16** were prepared using a similar procedure to that employed in **C14** from ligands **L2** and **L3** respectively. However the purification was done by column chromatography. A column was packed with silica gel and the products eluted with 5 % CH₂Cl₂ in hexane. A few drops of Et₃N were added to the mobile phase. Fractions were collected at regular intervals and purity determined by TLC.

4.4.5.: Synthesis and characterization of salicylaldiminato bi-nuclear Pd(II) complex, C17

In a Schlenk tube containing a yellow solution of 0.12 g (0.164 mmol) the unsubstituted salicylaldimine ligand, **L4**, in dry THF (10 mL) was added NaH 0.017 g (0.708 mmols). Immediate effervescence was observed. The yellow mixture was stirred at room temperature for 2 h after which the solution was filtered into another Schlenk tube through celite under nitrogen to remove excess NaH. To the clear yellow solution, Pd(OAc)₂·H₂O (0.04 g, 0.32

mmol) was added. As the acetate dissolves the solution acquired an orange-yellow colour that it retained over the 12 h period.

After the reaction time, all the volatiles were removed. To the orange yellow solid, 20 mL of water was added and the mixture stirred at room temperature for 20 minutes. The mixture was left to settle and the water syringed off. The remaining solid was then washed with acetone, (2 x 10 mL). After the washing, the yellow orange solid was dried under vacuum at elevated temperature (50 °C).

4.5: References

1. R. H. Holm, A. Chakravorty, L. J. Theriot, *Inorg. Chem.*, **5** (1966) 625.
2. K.-N. Yen, R. H. Barkery, *Inorg. Chem.*, **6** (1967) 830.
3. L. K. Johnson, C. M. Killian, M. Brookhart, *J. Am. Chem. Soc.*, **117** (1995) 6414.
4. G. J. P. Britovsek, V. C. Gibson, B. S. Kimberley, P. J. Maddox, S. J. McTavish, G. A. Solan, A. J. P. White, D. J. Williams, *Chem. Commun.*, (1998) 849.
5. Y. Yoshida, S. Matsui, T. Fujita, *J. Organomet. Chem.*, **690** (2005) 4382.
6. K. Vanka, Z. Xu, T. Ziegler, *Organometallics*, **23** (2004) 2900.
7. S. Matsui, Y. Yoshida, Y. Takagi, T. P. Spaniol, J. Okuda, *J. Organomet. Chem.*, **689** (2004) 1155.
8. C. N. Iverson, C. A. G. Carter, R. T. Baker, J. D. Scollard, J. A. Labinger, J. E. Bercaw, *J. Am. Chem. Soc.*, **125** (2003) 12674.
9. L.-P. He, J.-Y. Liu, L. Pan, J.-Q. Wu, B.-C. Xu, Y.-S. Li, *J. Polym. Sci. Part A: Polym. Chem.*, **47** (2009) 713.
10. V. C. Gibson, C. Newton, C. Redshaw, G. A. Solan, A. J. P. White, D. J. Williams, *Dalton Trans.*, (2002) 4017.
11. S. D. Drouin, H. M. Foucault, G. P. A. Yap, D. E. Fogg, *Can. J. Chem.*, **83** (2005) 748.

12. H. M. Foucault, D. L. Bryce, D. E. Fogg, *Inorg. Chem.*, **45** (2006) 10293.
13. J. Li, H. Song, C. Cui, *Appl. Organomet. Chem.*, **24** (2010) 82.
14. P. Pérez-Puente, E. de Jesús, J. C. Flores, P. Gómez-Sal, *J. Organomet. Chem.*, **693** (2008) 3902.
15. Y.-S. Li, Y.-R. Li, X.-F. Li, *J. Organomet. Chem.*, **667** (2003) 185.
16. J. Mugo, S. F. Mapolie, J. L. van Wyk, *Inorg. Chim. Acta.*, **363** (2010) 2643.
17. S. A. Carabineiro, L. C. Silva, P. T. Gomes, L. C. J. Pereira, L. F. Veiros, S. I. Pascu, M. T. Duarte, S. Namorado, R. T. Henriques, *Inorg. Chem.*, **46** (2007) 6880.
18. S. A. Carabineiro, R. M. Bellabarba, P. T. Gomes, S. I. Pascu, L. F. Veiros, C. Freire, L. C. J. Pereira, R. T. Henriques, M. C. Oliveira, J. E. Warren, *Inorg. Chem.*, **47** (2008) 8896.
19. Y-S. Li, Y-R. Li, X-F. Li, *J. Organomet. Chem.*, **667** (2003) 185.
20. H. Liang, J. Liu, X. Li, Y. Li, *Polyhedron*, **23** (2004) 1619.
21. G. Tian, H. W. Boone, B. M. Novak, *Macromolecules*, **34** (2001) 7656.
22. N. Meyer, M. Kuzdrowska, P. W. Roesky, *Eur. J. Inorg. Chem.*, (2008) 1475.
23. Y. Yang, S. Li, D. Cui, X. Chen, X. Jing, *Organometallics*, **26** (2007) 671.
24. C. Cui, A. Shafir, C. L. Reeder, J. Arnold, *Organometallics*, **22** (2003) 3357.
25. J. Lewiński, M. Dranka, I. Kraszewska, W. Sliwińska, I. Justyniak, *Chem. Commun.*, (2005) 4935.
26. H. Hao, S. Bhandari, Y. Ding, H. W. Roesky, J. Magull, H.-G. Schmidt, M. Noltemeyer, C. Cui, *Eur. J. Inorg. Chem.*, (2002) 1060.
27. Y. Yang, B. Liu, K. Lv, W. Gao, D. Cui, X. Chen, X. Jing, *Organomet.*, **26** (2007) 4575.
28. J-S. Mu, Y-X. Wang, B-X. Lia, Y-S. Li, *Dalton Trans.*, **40** (2011) 3490
29. G. Tian, H. W. Boone, B. Novak, *Macromolecules*, **34** (2001) 7656.

30. J. N. Mugo, MSc thesis, “*Mononuclear, Dendrimeric and MCM-41 Immobilized Pyrrole-Imine Complexes of Cu, Co and Ni as Catalytic Precursors in Oxidation Reactions*” University of the Western Cape, 2007.
31. W-Y. Huang, S-J. Chuang, N-T. Chunag, C-S. Hsiao, A. Datta, S.-J. Chen, C- H. Hu, J-H. Huang, T-Y. Lee, C-H. Linc, *Dalton Trans.*, **40** (2011) 7423
32. C. Wang, S. Friedrich, T. R. Younkin, R. T. Li, R. H. Grubbs, D. A. Bansleben, M. W. Day, *Organometallics*, **17** (1998) 3149.
33. D. Chandran, C. H. Kwak, C.-S. Ha, I. Kim, *Catal. Today*, **131** (2008) 505.
34. S. Arockiasamy, M. G. Johnsona, C. Mallikab, O.M. Sreedharana, K.S. Nagaraja, *Mater. Chem. Phys.*, **114** (2009) 456.
35. E. G. Bowes, G. M. Lee, C. M. Vogels, A. Decken, S. A. Westcott, *Inorg. Chim. Acta*, **377** (2011) 84.
36. D. B. G. Williams, M. Lawton, *J. Org. Chem.*, **75** (2010) 8351.
37. Kirk Marat, SpinWorks 3.1.7, Copyright © 2010 University of Manitoba.

Chapter 5 : Ring Opening Polymerization of D,L–Lactide using Salicylaldiminato Zn(II) Complexes

5.1: Introduction

5.1.1: *Lactide ring opening polymerization (ROP)*

Polymerization of cyclic monomers such as lactide is referred to as ring opening polymerization (ROP). It is a form of addition polymerization where the active species remains attached to the end of the growing polymer chain. The main routes employed for the catalytic ring opening polymerization of lactide include enzymatic, anionic, cationic and metal complex mediated. In the ring opening polymerization of cyclic esters, development of suitable catalysts/initiators has generated a lot of interest.

Polyesters can be prepared by polycondensation of hydroxycarboxylic acids e.g. lactic acid or ROP of cyclic esters e.g. lactide. Polyesters such as polylactide (PLA), polycaprolactones (PCL), polyglycolide (PGL), and their copolymers have attracted immense attention due to their biodegradability and biocompatibility.¹ ROP of cyclic esters is favoured because in most cases it yields polymers of higher molecular weight and has been shown to be a better technique in the production of copolymers of these cyclic esters.² These polyesters are most commonly used in the biomedical and pharmaceutical industries. They have found application as surgical sutures, scaffolds for tissue engineering, post-operative support pins and splints, as well as a delivery medium for controlled release of drugs.^{3,4} Physiological simple hydrolysis of the ester linkages in the polymer produces non-toxic products that are eliminated from the body through the Krebs cycle as water and carbon dioxide.⁵⁻⁸

The other uses for these polymers are in packaging materials, agricultural films and fibers. Due to their biodegradability, they have attracted attention as suitable environmentally friendly alternatives to the common polyolefins.⁹ In this case; their degradation is facilitated by naturally occurring organisms such as bacteria, algae and fungi.¹⁰

Another major advantage is that the monomers used to produce these polymers can be obtained from renewable resources. Lactide is obtained by fermentation of lactic acid which is abundant in crops such as corn, beets and sugar cane.¹¹

Metal alkoxides of Al, Li, Mg, Fe, Sn, and Zn are by far the most credited for the polymerization of cyclic esters. Tin and zinc have generated a lot of interest because they are the only metals approved by the food and drug administration (FDA) for their low toxicity in physiological systems.¹² Toxicity plays an important role in the biomedical applications of these polymers.¹³

Some racemic alkoxide initiators have been shown to produce stereoselective polymers. Unfortunately, chain transfer has been observed to be more rapid than the ring-opening.¹⁴ Chain transfer occurs where a bimolecular mechanism involving alkoxide bridges, $M(\mu\text{-OP})(\mu\text{-OP}')M'$, or in the presence of an alcohol. Alcohols are commonly used in conjunction with these metal alkoxides to control the number of growing chains and in return the molecular weight of the polymer.

Other common side reactions include trans-esterification and epimerization. There are two types of trans-esterification *viz*, inter-chain- and intra-chain-esterification with the latter leading to cyclic products. Trans-esterification competes with the chain growth due to the presence of carbonyl groups in the polymer. These reactions become significant in very active catalysts. The high basicity of the metal alkoxides can also result in epimerization. Epimerization usually occurs at the methine carbon. The methine carbon is deprotonated forming an enolate group. These reactions are mainly prevalent in the presence of alkoxide initiators of group 1 and 2 metals as well as those of lanthanides.¹⁵

Metal alkoxides in combination with other ancillary ligands have also been widely studied. It is generally believed that the M-O bond is the most crucial functionality in these complexes. Like any other catalytic processes, the choice of ligands bonded to the metal is

critical to the catalytic behaviour of the complexes. Thus the ancillary ligands are believed not to be directly involved in the polymerization but later in the tuning of the metallic center and in minimizing catalyst deactivation processes as well as controlling side reactions.¹⁶

Metal complexes without alkoxide groups have also been established to be effective initiators in the polymerization of cyclic esters provided a metal oxygen (M-O) bond is present. The ligand's architecture controls the activity, polymer architecture and polymer morphology. However these non-alkoxide metal complexes show lower activities as compared to alkoxide containing initiators.¹² Very few Schiff base complexes without an alkoxide group are reported in literature.^{17,18}

Schiff base metal complexes as catalysts for lactide polymerization have attracted interest because the ligands can stabilize different metals in various oxidation states and are relatively easy to prepare. Changing the substituents on either the amine or aldehyde also allows for varying the steric and electronic properties.¹⁹ In salicylaldiminato metal complexes, bulky substituents on the phenoxy ring have been used to significantly decrease side reaction. Electron withdrawing groups (EWG) have been reported to enhance activity while electron donating groups (EDG) have been shown to decrease the activity. The EWG groups enhance metal electrophilicity or increase the polarization of the initiating and propagating processes. The EWG have been reported to also reduce both inter-molecular and intra-molecular trans-esterification reactions in the polymerization of lactide.²⁰

Du *et al.*²¹ reported aluminium complexes supported by chiral tetradentate phenoxyamine (salan-type) ligands that polymerized D, L-lactide at M/Al = 50. When a chloro group was introduced in the *ortho* position relative to the phenoxide, 84 % conversion was obtained in 34 h as compared 85 % conversion in 53 h when a methyl substituent was present. Gibson *et al.*²² also reported a similar phenomenon in the polymerization of D, L-lactide with an aluminium complex supported by a tetradentate aminophenoxide ligand.

In these complexes, four chloro substituents were present at the *ortho*- and *para*-positions of phenoxide units. Darensbourg and Krarroonnirum have observed that when EWG's such as methoxy groups were introduced in a salen aluminium complex, the activity reduced considerably.²³

Although numerous papers as well as reviews have been published on the synthesis, characterization and applications of metallodendrimers, to our knowledge there are no reports of metallodendrimers as catalysts/initiator in the polymerization of lactide.²⁴

5.1.2: D, L-lactide isomers

Lactide is a cyclic dimer of lactic acid that is commercially available in two stereoisomers, Figure 5.1, L-lactide (S, S - lactide) or D-lactide (R, R-lactide) and as the equimolar racemic mixture of the D and L-lactide. The meso-lactide (R, S-lactide) form is not commercially available. The ring opening polymerization process is favorable due to the ring-strain in the lactide imposed by the presence of the two ester groups in the ring.²⁵

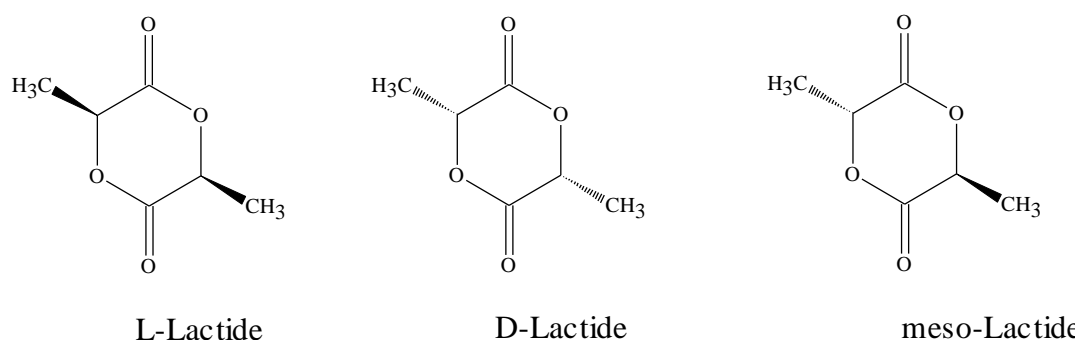


Figure 5.1: Lactide enantiomers

When the racemic mixture D, L-lactide is used in polymerization, the monomers may randomly add onto the growing chain and is described by pair-addition Bernoullian statistics.²⁶ Once polymerized, the ¹³C-NMR chemical shift of the methine carbon, CH (δ

68.5-69.5 ppm) and carbonyl carbon, CO (δ 169-170 ppm) are used to characterize the stereo-chemistry of the polymers. The configurations depend on the neighbouring asymmetric centers. Two possibilities exist.

- i. The adjacent asymmetric carbons have the same configuration; their relationship is termed as isotactic (*i*).
- ii. The adjacent asymmetric carbons have the opposite configuration; their relationship is termed as syndiotactic (*s*).

The difference in the stereo-chemistry gives the polylactide (PDLLA) differing physical and mechanical properties. The degradation is also closely dependent on the PDLLA stereochemistry of the polymer.¹

This chapter looks at the polymerization of D, L-lactide using some of the zinc complexes whose synthesis is described in Chapter 3. Our choice of zinc is motivated by its low toxicity and low cost. The complexes evaluated were mononuclear complexes with a *n*-propyl substituent at the imino nitrogen, **C1** – **C3**; Figure 5.2. Two other mononuclear complexes with an aromatic substituent on the imino nitrogen were also evaluated. These complexes were synthesized in our Laboratory and will be discussed herein as **C18** and **C19**, Figure 5.2.²⁷ The 1st and 2nd generation salicylaldiminato complexes, **C4** – **C6** and **C7** - **C9**, Fig. 5.3 and 5.4 respectively were also evaluated in solution and in the melt conditions.

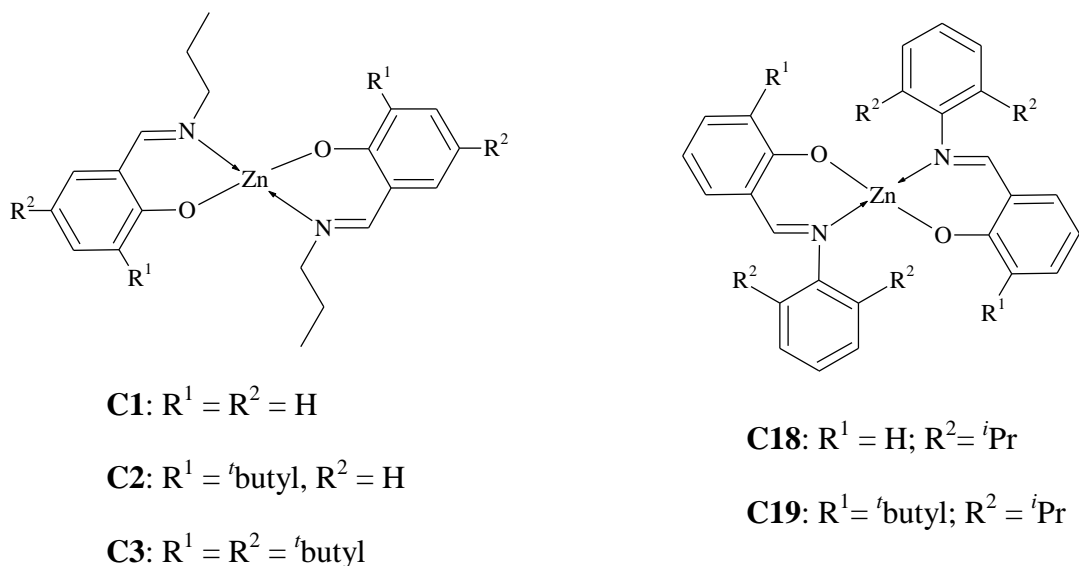


Figure 5.2: Structure of mononuclear salicylaldiminato Zn(II), **C1 – C3, C18** and **C19**

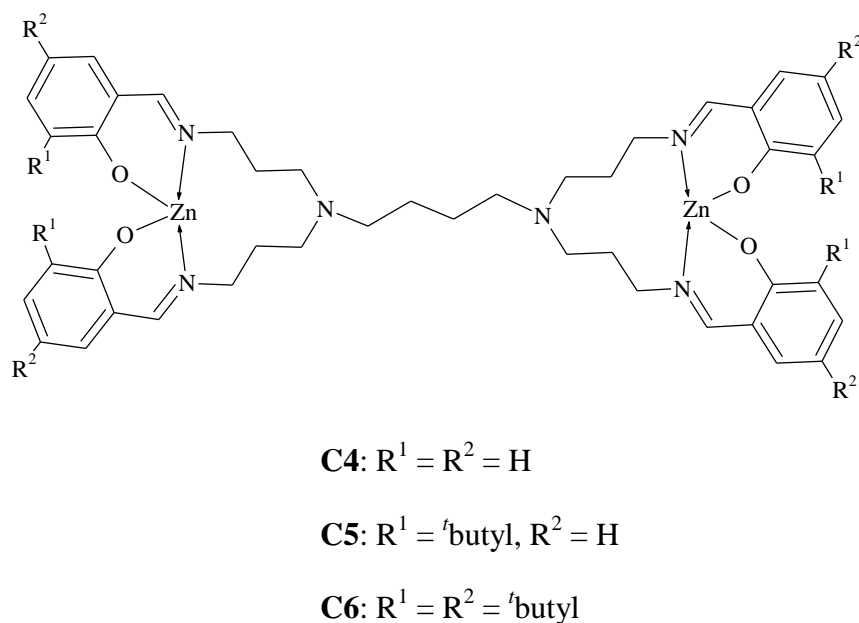
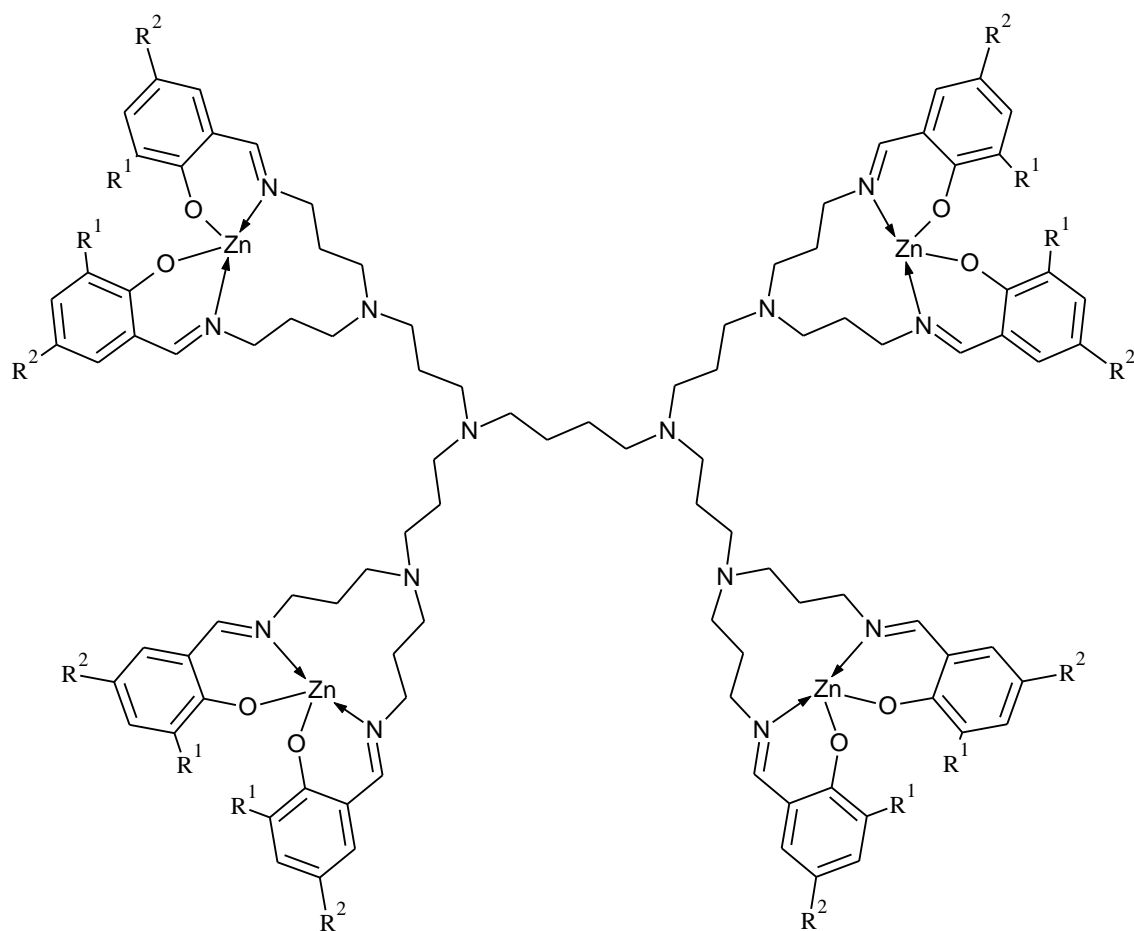


Figure 5.3: 1st generation (G1) dendritic salicylaldiminato Zn(II) complexes



C7: $R^1 = R^2 = H$

C8: $R^1 = t\text{butyl}, R^2 = H$

C9: $R^1 = R^2 = t\text{butyl}$

Figure 5.4: 2nd generation (G2) dendritic salicylaldiminato Zn(II) complexes

We investigated the activity of the complexes and morphological characteristics of the polymers obtained. We looked into the influence of substituting the aliphatic propyl chain at the imine nitrogen in **C1** and **C2** with an aromatic group, 2, 6 - diisopropylphenyl, in **C18** and **C19**. We also compared the efficiency of the mononuclear catalyst to that of the multinuclear analogues anchored on dendrimer scaffolds, **C4** – **C9**. In order to determine the optimum reaction conditions we investigated several reaction parameters such as metal concentration, reaction time, solvent type and temperature.

Polymers obtained were characterized using the following techniques: scanning electron microscopy (SEM), gel permeation chromatography (GPC), NMR and FT-IR (ATR) spectroscopy.

5.2: Results and discussions

5.2.1: Preliminary results on D, L-lactide polymerization

The polymerization was performed using the salicylaldiminato Zn(II) complexes shown in Figures 5.2 - 5.4. In the literature, toluene, dioxane and CH_2Cl_2 are the most commonly used solvents in these types of polymerization reactions. After solubility tests, toluene was selected as the best solvent in which to carry out the polymerization reactions. All complexes were completely soluble in toluene except the 1st generation complexes **C4** and **C5**, with **C4** being the least soluble.

The preliminary polymerization reactions were carried out under vacuum using the various complexes at a D, L-lactide to zinc mole ratio (M:Zn) of 50:1 in toluene at 70 °C. Reactions were allowed to proceed until some polymeric material was formed. After the reaction time, all volatiles were removed and ¹H-NMR spectrum of the crude product obtained in CDCl_3 . The methine proton of D, L-lactide is a quartet located at 5.07 ppm, while the methine protons of the polymer are multiplets falling between 5.12 - 5.22 ppm. This chemical shift difference is large enough to distinguish the methine of the monomer from that of the polylactide. The integration values of these methine protons were used to calculate the percentage conversion using Equation 1. Purification was done by recrystallization from a CHCl_3 solution with acidified CH_3OH in an ice bath. The results are summarized in Table 5.1.

$$\% \text{ Conversion} = \frac{I_{\text{CH}_{\text{polymer}}}}{I_{\text{CH}_{\text{monomer}}} + I_{\text{CH}_{\text{polymer}}}} \times 100 \quad (1)$$

$I_{\text{CH}_{\text{polymer}}}$: Intensity of the methine of the polymer

$I_{\text{CH}_{\text{monomer}}}$: Intensity of the methine of the monomer

Table 5.1: Preliminary polymerization results using $[M]/[Zn] = 50$, $[M] = 1 \text{ M}$

Complex	Solvent	Temp (°C)	Time (h)	Conversion (%) ^a
C1	Toluene	70	24	80
C2	Toluene	70	24	17
C3	Toluene	70	24	20
C4	Toluene	70	24	trace
C4	Toluene	70	48	25
C5	Toluene	70	24	trace
C5	Toluene	70	72	23
C6	Toluene	70	24	28
C18	Toluene	70	24	25
C19	Toluene	70	24	trace
C19	Toluene	70	48	26
C4	Dioxane	100	24	10
^b C4	neat	160	0.5	87

^aCalculated using Equation 1, ^bReaction done in the melt at 160 °C

The unsubstituted mononuclear salicylaldiminato Zn(II) complex, **C1**, showed the best activity. Up to 80 % of the lactide was converted in 24 h. Due to the nature of the coordination geometry of **C1**, it was easier for the monomer to access the zinc center. The structure of **C1** was previously reported by Torzilli *et al.*²⁸ and possesses tetrahedral geometry. Of the other mononuclear complexes with an aliphatic substituent on the imino nitrogen, **C2** and **C3** were the least active. Since Zn(II) is a d^{10} ion the ability of the phenoxy

oxygen to act as a π -donor is inhibited by the lack of empty d orbitals on the metal to accept electrons. Thus the electron releasing ability of the ^tbutyl groups has no impact on the π -bonding of the phenoxy group to the metal center. One can thus assume that in these zinc systems the ^tbutyl groups have a purely steric effect.

Wang and Ma observed a similar trend with Zn(II) complexes supported by multidentate aminophenolate ligands. When a bulky substituent such as ^tbutyl was introduced at the *ortho*- position relative to the phenoxide unit, a decline in the rate of polymerization of *rac*-lactide was recorded.²⁹ They attributed the reduction in activity to the steric hindrance induced the bulkiness of these groups.

The complexes with an aliphatic moiety at the imino nitrogen showed better monomer conversion compared to those with an aromatic, **C18** and **C19**. These two complexes have an aromatic moiety, 2, 6-diisopropyl phenyl, unlike **C1** and **C2** which have an aliphatic (*n*-propyl) group. It is postulated that the bulkiness of the 2, 6-diisopropyl phenyl hinders the coordination and subsequent insertion of the monomer into the Zn-O bond. Complex **C18** is a better catalyst/initiator than **C19** but still shows only 25 % conversion after 24 h. **C19** required 48 h to achieve 26 % conversion of the D, L-lactide. Again the presence of the ^tbutyl group at the ortho position relative to the phenoxide in **C19** was observed to induce steric hindrance at metal center slowing down the coordination of the lactide and subsequent chain growth via monomer insertion into the Zn-O bond.

Of the metallodendrimers, **C6** showed 28 % monomer conversion after 24 h unlike **C4** and **C5** which required longer reaction times to produce significant amount of polymers. Up to 72 h was required by **C5** to convert 23 % of the lactide. In these metallodendrimers, the ^tbutyl groups increased the solubility of the complex and in return the activity.

Carrying out the polymerization reaction using **C4** at higher a temperature (100) °C in dioxane did not improve conversion considerably. This reduction in activity may largely be

attributed to its low solubility. In this case, the system could essentially be regarded to as a heterogeneous system. It is well established that heterogeneous catalytic systems are less efficient as compared to homogeneous systems especially when operated in batch mode.

In a further effort to improve the efficiency of **C4**, the polymerization was attempted in the melt phase i.e. in the absence of any solvent. The reaction was carried out at a M/Zn ratio of 50:1 at 160 °C. It was previously established from TGA studies that **C4** is thermally stable at this temperature showing no decomposition. At this temperature, the lactide forms a melt in which the polymerization occurs. After 30 min, 87 % of the lactide was found to have been polymerized. This metallodendrimer proved to be more active than Cu(II) complexes of phenoxy-ketimine ligands reported by John *et al.*³⁰ and also evaluated under melt conditions. The most active Cu(II) complex of this series showed 86 % conversion of L-lactide after only 6 h.

Other zinc complexes have been reported as suitable catalysts in the polymerization of lactide under the melt conditions. However, these systems were evaluated under different conditions to those we employed for our dendritic Zn(II) complex. Jones *et al.*³¹ reported a series of mononuclear and trinuclear salicylaldiminato Zn(II) complexes that polymerized D, L-lactide in the melt (130 °C) at M/Zn = 300. The best performing complex gave up to 80 % conversion in 30 min. Börner *et al.*⁹ also published a series of Zn(II) complexes amongst them ZnCl₂ that polymerized D, L-lactide in the melt at 150 °C. ZnCl₂ showed 85 % conversion after 48 h at a M:I ratio of 500: 1.

In the Zn(II) complexes evaluated here, polymerization is assumed to occur via a coordination-insertion mechanism involving the M-O bond. In an attempt to understand the mechanism we tried to probe the polymerization process using ¹H-NMR spectroscopy. In an NMR tube, D, L-lactide (0.015 g, 0.104 mmols) and **C1** (0.04 g, 0.103) were mixed in CD₂Cl₂ as solvent and the ¹H-NMR spectrum acquired immediately and thereafter spectra

were recorded at time intervals of 24 and 120 hours. The NMR sample was stored at 25 °C under a nitrogen atmosphere.

In the initial ^1H -NMR spectrum, Figure 5.5, the signals arising from the complex, **C1**, were similar in position, multiplicity and integration to those of the pure complex as discussed in Chapter 3. Changes in the NMR spectrum were monitored over time. The lactide signals that were monitored are those observed at δ 5.03 (methine) and 1.63 ppm (methyl). At the same, time the intensities of the two imine peaks at δ 8.35 and 8.20 ppm were monitored as the reaction progressed. The peak at δ 8.20 ppm was assigned to the imine of the complex **C1**, while that at δ 8.35 ppm is that of uncoordinated imine which is formed once the lactide monomer coordinated and subsequently inserted into the Zn-O bond. There is a significant increase in the intensity of the peak at δ 8.35 ppm relative to that at δ 8.20 ppm over time. The ratio of the aforementioned imine peaks were calculated over the course of the reaction. At time 0 h (Fig. 5.5.) a ratio of 1:9 was observed for the peak at δ 8.35 ppm to that at δ 8.20 ppm. After 24 h the ratio was 1:2, while after 120 h a further reduction to 1:1.5 was observed.

All the peaks broaden and lose their resolution due the overlapping of the protons from the complex (**C1**) and those of the activated complex. In this mixture, the complex **C1** can be in three different structural conformations as shown Scheme 5.1. These changes in the ^1H NMR spectra confirm the assumption that a new complex with a slightly altered structure is formed. Pastusiak *et al.*³² performed a study using $\text{Zn}(\text{acac})_2$ with L-lactide at 1:1 mole ratio and made similar observations in the ^1H -NMR spectra. They reported the presence of free acetylacetone (Hacac) proving dissociation of one of the ligands.

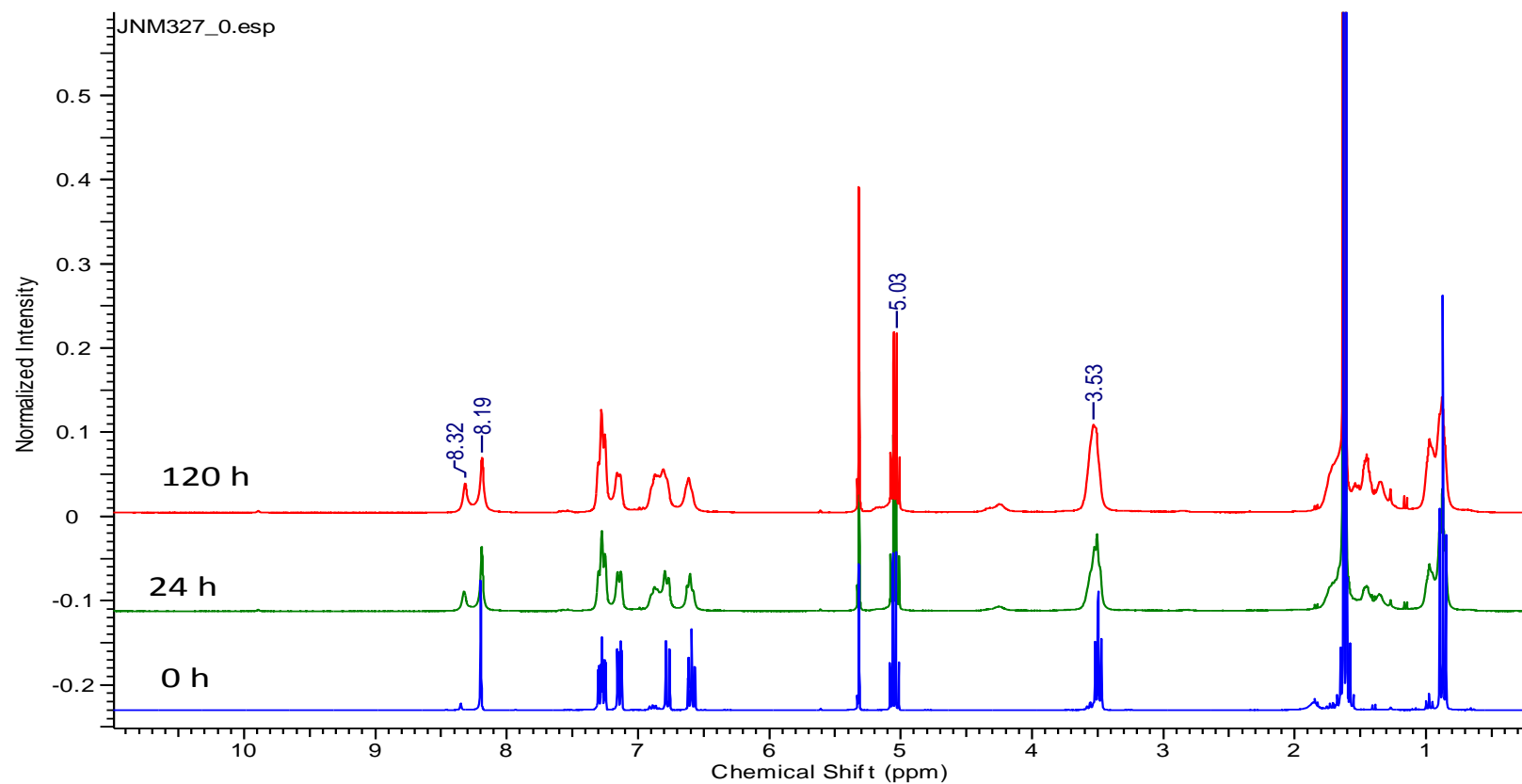
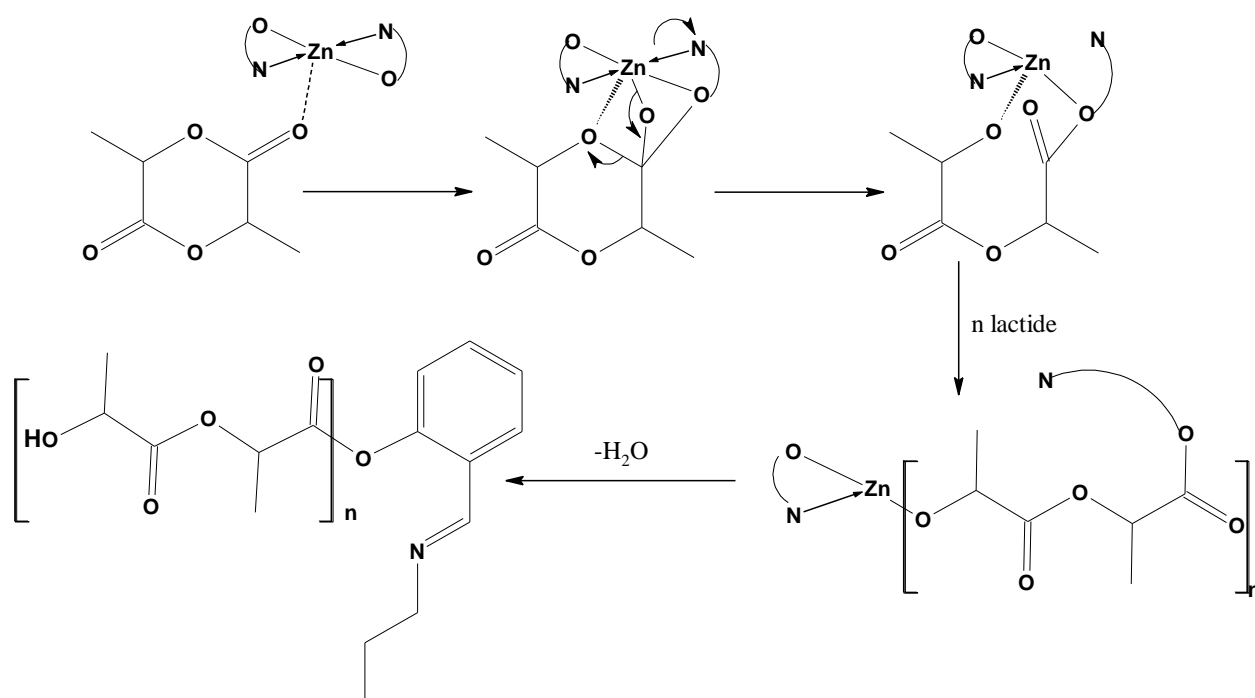


Figure 5.5: ¹H-NMR spectra obtained for M:Zn = 1 for C1 in an NMR tube at time (t = 0, 24 and 120 h).

The coordination of the oxygen of the lactide to the electrophilic metal center activates the carbonyl carbon towards nucleophilic attack by the phenoxide group of the metal complex. This is followed by ring-opening of the lactide and the formation of a metal-oxygen bond, Scheme 5.1.³³ The imino nitrogen dissociated creating vacant a coordination site onto which the cycle is repeated upon coordination of another monomer.



Scheme 5.1: Mechanism for the coordination and insertion of the D, L – lactide into **C1**'s Zn-O bond

5.2.2: Kinetic studies

5.2.2.1: Effect of [Zn], M/I ratio, using **C1**

The kinetics of the most active complex **C1** were evaluated at M/Zn ratios of 100, 50 and 25. The polymerization reactions were carried out in toluene at 70 °C and data collected over time. The monomer concentration was maintained at 1 M. The % conversions were calculated from the ¹H-NMR spectrum of the crude material using Equation 1, Table 5.2.

Table 5.2: Polymerization of D, L-Lactide using complexes **C1** at different M/Zn ratios^a

M/Zn	Time (h)	^b Conv %	x 10 ³ g mol ⁻¹			^d PDI
			^c M_n (Calc.)	^d M_n (GPC)	^e M_n (corrected)	
25	2	22.7	0.82	0.27	0.15	3.2
	5	68.35	2.46	2.23	1.29	1.6
	10	80.5	2.90	12.07	6.99	1.5
	20	92.4	3.33	24.42	14.16	1.4
	24	97.5	3.51	27.88	16.18	1.3
50	^f 5	15.7	1.13	n.d.	n.d.	n.d.
	10	53.7	3.87	2.40	1.39	2.5
	24	79.9	5.75	2.56	1.49	2.6
	48	89.3	6.43	9.59	5.56	1.6
	72	96.1	6.92	33.68	19.53	1.7
100	24	67.9	9.77	1.86	1.08	2.7
	48	74.2	10.68	3.77	2.19	1.8
	72	90.7	13.06	6.74	3.91	1.9
	96	94.5	13.61	44.86	26.02	1.5

^aConditions: toluene, 70 °C, ^bCalculated using equation 1, ^cCalculated using equation 6, [M/I x 144 x % conversion], ^dDetermined by GPC relative to polystyrene standards, ^eObtained after multiplying GPC values with the correction value of 0.58 see ref. 35, ^fSufficient polymeric material for GPC analysis could not be obtained after purification.

A plot of $\ln\{[M]_0/[M]_t\}$ vs time (t) is shown in Figure 5.6. The linearity of this semilogarithmic plot supports a living polymerization process since the concentration of the active species remained unchanged.³⁴ The gradient also increases as the concentration of the Zn metal increases. This indicates that the polymerization follows 1st order kinetics with respect to D, L-lactide. The order of the reaction can be calculated from the Equations in

Scheme 5.2. The propagation rate constants for different metal concentrations were determined by the slope of the plot using Equation (5) in Scheme 5.2.

(2)

(3)

(4)

(5)

$[M]_0$ = initial monomer concentration, t = time,

$[M]_t$ = monomer concentration at time t , c = integral constant

Scheme 5.2: Equations to determine the order of the polymerization reaction using of D, L-Lactide as monomer.

At various metal concentrations of $[Zn] = 0.01, 0.02$ and 0.04 M, the apparent polymerization rate constants (k_{app}) were established as $2.63, 3.80$ and $13.62 \times 10^{-2} \text{ h}^{-1}$ respectively from Figure 5.6. As the concentration of Zn is increased, the k_{app} values increase indicating that the order with respect to Zn is also first order. The nonzero x, y intercept suggests that there is a significant induction period for the process. The induction is possibly due to the steric hindrance around the zinc center as a result of the bulky ligands thus necessitating an induction period for these complexes. Bero *et al.*³⁵ attributed such an induction period to the presence of impurities in the reaction mixture. Although precautions were taken this cannot be entirely ruled out in our reactions.

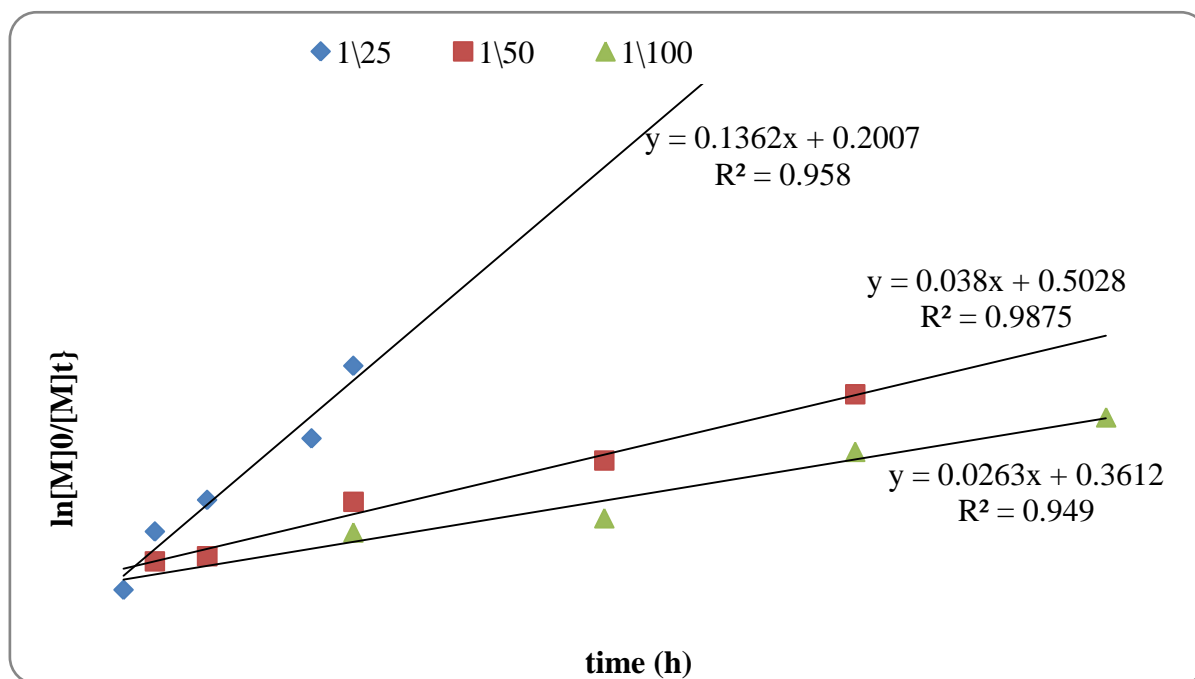


Figure 5.6: A plot of $\ln\{[M]_0/[M]_t\}$ vs time (h) for complexes **C1** at $M/Zn = 25, 50$ and 100

5.2.2.2: Polymerization using complexes **C1** – **C3**

Relationship between reaction rates and nature of ligand

The rates of polymerization using complexes **C1** – **C3** were evaluated at $M/Zn = 50$ and the results are shown in Table 5.3. A plot of $\ln[M]_0/[M]_t$ against time for complexes **C1** – **C3** is showed in Figure 5.7. The semilogarithmic plots showed that the polymerization reaction followed first order kinetics for the three complexes. The polymerization rate constants for each of the reactions using the different complexes were established to be 3.80, 2.37 and $0.73 \times 10^{-2} \text{ h}^{-1}$ for **C1**, **C2** and **C3** respectively at a $[Zn] = 0.02 \text{ M}$.

Complexes **C1**, **C2** and **C3** have similar structures with the only difference being the ^tbutyl substituents in the *ortho*- and *para*- positions on the phenoxy ring. The order of activity was observed to be **C1** > **C2** > **C3**. The presence of the ^tbutyl groups imparts steric effects on complexes **C2** and **C3** leading to a decrease in the activity as compared to **C1**.

Table 5.3: Lactide polymerization using mononuclear complexes **C1 – C3**^a

	Time (h)	^b Conv %	x 10 ³ g mol ⁻¹			PDI
			^c <i>M_n</i> (Calc.)	^d <i>M_n</i> (GPC)	^e <i>M_n</i> (corrected)	
C1	5	15.7	1.13	n.d.	n.d.	n.d.
	10	53.7	3.87	n.d.	n.d.	n.d.
	24	79.9	5.75	2.56	1.49	2.6
	48	89.3	6.43	9.59	5.56	1.5
	72	96.1	6.92	33.68	19.53	1.7
C2	10	6.6	0.47	n.d.	n.d.	n.d.
	24	16.5	1.19	n.d.	n.d.	n.d.
	48	37.1	2.71	8.23	4.77	1.2
	72	65.6	4.72	14.86	8.62	1.2
C3	10	trace				
	^f 24	20.0	1.44	n.d.	n.d.	n.d.
	48	32.6	2.36	2.30	1.13	1.4
	72	39.2	2.82	9.61	5.57	1.1
	96	56.3	4.06	17.23	9.99	1.4
	144	65.8	4.74	39.90	23.14	1.6

^aConditions: toluene, 70 °C, M/Zn = 50, ^bCalculated using Equation 1, ^cCalculated using Equation 6,

^dDetermined by GPC relative to polystyrene standards, ^eObtained after multiplying GPC values with the correction value of 0.58, ^fSufficient polymeric material could not be obtained after purification for GPC analysis

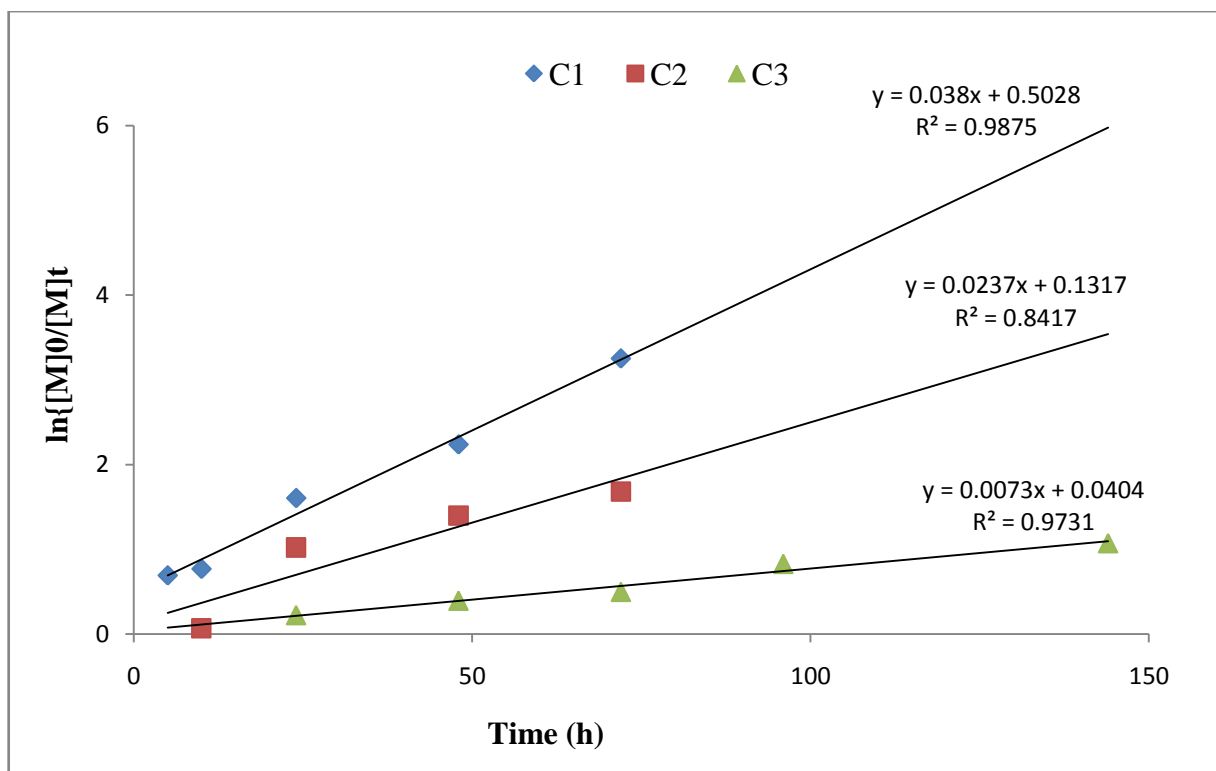


Figure 5.7: A plot of $\ln\{[M]_0/[M]_t\}$ vs time (h) for the salicylaldiminato Zn(II) complexes, **C1 - C3**, at $M/Zn = 50$

Assuming the other two complexes adopt a similar geometry to that reported for **C1**, then the *t*-butyl groups would be positioned close to the metal center. This results in the blocking of the Zn center thus inhibiting access of the monomer to the active site which results in lower activities for **C2** and **C3**. Complex **C3** with two *t*-butyl substituents showed the lowest rate of polymerization and also has an induction period of almost 10 h.

Gel permeation chromatography analysis of the polymers produced using C1 – C3

The GPC traces obtained were essentially monomodal in character and in a few exceptions bimodal. The molecular weights obtained from GPC, $M_n^{(GPC)}$, increased as the % conversion increase over time, Table 5.2 and 5.3. The expected molecular weights, $M_n^{(Calc)}$, of the polymers were estimated using Equation 6. In this calculation, it was assumed that all the polymerization occurred with no side reactions. A lower $M_n^{(GPC)}$ compared to the $M_n^{(Calc)}$

indicates intra-chain trans-esterification while a higher value points to inter-chain trans-esterification. In inter-chain trans-esterification, two polymeric chains are combined leading to very high molecular weight while in the intra-chain cyclic products are formed.³³

(6)

Polymers obtained using catalyst **C1** showed a very high degree of intra-chain trans-esterification. The calculated molecular weight ($M_n^{(\text{calc})}$) of the polymer obtained after 24 h was 5.75×10^3 while that obtained from GPC ($M_n^{(\text{GPC})}$) was 2.56×10^3 with a PDI of 2.6. On the other hand after longer reaction time, the polymers obtained had a much higher $M_n^{(\text{GPC})}$ value as compared to the $M_n^{(\text{calc})}$. After 72 h, a $M_n^{(\text{GPC})}$ of 3.37×10^4 was obtained. This value is almost 5 times higher than the calculated one, $M_n^{(\text{calc})} = 6.92 \times 10^3$. As the monomer concentration decreases, inter-chain trans-esterification becomes more pronounced. As the concentration of the monomer decreases, the inter chain trans-esterification reactions becomes more likely for very active catalysts.

There was a decrease in the average molecular weight of the polymers as the steric bulk of the ligand increased. At 72 h, the $M_n^{(\text{GPC})}$ were 3.37×10^5 , 1.49×10^4 and 9.07×10^3 for **C1**, **C2** and **C3** respectively. The Zn center is more sterically crowded in **C3**, thus the monomer coordination and subsequent insertion into the Zn-O bond becomes more difficult.

The presence of the ^tbutyl groups in **C3** had little influence on limiting the trans-esterification reactions. Prolonged reaction time (144 h) yielded polymers with $M_n^{(\text{GPC})} = 3.98 \times 10^4$ which was higher by a factor of 8 when compared to the $M_n^{(\text{calc})}$ (4.74×10^3). This was similar to what was observed by Chisholm.³³ As the % conversion increased and the monomer concentration decreases, the PDI also increased. The broad molecular

weight distribution provides further evidence for the inter-chain trans-esterification reactions.³⁷

5.2.2.3: Polymerization using complexes **C18** - **C19**

Relationship between ligand structure and rate of polymerization

The polymerization reactions using these two complexes also followed first order kinetics similar to what was observed for the aliphatic analogues. The ^tbutyl groups also played a very significant role in influencing the rate of initiation and propagation for the polymerization. **C18** has a less crowded coordination sphere thus allowing for faster initiation of the reaction than **C19**, Table 5.4. This is similar to what was observed for the aliphatic analogues **C1** and **C3**. Thereafter; once the insertion was accomplished the rate of propagation was slightly faster in **C19** than in **C18**. Complete lactide conversion was achieved in 96 h for **C19** while **C18** showed 94 % conversion after 100 h. The propagation rate constants were determined to be 5.59 and $6.04 \times 10^{-2} \text{ h}^{-1}$ for **C18** and **C19** respectively. It is postulated that the presence of the ⁱPr and ^tbutyl substituents on the amino and phenoxy moieties in **C19**, enhances the thermal stability of the catalyst leading to a more stable catalyst over time.

*Gel permeation chromatography analysis for the polymers produced by **C18** and **C19***

Complex **C18** being the less sterically hindered gave polymers with higher molecular weights compared to that of **C19**. Polymers of high M_w were obtained with increased % conversion. At lower M/Zn ratios, the polymerization seemed to be more controlled as evident from the low PDI values. The M_n of polymer from complexes **C18** and **C19** were much higher than those from the aliphatic analogues. The differences could be due to the higher stability of the **C18** and **C19** complexes under the conditions employed.

Table 5.4: Lactide polymerization using mononuclear complexes **C18** and **C19**^a

Catalyst	M/Zn	Time (h)	^b Conv %	x 10 ³ g mol ⁻¹			PDI
				^c M _n (Calc.)	^d M _n (GPC)	^e M _n (corrected)	
C18	50	24	24.8	1.79	4.31	2.50	2.7
		48	54.6	3.93	45.53	26.41	2.2
		72	70.2	5.05	120.48	69.88	1.8
		100	93.8	6.75	143.1	82.98	1.6
	25	10	20.6	0.74	33.09	19.19	1.2
		15	46.5	1.67	43.63	25.31	1.3
		20	87.9	3.16	46.84	27.17	1.7
		30	92.8	3.34	52.28	30.49	1.8
C19	50	24	trace	-			
		48	25.8	1.86	15.53	9.01	1.7
		68	62.5	4.50	17.87	10.33	1.8
		96	100	7.19	18.93	10.98	1.6
	25	15	trace	-			
		20	46.2	1.66	12.0	6.96	1.5
		30	62.5	2.25	15.34	8.90	1.7
		48	100	3.60	17.85	10.35	1.7

^a Conditions: toluene, 70 °C, M/Zn = 50, ^bCalculated using Equation 1, ^cCalculated using Equation 6, ^dDetermined by GPC relative to polystyrene standards, ^eValues obtained from GPC values multiplied by 0.58

5.2.2.4: Polymerization using dendritic complexes **C5** and **C6**

Relationship between nature of ligand and the rate of polymerization

The zinc metallodendrimers **C5** and **C6** showed some activity in lactide polymerization with **C6** being the most active, Table 5.5. Up to 6 days were required for **C6** to polymerize 93 % of the monomer. On the other hand **C5** afforded only 36 % conversion after 5 days. The propagation constants obtained were 0.48 and 1.92 x 10⁻² h⁻¹ for **C5** and **C6** respectively.

The presence of ^tbutyl groups dramatically improved the solubility of the complexes and in return the activity. In essence the polymerization reaction was greatly affected by the low solubility of these dendritic complexes.

Gel permeation chromatography analysis of the polymers produced using C5 – C6

The M_n of polymer from **C5** was very high as compared to that produced using **C6**. The difference in these two systems could be due to the fact that **C5** is not completely soluble in the reaction solvent leading to a less controlled system.

Table 5.5: Solution polymerization of D, L-lactide using dendritic complexes **C5** and **C6** as catalyst^a

	Time (h)	^b Conv %	$\times 10^3 \text{ g mol}^{-1}$			PDI
			^c M_n (Calc.)	^d M_n (GPC)	^e M_n (corrected)	
C5	48	trace				
	72	22.7	1.64			
	96	31.9	2.30	44.29	25.69	1.3
	120	36	2.59			
C6	24	27.7	1.99	4.07	2.36	1.2
	48	55.6	4.01			
	72	70.9	5.12	11.36	6.59	1.3
	96	74.6	5.37			
	144	93.5	6.73	28.72	16.66	1.2

^a Conditions: toluene, 70 °C, M/Zn = 50, ^bCalculated using Equation 1, ^cCalculated using Equation 6,

^dDetermined by GPC relative to polystyrene standards, ^eValues obtained from GPC values multiplied by 0.58

5.2.2.5: Effects of solvent and temperature on the polymerization reactions

Complex **C1** was chosen for the study of the influence of temperature and solvent type on the polymerization reactions because of its high activity. In toluene at 70 °C and M/Zn

ratio of 25:1, up to 98 % conversion was obtained in 24 h, Table 5.6. However when the reaction was done at 25 °C in the same solvent, only traces of polymeric material was observed. When the polymerization reaction was conducted at 25 °C in CH₂Cl₂, 20 % conversion was obtained in 24 h.

Kang and co-workers also observed a decrease in catalytic activity of Zn(II) complexes bearing pyrazole-based ligands as temperature was reduced from 25 to -20 °C. In this case the polymerization reactions were done in toluene at a M/Zn ratio of 50. Up to 93 % conversion was obtained in 2 h at 25 °C as opposed to 52 % after 12 h at -20 °C.³⁷

High D, L-lactide conversions were also reported by Wang and Ma at ambient temperature in THF or toluene in the presence of a series of zinc silylamido complexes as catalysts. In each case conversion of between 67 – 95 % were achieved in 50 min, M/Zn = 200. Under the polymerization conditions used, very slight solvent effects were observed for the same complex in the solvents.²⁹

Another significant observation from these studies was that at lower temperature, 25 °C, the polymerization progressed in a more controlled fashion even though the conversion was lower. Lower PDI's were obtained when reactions were carried out in CH₂Cl₂ as opposed to toluene.

Table 5.6: Effect of solvent and temperature in the polymerization of D, L-lactide using **C1** at M/Zn = 25.

Solvent	Temp (°C)	Time (h)	^a Conv %	$\times 10^3 \text{ g mol}^{-1}$			PDI
				^b M_n (Calc.)	^c M_n (GPC)	^d M_n (corrected)	
Toluene	70	2	22.7	0.82	0.27	0.15	3.2
		5	68.35	2.46	2.23	1.29	1.6
		10	80.5	2.90	2.49	1.45	1.5
		20	92.4	3.33	2.44	1.42	1.4
		24	97.5	3.51	12.07	6.99	1.3
Toluene	25	24	trace	-	-	-	-
CH ₂ Cl ₂	25	^e 24	22.1	n.d.	n.d.	n.d.	n.d.
		72	34.2	1.23	1.32	0.77	1.3
		96	42.9	1.54	2.24	1.30	1.3
		120	51.2	1.84	3.043	1.765	1.2

^aCalculated using Equation 1, ^bCalculated using Equation 6, ^cDetermined by GPC relative to polystyrene standards, ^dValues obtained from GPC values multiplied by 0.58, ^eSufficient polymeric material could not be obtained after purification for GPC analysis

5.2.2.6: Melt polymerization reactions using dendritic complexes **C4** – **C9**

Due to the low polymerization activity of the 1st generation metallodendrimers in solution, it was decided to evaluate these complexes as catalyst for the polymerization of D, L-lactide under melt conditions. The Zn(II) metallodendrimers were evaluated for the polymerization of D, L-lactide under solvent free melt conditions at a M/Zn ratio of 50:1. A typical polymerization experiment involved heating D, L-lactide to 160 °C with the appropriate metallodendrimer. The lactide forms a melt in which the polymerization can occur. The results are summarized in Table 5.7

Table 5.7: Polymerization of D, L-lactide using **C4** – **C9** under melt conditions

	M/Zn	Temp (°C)	Time (min)	Conv. (%) ^a	($\times 10^3$ g mol ⁻¹)			PDI ^c
					M_n (calc) ^b	M_n (GPC) ^c	M_n (corrected) ^d	
C4	^e 50	160	10	33.8	2.43	n.d.	n.d.	n.d.
	50	160	15	58.9	4.24	1.38	0.81	1.6
	50	160	30	86.6	6.21	2.55	1.48	1.7
	50	160	1440	99.8	7.19	6.12	3.55	1.6
	100	160	30	64.0	9.22	1.24	0.72	1.6
C5	50	160	10	68.9	4.96	1.65	0.95	1.8
	50	160	15	80.6	5.80	1.94	1.12	1.8
	50	160	30	96.7	6.63	3.37	1.96	2.1
	100	160	30	79.3	11.42	3.41	1.98	2.1
C6	50	160	10	74.2	5.34	1.62	0.94	1.7
	50	160	15	86.6	6.24	1.86	1.08	1.8
	50	160	30	99.0	7.13	2.04	1.19	2.0
	50	140	30	77.4	5.57	1.42	0.83	1.5
	50	120	30	56.7	4.08	1.38	0.80	1.5
	100	160	30	84.0	12.14	2.83	1.64	2.2
C7	50	160	10	78.1	5.62	1.49	0.86	1.6
	50	160	30	82.8	5.96	1.98	1.15	1.8
	100	160	30	40.3	5.80	2.59	1.50	1.8
C8	50	160	10	80.5	5.80	1.84	1.06	1.7
	50	160	30	99.0	7.13	2.16	1.25	1.9
	100	160	30	68.5	9.86	2.83	1.64	2.4
C9	50	160	10	81.9	5.90	1.04	0.60	2.7
	50	160	30	99.0	7.13	2.68	1.55	2.2
	50	140	30	73.6	5.30	2.25	1.30	2.2
	50	120	30	27.7	2.71	1.75	1.01	1.83
	100	160	30	80.2	11.55	2.93	1.70	2.8

^aCalculated using Equation 1, ^bCalculated using Equation 6, ^cDetermined by GPC in THF at 30 °C relative to polystyrene standards, ^dCorrection factor of 0.58 applied to the GPC values, ^eSufficient polymeric material could not be obtained after purification for GPC analysis.

The 1st generation metallodendrimers showed a rapid rate of polymerization. High conversions of 87, 97 and 99 % were obtained for **C4**, **C5** and **C6** respectively in 30 min.

For the 2nd generation metallodendrimers, a similar trend to that of the 1st generation was observed. **C9** which possess ^tbutyl groups at the *ortho*- and *para*- positions relative to the phenoxide was the most active.

The effect of the temperature on the polymerization was investigated using the most active G1 (**C6**) and G2 (**C9**) catalyst. The M/Zn ratio was maintained at 50:1 and the reactions performed at 120, 140 and 160 °C. It was observed that the catalytic activity of these metallodendrimer increased with increase in temperature.

Gel permeation chromatography analysis of the polymers produced using C4 – C9 under melt condition

The molecular weights of the polymers obtained experimentally using GPC were much lower than the theoretical values. This may suggest that there could be intra-molecular transesterification occurring leading to formation of cyclic products. At shorter reaction times i.e. 10 min, relatively high PDI values were recorded.

However, several other initiators have also been reported to produce polymers of higher molecular weight in the solvent free melt conditions. Jensen *et al.*⁴⁰ reported bidentate pyridyl-NHC Zn(II) complexes that polymerized lactide only in the melt phase and in the presence of BnOH. The evaluation was done at 140 °C with varying M/Zn mole ratios started from 50 to 200. They observed very rapid rates of polymerization with 97 % conversion in 5 min at M/Zn ratio of 50:1.

5.2.3: Characterization of polylactides produced

5.2.3.1: Stereochemistry of polymers

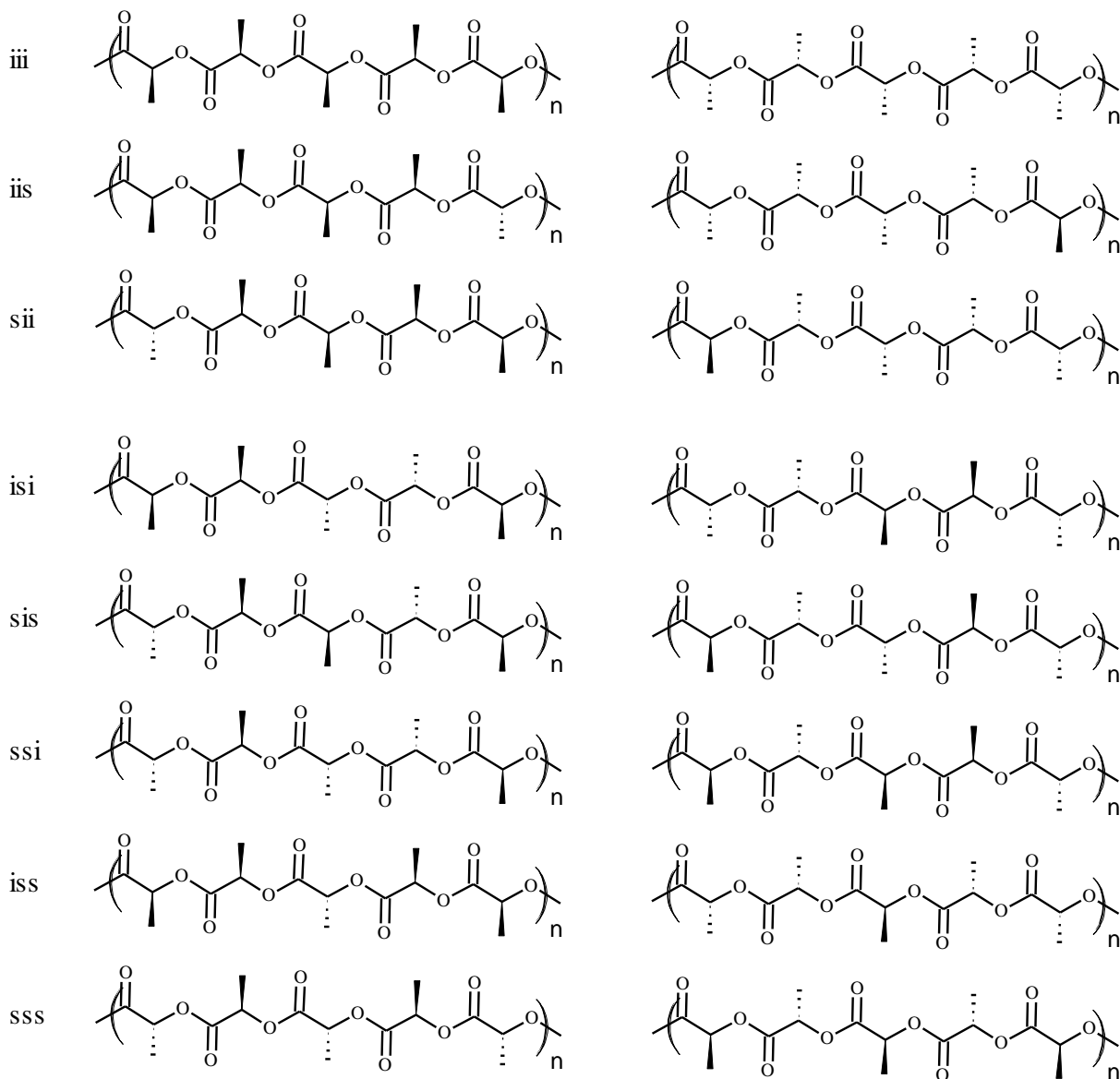
Microstructure using ^{13}C -NMR spectroscopy

NMR spectroscopy of polymers has been established as a powerful technique in the determination of polymer microstructure. Polylactide can either be isotactic, syndiotactic or atactic. Sequences of up to eight asymmetric centers can be differentiated in a completely atactic-PLA (Scheme 5.3), however only chemical shifts of stereosequences on the tetrad level have been assigned for which there are three pair-wise relationships.

For example a (R,R,R,R) or (S,S,S,S) tetrad would be denoted as *iii* and a (R,R,S,S) or (S,S,R,R) as *isi* as illustrated in Figure 5.3 where *i* and *s* denotes isotactic and syndiotactic respectively.⁴¹ D, L-lactide polymerization devoid of epimerization and trans-esterification can only produce five tetrad sequences *viz.* *iii*, *iis*, *sii*, *isi* and *sis*. In the polymerization of D, L-Lactide there can be no *ss* junction ruling out the *sss*, *ssi* and *iss* tetrads. ^{13}C NMR analysis of some of the PDLA obtained using some of the zinc complexes is summarized in Tables 5. 8 and 5.9.

It was observed that the *iii*, *iis*, *sii*, *sis* tetrads were present between 62 and 69 % with only one exception. The presence of the other tetrads, *iss*, *sss* and *ssi*, further supports the occurrence of trans-esterification reactions. The presence these other tetrads in such significant proportions ~30 % indicates that in these catalysts systems do not have stereoselectivity for either the D or the L-lactide. The substituents on the phenoxy moiety do not seem to play a very significant role in the controlling the stereochemistry of the polymers produced either. The stereochemistry of the approaching lactide unit is probably more influenced by the previously incorporated lactide unit in the polymer chain. Polymers produced using **C1** at $M/Zn = 50$ differed significantly from those obtained from other

catalysts. The melt polymerization products are similar to those obtained in solution. The metallo dendrimers are also not selective for either D or L-lactide.



Scheme 5.3: Tetrads from the possible stereosequences of lactide polymers¹³

Table 5.8: Intensities of different tetrad stereo-sequences of the polymers from solution reactions calculated from the ^{13}C -NMR spectra.^a

Catalyst	M/I	Time	Conversion	Tetrad intensities			
				iii, iis, sii, isi, sis	iss	sss	ssi
C1	25	2	22.7	51.3	25.1	15.6	8.1
C1	25	5	68.4	63.4	32.7	2.3	1.6
C1	50	48	89.3	65.4	28.9		
C2	50	72	65.6	67.0	22.9	4.3	5.9
C3	50	96	56.3	68.0	27.5		4.5
C18	50	72	70.2	68.5	29.3	2.3	
C19	50	68	62.5	62.2	23.9	10.5	3.4

^aConditions: toluene, 70 °C**Table 5.9:** Intensities of different tetrad stereo-sequences of the polymers calculated from the ^{13}C -NMR spectra of the polymers from melt reactions.

Complex	M/I	Time (min)	Temp (°C)	Conv. (%)	Tetrad intensities				
					sis, iis, sii, iii	isi	iss	sss	ssi
C4	50	10	160	33.8	64.8	8.9	20.7	3.1	2.6
C4	50	30	160	86.6	49.7	11.3	27.2	5.7	6.4
C5	50	30	160	96.7	66.3	0	27.3	2.7	3.6
C6	50	30	160	99.0	59.7	0	29.9	4.1	6.2
C6	50	30	140	77.4	57.3	0	30.4	5.4	7.0
C6	50	30	120	56.7	63.5	0	30.6		6.0
C4	100	30	160	64.0	60.6	7.4	24.0	3.7	4.2
C5	100	30	160	79.3	64.2	0	28.2	2.7	4.9
C6	100	30	160	84.0	61.1	0	27.5	4.2	7.3
C7	50	30	160	82.8	67.0	0	27.4	0	5.6
C8	50	30	160	99.0	62.9	0	24.3	5.8	6.9
C9	50	30	160	99.0	65.9	0	25.2	3.3	5.6

5.2.3.2: Polymer morphology

IR (Crystallinity, morphology)

The crystallinity of a polylactide can be gauged using infrared spectroscopy. Ribeiro *et al.*⁴⁵ summarized all the relevant bands associated with different phases. The FT-IR data was compared to those published in order to establish the phase of the polymer. The FT-IR spectrum of pure D, L-lactide is shown in Figure 5.8. The shift in the absorption bands are compared to those of the polymers obtained.

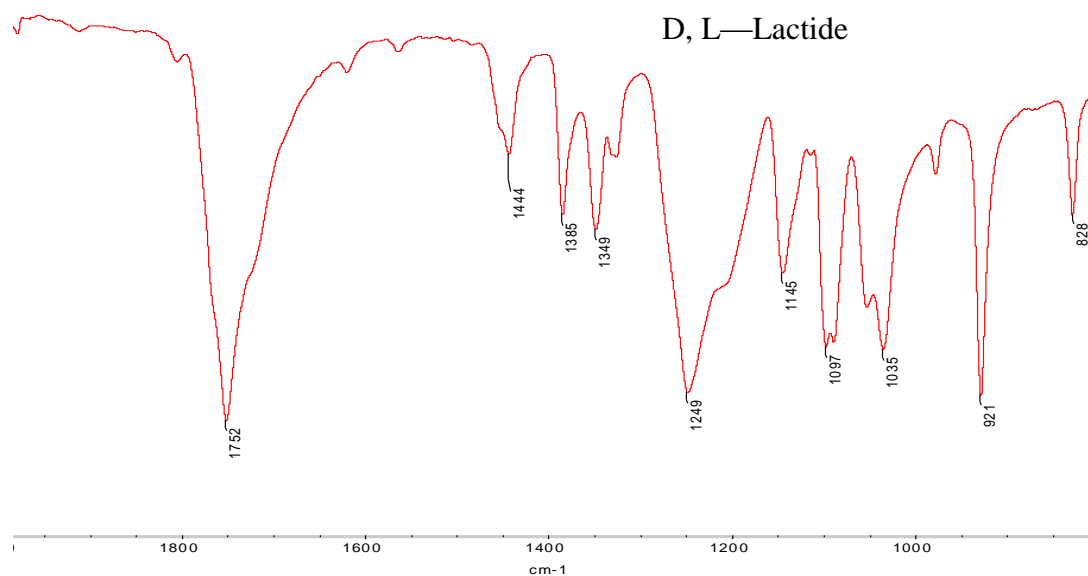


Figure 5.8: FT-IR (ATR) spectrum of D, L – Lactide

Complex **C1** produced amorphous polymers with similar properties irrespective of the concentration of the catalyst, $M/Zn = 25, 50$ or 100 . Figure 5.9 shows an overlay of spectra of polymers obtained at $M/Zn = 25$ after 5, 20 and 24 hours. The three polylactide samples showed similarity in their stereo-chemistry. The most significant bands were observed as very strong peaks at 1746 cm^{-1} due to the stretching vibration (α , $\nu(C=O)$), 1261 cm^{-1} $\nu(-C-O-C-)$, 1182 (amorphous or α' and α , $\nu_{as}(C-O-C) + \nu_{as}(CH_3)$), and 1044 (amorphous or α , $\nu(C-CH_3)$). The peak at 866 cm^{-1} can be assigned to the $\nu(-C-C-)$ skeletal stretching and rocking of

the amorphous phase. Another significant peak was the one which occurred at 955 cm^{-1} . This peak can be assigned to the coupling of the C-C backbone stretching with that of the CH_3 rocking in the amorphous phase. Amorphous polymers are commonly obtained when D, L-lactide is used as monomer.^{45, 46}

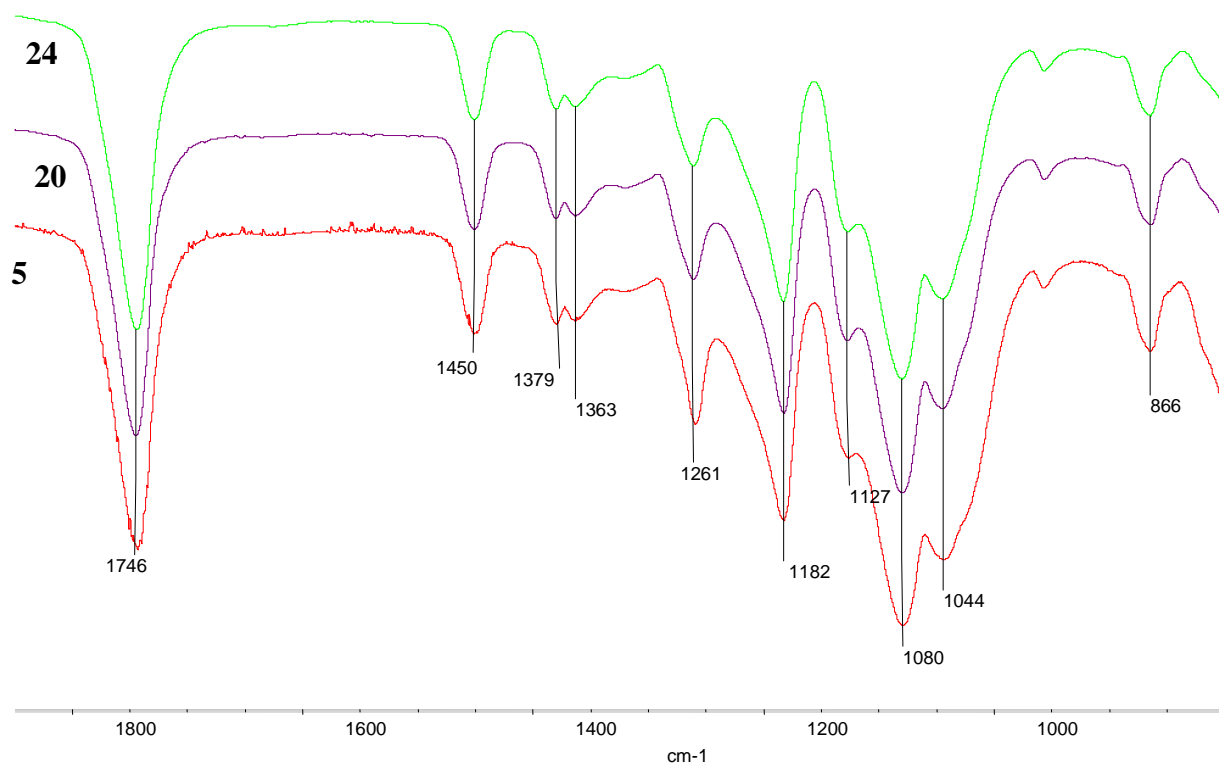


Figure 5.9: FT-IR spectra of polymer produced by **C1** as catalyst at various times, $M/Zn = 25$

FT-IR (ATR) spectra of polymers produced using **C1**, **C2** and **C3** at $M/Zn = 50$ revealed significant differences, Figure 5.10. The morphology of the polymers produced using **C2** (72 h) differed from those produced using **C1** (72 h) and **C3** (96 h). The polymers synthesised using **C1** and **C3** were amorphous and similar in nature to those produced using **C1** at $M/Zn = 25$.

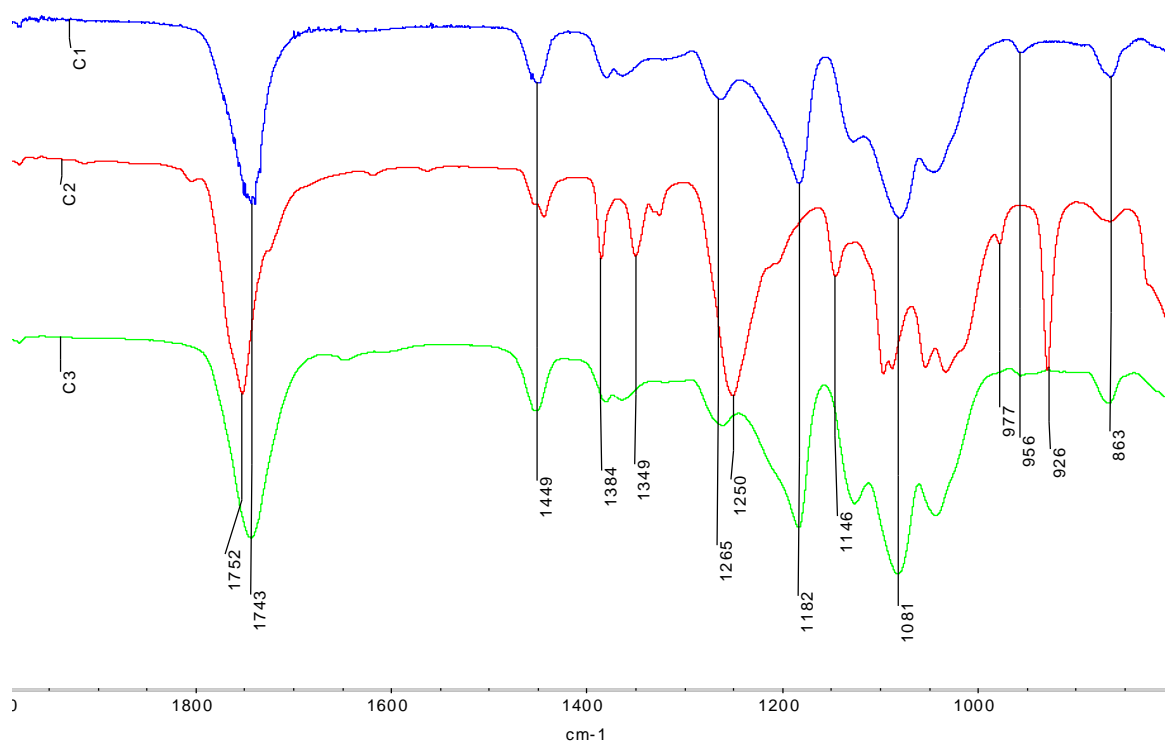


Figure 5.10: FT-IR spectra of polymer; M/Zn = 50, **C1** and **C2** at 72 h, and at 96 h for **C3**.

The spectrum of the polymer produced by **C2** shows bands at (cm^{-1}) 1752 (amorphous or α , (C=O)), 1249 (C-O), 1146 (amorphous, $\nu_{\text{as}}(\text{C-O-C}) + \nu_{\text{as}}(\text{CH}_3)$), 1087 and 1097 (α' and α , $\nu_{\text{s}}(\text{C-O-C})$), and 1053, 1033 (amorphous or α , $\nu(\text{C-CH}_3)$). The peak at 1249 cm^{-1} in the polymer produced using **C2** is very strong compared to that of the polymers from the other two catalysts. The presence of the peak at 926 cm^{-1} is characteristic of the α -crystalline phase coupling of the C-C backbone stretching with the CH_3 rocking only.⁴⁵ Due to this peak it can be concluded that polymers produced by **C2** is in the α -crystalline phase with a small amount in the amorphous phase indicated by the weak peak at 866 cm^{-1} .

FT-IR (ATR) spectra, Fig. 5.11, of polymers produced at M/Zn =50 for **C5**, **C6** and **C18** after 72 h showed characteristics of an amorphous polymer. Similarly **C19** also produces amorphous polymers after 68 h.

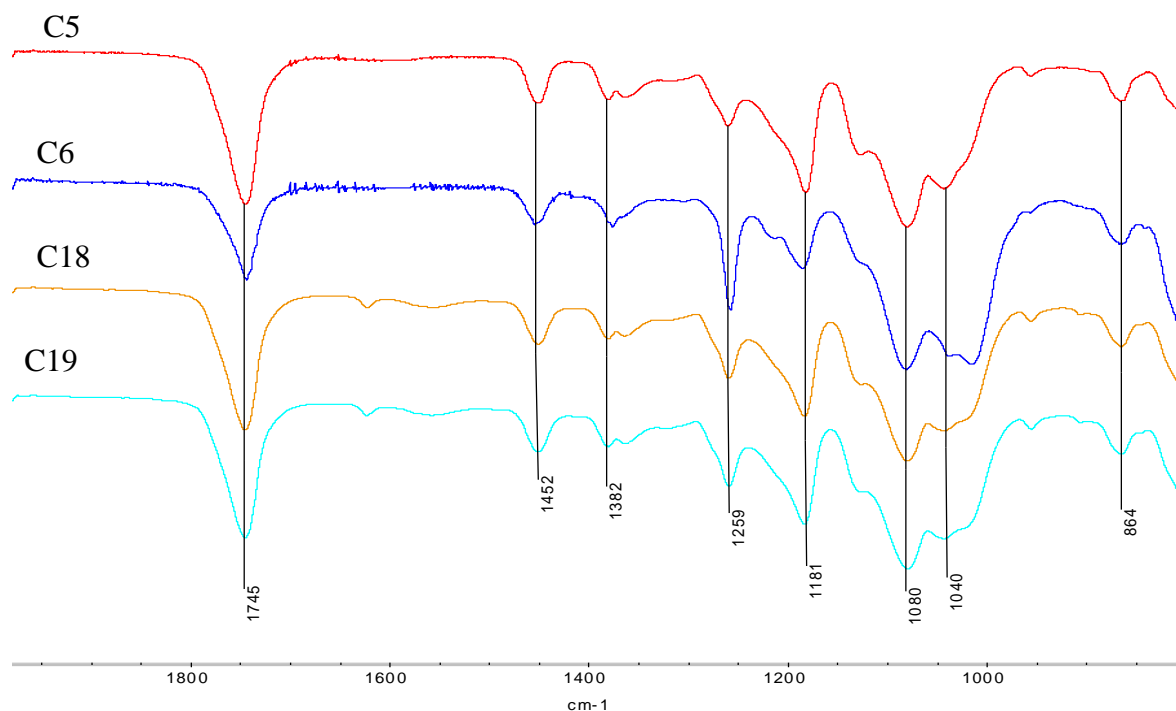
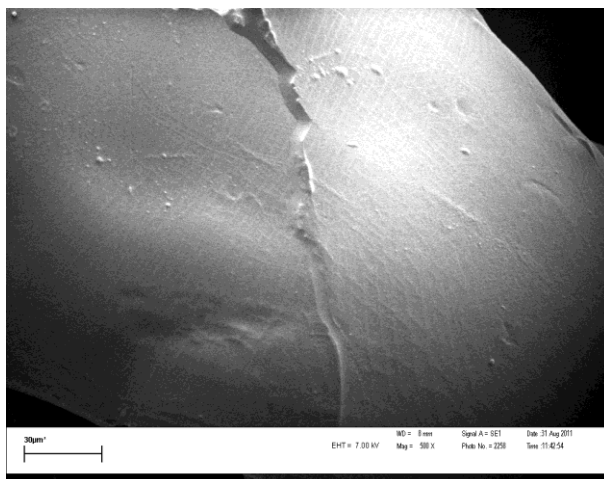


Figure 5.11: FT-IR spectra of polymer of **C5**, **C6** and **C18** at M/Zn = 50 after 72 h, **C19**, M/Zn = 50 after 68 h

Scanning electron microscopy (SEM) (visual morphology)

SEM was used to investigate the surface patterns of the polymer. The polymers produced displayed different morphological patterns, Figure 5.12 – 5.14. Wu *et al.*⁴⁷ proposed that polymers of D, L-lactide could form self organized double strand helix when mixed at a 1:1 ratio. Note, that labeling of the SEM images, **C1-25-20** represents; Complex used-M/Zn ratio- total time of reaction

C1-25-20



C1-50-72

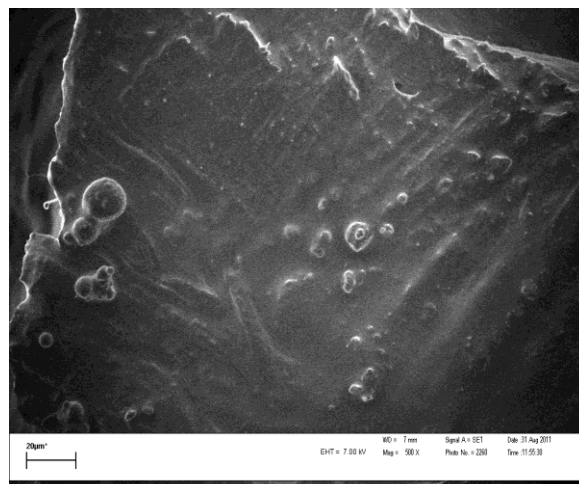
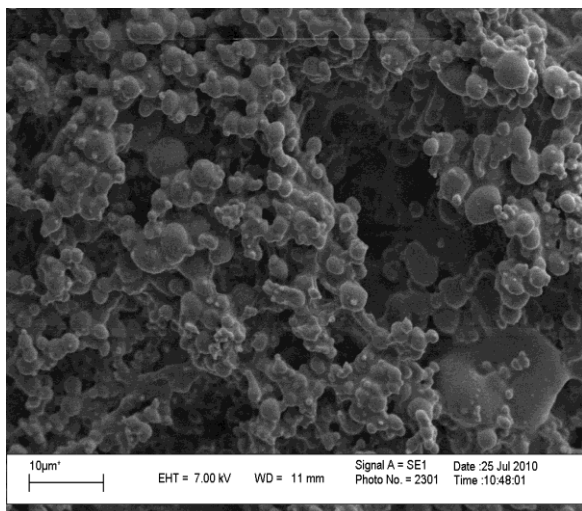


Figure 5.12: SEM images of PDL-LA obtained using C1.

C5-50-72



C6-50-72

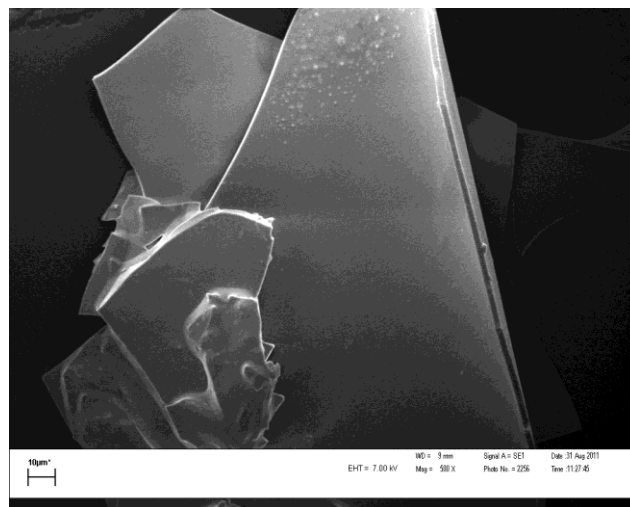


Figure 5.13: SEM images of various PDL-LA obtained using C5 and C6 at M/Zn = 50, 72 h.

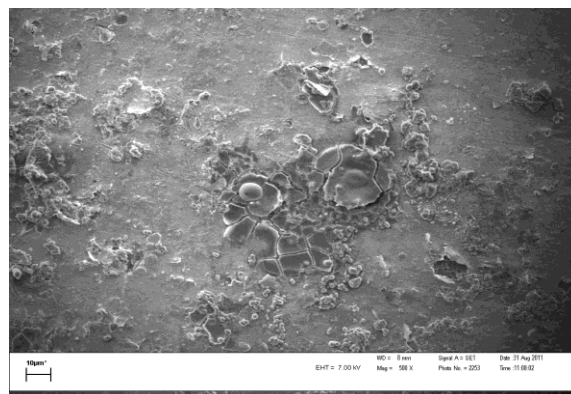
C18-25-20**C19-25-20**

Figure 5.14: SEM images of various PDL-LA obtained using **C18** and **C19** at $M/Zn = 25$, 20 h.

Most of the polymers obtained displayed smooth surfaces. In a few exceptions e.g. **C5** and **C19** gave the polymers that had bead like structures on the surface.

5.2.3.3: Thermal properties of polymers produced

Thermal gravimetric analysis (TGA) for C4 – C6

Only polymers produced using catalyst **C18** and **C19** were characterized by TGA. The thermogram obtained for the polymers produced using **C18** at $M/Zn = 50$ after 96 h is shown as an example, Figure 5.15. The 1st stage of thermal decomposition begins at around 200 °C and progresses gradually till 280 °C where *ca* 20 % of the initial mass is lost. The next stage of decomposition occurs between 300 – 380 °C and progresses much faster with complete loss of the remaining 80 % of the mass. There is complete decomposition at 380 °C. Polylactide from our Zn(II) catalyst were more thermally stable compared to those produced using Mn(II) and Fe(II) salen catalysts. Idage *et al.* reported that the PLLA prepared using Mn and Fe completely decomposed at 260 °C.⁴⁹

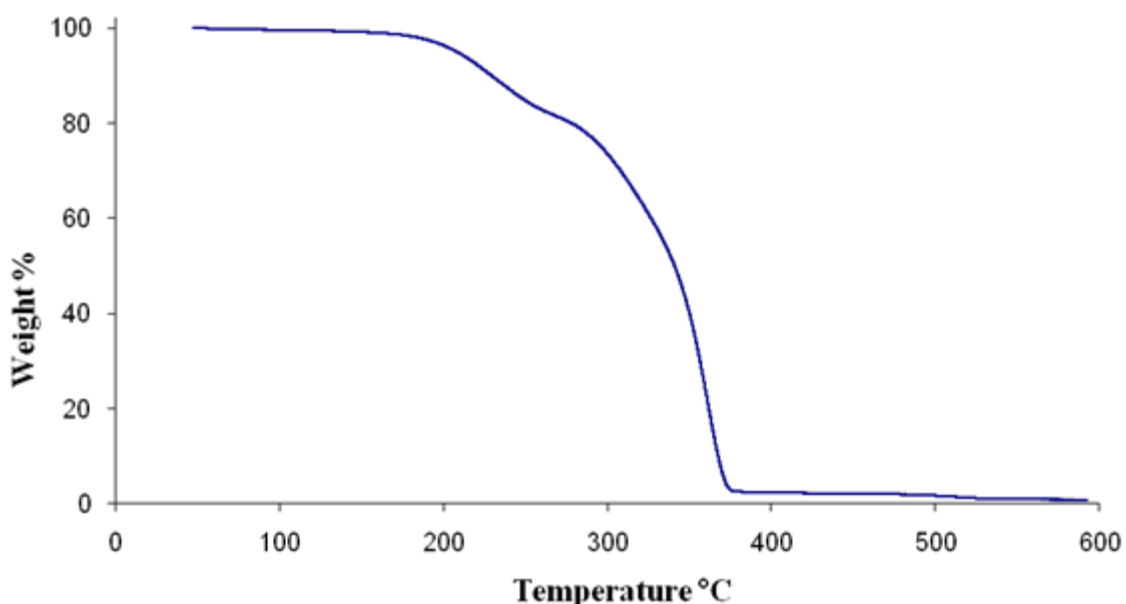


Figure 5.15: Thermogram for polymer obtained from **C18**, M/Zn = 50, 96 h

Differential scanning calorimetry (DSC)

The DSC analysis for polymers produced using **C18** and **C19** were done over the temperature range of 0 to 180 °C. This temperatures range was selected after recording the TGA analysis. PLLA with 100 % L content and a PDLLA with complete racemic and random sequence normally have glass transition temperatures (T_g) around 62 and 45 °C respectively. These polymers obtained from **C18** and **C19** showed the presence of T_g 's at 54 and 56 °C respectively. These values are characteristic of isotactic polylactide and are similar to those we reported for Cu(II) complexes with similar ligands systems.²⁷ Urayama *et al.*⁴⁹ also published similar values for isotactic polymers. It has been reported that as the isotacticity increase (moving from a purely PLLA to PDLLA), the T_g temperature increases.

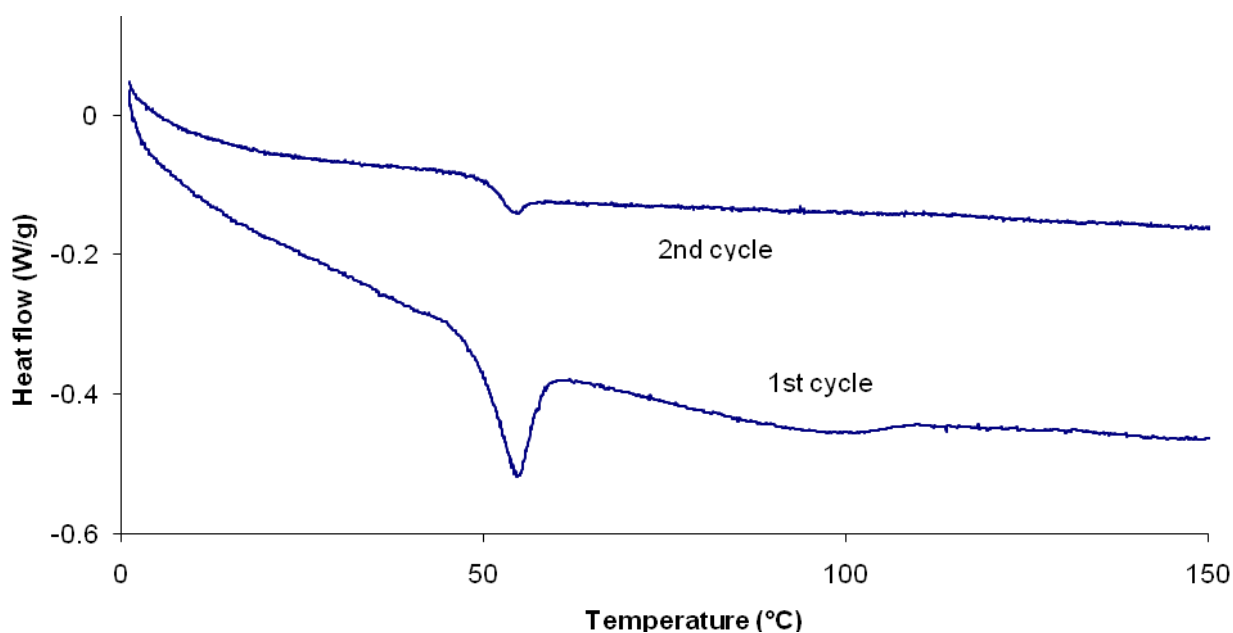


Figure 5.16: DSC plot for **C18**, M/Zn = 50, 96 h; 1st cycle of heating, 2nd cycle of heating after cooling

5.3: Conclusions

The mononuclear (**C1-C3**, **C18**, **C19**) and the multinuclear (**C4 - C9**) Zn(II) complex were investigated as catalysts for the polymerization of D, L-lactide. The reactions were monitored using ¹H-NMR to establish the % conversion for the polymerization reaction. Other techniques such as GPC and ¹³C-NMR were employed to establish the M_n and stereochemistry of the polymers. FT-IR was also employed to probe the crystallinity of the polymers.

Catalyst **C1** was the most active of the systems evaluated in solution with up to 96 % conversion after 72 h. In the mononuclear catalytic systems, bulky substituents on the phenoxy moiety lead to a decrease in activity. These systems showed a linear relationship between molecular weight and monomer conversion at different M/Zn ratios indicating the living nature of the polymerization.

Under the melt polymerization conditions, the G2 metallodendrimers were observed to be the more active than the G1 analogues. However the M_n of the polymers were much lower compared to that of the products obtained in solution.

These catalysts did not show any selectivity for either the D or the L-lactide thus yielding amorphous polylactide.

5.4: Experimental

5.4.1: Materials and instrumentation

All solvents used were of analytical grade and were dried and distilled prior to use. Toluene was dried over and distilled from sodium/benzophenone, methanol from magnesium turnings/iodine and dichloromethane over phosphorous pentoxide. Dioxane was distilled and collected at its boiling point and stored over 4 Å molecular sieves. D, L-lactide was obtained as a research gift from Purac Biochem Netherlands, and was used without further purification.

The NMR spectra were recorded on a Varian 300 VNMRS spectrometer (^1H at 300 MHz ^{13}C at 75.4 MHz unless otherwise stated) at room temperature using tetramethylsilane as an internal standard. The chemical shifts are reported in δ (ppm) and referenced to the signal for the residual proton in CDCl_3 , or CD_2Cl_2 , the NMR solvent. $^{13}\text{C}\{^1\text{H}\}$ NMR chemical shifts are given in δ ppm and referenced to the residual ^{13}C in solvents. Infrared spectra were recorded on a Nicolet Avatar 330 FT-IR spectrophotometer using an ATR accessory and employing a resolution of 1 cm^{-1} . The spectrophotometer was equipped with an attenuated-total-reflection (ATR) accessory with a selenium crystal.

Gel permeated chromatography (GPC)

The determination of molecular weights and molecular weight distributions was carried out on a Polymer Standards Systems (PSS) GPC apparatus equipped with a refractive index detector. Calibration was done using polystyrene standards. The instrument comprised a Waters 1515 isocratic pump, a Waters inline degasser AF, a Waters 717 plus auto sampler with a 100 μL sample loop, a Waters 2487 dual wavelength absorbance UV detector, a Waters 2414 refractive index detector at 30 $^{\circ}\text{C}$. GPC measurements were performed on a set of two PLgel columns (Polymer Laboratories) 5 μm Mixed-C (300 x 7.5 mm^2) connected in series along with a PLgel guard column (50 x 7.5 mm^2). THF (stabilized by 0.125% BHT) was used as mobile phase at a flow-rate of 1.00 mL/min. Sample concentrations were 1.0–5.0 g/L and injection volumes were 100 μL . The columns were calibrated with PS standards from Polymer Laboratories (Church Stretton, Shropshire, UK). Data processing was performed by Breeze version 3.30 SPA (Waters) software.

Scanning electron microscopy (SEM)

Imaging of the samples was accomplished using a Leo® 1430VP Scanning Electron Microscope at the Stellenbosch University. Prior to imaging the samples were mounted on a stub with double sided carbon tape. The sample was then coated with a thin layer of gold for 90s in a 20 mV argon atmosphere on S150A sputter coater. This was done in order to make the sample surface electrically conducting. Beam conditions during surface analysis were 7 KV and approximately 1.5 nA, with a working distance of 9 mm and a spot size of 150.

5.4.2.1: General polymerization procedure of D, L-lactide in solution

In a typical polymerization, D, L-lactide (0.72 g, 5 mmol) was dissolved in the appropriate solvent (5 ml) in a Schlenk tube and the required amount of initiator was added.

The solution was degassed, stirred or heated for the appropriate amount of time. In the case where CH_2Cl_2 was used the solution was stirred at 25 °C under nitrogen. For the higher temperature reactions, the solution/mixture was heated under vacuum in either toluene or dioxane at 70 °C or 100 °C respectively. After the reaction time, each sample had all volatiles removed and a $^1\text{H-NMR}$ spectrum of the crude material obtained in CDCl_3 . The integration values of the methine proton of the monomer and that of polymer were used to calculate the percentage conversion using Equation 1.

5.4 2.2: General polymerization reaction procedure under the melt condition

In a typical polymerization experiment D, L-lactide (0.72 g, 5 mmol) and appropriate metallodendrimer were charged into a 25 mL round bottomed flask. The flask was evacuated and placed in an oil bath at appropriate temperature for the appropriate time. Under these conditions, the reaction mixture turned into a melt in which the polymerization occurred. The molten mixture was cooled by immersing the round bottomed flask in an ice bath to stop the polymerization. Conversion was determined by $^1\text{H-NMR}$ spectroscopy of the crude reaction mixture in CDCl_3 using Equation 1.

5.5: References

1. H.-Y. Chen, B.-H. Huang, C.-C. Lin, *Macromolecules*, **38** (2005) 5400.
2. K. M. Stridsberg, M. Ryner, A.-C. Albertsson, *Advances in Polym. Sci.*, **157** (2002) 41.
3. R. P. Lanza, R. Langer, J. Vacanti, *Principles of Tissue Engineering*. Academic Press, San Diego, CA (2000).
4. Y. Ikada and H. Tsuji, *Macromol. Rapid Commun.*, **21** (2000) 117.
5. O. Dechy-Cabaret, B. Martin-Vaca, D. Bourissou, *Chem. Rev.*, **104** (2004) 6147.
6. H. J. Sanders, *Chem. Eng. News*, **63** (1985) 30.

7. Y. M. Bero, P. Dobrzyński, J. Kasperczyk, *Rapid Commun.*, (1999) 4038.
8. K. E. Uhrich, S.M. Cannizzaro, R. S. Langer and K. M. Shakesheff, *Chem. Rev.*, **99**, (1999) 3181.
9. J. Börner, U. Flörke, A. Döring, M. D. Jones, S. Herres-Pawlis, *Sustainability*, **1** (2009) 1226.
10. A. J. Nijenhuis, D. W. Grijpma, A. J. Pennings, *Macromolecules*, **25** (1997) 6419.
11. R. E. Drumright, P. R. Gruber and D. E. Henton, *Adv. Mater.*, **12** (2000) 1841.
12. C. Zhang, Z.-X. Wang, *J. Organomet. Chem.*, **693** (2008) 3151.
13. J. Wu, T.-L. Yu, C.-T. Chen, C.-C. Lin, *Coord. Chem. Rev.*, **250** (2006) 602.
14. T.M. Ovitt, G.W. Coates, *J. Am. Chem. Soc.*, **124** (2002) 1316.
15. S. Dutta, W.-C. Hung, B.-H. Huang, C.-C. Lin, *Adv. Polym. Sci.*, DOI: 10.1007/12_2011_156.
16. Y. Sarazin, R. H. Howard, D. L. Hughes, S. M. Humphrey, M. Bochmann, *Dalton Trans.*, (2006) 340.
17. J.-C. Wu, B.-H. Huang, M.-L. Hsueh, S.-L. Lai, C.-C. Lin, *Polymer*, **46** (2005) 9784.
18. A. John, V. Katiyar, K. Pang, M. M. Shaikh, H. Nanavati, P. Ghosh, *Polyhedron*, **26** (2007) 4033.
19. J. Wu, T.-L. Yu, C.-T. Chen, C.-C. Lin, *Coord. Chem. Rev.*, **250** (2006) 602.
20. G. Montaudo, M. S. Montaudo, C. Puglisi, F. Samperi, N. Spassky, A. LeBorgne, M. Wisniewski, *Macromolecules*, **29** (1996) 6461.
21. H. Du, A. H. Velders, P. J. Dijkstra, J. Sun, Z. Zhong, X. Chen, J. Feijen, *Chem. Eur. J.*, **15** (2009) 9836.
22. P. Hornum, E. L. Marshall, V. C. Gibson, A. J. P. White, D. J. Williams, *J. Am. Chem. Soc.*, **126** (2004) 965.
23. D. J. Darenbourg, O. Krarroonnirum, *Organometallics*, **29** (2010) 5627.

24. D. Astruc, E. Boisselier, C. Ornelas, *Chem. Rev.*, **110** (2010) 1857.
25. G. J. Van Hummel, S. Harkema, F. E. Kohn, J. Feijen, *Acta Crystallogr.*, **B38** (1982) 1679.
26. F. Chabot, M. Vert, *Polymer*, **24** (1983) 53.
27. S. Bhunora, J. Mugo, A. Bhaw-Luximon, S. Mapolie, J. L. van Wyk, J. Darkwa, E. Nordlander, *Appl. Organometal. Chem.*, **25** (2011) 133.
28. M. A. Torzilli, S. Colquhoun, J. Kim, R. H. Beer, *Polyhedron*, **21** (2002) 705.
29. L. Wang and H. Ma, *Dalton Trans.*, **39** (2010) 7897.
30. A. John, V. Katiyar, K. Pang, M. M. Shaikh, H. Nanavati, P. Ghosh, *Polyhedron*, **26** (2007) 4033.
31. M. D. Jones, M. G. Davidson, C. G. Keir, L. M. Hughes, M. F. Mahon, D. C. Apperley, *Eur. J. Inorg. Chem.*, (2009) 635.
32. M. Pastusiak, P. Dobrzynski, B. Kaczmarczyk, J. Kasperczyk, A. Smola, *Polymer*, **52** (2011) 5255.
33. M. H. Chisholm, *J. Organomet. Chem.*, **693** (2008) 808.
34. Silvestri, F. Grisi, S. Milione, *J. Polym. Sci., Part A: Polym. Chem.*, **48** (2011) 3632.
35. M. Bero, J. Kasperczyk, Z. Jedlinski, *Die Makromolekulare Chemie*, **191** (1990) 2287.
36. H. Ma, J. Okuda, *Macromolecules*, **39** (2006) 128.
37. H. Sun, J. S. Ritch, P. G. Hayes, *Inorg. Chem.*, **50** (2011) 8063.
38. Y. K. Kang, J. H. Jeong, N. Y. Lee, Y. T. Lee, H. Lee, *Polyhedron*, **29** (2010) 2404.
39. T. R. Jensen, C. P. Schaller, M. A. Hillmyer, W. B. Tolman, *J. Organomet. Chem.*, **690** (2005) 5881.
40. M. H. Chisholm, Z. Zhou, *J. Mater. Chem.*, **14** (2004) 3081.
41. J. Baran, A. Duda, A. Kowalski, R. Szymanski, S. Penczek, *Macromol. Rapid Commun.*, **18** (1997) 325.

42. N. Spassky, V. Simic, M. Montaudo, G. Hubert-Pfalzgraf, *Macromol. Chem. Phys.*, **201** (2000) 2432.
43. M. H. Chisholm, J. C. Gallucci, K. T. Quisenberry, Z. Zhou, *Inorg. Chem.*, **47** (2008) 2613.
44. J. Coudane, C. Ustariz-Peyret, G. Schwach, M. Vert, *J. Polym. Sci. A: Polym. Chem.*, **35** (1997) 1651.
45. C. Ribeiro, V. Sencadas, C. M. Costa, J. L. G. Ribelles, S. Lanceros-Méndez, *Sci. Technol. Adv. Mater.*, **12** (2011) 015001 and references herein
46. B. B. Idage, S. B. Idage, A. S. Kasegankar, R. V. Jadhav, *Mater. Sci. Eng. B*, **168** (2010) 193.
47. S. Kang, S. L. Hsu, H. D. Stidham, P. B. Smith, M. A. Leugers, X. Yang. *Macromolecules*, **34** (2001) 4542.
48. J. Wu, B. Huang, M. Hsueh, S. Lai, C. Lin, *Polymer*, **46** (2005) 9784.
49. H. Urayama, S.-I. Moon, Y. Kimura, *Macromol. Mater. Eng.*, **288** (2003) 137.

**Chapter 6 : Preliminary Evaluation of Pd(II)
Complexes as Pre-catalysts for α -Olefin
Transformation**

6.1: Introduction

Development of new non-metallocene homogeneous catalysts for the oligomerization and polymerization of olefins with improved activity and selectivity is a major research area in the field of organometallic chemistry.¹

Linear alpha olefins (1-C₄ to 1-C₂₀) are useful intermediates in many processes amongst which are the manufacture of co-polymers, detergents, synthetic lubricants, plasticizers and long chain alcohols.² There has been considerable effort in the development of late transition metal catalysts for the oligomerization and polymerization of these low carbon number olefins in both academia and industry.³ However the higher olefins (C₆ and above) have not received as much attention as lower molecular weight monomers such as ethylene and propylene.⁴ These higher α -olefins can also undergo other transformations such as hydrogenation, cyclization and isomerisation.^{5,6}

In the last three decades, there has been a tremendous amount of academic and industrial research focused on the development of well-defined, highly active homogeneous catalysts for the oligomerization and polymerization of olefins unlike the multi-sited heterogeneous Ziegler–Natta catalysts.⁷⁻⁹ Some homogeneous catalytic systems have also been commercialized e. g. the SHOP process by Shell.

An efficient catalytic system for olefin polymerization/oligomerization should have the following properties.¹⁰

- I. High olefin-insertion ability
- II. Availability of two cis-located sites
- III. High stability under the reaction conditions employed

These properties are greatly induced by the ligand system and the nature of the co-catalyst.¹¹ Oligomerization and polymerization of olefins are typically carried out using

transition metal catalysts. Late transition metals have been shown to be more tolerant of polar-functionalized α -olefins compared to the early transition metals because they are less oxophilic in nature. Nevertheless, late transition metals catalysts are less active in the polymerization of simple olefins.

However after Brookhart and co-workers reported Ni(II) and Pd(II) diimine based complexes as efficient ethylene catalysts, there has been considerable effort in developing nitrogen based donor ligands.¹² These researchers observed that the use of sterically hindered ligands improved catalyst activity by limiting chain termination processes. Grubbs *et al.*¹³ later reported a series of salicylaldiminato nickel catalysts with bulky imino substituents that exhibited moderate activity in ethylene polymerization.

The interest in the metal complexes containing pyrrolide ligands (which is also a nitrogen donor ligand) has been renewed since the discovery of chromium pyrrolyl compounds that efficiently catalysed the trimerization of ethylene.¹⁴

In this chapter we discuss the application of the palladium complexes (**C10** – **C17**) covered in Chapter 4 in the transformation of α -olefin. Our main objective in this study was to apply these complexes as catalysts in the oligomerization of ethylene and other α -olefins. The activity of some of the mononuclear complexes, Figure 6.1 was also compared to that of the multinuclear complexes (metallodendrimers), Figure 6.2 and 6.3. We also compare N,N versus N,O chelate ligands in this catalytic process.

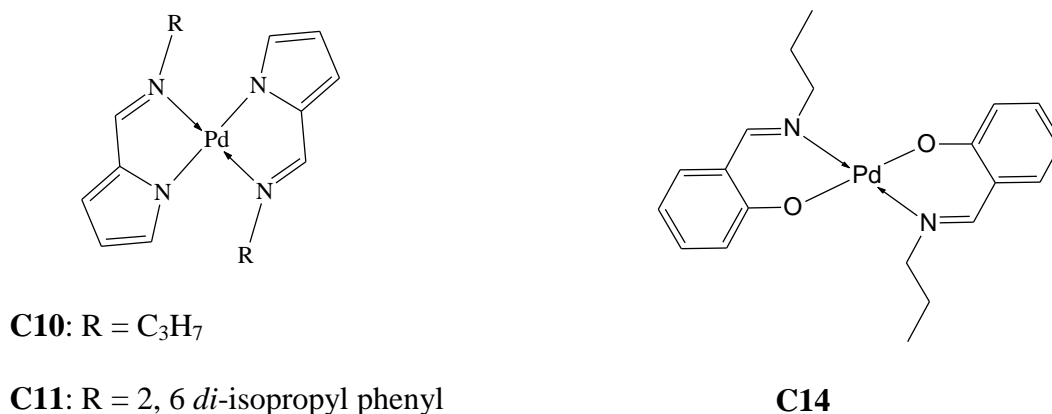


Figure 6.1: Structure of mononuclear pyrrolylaldiminato Pd(II) complexes, **C10** and **C11**

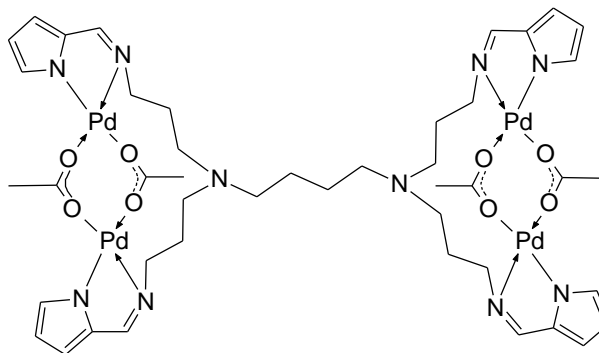


Figure 6.2: 1st generation (G1) dendritic pyrrolylaldiminato Pd(II) complex, **C12**

6.2: Results and discussion

6.2.1: Ethylene oligomerization

The ethylene oligomerization reactions were carried out in a 300 mL stainless steel autoclave. Various reaction conditions namely, temperature, Al:Pd ratio and ethylene pressure were investigated to establish the optimal conditions. The metal concentration was kept constant irrespective of the pre-catalyst employed.

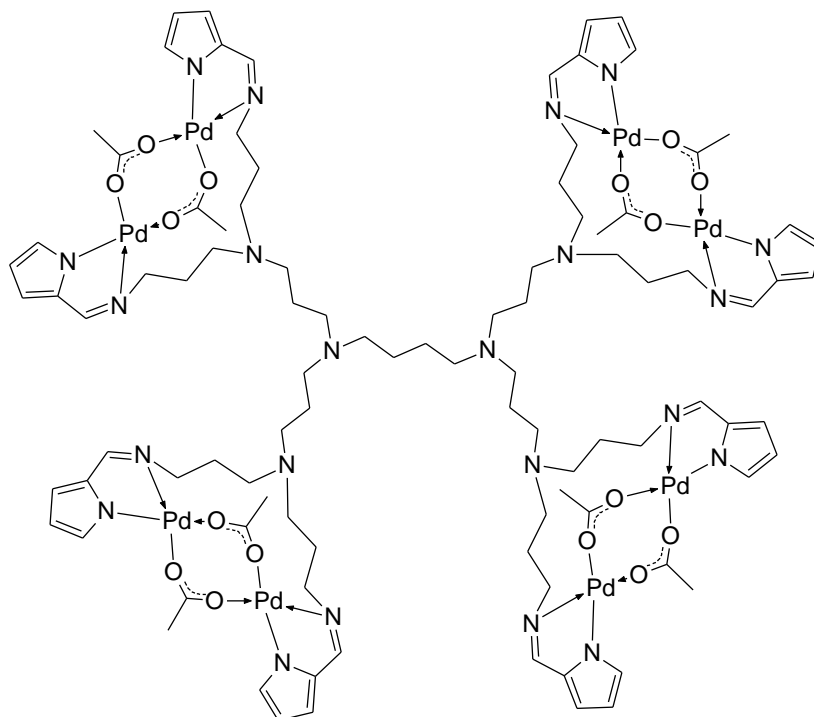


Figure 6.3: 2nd generation (G1) dendritic pyrrolylaldiminato Pd(II) complex, **C13**

6.2.1.1: Evaluation of mononuclear pyrrolylaldiminato Pd(II) complexes under various reaction conditions, complex C11

Preliminary investigations were done using the pyrrolylaldiminato complex **C11** in the presence of EtAlCl₂ to establish the optimal reaction conditions to employ, Table 6.1. It was established that the amount of co-catalyst played a very important role. At Al:Pd ratios below 1000:1, **C11** was not active even at an ethylene pressure of 20 bar.

When the amount of co-catalyst was increased, (Al:Pd = 2000:1) oligomers were obtained even at a much lower pressure of ethylene. At an ethylene pressure of 10 bar, a TOF value of 60 kg product (mmol Pd)⁻¹ h⁻¹ was obtained while at 20 bar, the TOF was 920 kg product (mmol Pd)⁻¹ h⁻¹. The higher activity for this pre-catalyst at an ethylene pressure of 20 can be attributed to higher monomer concentration in the reaction mixture. Increase in activity with increased ethylene pressure has been widely reported in literature for various metal complexes.^{15, 16}

Other pyrrolylaldiminato transition metal complexes have been reported to oligomerize or polymerize ethylene in the presence of co-catalysts such as MAO or Et₂AlCl. However, our complexes were inactive when MAO or Et₂AlCl were employed as co-catalysts.

Table 6.1: Ethylene oligomerization data **C11**^a

Al:Pd	P (bar)	TOF ^b	Oligomers (%)	Alkylation products (%)	Alkylation products selectivity (%) ^c	
					C ₁₁	C ₁₃
1000:1	10	-				
1000:1	20	680	52.6	47.4	70.2	29.8
2000:1	5	-				
2000:1	10	60				
2000:1	20	920	43.8	56.2	65.6	34.4

^aReaction conditions: 5 μmol Pd, 50 mL toluene time 1 h, temperature 25 °C ^bTurn Over Frequency (TOF) Kg product (mmol Pd)⁻¹ h⁻¹, ^cExpressed as a % of the total product mixture, ^d% of alkylation products relative to each other

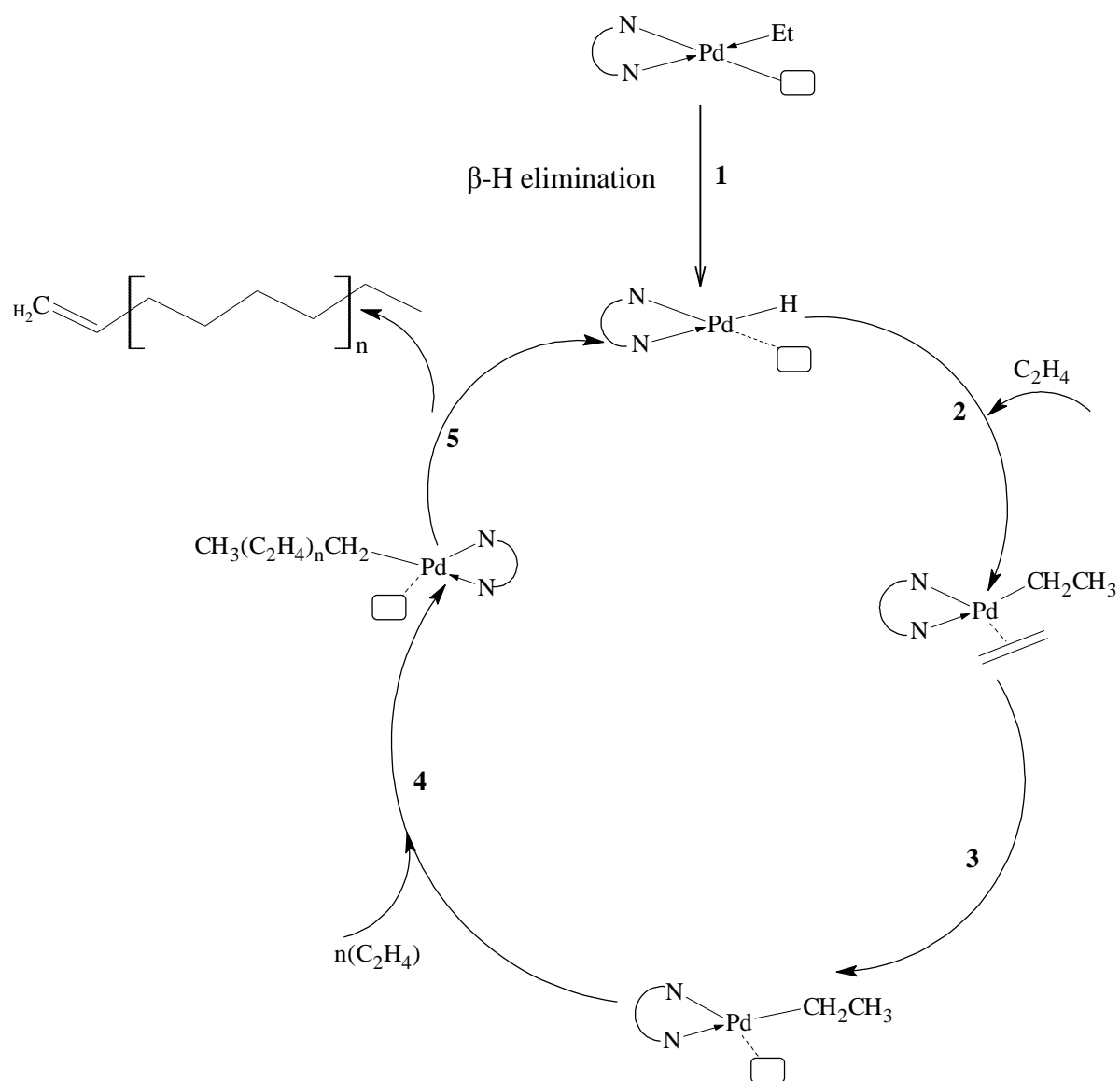
Mu *et al.*¹⁷ recently reported a V(III) pyrrole-imine complex bearing the same ligand on which complex **C11** is based and which polymerized ethylene with an activity of 12.6 kg PE (mmol V)⁻¹ h⁻¹. In this case the vanadium complex was activated with Et₂AlCl while using Cl₃C₂O₂Et as a promoter. These reactions were however done at a higher temperature of 50 °C.

An *in-situ* generated Cr(III) complex based on the same ligand as **C11** also exhibited very low activity in the polymerization of ethylene. For this Cr catalyst system, He *et al.*¹⁸ reported an activity of 0.08 kg PE (mmol Cr)⁻¹ h⁻¹ while using MMAO as co-catalyst, Al:Cr = 2000:1, at 25 °C in 50 mL toluene with an ethylene pressure of 1 atm.

A proposed catalytic cycle for the ethylene oligomerization is shown in Scheme 6.1. The first step involves the alkylation of the Pd pre-catalyst with EtAlCl_2 followed by β -hydride elimination to form a Pd-H species thought to be the active species, step 1. Ethylene then coordinates to the metal center, step 2, followed by insertion of the monomer into the metal hydride bond to produce a Pd-ethyl species, step 3. This subsequently reacts with additional ethylene leading to chain growth, 4. Chain termination occurs via β -hydride elimination of the growing alkyl chain to produce the olefin regenerating the Pd-H active species (step 5).¹⁹

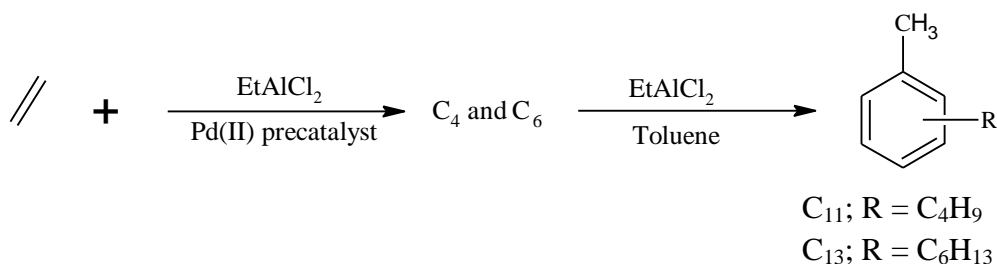
While employing EtAlCl_2 no short chain oligomers were detected when analysing the reaction mixture using gas chromatography (GC). Instead the formation of alkyl toluenes was observed. These alkyl toluenes are formed as a result of Friedel-Crafts alkylation of the solvent, toluene, by the reaction of the α -olefins present in the mixture. The Friedel-Crafts alkylation is mediated by the co-catalyst, EtAlCl_2 . Such Friedel-Craft alkylations of toluene during ethylene oligomerization have recently been reported by Darkwa *et al.*²⁰ It should be noted that no toluene alkylation occurs when Et_2AlCl and MAO were employed as co-catalyst. This is presumably due to the fact that these two organo-aluminium species are not Lewis acidic enough to interact with the alkenes to form the carbonium ion which is a crucial intermediate in the Friedel-Crafts alkylation process.

In the case where **C11** was employed as pre-catalyst, a range of alkyl toluenes were detected. The proportion of the alkyl toluene products consisted largely of butyl-toluenes (C_{11}) and hexyl-toluenes (C_{13}) with the butyl-toluenes being the major fraction, Table 6.1.



Scheme 6.1: Proposed mechanism for the oligomerization of ethylene

These observations are consistent with a two-stage process whereby, ethylene is oligomerized generating C_4 and C_6 alkenes, Scheme 6.1. The Friedel-Crafts alkylation of toluene by the generated alkenes then occurs, Scheme 6.2. In addition to the alkyl-toluenes, it was also found that on removal of solvent from the reaction mixture an oily residue was in fact long chain oligomers of ethylene.



Scheme 6.2: Two-stage process for ethylene oligomerization and subsequent alkylation of toluene

Dyer *et al.*²¹ also reported a similar observation where C₄, C₆, C₈, and C₁₀ alkyl-substituted toluenes were obtained while using a Ni(II) complex with a guanidine P, N ligand. In this case, much milder conditions were employed, Al:Ni = 14:1, 1 bar ethylene pressure and reaction time of only 20 min. However, when they changed the solvent to CH₂Cl₂ or chlorobenzene only traces quantities of butenes and hexenes were detected by GC.

In an attempt to eliminate the possibility of the low molecular weight oligomers interacting with the solvent, subsequent reactions were conducted in a non-aromatic solvent such as hexane. This is discussed in the following section.

6.2.1.2: Effect of reaction conditions on **C10** – **C13** as catalyst precursors for ethylene oligomerization

The four pyrrolylaldiminato complexes were then evaluated as ethylene oligomerization catalysts in hexane as solvent using the reaction conditions established for the toluene system. Using **C11** the pre-catalyst was tested at ethylene pressure 20 bar, temp 25 °C, Pd:Al ratio of 1000:1 for 1 hour, an activity of up to 116 kg product (mmol Pd)⁻¹ h⁻¹ was obtained. This TOF value was much lower than that observed using toluene as solvent. The lower activity in hexane could possibly be due to the low solubility of the **C11** in hexane.

Under similar conditions as those employed for **C11** the other pyrrolylaldiminato complexes **C10**, **C12** and **C13**, were observed to be inactive in hexane. We therefore set out

to find alternative reaction conditions for the afore-mentioned pre-catalysts using **C10** by varying the amounts of co-catalyst and changing the reaction temperature. The results are summarized in Table 6.2. The ethylene pressure was maintained at 20 bar and the temperature at 25 °C while the amount of co-catalyst was increased up to a Al:Pd ratio 2000:1. Some catalytic activity was observed but only after the reaction had proceeded for 3 hours.

Table 6.2: Ethylene oligomerization catalysed by **C10**, **C11** and **C14**^a

	Al:Pd	Time (h)	Temp (°C)	P (bar)	TON	TOF ^b
C11	1000:1	1	25	20	116	116
C10	500:1	1	25	20		-
	1000:1	1	25	20		-
	2000:1	1	25	20		-
	2000:1	3	25	20	240	80
	2000:1	3	30	20	342	114
	2000:1	5	30	20	470	94
C14	2000:1	1	25	10		-
	2000:1	1	25	20		-
	2000:1	1	30	20	197	197

^aConditions: 50 mL n-hexane, 5 μmol Pd, ^b TOF = kg product (mmol Pd)⁻¹ h⁻¹, ^cTurn-over number (TON) = kg product (mmol of Pd)⁻¹

Raising the temperature to 30 °C improved the catalytic activity of **C10** but again up to 3 hours reaction time was required. However prolonged reaction time of up to 5 h resulted in a decrease in catalytic activity. For a reaction time of 5 h an activity of 94 kg product

$(\text{mmol Pd})^{-1} \text{ h}^{-1}$ was obtained at Al:Pd ratio of 2000:1 compared to 114 kg product $(\text{mmol Pd})^{-1} \text{ h}^{-1}$ (Al:Pd 2000:1) obtained after 3 hours. This may imply that catalyst deactivation occurs over extended period of time. It could be that the catalyst is not stable in solution over extended times.

Under the conditions employed for **C10**, no activity was observed in the case of **C12** and **C13**. The inactivity may be due to the low solubility of these metallodendrimers in hexane.

6.2.1.3: Effects of changing the ligand system on the oligomerization

Comparison between different donor atom systems was accomplished by changing from the pyrrolylaldimine ligand in **C10** to a salicylaldimine system in **C14**. The salicylaldiminato complex **C14** proved to be a better catalyst. A TOF value of 197 kg product $(\text{mmol Pd})^{-1} \text{ h}^{-1}$ was obtained at 30 °C, 20 bar ethylene pressure and in 1 hour of reaction time. We propose that the oligomerization follows a similar mechanism to that of the pyrrolylaldiminato complexes

6.2.3: Characterization of the oligomers obtained using C10, C11 and C14 pre-catalysts

These three pre-catalysts oligomerized ethylene yielding predominantly long chain oligomers when evaluated in toluene and hexane as solvents. The oils were only slightly soluble in THF and chlorobenzene.

FT-IR spectroscopy

The FT-IR spectrum of these oil showed that the material was a hydrocarbon, Figure 6.4. The spectrum obtained suggested that the oligomers obtained were saturated hydrocarbons. Thus it could be concluded that chain termination occurs through protonolysis

of the metal alkyl on treatment with HCl. Another reason for the saturated hydrocarbon could be due to the presence of chain transfer to aluminium as a termination mechanism as proposed by Khamker *et al.*²²

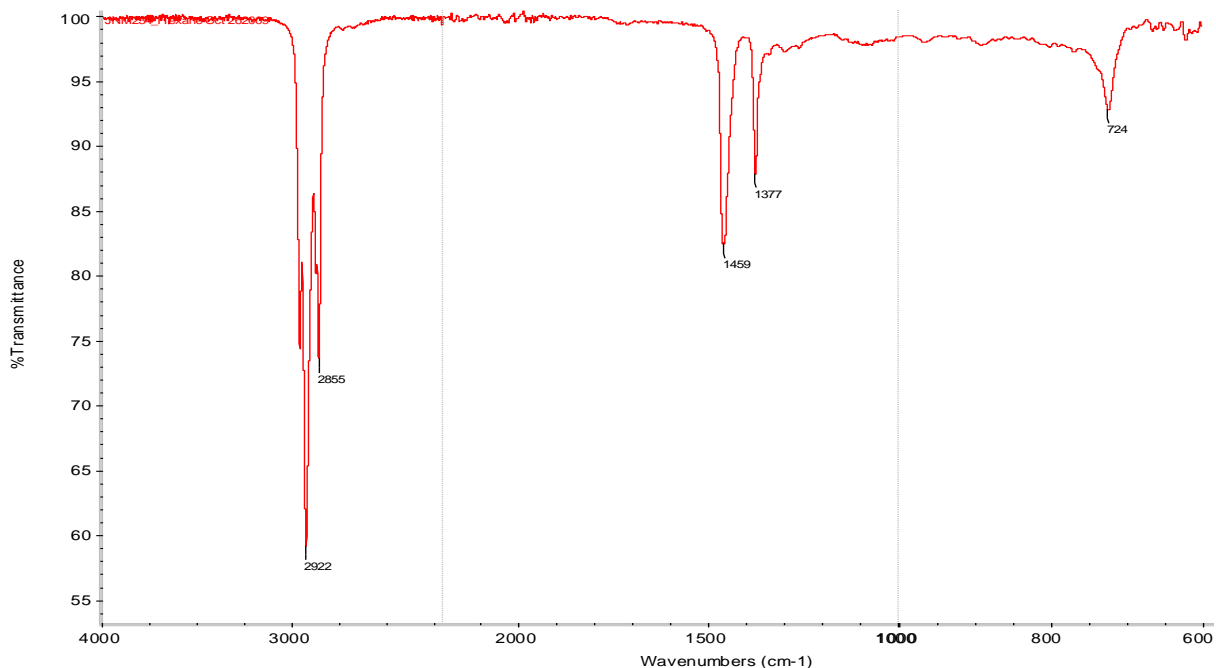


Figure 6.4: FT-IR spectrum of oligomers obtained using **C11** (1000:1, toluene, 25 °C, 20 bar)

Atmospheric pressure chemical ionization mass spectrometry (APCI-MS)

APCI-mass spectra were also obtained for all the oligomers (oil products). The oligomers produced employing **C11** appeared to be the most viscous of the lot and also had the highest molecular weight. The oily products were mainly composed of even carbon numbered oligomers with broad molecular weight distribution. Complex **C11** seems to favour chain propagation with oligomers of up to C₆₄ being obtained (see APCI-mass spectrum, Figure 6.5). The mononuclear pyrrolylaldiminato complex **C11** gave oligomers with higher molecular weight compared to those produced by **C10**, (Figure 6.6). **C11** is more sterically hindered than **C10**. In **C11**, the moiety on the imino nitrogen is 2,6-diisopropyl phenyl while in **C10** it is a *n*-propyl group. Other researchers have made similar observations

whereby an increase in the steric bulk of the ligand leads to an increase in the catalytic activity and hence higher molecular weight polymers.¹³

6.2.1.2: Attempted oligomerization of 1-hexene

In an attempt to oligomerize 1-hexene using **C10** - **C14** as pre-catalysts in the presence of EtAlCl₂ as co-catalyst in toluene as solvent, interesting observations were made. Only odd carbon numbered compounds arising from Friedel-Crafts (F-C) alkylation of toluene were detected using gas chromatography with no dimers or trimers of 1-hexene being observed. These (F-C) products were the *mono*-alkylated toluene (C₁₃) and *di*-alkylated toluene (C₁₉) arising from the reaction of the toluene and 1-hexene.

Alkylation of toluene in the presence of 1-hexene was subsequently established to also occur readily using EtAlCl₂ in the absence of a transition metal complex. At this stage it is presumed that the palladium complex plays no role in the alkylation of toluene but may be mediating in the isomerization of 1-hexene to internal olefins.

GC-MS analysis of the reaction mixture obtained using **C10** and **C14** revealed the formation of two products whose molecular ions were observed at $m/z = 176$ and 260 , Figure 6.7. These ions correspond to the *mono*- and *di*-alkylated toluene product C₆H₁₃-toluene and (C₆H₁₃)₂-toluene respectively. The GC and GC-MS showed the presence of regio-selectivity for the alkylated products, five peaks were observed for the C₁₃ cluster with retention times of 10.97, 11.15, 11.20, 11.36 and 11.56 min. These could be due to alkylation of toluene by the 1-hexene in the *ortho*, *meta*, or *para* positions. The additional peaks could be due to the alkylation of toluene by the internal hexene isomers in either the *ortho*, *meta* or *para* positions.

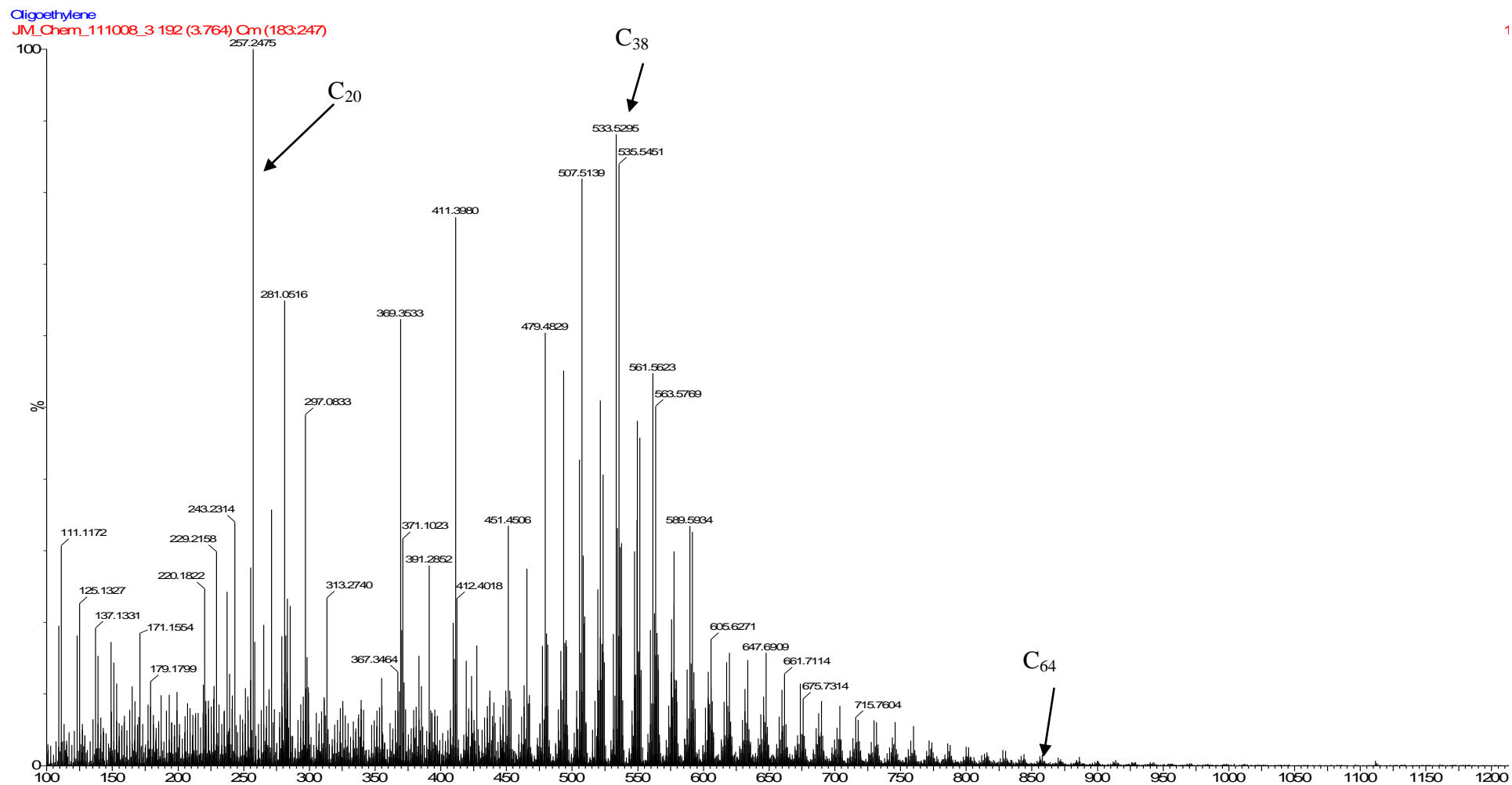


Figure 6.5: APCI-mass spectrum obtained for C11 Al:Pd (2000:1), 1 h, 25 °C in toluene.

JNVL_343

JNM_CHEM_111020_3_73 (1.458) Cm (71:74)

1: TOF MS ASAP+
1.48e4

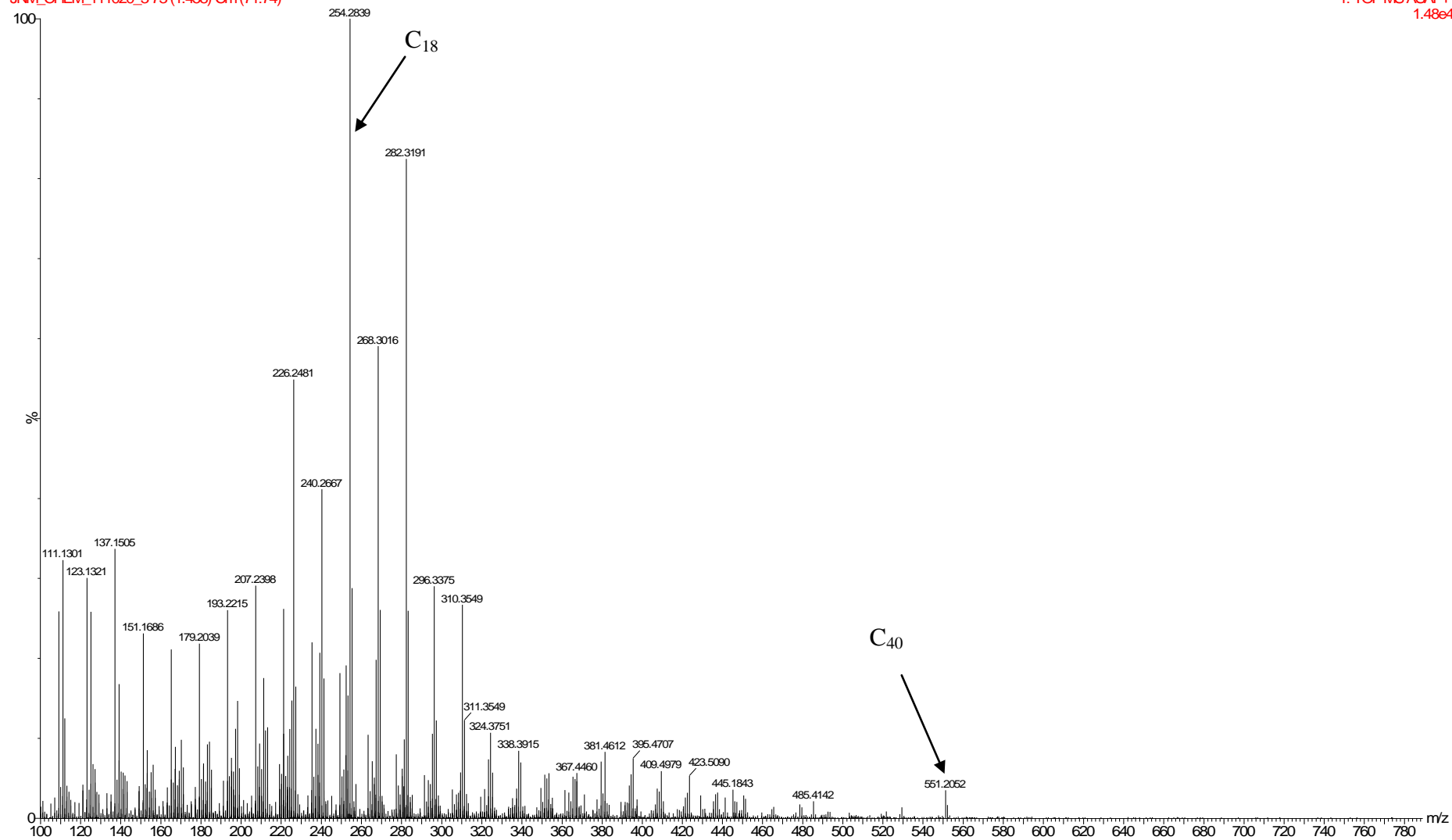


Figure 6.6: APCI-mass spectrum obtained for C₁₀ (Al:Pd 2000:1 , 3 h, 30 °C in Hexane).

The peaks with retention time of 10.97, 11.15 and 11.20 min are thought to be those of the linear alkylation products. These three regioisomers show an identical fragmentation pattern where the hexyl substituent is lost sequentially, Figure 6.8. The fragmentation pattern inferred from GC - mass spectrum followed a pattern typical of linear alkanes. An ethyl group was lost first giving rise to a fragment at m/z 147 followed by the loss of 4 methylene groups as individual fragments yielding an ion at m/z 91 that corresponds to a toluene fragment.

The other chromatographical peaks with retention time of 11.36 and 11.50 min were assigned to the products formed after the alkylation of the toluene with the internal hexene. This interaction yielded branched alkylation products. The GC - mass spectra of the two isomers showed a slightly different fragmentation pattern to that of the linear analogues. There was an initial loss of a *n*-butyl fragment resulting in an ion peak at m/z 119 followed by two methylene ions giving rise to an ion at m/z 91.

The differences in the fragmentation pattern lead us to the assumption that our palladium system isomerized 1-hexene to the internal olefin. Subsequent to the isomerization, the EtAlCl_2 mediated the alkylation of toluene with the internal hexene.

The products with retention times between 14.60 to 15.61 min are those of the *di*-alkylated toluene products. The fragmentation patterns of these products were more complicated than those of the C_{13} isomers. The C_{19} products are obtained after the F-C alkylation occurring at any two of the three probable positions (*ortho*, *meta*, *para*) with either α or the internal hexene.

In an attempt to eliminate the F-C alkylation, reactions were repeated in hexane as solvent employing EtAlCl_2 in hexanes as co-catalyst similar to what was done in the ethylene oligomerization reactions. After reactions of up to 3 hours with sampling at regular intervals, no oligomers were detected using GC.

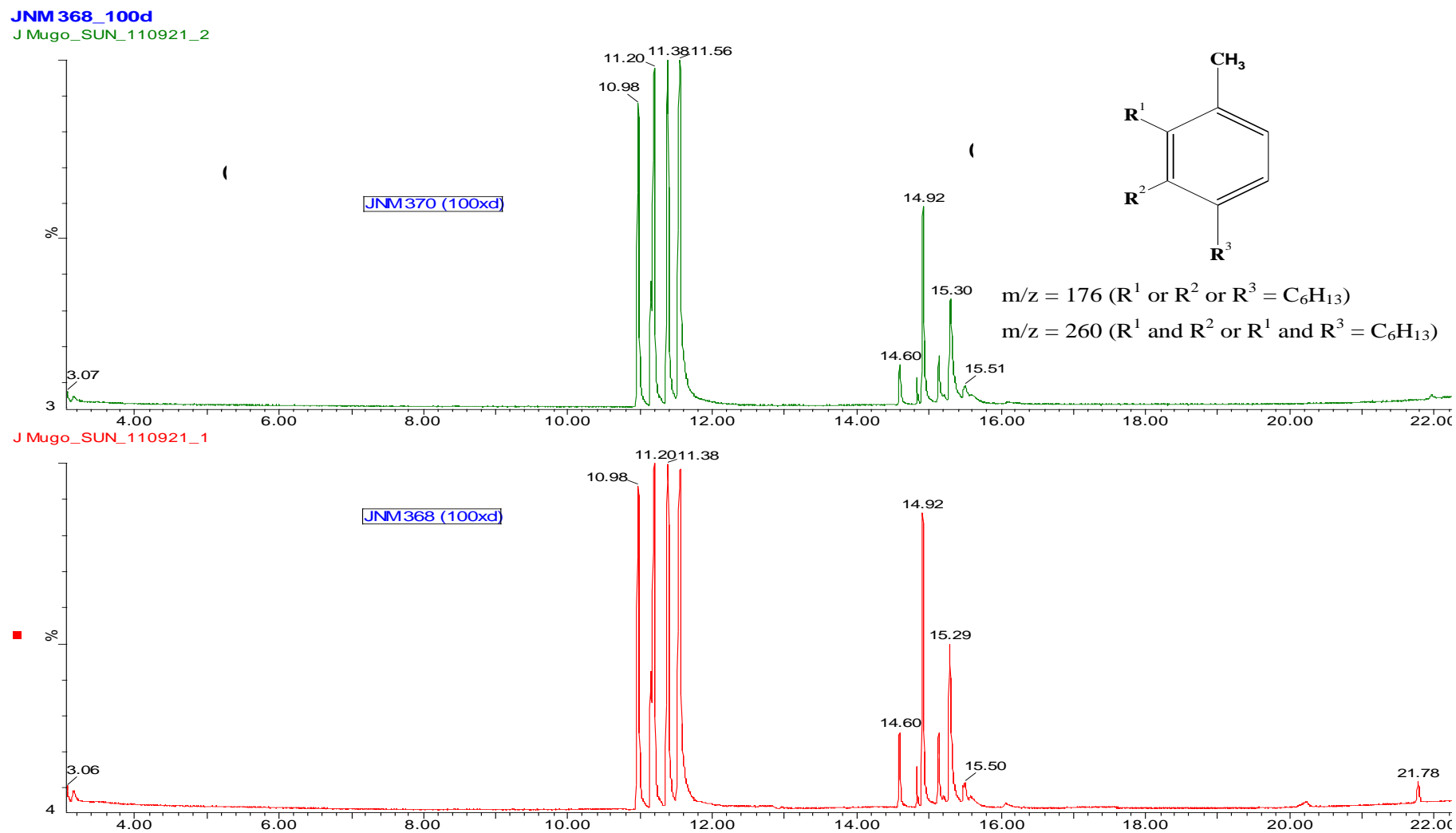
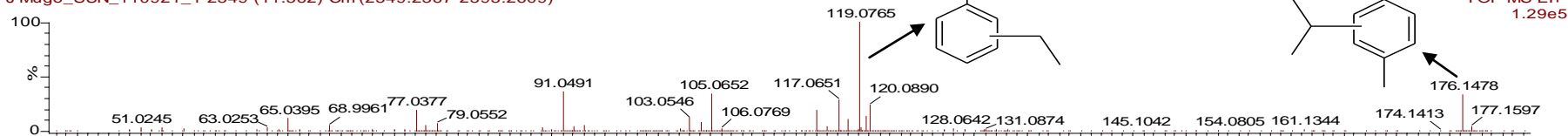


Figure 6.7: GC-MS chromatogram indicating Friedel-Craft alkylation of toluene with 1-hexene while using **C10** and **C14** as pre-catalysts

JNM368_100d

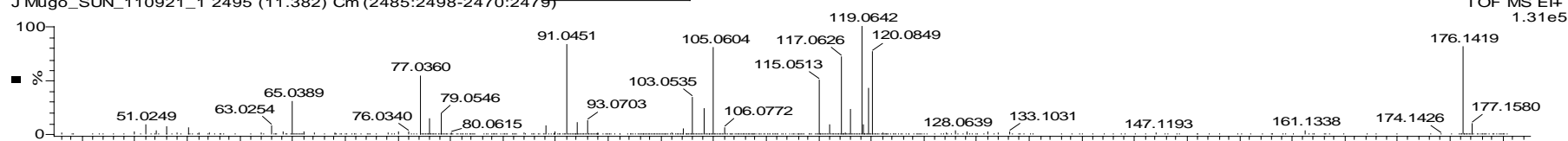
J Mugo_SUN_110921_1 2549 (11.562) Cm (2549:2567-2595:2609)

Peak at 11.56 min



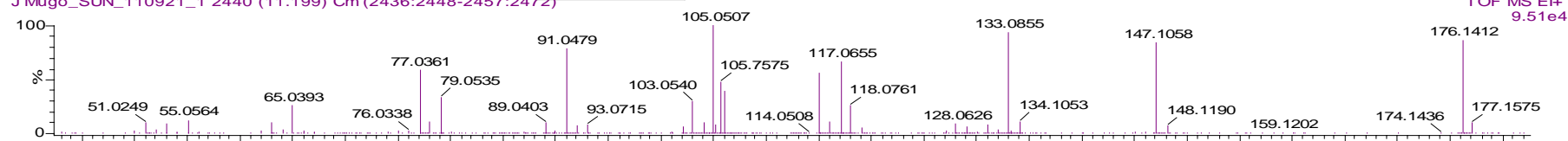
J Mugo_SUN_110921_1 2495 (11.382) Cm (2485:2498-2470:2479)

Peak at 11.38 min



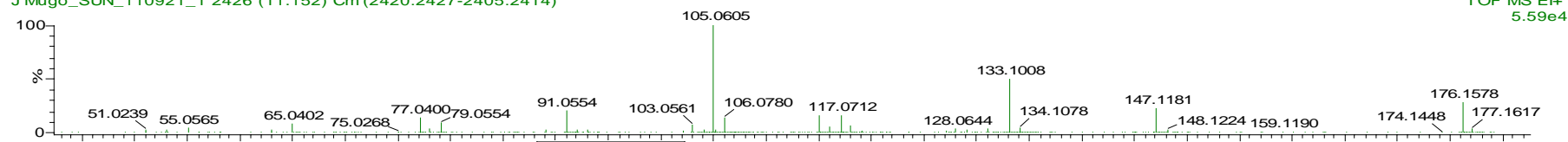
J Mugo_SUN_110921_1 2440 (11.199) Cm (2436:2448-2457:2472)

Peak at 11.20 min



J Mugo_SUN_110921_1 2426 (11.152) Cm (2420:2427-2405:2414)

Peak at 11.152 min



J Mugo_SUN_110921_1 2370 (10.965) Cm (2360:2370-2344:2352)

Peak at 10.97 min

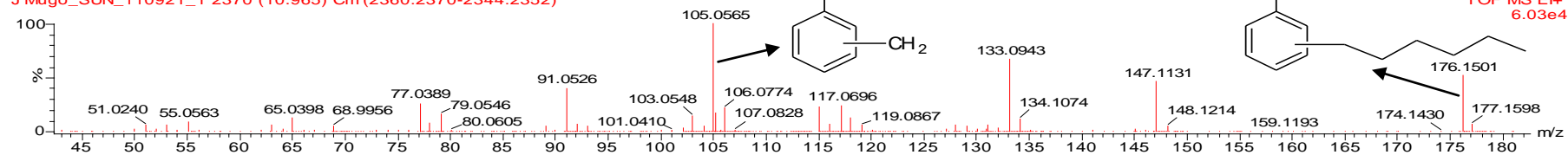


Figure 6.8: GC-MS spectra of the fractions with retention time of between 10.97 and 11.56 min for the products produced using **C10** and 1-hexene

In addition no long chain oligomers were isolated on removal of the solvent from the reaction mixture. These complexes are thus inactive in hexane as solvent.

It would thus appear that these palladium systems are unable to mediate the oligomerization of the higher α -olefins. Varying the parameters such as increasing the catalyst loading to 20 μ mol, or Al: Pd ratio to 1000:1 did not result in any oligomerization.

Other researchers have observed a similar trend where α -olefins alkylate aromatic hydrocarbons such as toluene and benzene. This phenomenon of alkylation has also been observed by others in our research group. Malgas-Enus²³ recently reported salicylaldiminato and iminopyridyl Ni(II) metallodendrimers that were also involved in alkylation of toluene. 1-pentene and 1-octene have also been shown to alkylate toluene under similar conditions to those employed in the 1-hexene reactions.

The presence of the transition metal pre-catalyst influenced the distribution of the alkylation products. C₁₃ was formed in higher % yield compared to C₁₉ in all the catalytic systems, Table 6.3.

Table 6.3: Selectivity of the Friedel-Craft alkylation products using **C10 - C14**^a

Complex	Friedel-Crafts alkylation product distribution	
	C ₁₃	C ₁₉
C10	66.9	33.1
C11	82.3	17.6
C12	87.5	12.4
C13	78.0	22.0
C14	70.8	29.2

^aReaction conditions: Temp 25 °C, time 30 min, Pd:Al:C₆H₁₂ ratio of 1:200:1600

The oligomerization of higher olefins thus proved unsuccessful in both toluene and *n*-hexane. When toluene was employed as solvent the substrate was consumed in the alkylation process before any oligomerization could be occur.

6.3: Conclusions

Pyrrolylaldiminato and salicylaldiminato palladium complexes were evaluated as pre-catalysts in the presence of EtAlCl₂. The active species that facilitates oligomerization was generated by alkylation of **C10**, **C11** and **C14**. Moderate activity of up to 920 kg (mmol Pd)⁻¹ h⁻¹ were obtained for the most active complex **C11**. The higher catalytic activity of this species is probably due to the higher stability of the active species of **C11** under the conditions employed. The inactivity of metallodendrimers **C12** and **C13** may be attributed to their low solubility in the solvents employed.

6.4: Experimental

6.4.1: Materials and instrumentation

All solvents used were of analytical grade and were dried and distilled prior to use. Toluene and *n*-hexane were dried over and distilled from sodium/benzophenone and ethanol from magnesium turnings/iodine. EtAlCl₂ (1.0 M in hexanes or 1.8 M in toluene) was obtained from Sigma Aldrich and used without any further purification. Ethylene (99.9 %) was obtained from Afrox.

The GC analysis was done using a Varian CP-3800 gas chromatograph equipped with a flame ionization detector (GC-FID) using a HP PONA column. *o*-Xylene was used as the internal standard during the GC analysis. Infrared spectra were recorded on a Nicolet Avatar 330 FT-IR spectrophotometer using an ATR accessory with a ZnSe crystal. The atmospheric pressure chemical ionization mass spectrometry (APCI-MS) was done on a Waters Synapt

G2 spectrometer introduced via an ASAP probe in the positive mode at Central Analytical Facilities, Stellenbosch University. GC-MS was done on a Waters GCT Premier spectrometer equipped with a HP5 column (30 m, 0.25 mm ID, 0.25 μm film thickness) at Central Analytical Facilities, Stellenbosch University.

Ethylene oligomerization

The ethylene oligomerization reactions were carried out in a 300 mL stainless steel autoclave equipped with an overhead stirrer and a heating mantle controlled by a thermocouple dipped into the reaction mixture. The autoclave was loaded with pre-catalyst, the required amount of co-catalyst (EtAlCl_2) and 50 ml of either dry toluene or n-hexane. The amount of pre-catalyst was varied to ensure that 5 μmol Pd was employed irrespective of the nature of the complex. The loading of the reactor was done in a nitrogen-purged glove box. The autoclave was sealed, removed from the glove box. The reactor was flushed twice with ethylene and heated to set temperature. The desired ethylene pressure was set and a constant flow was maintained through the reaction time. Various reaction conditions namely, temperature, Al:Pd ratio and ethylene pressure were investigated

At the end of reaction, the ethylene feed was stopped and the autoclave vented. The oligomerization was stopped by quenching the reaction mixture with 10 mL acidified ethanol (ethanol:HCl, 95:5). A GC aliquot was taken after which all volatiles were removed from the remaining mixture via rotary evaporation. Remaining non-volatiles material was subjected to atmospheric pressure chemical ionization mass analysis (APCI-MS) and IR spectroscopy.

Reaction conditions for toluene alkylation using 1-hexene

In a Schlenk tube containing appropriate amount of catalyst (Pd, 10 μmol), toluene (10 mL) and 1-hexene (2 mL, 1.6×10^4 mol) was added EtAlCl_2 (2 mL, 2.0×10^3 mol). The

solution acquires a light orange colour on addition of the co-catalyst. The solution is stirred at room temperature for 3 hours. The ratios of Pd:Al:C₆H₁₂ were maintained at 1:200:1600 irrespective of the complex used. After the reaction time, the mixture was quenched using 10 mL acidified ethanol.

After taking GC and GC-MS samples, all volatiles were removed from the reaction mixture via rotary evaporation.

6.4: References

1. G. J. P Britovsek, V. C. Gibson, D. F. Wass, *Angew. Chem. Int. Ed.*, **38** (1999) 428.
2. S. Kuhlmann, C. Paetz, C. Hägele, K. Blann, R. Walsh, J. T. Dixon, J. Scholz, M. Haumann, P. Wasserscheid, *J. Catal.*, **262** (2009) 83.
3. S. Mecking, *Coord. Chem. Rev.*, **203** (2000) 325.
4. A. de Klerk, *Ind. Eng. Chem. Res.*, **44** (2005) 3887.
5. J. T. Dixon, M. J. Green, F. M. Hess, D. H. Morgan, *J. Organomet. Chem.*, **689** (2004) 3641.
6. Y. Yoshida, S. Matsui, T. Fujita, *J. Organometal. Chem.*, **690** (2005) 4382.
7. K. Vanka, Z. Xu, T. Ziegler, *Organometallics*, **23** (2004) 2900.
8. K. Vanka, Z. Xu, T. Ziegler, *Organometallics*, **24** (2005) 419.
9. K. P. Bryliakov, E. A. Kravtsov, L. Broomfield, E. P. Talsi, M. Bochmann, *Organometallics*, **26** (2007) 288
10. K. C. Gupta, A. K. Sutar, *Coord. Chem. Rev.*, **252** (2008) 1420.
11. M. K. Das, K. Niedenzu, *Inorg. Chim. Acta.*, **150** (1998) 47.
12. L. K. Johnson, C. M. Killian, M. Brookhart, *J. Am. Chem. Soc.* **117** (1995) 6414.
13. C. Wang, S. Friedrich, T. R. Youkin, R. T. Li, R. H. Grubbs, D. A. Bansleben, M. W. Day, *Organometallics*, **17** (1998) 3149.

14. S. Kuhlmann, C. Paetz, C. Hägele, K. Blann, R. Walsh, J. T. Dixon, Judith Scholz, M. Haumann, P. Wasserscheid, *J. Catal.*, **262** (2009) 83 and references therein.
15. F. A. Hicks, J. C. Jenkins, M. Brookhart, *Organometallics*, **22** (2003) 3533.
16. G. J. P. Britovsek, M. Bruce, V. C. Gibson, B. S. Kimberley, P. J. Maddox, S. Mastroianni, S. J. McTavish, C. Redshaw, G. A. Solan, S. Strömberg, A. J. P. White, D. J. Williams, *J. Am. Chem. Soc.* **121** (1999) 8728.
17. J.-S. Mu, Y.-X. Wang, B.-X. Lia, Y.-S. Li, *Dalton Trans.*, (2011) 3490.
18. L.-P. HE, J.-Y. LIU, L. PAN, J.-Q. WU, B.-C. XU, Y.-S. LI, *J. Poly. Sci. Poly. Chem.*, **47** (2009) 713.
19. S. Mecking, *Angew. Chem. Int. Ed.*, **40** (2001) 534
20. S. O. Ojwach, I. A. Guzei, L. L. Benade, S. F. Mapolie, J. Darkwa, *Organometallics*, **28** (2009) 2127.
21. W. Dyer, J. Fawcett, M. J. Hanton, *Organometallics*, **27** (2008) 5082.
22. Q. Khamker, Y. M. Champouret, K. Singh, G. A. Solan, *Dalton Trans.*, (2009) 8935.
23. R. Malgas-Enus, PhD., *Thesis title, The Preparation and Characterization of Multinuclear Catalysts Based on Novel Dendrimers: Application in the Oligomerization and Polymerization of Unsaturated Hydrocarbons*, Stellenbosch University, 2011.

Chapter 7 : Summary and Future Work

7.1: Summary

Homogeneous and heterogeneous transition metal complexes of salicylaldimine and pyrrolylaldimine have been reported as catalysts in various catalytic processes. Their uses especially in the polymerization of cyclic esters and the polymerization and oligomerization of α -olefins are summarised in Chapter 1. These two catalytic processes were the main focus of this research project.

A series of monofunctional and multifunctional (dendritic) salicylaldimine and pyrrolylaldimine ligands were successfully synthesised in good yields. The multifunctional ligands were obtained by modifying the periphery of the 1st and 2nd generation diamino-butane poly(propyleneimine) dendrimers, DAB-(NH₂)_n (where n = 4 or 8). Zn(II) complexes of the salicylaldimine ligands, **L1** – **L9**, were prepared using Zn(Et)₂ and isolated in moderate to good yields. Palladium analogues of ligands **L1** - **L4** were successfully synthesised in moderate yields. The palladium complexes of the pyrrole-imine ligands, **L10** – **L13** were also successfully prepared.

All the compounds were comprehensively characterized using a range of analytical techniques which include FT-IR, NMR, and ICP-AES spectroscopy, thermal analysis (DSC, TGA), mass spectrometry and elemental analysis. Single crystal x-ray diffraction was also employed in the characterization of compounds **L5** and **C14**. The data acquired from all these techniques confirmed the nature of the ligands and metal complexes. We were however not successful in isolating the Pd(II) metallodendrimers of ligands **L5** – **L9** in pure form. Although coordination of these ligands to the palladium was successful as illustrated with **L5** in Chapter 4, purification of the material was problematic. Hydrolysis of the imine occurred during the various attempts we made to isolate a pure product.

We set out to evaluate the Zn(II) complexes as catalysts for the polymerization of D, L-Lactide. The reactions were performed in solution in the case of the mononuclear and

the 1st generation metallodendrimers. Various reaction parameters including time, M:Zn ratio and solvent were investigated. The mononuclear complexes **C1 - C3**, **C18** and **C19** showed moderate to high activity. However the dendritic systems **C4 – C6** showed poor activity in solution which was thought to be as a result of their low solubility in the solvents employed. Due to the low activity of the G1 zinc metallodendrimers in solution; further catalytic testing of the metallodendrimers was done under melt conditions.

Although **C1** was the most active of the lot, **C18** and **C19** gave polymers of highest molecular weight under similar conditions. This was attributed to the catalyst stability under the conditions employed. The polymers produced by these catalysts were mainly amorphous in nature. This indicates the lack of selectivity for the D or the L-lactide during the polymerization process. The metallodendrimers exhibited very high activity under the melt conditions but produced largely cyclic polyesters.

Preliminary evaluation of the Pd(II) complexes as catalysts in the oligomerization of α -olefins was carried. It was established that complexes **C10 – C14** in conjunction with EtAlCl₂ oligomerized ethylene to long carbon chain oligomers. Attempts to oligomerize higher α -olefins such as 1-hexene and 1-pentene proved unsuccessful.

7.2: Future work

In the D, L-lactide polymerization, further investigation under the melt conditions is required in order to understand why the metallodendrimers produced polymers of low molecular weight. MALDI-TOF mass spectrometry should be employed so as to determine the end groups in the polymer produced, especially for the polymers obtained under the melt conditions. Further research in this area would include modifying the catalyst systems by introducing electron withdrawing groups in the phenoxide moiety to establish how that would affect the rate of the polymerization and the prevalence of side reactions.

In the α -olefin oligomerization reactions, further optimization of the catalytic process conditions is required. A more comprehensive study of the various reaction parameters should be carried out. Reaction conditions such as higher reaction temperatures and higher ethylene pressure should be explored. Mechanistic studies for the alkylation of aromatics solvents by these olefins should also be probed to provide a better understanding of the role of the transition metal for further catalyst development.